APPLICATIONS OF GEOPHYSICAL METHODS FOR MONITORING ACID MINE DRAINAGE

MEND Project 4.6.1

December 1994

APPLICATIONS OF GEOPHYSICAL METHODS
FOR
MONITORING ACID MINE DRAINAGE

A. King
INCO Exploration and Technical Services Inc.
Copper Cliff, Ontario
Preliminary Report
April 22, 1994

EXECUTIVE SUMMARY

Following preliminary studies that indicated the potential for using geophysical methods for mapping acid mine drainage (AMD), the Mine Environmental Neutral Drainage (MEND) program sponsored a study to demonstrate the applications of geophysical methods to the AMD problem. Funding was provided by INCO Limited and the federal and provincial governments through the Northern Ontario Development Agreement.

The resource exploration industries have developed sophisticated instrumentation for mapping the electrical properties of the subsurface. In recent years, this equipment has been adapted for engineering and environmental applications, including determination of ground water quality.

Any increase in total dissolved solids (ADS) in groundwater results in an increase in electrical conductivity. Using commercially available equipment, the lateral and vertical variation of conductivity can be mapped, although resolution decreases with increasing depth.

Where the conductivity due to man-made contaminants such as AMD exceeds the natural variations in background conductivity, geophysical surveys can be used to map the subsurface distribution of AMD in three dimensions.

Other geophysical methods can be used to map the distribution of disseminated sulphides and zones of active oxidation or reduction reactions. The induced polarization method (IP) was developed to assist in mapping disseminated sulphides such as those found in porphyry copper deposits. This method can be used to map the lateral and vertical distribution of sulphides in tailings as part of programs to assess the acid-generating potential of tailings areas. The self potential (SP) method measures the passive voltage distribution and can indicate zones of active oxidation and reduction.

Under suitable conditions, the combination of electrical conductivity measurements, IP, and SP can be used to map:

    i) sulphides - the source of AMD,
    ii) zones of active oxidation, and
    iii) the distribution of the reaction resultant AMD.

High-quality airborne, ground and borehole geophysical data were acquired over areas with well-documented AMD problems. The geophysical data were correlated with hydrological and chemical data from ongoing ground water investigations to establish the utility of the methods.

The results confirmed that electromagnetic (EM) methods that remotely measure the conductivity of the subsurface are very useful for location and detailed three- dimensional mapping of AMD in groundwater. Airborne surveys can provide rapid reconnaissance scale surveys, while ground surveys and borehole surveys provide progressively more detail.

In addition to the EM work, combined IP and electrical conductivity surveys were tested on a large revegetated tailings area. The IP method detected disseminated sulphides as expected, and the combination of IP and conductivity surveys can be used for simultaneous three-dimensional mapping of sulphides and ground water quality in tailings. United SP surveying showed strong SP anomalies over the tailings however, additional SP data and

information on the distribution of the oxidation found on the tailings is required to properly assess this method.

All of these methods require measurement of the electrical properties of the subsurface and are adversely affected by electrical noise from power lines and surface and buried metal. The response of AMD may be masked by naturally conductive ground water, bedrock lithologies, or clay soils.

RÉSUMÉ À L'INTENTION DE LA DIRECTION

Après des études préliminaires qui ont indiqué le potentiel de des méthodes géophysiques pour cartographier le drainage minier acide (DMA), le Programme de neutralisation des eaux de drainage dans l'environnement minier ou NEDEM, a parrainé une étude permettant de démontrer les applications des méthodes géophysiques à la résolution des problèmes de DMA. Le financement a été assuré par l'INCO Limitée et les gouvernements fédéral et provinciaux par le biais de l'Entente d'exploitation du Nord de l'Ontario.

Les industries de la prospection des ressources ont mis au point des instruments sophistiqués pour cartographier les propriétés électriques du souterrain. Ces dernières années, ce matériel a été adapté à des usages techniques et environnementaux, notamment à la détermination de la qualité des eaux souterraines.

Un accroissement des concentrations de solides totaux dissous (STD) dans les eaux souterraines provoque une augmentation de la conductivité électrique. En employant les appareils disponibles dans le commerce, on peut cartographier les variations latérales et verticales de la conductivité, même si la résolution diminue en fonction de la profondeur.

Lorsque la conductivité due à des contaminants anthropiques tels que le DMA dépasse les variations naturelles de la conductivité de fond, on peut employer des levés géophysiques pour cartographier la distribution du souterraine du DMA en trois dimensions.

On peut faire appel à d'autres méthodes géophysiques pour cartographier la distribution des sulfures disséminés et des zones d'oxydation ou de réduction actives. On a mis au point la méthode de polarisation induite (PI) pour aider à cartographier les sulfures disséminés tels que ceux rencontrés dans les gîtes porphyriques sulfurés de cuivre. Cette méthode peut servir à cartographier la distribution latérale et verticale des sulfures dans les résidus, dans le contexte des programmes d'évaluation du potentiel générateur d'acides des résidus. La méthode du potentiel spontané (PS) permet de mesurer la distribution du voltage passif et peut indiquer les zones d'oxydation et de réduction actives.

Dans des conditions appropriées, on peut employer les mesures combinées de la conductivité électrique, de la PI et du PS pour cartographier:

i) les sulfures - source du DMA
ii) les zones d'oxydation active, et
iii) la distribution du DMA résultant des réactions.

On a acquis des données géophysiques de haute qualité, faites par levés aéroportés, levés au sol et relevés dans les trous de sondage, dans des secteurs où les problèmes de DMA sont bien documentés. On a corrélé les données géophysiques avec les données hydrologiques et les données chimiques provenant d'études actuelles des eaux souterraines pour établir l'utilité des méthodes.

Les résultats ont confirmé que les méthodes électromagnétiques permettant de télémesurer la conductivité du souterrain sont très utiles pour situer et pour cartographier de façon détaillée en trois dimensions le DMA dans les eaux souterraines. Les levés aéroportés peuvent fournir rapidement des levés de reconnaissance, tandis que les levés terrestres et les relevés effectués dans les trous de sondage fournissent progressivement

plus de détail.

Outre le travail de levés EM, on a mis à l'épreuve des levés combinés PI et de conductivité électrique sur une vaste zone de résidus que l'on a recouverts de végétation. La méthode PI a permis de déceler les sulfures disséminés comme prévu, et la combinaison des levés PI et de conductivité peut servir à la cartographie simultanée en trois dimensions des sulfures et de la qualité des eaux souterraines à l'intérieur des résidus. Un travail de levés PS limités a indiqué de fortes anomalies PS dans les résidus; cependant, des données PS additionnelles et l'information sur la distribution de l'oxydation rencontrée dans les résidus sont nécessaires pour évaluer correctement cette méthode.

Toutes ces méthodes exigent la mesure des propriétés électriques du souterrain et sont gênées par le bruit électriques des lignes de transport d'électricité et par les métaux présents en surface et dans le sous-sol. La réponse du DMA peut être masquée par les eaux souterraines naturellement conductrices, par la lithologie du substratum rocheux, ou par les sols argileux.

Index

List of Figures

* These figures are not included in this report but copies may be obtained, at extra cost, from the MEND Secretariat.

List of Tables

1.0   INTRODUCTION

The purpose of this work is to demonstrate and document the application of geophysical methods for monitoring acid mine drainage (AMD). AMD has been identified as the largest single environmental problem facing the Canadian mining industry (Filion et al., 1990). Because AMD investigations have traditionally relied on surface sampling and drilling and sampling of the subsurface, they can be expensive and slow. In suitable environments geophysical methods offer the potential for rapid, non-intrusive mapping of significant AMD problems.

We have not attempted to cover all possible geophysical applications in detail but have, after a review of the literature and current geophysical practice, focused on the electrical and electromagnetic methods. In appropriate environments these methods have the potential to directly detect and map the following:

- sulphides which are the source of AMD,
- areas of active chemical oxidation, and
- acid mine drainage itself.

These methods specifically target AMD, and we believe their application would offer the most immediate benefit to the mining industry.

Geophysical studies involve the measurement of various fields and waves (gravitational, electromagnetic, acoustic, etc.) that penetrate the earth, and provide information on variations in the physical properties (density, electrical conductivity, acoustic velocity, etc.) of the subsurface. They are non-intrusive but penetrating.

Geophysical methods remotely measure variations in physical properties, but are distinct from conventional remote sensing techniques that rely exclusively on high-frequency electromagnetic radiation, visible and otherwise, and have essentially no depth penetration.

Geophysical measurements can be used to map three-dimensional variations in subsurface physical properties and to locate and map geological features at depth where these features are associated with some measurable physical property contrast.

In most methods the depth of penetration is limited only by the power and sensitivity of the measuring system and/or the size of the source; however, resolution decreases with depth penetration so that only large features can be resolved at greater depths.

Geophysical methods have been used for many years by the mining industry in exploration and geotechnical investigations. The basic techniques for mapping variations in physical properties of the subsurface have been adapted to meet the

special needs of resource exploration and development in the coal, potash, oil sands, industrial minerals, precious metals and base metal industries. For suitable targets the use of geophysics can reduce "finding costs" by orders of magnitude while simultaneously improving the reliability of the search methods.

As in the search for buried ore deposits or in geotechnical investigations, geophysics can be a valuable aid in subsurface environmental investigations. Investigations can be remedial, involving the location or monitoring of existing problems, or preventive, where problem areas are identified or background values are established before site development. In either case, geophysical methods should not be considered as a substitute for drilling. Geophysical interpretations in general do not provide the detail required for a complete environmental or geotechnical investigation. They are most useful as rapid reconnaissance methods for targeting subsequent drilling, or for interpreting subsurface conditions away from or between drill holes.

Table 1 lists the common geophysical methods and the physical properties they are sensitive to. The methods that we have chosen to focus on in this study are the electrical and electromagnetic methods for mapping ground conductivity, the induced polarization method for measuring low frequency ground electrical polarization, and the self-potential method for measuring natural earth voltages. These methods have the potential, in most AMD environments, for direct detection of:

i) the AMD product (conductive acidified groundwater),
ii) the source (polarizable sulphides), and
iii) the chemical reactions (which generate natural voltages or potentials).

They are discussed in more detail in Section 2.

Other geophysical methods may have direct applications in special AMD environments, or indirect applications where they are used to characterize the subsurface geology. Some of these applications are briefly summarized below.

Airborne, ground and borehole radiometric measurements can be very useful for investigations of radioactive tailings (King and Pesowski, 1991). It should be noted that ionizing radiation does not normally penetrate more than a metre of soil or water, so depth penetration is limited. A possible exception to this is the use of alpha particle detectors for detecting radon gas that may migrate from depth.

Magnetic measurements have been used to map the distribution of pyrrhotite, the most magnetic of the metallic sulphides, in tailings (Clark, 1991). They can also be useful as an auxiliary tool for separating conductive but nonmagnetic AMD from buried conductive and magnetic ferrous metal.

Seismic methods may have important but indirect applications to the AMD problem. Seismic refraction is a standard engineering geophysical tool and can be used to map the depth to bedrock under tailings (Berrer and King, 1992). This can be useful for estimating total volume of tailings and for determining groundwater volumes and flow paths. The seismic reflection method may also be used for mapping the bedrock surface, and possibly layering within tailings and the tailings-overburden boundary. To our knowledge no seismic reflection surveys have been done on tailings but proposals for test work have been submitted to the MEND group.

Because of the heat released in the oxidation of sulphides, thermal measurements may have some application for mapping AMD. These could include airborne infrared thermal imaging and borehole thermal measurements. AECL, together with Intera-Kenting, have carried out thermal imaging of the Rabbit Lake uranium tailings in northern Saskatchewan. Again, the method is limited to surface mapping because of the negligible depth penetration. To our knowledge no borehole thermal measurements have been done on tailings but it is planned to test the GSC multiparameter borehole logging system, which includes a temperature probe, at the Sudbury test sites established in the course of this work.

It is expected that applications of ground-probing radar to AMD problems will be limited due to the reduced depth penetration in conductive environments. The gravity method, which is sensitive to density variations, has little application due to its poor resolution.

2.0   BASIC PRINCIPLES

2.1   Electrical Conductivity in the Earth

Measurement of the electrical properties of the subsurface using geophysical methods has been a standard procedure in resource and groundwater exploration for many decades. The conductivity of earth materials is determined by the conductivity of the soil or rock matrix, the conductivity of the pore fluid or groundwater, and the thermal state of the soil or rock. The basic equations governing conductivity are discussed in Technical Note 5 (Geonics, 1981).

Natural variations in electrical conductivity can assist in the mapping of soil types as shown in Figure 2.1. The location of less conductive, coarse-grained material such as sand and gravel prior to development can be useful in establishing potential groundwater flowpaths. More conductive, fine-grained clay soils are relatively impermeable and can be used as a natural barrier to fluid flow.

In general, the crystalline bedrock of the Canadian Shield is non-conducting; however, highly conductive bedrock sources such as sulphide deposits and graphitic schists are found in some areas. In fact, sulphide deposits are always found in the immediate vicinity of any sulphide tailings or waste rock piles and can be expected to complicate the interpretation of electrical measurements.

The addition of inorganic ions such as salts, acids, bases, metallic ions, etc., increases groundwater conductivity dramatically, and geophysical maps of the electrical properties of the subsurface can be very useful in locating or monitoring areas of inorganic contamination. The relative electrical activity of some of the common groundwater ions is shown in Figure 2.2.

The level of contamination that can be detected is dependant on the natural conductivity background. If pre-development conductivity surveys are available relatively small changes in conductivity due to contamination can be detected. In areas of high and variable natural conductivity, low levels of contamination may not be detectable without prior surveys.

The oxidation of sulphides yields sulphate, hydronium (H^+) and metal ions that raise the conductivity of groundwater. The principal contributors to increased conductivity are the sulphate and metal ions. Acidified groundwater is a weak solution of sulphuric acid, which is a well known electrical conductor. The iron ions and other metals dissolved by acidic groundwater make additional contributions to groundwater conductivity.

It is apparent in Figure 2.2 that the combination of H+ ions and sulphate ions results in the highest conductivity of the usual ionic pairs (compared to Na+ and Cl- for example). The thermal state of earth materials also influences their conductivity. As shown in Figure 2.3, electrical conductivity decreases slowly with temperature to the

freezing point and drops rapidly below the freezing point. The strong correlation between conductivity and AMD was first demonstrated by hydrological studies by the University of Waterloo at the Nordic Mine tailings near Elliot Lake (Blair et al, 1980).

Pyrite-bearing uranium ore was mined at the Nordic Mine from 1957 to 1968. An estimated 15 million tons of tailings cover 85 hectares to an average thickness of 10 m. The tailings contain approximately five percent pyrite. Oxidation of pyrite in the tailings has generated acid that, together with Radium 226 and heavy metals, has contaminated a 20 to 30 m thick sandy aquifer underlying the tailings. Figure 2.4 shows a plan view of part of the tailings dam with contours of sulphate concentration as measured in piezometers. These measurements, taken in 1979, indicate a plume of contaminated groundwater extending approximately 400 m from the tailings dam. The high sulphate concentrations result in high ground conductivities that can be mapped using surface geophysical methods. The correlation between sulphates and conductivity has been well established at this site by laboratory measurements of conductivity and sulphate content of groundwater samples from multi-level piezometers, as shown in section in Figures 2.5A and B. It is obvious from this data that maps of conductivity could be used to locate the contamination plume. Figure 2.5C shows a typical heavy metal distribution, in this case Radium 226, in the same plume. The heavy metal distribution is confined to the plume, as defined by the sulphates and the conductivity.

This site was also surveyed using electrical and electromagnetic geophysical methods (Pehme, 1981). The examples in the following section are drawn from this work, which demonstrated, for the first time, the application of geophysical methods for mapping AMD. The results of this work are summarized below, since we have used this work as a base, expanding the DC electrical resistivity (resistivity is the inverse of conductivity) method to include the IP and SP methods, and the EM work to demonstrate the newer surface systems designed specifically for engineering and groundwater applications as well as airborne and borehole systems and advanced processing and imaging techniques.

2.2   DC Resistivity Method

There are several methods of remotely measuring ground conductivity or its inverse, resistivity. The galvanic or direct current (DC) resistivity method is illustrated in Figure 2.6. A constant or DC electrical current is passed through the earth between two current electrodes. The voltage between two potential electrodes is measured at various points on the surface, and the resistivity of the ground is calculated from the ratio of measured voltage to transmitted current, with appropriate geometric factors (Telford, 1976).

As shown in Figure 2.7 the current is turned off and reversed periodically. This prevents polarization (and hence corrosion) of the electrodes and also allows induced polarization (IP) measurements following the current shut off.

In the profiling mode, the entire electrode array is moved along a survey line, generating a continuous profile of resistivity along the line. In the sounding mode, the distances between the electrodes are progressively expanded. At larger separations, current flows to a greater depth, and an estimate of the variation of resistivity with depth can be obtained by comparing measurements made at different electrode separations.

Both sounding and profiling modes were used in an investigation of the contamination plume originating from tailings at the Nordic Mine site (Pehme, 1981).

Resistivity data were acquired along several profiles over the plume area. The data from Profile B, which runs parallel to the dam and crosses the plume as shown in Figure 2.4, are shown in Figure 2.8. The centre of the plume around piezometer M8 is clearly indicated by resistivity lows in the larger electrode spacings. Data from the shortest array reflect near-surface conditions while the wide-spaced arrays provide more information on deeper resistivity values. Like many geophysical methods, there is a trade off between depth and resolution. The longest array, with a depth penetration of the order of 30 m, averages resistivities over the 90 m length of the array. This results in a smoothing of the deep resistivity data and blurs the edges of the plume.

In general, the vertical resolution in the sounding mode is better than the lateral resolution in the profiling mode. A resistivity sounding at piezometer M8 is shown in Figure 2.9. In this case, the centre of the array is fixed and the electrodes are expanded symmetrically about the centre.

The resistivity data show a thin, resistive surface layer, consisting of dry soil; a highly conductive, intermediate layer corresponding to the contaminant plume; and deep, resistive bedrock.

Sounding data can be interpreted quantitatively for layer thickness and resistivity, as shown in the resistivity model (Figure 2.9). In this case, the responses of theoretical models were calculated until a good match to the observed data was obtained.

The modelled layer boundaries match the boundaries as observed in drill hole M8. As expected, the bulk resistivity of the plume, as indicated by the geophysics, is higher than the resistivity of the water in the pores as determined from groundwater samples. This is because the bulk resistivity includes the effect of the mineral grains.

Fixed electrical arrays can also be used for continuous monitoring. In this case, electrodes installed at a site are monitored to detect variations in resistivity with time. Since readings can be recorded automatically, this method is particularly

suitable to long-term monitoring of remote sites.

2.3   Electromagnetic Methods

Ground conductivity can also be measured using electromagnetic (EM) measuring devices. A generalized EM system, as shown in Figure 2.10, consists of a source antenna and a receiving antenna. An alternating magnetic field generated by the source induces alternating currents in the ground. These, in turn, generate secondary magnetic fields that are detected at the receiver (Rx). As secondary currents are selectively induced in conductive material, this method is most sensitive to the presence of conductive bodies in the subsurface (McNeill, 1980b).

EM methods require no ground contact, which permits operation in frozen terrain or from aircraft. In general, the method provides better lateral resolution than the galvanic methods, and data can be acquired more quickly.

A wide variety of EM systems are available. The choice of systems usually depends on the type of problem at hand. The very low frequency (VLF) method uses distant US Navy navigation and communication radio beacons as sources, and small, one-man, portable receivers. Resistivities are derived from a combination of magnetic and electrical field measurements. The VLF method was used by Pehme (1981) to map the extent of the low-resistivity area associated with the Nordic contamination plume, as shown in Figure 2.11. The VLF apparent resistivity data correlate well with the extent of the plume, as shown in Figure 2.4, and provide considerably more information at the edges of the plume where detailed traverses were carried out. The basic survey data, consisting of 70 stations, were acquired in one day by a single operator.

Small one- or two-man, portable, two-coil, EM systems specially adapted for engineering and environmental applications by Geonics (McNeill, 1980b) are most commonly used now in site investigations. These instruments, known as ground conductivity meters, are easy to use, and read directly in conductivity units.

Readings taken with different coil orientations with the EM31 and at different coil separations and orientations with the EM34 permit measurements to various depths ranging from 1 to 48 m as shown in Table 1. Comparison of readings with different depth of penetration can provide information on the variation of conductivity with depth.

The apparent conductivity data obtained from different depths of exploration at any measurement station can be used to estimate the conductivity stratification of the subsurface in the vicinity of that station. This is discussed in more detail in the section on inversion methods in Section 4.4.

2.4   Induced Polarization

The IP method uses the same arrays as the DC resistivity method, but measures

the time decay of the voltage in the ground after the shut off of a current pulse. This provides a measure of the low-frequency electrical polarization or chargeability of the subsurface. The strongest source of the IP effect is polarization at the boundary between electrolytic conduction in groundwater and metallic conduction in sulphide grains or metallic objects. Electrochemical effects in clays may also produce weak IP effects.

The principal use of the IP method in exploration has been the mapping of disseminated sulphides in bedrock for gold deposits or large low-grade sulphide systems. It is proposed here that the method could be used to map the distribution of sulphides in tailings.

The IP effect can also be measured using frequency domain systems that transmit a continuous sine wave current and measure the phase difference between the transmitted and received waveforms, or the change in impedance at slightly different frequencies. Time domain systems provide data over a broader bandwidth with a single reading and are more resistant to interference between Rx and Tx wires, while frequency domain systems give better signal in low-signal, high-noise environments.

2.5 Self-Potential Method

The SP method measures the natural voltages between receiving electrodes, and can be measured simultaneously with resistivity and IP. The natural voltage signal is sensitive to active oxidation-reduction reactions and could be useful in mapping the reaction rate of sulphide oxidations.

3.0   DESCRIPTION OF METHODS

This section describes the specific systems that were used as well as procedures and calibrations.

3.1   Electromagnetic Methods

Due to their ease of use electromagnetic methods were preferred for mapping subsurface electrical conductivity for this study. The work started with test surveys using small, ground EM systems in areas of known AMD. Subsequently, airborne EM (AEM) data became available and was incorporated into the study. In some cases, additional ground data was acquired to cover areas of interest, as indicated by the AEM results. On completion of the ground work, test holes were drilled and cased in plastic to collect water samples and to provide for borehole EM (BHEM) surveys.

Each stage of this work, from AEM to ground EM to BHEM, provides progressively greater detail at progressively greater cost per unit area covered for acquiring new data. In many cases surveys can share resources with other data-gathering activities to reduce costs. For example, in this project:

? AEM data from an exploration survey was reprocessed and presented in a form suitable for groundwater studies. Most mining areas in Canada have been covered by AEM surveys. In many areas reconnaissance AEM data is available from the provincial governments for the cost of reproduction. Companies should check with their exploration departments or an exploration consultant for details on acquiring and reprocessing this and other geological, geochemical and geophysical exploration data. In most areas there is a great deal of valuable data in government and private company files, with direct application to environmental investigations in general and AMD problems in particular.

? Data from multilevel piezometer tests previously established by the University of Waterloo were used to provide groundwater data for nearby geophysical wells.

? New holes drilled by consulting engineers as part of ongoing groundwater and geotechnical investigations were cased in plastic (minimum 2 inches with plastic screens) and logged for conductivity. On investigation it was remarkable how many new and old holes there were. It was estimated that approximately 1,000 holes had been drilled for groundwater and geotechnical investigations on the Copper Cliff Tailings alone and new holes were being drilled regularly to provide information on dam stability, depth to bedrock, etc., as well as groundwater. Unfortunately, most of these holes have not been preserved and some of those that were are

steel-cased. If all holes are completed as described above, at an extra cost of a few hundred dollars per hole, and preserved, they can be an extremely valuable asset for detailed three-dimensional monitoring of groundwater quality before and after mine closure.

3.1.1   Surface Systems

Small frequency (FEM) systems were used for shallow (0 to 40 m) investigations. These systems are fast, easy to operate, and relatively inexpensive to rent or purchase. Unfortunately, the deeper penetrating system saturates in high-conductivity environments (>100 milliSiemens/metre or mS/m). For deeper investigations or very conductive environments a Transient EM (TEM) system was used. This system can penetrate to at least 100 m and has a much higher conductivity threshold but is expensive and is usually operated by specialist contractors.

FEM systems

The Geonics EM31 and EM34 systems were used for this work. These systems were designed specifically for environmental and geotechnical investigations. They read directly in conductivity units (mS/m) and do not require geophysical specialists to operate.

The EM31 is a one-man unit with a 36 m long rigid boom which contains a transmitting (Tx) coil in one end and a coplanar receiving (Rx) coil in the other end. In the EM34 the Tx and Rx are separated and are linked by a cable. This permits larger coil separations (10, 20 or 40 m) and hence greater depth penetration, but requires two people to operate. On both systems data is displayed on an analogue meter and can be recorded with an external digital logger. Detailed equipment specifications are given in Appendix B.

Readings taken with different coil orientations with the EM31, and at different coil separations and orientations with the EM34, permit measurements to various depths, ranging from 1 to 40 m as shown in Table 2. In each case the effective depth is the maximum depth of penetration and the reading is the apparent conductivity, which is a weighted average of the conductivity to the effective depth of penetration. For more details on the relationship of the apparent conductivity to the true conductivity structure see TN6 in Appendix A.

The system calibrations were checked daily using the procedures described in the instrument manuals.

TEM system

The Geonics EM47 system was used in high-conductivity areas or for deep targets. Instead of transmitting a single frequency sinusoidal current through the Tx, TEM systems transmit discrete current pulses with a precisely controlled ramp turn off. The turn off of the current pulse creates a changing magnetic field that, like the

sinusoidal waveform in the FEM systems, induces secondary currents in subsurface conductors. These secondary currents decay with time and produce a decaying secondary magnetic field that is detected as a voltage pulse at the Rx coil. The amplitude of the signal is measured in a series of 20 logarithmically spaced channels located after the end of the turn off. In general, for layered earth geometries, the signal amplitude is proportional to the conductivity of the layers, with signal values in later time corresponding to deeper layers. The calculations for converting voltages to apparent resistivity are described in more detail in Technical Note 7 in Appendix A. A sample output plot is shown in Figure 3.1A with resistivity plotted against time (equivalent to depth) on log-log scales. Each reading is effectively a 20 electromagnetic depth sounding with 20 depth points. The depth soundings are interpreted by computer curve matching or data inversion programs.

The survey geometry is shown in Figure 3.1B. A large Tx loop (minimum 20 m by 20 m) is laid out on the ground and is energized by a small battery-powered Tx. A motor generator-powered Tx is available for larger loops where more depth penetration is required. The Rx can be located anywhere except near the Tx wire. For larger loops the simplest geometry is with the Rx at the centre of the Tx loop. For smaller loops the central location is too close to the Tx wire and the Rx is located outside the Tx loop.

Data are recorded digitally with a built-in data logger that is dumped to a field computer. Programs supplied by the manufacturer are available for converting raw data to apparent resistivity.

An internal calibration signal is generated periodically to ensure the calibration of the Rx electronics. The Tx current and turn off time is measured at each station using an internal digital ammeter and clock. Synchronization between the Tx and Rx is maintained by a cable link.

3.1.2 Airborne Systems

Helicopter AEM systems, as shown in Figure 3.2, are similar to the EM31 in that they are mounted in a short fixed boom; however, instead of a single coplanar coil pair operating at a single frequency, it has multiple coil configurations operating at multiple frequencies. The Aerodat system used for the Sudbury Basin survey had vertical coplanar, horizontal coplanar and coaxial coil pairs operating at 900 Hz, 4,000 Hz and 32,000 Hz. These multiple data sets allow some depth and conductor geometry discrimination from a single pass survey. In general, lower frequencies penetrate further into the earth and different coil configurations have characteristic responses to different conductor geometries. For example, the horizontal coplanar pair has maximum response to the flat-lying conductors typical of water-saturated overburden, while the coaxial pair has maximum response to the subvertical conductors typical of bedrock conductors in the Canadian Shield.

The data were recorded digitally and calibrations were carried out regularly to

ensure data quality.

3.1.3   Borehole Systems

Borehole EM (BHEM) surveys are based on the same principles as surface and airborne. As shown in Figure 3.3 Tx and Rx coils are mounted in a small-diameter (32 mm) waterproof sensor that is lowered down plastic-cased boreholes. The average or apparent conductivity within effective range of the hole is measured at intervals down the hole and is presented in profile form. For this work the Geonics EM39 BHEM system was used. This system incorporates auxiliary focusing coils that reduce the sensitivity of the sensor to conductivity variations in the immediate vicinity of the hole. These variations may be due to the fluid in the hole, the casing material, or disturbed material around the casing. This ensures that, in so far as possible, the conductivity measurements are representative of undisturbed material. The effective range of the EM39 sensor is about 0.8 m from the hole.

Distance down the hole is measured using a counter mounted on a pulley. The cable attached to the sensor is passed over the pulley under tension. Depth measurements are accurate to a few centimetres.

For some of the BHEM work Geonics Ltd. made available, at nominal cost, a natural gamma radiation sensor. This measures the total natural gamma radiation emitted from material within about 0.3 m of the hole. The only significant natural gamma emitters are the radioactive isotopes of uranium, thorium and potassium. The concentrations of these elements (trace values only for uranium and thorium) are usually highest in fine-grained soil materials such as clays. Concentrations normally decrease steadily with increasing grain size, with the lowest values in clean sands. Gamma measurements provide an independent parameter for classifying soil type on the basis of physical properties. They are particularly useful in studies of groundwater contamination where natural conductivity values, which are generally characteristic of soil type, are affected by contaminants.

The EM39 system records depth down the hole, conductivity and total gamma values digitally at preset intervals down the hole. Data are dumped to personal computers using software supplied by the manufacturer.

3.2   Electrical Methods

Resistivity, Induced Polarization and Self Polarization Measurements

These measurements can all be acquired simultaneously using grounded electrical arrays, as shown in Figure 2.6. Currents are generated by battery- or motor generator-powered transmitters connected to the ground using stainless steel stakes. The potentials or voltages are measured simultaneously at multiple electrical dipole locations using a multichannel digital recording system. To avoid contamination of the data by electrodal polarization effects these dipoles are connected to the earth with nonpolarizable copper-copper sulphate electrodes. This ensures that the only polarization in the received signal is due to earth polarization.

The self potential or natural voltage is measured first, during the current off-time, and is automatically subtracted from the subsequent on-time (resistivity) and pulse decay (IP) readings.

The resistivity is determined from the receiver voltage measured during the on-time, the transmitted current, and the array geometry. Voltage divided by current gives the resistance of the earth, and normalization by the appropriate geometric factor gives the resistivity.

Chargeability is determined from the decay of the voltage in the earth after current shut off (time domain) or by phase shift or resistivity ratios (frequency domain). Chargeability and resistivity are often used to calculate the metal factor, which is the product of chargeability and conductivity. The metal factor responds most strongly to connected but not massive sulphides that are both chargeable and conductive.

Both time and frequency domain methods were tested. Data were digitally recorded by the receivers. Each evening the data were dumped to the computer and plotted in pseudosection form.

4.0   DESCRIPTION OF WORK

Regional Geology and Site Selection - Sudbury Basin
The Sudbury igneous complex (SIC), shown in Figure 4.1, hosts one of the largest concentrations of economic sulphide deposits in the world, with production of nickel, copper, cobalt and platinum group elements. The SIC is the result of a major meteor impact approximately 1.8 billion years ago. It is believed that the complex was originally circular in shape and subsequent tectonic events have deformed it to its present elliptical shape. It consists of a series of crystalline intrusive rocks overlain by rocks of the Sudbury basin: a tuff-like fallback breccia (Onaping formation) and an upper layer of carbonaceous sediments (Onwatin formation).

The major deposits and the associated mine facilities are all found at or near the contact between the basal crystalline intrusive rocks of the complex and surrounding metamorphosed volcanic, sedimentary and intrusive rocks. These host rocks are all electrically very resistive (an important factor in the application of electrical geophysical methods). The only electrically conductive rock formations in the area are the carbonaceous slates of the Onwatin formation. The ore-bearing sulphides are also highly conductive but are found only in restricted areas at or near the base of the SIC.

The first deposits were discovered in the 1890s and have been mined continuously since then. There are currently 14 operating mines, 40 abandoned sites, and four major tailings areas.

Mining has produced approximately 900 million tonnes of reactive sulphide-bearing waste rock. Most of this is in tailings, with some in waste rock piles. The principal sulphide in the waste rock is pyrrhotite, with concentrations in tailings ranging from less than one percent to more than 60% sulphides in pyrrhotite storage areas. As is well known, on exposure to air the sulphides oxidize to produce dilute sulphuric acid plus metals, mainly Fe, with small quantities of Ni and Cu.

Tailings
The tailings are stored in large impoundments in topographically low areas and contained where necessary by large, semi-permeable dams. The two main INCO tailings are at Copper Cliff (2,225 hectares) and Levack (80 hectares). The Copper Cliff tailings are being expanded to handle future mine waste and are currently receiving about 36,000 tonnes per day of tailings. The Levack tailings are no longer active. Ongoing geotechnical and hydrogeological studies at both sites are gathering the detailed information required to design optimum containment, treatment and eventual closure plans.

Groundwater Flow

The tailings areas are net recharge areas due to natural precipitation and the addition of mine waters. The hydraulic gradients in the tailings areas are generally downward and outward, resulting in groundwater flow through and below the dams. This results in plumes of tailings water which manifest themselves as low pH, high sulphate, high iron, surface AMD seeps. All surface drainage is collected through an extensive network of interception ponds and pumping stations, and treated.

Study areas

Two sites, one at Pistol Dam on the Copper Cliff tailings and the other at the INCO Levack tailings, were originally selected for geophysical tests. Subsequently, some excellent data provided by Falconbridge at their Fault Lake tailings near Falconbridge resulted in the inclusion of this site in the study as well. These areas were selected as known AMD sites where data from concurrent geotechnical and hydrological studies could be used to correlate with our geophysical work.

Site Selection and Preparation

Ground test sites, as shown in Figure 4.1, were selected in areas of known AMD problems. Sites where some data were available, or would become available during the study, were given priority. This ensured that the sites would be suitable for geophysical tests and provided data above and beyond that provided for (and paid for) by the MEND budget. The INCO sites were prospected with the EM31 prior to final selection to assist in the survey grid layout. This included a complete line around the base of the Copper Cliff tailings prior to the start of the MEND work.

At all sites ground survey grids tied to topographic features or survey markers were laid out. Some line clearing was required in areas where vegetation was thick. It should be noted that line clearing can be a significant cost of a ground geophysical survey. In areas of thick bush it can equal or exceed the cost of acquiring the geophysical data.

The AEM data used in this study was taken from a survey, flown for exploration purposes, which covered most of the Sudbury Basin.

4.1 EM

4.1.1 Airborne EM

Approximately 40,000 kilometres of multi-frequency helicopter EM (HEM) data were acquired as part of a regional exploration survey of the Sudbury Basin. The survey was carried out by Aerodat Ltd. of Toronto for Falconbridge Ltd. and was made available to INCO under a data-sharing agreement for mineral exploration. Permission to release parts of this data for this study was granted by the Falconbridge and INCO exploration groups, and we would like to acknowledge the contribution of this valuable data set. The outline of the survey area and the portions used in this study are shown in Figure 4.1.

The survey lines were flown at 100 m line spacing, generally perpendicular to the contact between the Sudbury Igneous Complex (SIC) and the surrounding rocks, with the helicopter at a height of 80 m and the EM bird at 30 m above the ground. Navigation was by satellite-based Global Positioning System (GPS) and ground radio navigation beacons. It is estimated that the position of the helicopter has been recovered to within a 5 m accuracy at most locations. As well, a downward-looking video camera mounted on the helicopter recorded the flight path in detail. These videos are available for flight path confirmation. They can also be used to identify sources of anomalous conductivity if these are apparent at surface.

It is interesting to note that magnetic data was acquired simultaneously with the EM data. This data has not been used in this study; however, it does demonstrate the potential for the acquisition of multiple data sets.

The AEM data was processed for INCO by Aerodat to produce colour contour, apparent resistivity maps from the 4,000 Hz data at 1:50,000. This map, together with clear plastic overlays of the geology and topography, were used to select areas in the vicinity of the Levack and Fault Lake test sites for further processing for this study. In the Levack area 1,500 kilometres of data were reprocessesed to produce apparent conductivity maps, which emphasized shallow conductivity variations by using a single 10 m thick layer to model the data, at three frequencies (900 Hz, 4,000 Hz and 32,000 Hz). Detailed equipment specifications are given in Appendix B.

4.1.2 Ground EM
Surface EM surveys using the Geonics EM31 and EM34 ground conductivity meters were conducted on seven lines at the Pistol site and on 20 lines at the Levack site. A previous EM31 and EM34 survey, carried out by a contractor at the Fault Lake site, was contributed to the study by Falconbridge.

For the MEND work EM31 readings with depth penetrations of 1.5, 2.5 and 5 m were taken at 10 m intervals along all survey lines. EM34 readings with depth penetration of 10 and 20 m were taken at 20 m intervals along all lines. On a few lines where maximum depth penetrations was desired EM34 readings with a depth penetration of 48 m were acquired.

4.1.3 Borehole EM
To establish a correlation with chemical analyses from multilevel sampling in the groundwater sampling wells, downhole conductivity surveys were conducted in all available holes. Downhole natural gamma surveys were carried out at the same time to assist in mapping soil stratigraphy.

Pistol Dam
A total of six holes were logged with borehole EM and gamma at Pistol Dam. Three of these holes were drilled and cased with MEND funds. The other three holes were

drilled and cased by the University of Waterloo at no cost to the MEND program. Five of these plastic-cased wells were established next to small-diameter, multilevel piezometers previously established by the University of Waterloo as part of their ongoing study of the tailings-derived groundwater plume at Pistol Dam (Robertson et al., 1992). This pairing of multilevel water sampling wells and plastic-cased geophysical holes was designed to provide data for the correlation of stratigraphy and groundwater chemistry with borehole geophysical data. The sixth hole was drilled in an area of deep overburden where the small University of Waterloo drill rig was not able to penetrate to bedrock. This hole was completed as a single-point water sample well with the well screen in the basal aquifer.

Five of the new holes were cased using 3" inside diameter plastic casing to accommodate the suite of downhole sensors operated by the GSC borehole logging group. They have been invited to survey these holes in conjunction with borehole surveys at the nearby Garson test area. Their borehole logging tools include thermal, and nuclear density and porosity.

At the Levack tailings, as part of an ongoing program of groundwater monitoring, a total of 22 new water sampling wells were established on and around the tailings at ten separate locations. Six of these locations are multi-well installations with the capability of sampling the groundwater at multiple levels. Only four of these wells were paid for by the MEND program; however, all the data from these holes have been made available for this study.

At all accessible well locations the deepest well (usually drilled to bedrock) was surveyed to provide a single complete geophysical log. All wells shown in the logs were drilled to refusal or bedrock.

Fault Lake
At the Fault Lake tailings two new wells were drilled to provide groundwater chemistry and access for borehole geophysical logs. Geochemical data from a nearby small diameter well previously drilled and sampled by Falconbridge were made available for this study.

4.1.4   Repeat Ground EM Surveys
Repeat EM31 surveys were conducted on line 1070S on the South Dam grid at Levack in 1991, 1992 and 1993. The purpose of repeat surveys is to monitor the change in ground conductivity and, indirectly, groundwater chemistry with time. If previous conductivity surveys are available then subtle features of changing groundwater conductivity can be resolved.

For example, in an area of widely varying natural conductivity a single survey can only reliably detect contaminated groundwater when the contamination, and hence the conductivities, are well above the natural background variations. However, if a pre-development survey is available for comparison then low-level changes in

conductivity can be attributed to changes on groundwater conductivity. As well, surveys carried out before and after remedial work can be used to monitor the effects of the remedial work.

It is important for this type of work that the survey points are reoccupied exactly and that the instruments be accurately calibrated. To preserve the value of data for repeat surveys, it is recommended that all survey grids be accurately established and tied to permanent markers in the field, and the location of the permanent markers be documented in the report.

4.2   IP/SP/Resistivity

The Copper Cliff tailings were selected for the test work because of the easy access (most of the tailings are revegetated and dry) and the availability of University of Waterloo test holes along two profiles that cross the tailings. Surveys were carried out along these two lines so that the results could be correlated with the test hole results. One new drill hole beside University of Waterloo sample well IN10 was surveyed as well to provide more detailed vertical resolution and to demonstrate the use of downhole electrical surveying.

Both time and frequency domain methods were tested using dipole-dipole arrays for the surface work. The dipole-dipole array consists of in-line Rx and Tx dipoles of equal length L. Six Rx dipoles at Tx-Rx spacings of NL, where N=1, 2, 3, 4, 5, 6 are acquired simultaneously. Then the whole array is moved a distance L down the line and the reading is repeated. This provides data in profile and sounding mode simultaneously. When the data is plotted in pseudosection form (see IP/Resistivity data), with the data from larger Rx-Tx spacings plotted at greater depths, it provides a crude vertical section showing the variation of IP and resistivity with depth.

IP, SP and resistivity data are acquired simultaneously. Initial work by a crew from McMaster University used a battery-powered time domain system. This system is very portable, relatively safe, and easy to use; however, it was not able to acquire reliable data due to low signal values and high noise. The Copper Cliff tailings environment combines several features that make electrical surveys difficult. These include:

> i) A resistive surface layer of dry sand that limits the current that can be put into the ground.
> ii) A very conductive deeper layer, the saturated tailings, that reduces the measured voltage.
> iii) Nearby high-voltage power lines that add man-made noise to the readings.

It was apparent after several days of tests that a higher powered system would be necessary.

The work was completed by a contract crew from Walcer Geophysics.

A BRGM six-channel receiver was used for the time domain work and a Phoenix six-channel V4 receiver was used for the frequency domain work. A Phoenix 3 kilowatt motor generator-powered transmitter was used to power both time and frequency domain systems.

The surface surveys were carried out with a dipole-dipole array with electrode separations of 10 m and 20 m. The 10 m dipole data gives an effective depth penetration of about 20 m, with six measurements spread over this depth and readings every 10 m along the line. This configuration provided very detailed information on the top 20 m, which was desirable for correlation with the shallow University of Waterloo holes; however, it was relatively slow and did not penetrate the full thickness of the tailings. The 20 m spacing provided faster reconnaissance coverage and, in most locations, penetrated to bedrock. The two survey modes were overlapped on one line for comparison purposes.

The quality of the surface IP and resistivity data acquired by the Walcer crew was generally good. However, the surface dipole SP data were noisy, did not repeat well, and are not presented in this report. It is recommended that, in future, SP surveys be carried out on their own with longer signal averaging times and pole-pole arrays. Pole-pole SP surveys by the McMaster group provided good data and are included in this report.

To carry out the borehole IP and resistivity survey a new hole with special casing was required. As opposed to electromagnetic surveys, which do not require contact with the ground, electrical surveys require electrical contact at both the receiver and transmitter electrodes and, hence, cannot be conducted in holes cased in solid plastic. For this work a new hole, IN10G, was drilled beside the University of Waterloo hole IN10 and cased with plastic well screen over the full length of the hole. The well screen has thin (about 1 mm) horizontal slots at about 5 mm intervals down its length. These slots provide electrical contact between the water in the drill hole and the surrounding material.

Borehole data were acquired with a pole-dipole array using an electrode separation of 1 m. This gives penetration of about 0.5 m into the tailings surrounding the hole. A separate SP survey of the hole using a pole-pole array was also carried out.

4.3   Sampling and Geochemical Analysis

At Levack, soil and water sampling was done by Trow Engineering, with chemical analysis by INCO labs. Sampling and chemical analysis at the Copper Cliff tailings and Pistol Dam were done by the University of Waterloo under research programs funded by INCO.

4.4   Inversion Software

The apparent conductivity data obtained from different depths of exploration at any measurement station can be used to approximate the true conductivity stratification of the subsurface in the vicinity of that station.

Geo-Physi-Con Co. Ltd. of Calgary has developed a computer inverse modelling program to calculate the conductivity stratification at measurement stations using multiple apparent conductivity readings with different depths of penetration as input (Sartorelli et al., 1990).

The program output consists of a numerical approximation of the conductivity variation with depth at each measurement station. Conductivity estimates can be contoured in vertical section form (along each survey line) or in plan view (at different depths). In fact, the conductivity values from data acquired over a grid form a three-dimensional data volume that can be sliced in any direction for presentation.

Selected data from the Levack area were processed with this software.

5.0 RESULTS AND INTERPRETATION

5.1 Pistol Dam

Site Description
A schematic of the Copper Cliff tailings area is shown in Figure 5.1.1. Approximately 600 million tons of tailings are contained in a series of contiguous tailings disposal areas covering a total of about 8,000 acres. Fine- to medium-grained sand-sized tailings were deposited on top of pleistocene sediments or exposed bedrock in broad valleys. Deposition of the tailings commenced in 1937. Maximum depth of the tailings is 45 m with an average depth of about 20 m.

The sulphide content of the tailings, mainly pyrrhotite, ranges from less than 1% by volume to about 7% except for the pyrrhotite storage areas where pyrrhotite levels over 50% are the norm.

Oxidation of the sulphides has produced a large volume of acidified groundwater. Seepage from the base of the tailings dams is common, and a network of drainage ditches, collection ponds and pumping stations has been installed to intercept acid drainage and route it to treatment facilities.

Prior to the start of this project 15 kilometres of reconnaissance conductivity surveys using the Geonics EM31 were carried out along the south, west and north sides of the tailings area at the base of the dams. In general, areas of high conductivity were associated with areas of visible seepage.

Work by the University of Waterloo (Robertson et al., 1992) has shown that the main drainage from the tailings is to the south and west through the large dams that retain the tailings on these sides. Surface seepage is collected in ditches and ponds at the base of the dams but groundwater flow carries some of the tailings water below the interception system, forming plumes of tailings-derived water below the dams.

A group from the University of Waterloo (De Vos, 1992; Robertson et al., 1992) has made a detailed study of the tailings water plume below Pistol Dam. As shown in Figure 5.1.1, Pistol Dam is located on the southeast side of the tailings area. The dam, 35 m high and about 300 m long, is constructed mainly of compacted tailings.

About 20 multilevel small-diameter water sampling wells have been completed in the Pistol plume by the University of Waterloo group, and the upper part of the plume has been well defined by chemical analysis and electrical conductivity measurements of groundwater samples. The basal aquifer plume, as defined in 1992 by electrical conductivity measurements on water samples, is shown in plan in Figure 5.1.2 and in section in Figure 5.1.3.. At this time the plume extended 400 m from the base of the dam and was open to the south. As shown in the section, the plume south of borehole IN19 is split by a thickening wedge of clayey silt into a near-

surface component, which is largely due to surface run-off, and a deep plume which flows through the basal sand and gravel aquifer. At borehole IN81 the high conductivity part of the deep plume is below 25 m and relatively thin.

5.1.1 Surface Surveys

Pistol Dam

Surveys were conducted on seven lines extending from Pistol Dam to about 800 m downstream of the dam. Surveys on several other lines were attempted but abandoned due to power line interference. Plots of the results are shown in plan form in Figures 5.1.1.1 to 5.1.1.4 and in profile form in Figures 5.1.1.5 to 5.1.1.11.

In general, the EM data shows high conductivities at shallow depths extending south of Line 1. This corresponds with an area of surface AMD seeps and the area of high-conductivity surface run-off, as outlined by the University of Waterloo work. South of the highway, high shallow conductivities on Line 5 are due to salt-saturated run-off from the MOT road salt storage domes, located just to the north of the line at the edge of the swamp, as well as surface tailings water run-off.

High conductivity to 10 m in depth, which is approximately the depth to bedrock near the base of the dam, is apparent in the EM34 data 20H (20 m coil separation, horizontal dipoles) to Line 4. This is the deep plume as mapped by the University of Waterloo group. South of the highway on Line 5, where the plume is in the basal aquifer below 20 m, it is difficult to confirm that the deep plume has been detected because of interference from the salt, man-made features such as fences and culverts, and the absence of samples over the peak of the deep conductivity anomaly on this line. Specific features on each line are discussed below with reference to the profile data.

Line 1

This line is located 15 m above the base of the dam on the dam face. It is apparent from the data that there is high-conductivity water within a few metres of the surface of the dam. The area of highest conductivity at 150W suggests that this is the main flow path through the dam. It is likely that a more detailed survey of the dam face could be used to map the areas of highest permeability in some detail. The conductivity low at 125E in the EM34 data is probably due to a bedrock high.

Line 2

This line was run along the base of the dam over moderately rough ground. The variations in the EM31 data are due to a combination of topographic and conductivity variations. The EM34 data, since it is less affected by topography, gives a better picture of the ground conductivity, with major conductivity peaks and presumably, groundwater migration channels at 110E and 50W. The EM34 40V data penetrates to about 20 m. With electrically resistive bedrock at about 10 m, the average conductivity as measured by the instrument includes about 10 m of bedrock, resulting in considerably lower readings.

Line 3
This line is located just north of the seepage pond and passes over or near IN23, 21 and 25 with IN21 at 0+00. The EM31 data shows the highest conductivity in the top 2 m, and slowly decreasing conductivity to a depth of 5 m. This is consistent with the University of Waterloo work, which shows conductivity gradually increasing with depth at this location. The lower values in the swampy area may be due to fresh water flushing of the shallow aquifer, or lower porosity clayey soils.

The peak of the EM34 data at 20W is 50 m east of the highest EM31 values and probably represents the main groundwater migration channel through the deepest part of the valley with the highest conductivity values at depth.

Line 4
This line is located just south of the railway tracks. A nearby powerline prevented the acquisition of EM34-40V data. Sample well IN19, located in the middle of the line, shows a relatively uniformly saturated overburden with conductivity increasing slightly with depth. The EM31 and EM34 values are generally similar except for a pronounced, low-conductivity channel at 20E. This is due to a small stream at this location where surface run-off water appears to be diluting the tailings-derived groundwater.

Line 5
This line crosses the north end of a large swamp just south of the highway. Shallow higher conductivity values are due to road salt as well as surface tailings water run-off. The deep plume is located below 25 m depth at this point and there is no obvious increase in the deep readings to indicate this plume. The plume is a thin conductive layer at the limits of penetration of the EM34, and detection was expected to be difficult. This line and the swamp to the south were surveyed with the deeper penetrating EM47 in an attempt to track the deep plume beneath the swamp.

Line 6
This line was located across the south end of the swamp. The University of Waterloo work and the geophysical work traced the deep plume beneath the north edge of the swamp, but it was not known whether it extended to the south end of the swamp and, if so, where the exit point or points from the swamp (which is bounded on most sides by rock) were located.

Line 6 crosses the south end of the swamp where bedrock rises to surface and only a few narrow, swampy valleys form possible paths for groundwater migration. Conductivity values across most of the line are low; however, they start to rise at the east end of the line where a small creek exits the swamp. Unfortunately, powerlines along Fielding Road and bedrock on the other (east) side of the road prevented the acquisition of further data. It appeared that the plume, much attenuated, was exiting

the swamp through this narrow valley. Subsequent drilling and sampling by the University of Waterloo group in this valley has confirmed the presence of dilute tailings water. This, then, is approximately the southern limit of the plume. Most of the plume is confined to the rock-bounded valley immediately south of the Pistol Dam and the deep aquifer under the swamp which itself is bounded by rock on most sides.

Thus, the limits of the plume have been defined by a combination of drilling and geophysics.

Line 7
This line was located along the east side of the large swamp below Pistol Dam over University of Waterloo wells 92, 91, 100, 101 and 102. Well 92 showed significant contamination by tailings water below 10 m depth. Hydrological data (hydraulic head) show that this water is derived from the next dam to the east, not Pistol Dam, indicating that the plumes from the dams on the southeast boundary probably join in the valley. The other wells further to the south had normal groundwater, so the inferred migration path of the tailings water is from well IN92 into the large swamp where it joins the Pistol plume.

Some surficial contamination was expected from the Copper Cliff nickel refinery located just to the east of the line. This is apparent in the data, with shallow values of 20 mS/m to 30 mS/m higher than normal background for this area. Higher conductivity values at the northwest end of the line, in particular a 60% increase in the EM34-40V data, which is the only reading with penetration below 10 m, correlates with the tailing-derived water in the basal aquifer between 10 m and 15 m depth in well 92.

Lines 5, 6 and 7 were located along the edges of the large swamp where bedrock was thought to be within 20 m of the surface.

No FEM surveys were conducted over the large swamp - since it was apparent that the FEM systems were not penetrating to the basal aquifer beneath the swamp - and because of deep water in the swamp at the time of the surveys. In order to map the conductivity structure under the swamp to bedrock, which was expected to be as deep as 50 m, a TEM survey was conducted on the ice in winter.

TEM

Deep-penetrating time domain EM surveys using the Geonics EM47 were completed over the frozen swamp south of the highway below Pistol Dam in an effort to trace the main path of the plume at depth. Preliminary results were used to locate a deep well at 104G. The data acquisition and processing were done by Hyd-Eng Geophysics, and selected figures from their report are included as a separate set of figures.

It is known from well 81G on Line 5 that a deep plume of conductive groundwater derived from the tailings extended south of Line 5 in a 5 m thick sand and gravel aquifer located just above the bedrock surface at a depth of 30 m. The bulk conductivity of this zone was estimated from the BHEM log to be about 50 mS/m. This thin conductor is a difficult target under the overlying silty clays and silts and is not apparent in the EM34 data on Line 5; however, results from the BHEM log show surprisingly low resistivities in the immediately overlying thick silts (around 5 mS/m). With these low values this thin, deep conductor may be detectable with a broader band, deeper penetrating EM system such as the EM47. It was also possible that hole 81G had only intersected the edge of a thicker plume.

Figure H1 shows the survey area and the drill hole control. Holes 29, 90, 96, 103 and 105 were completed recently by the University of Waterloo, and not all data is available yet. Borehole conductivity logs are available in 81G and 104G. Figures H2, H3 and H4 show the values of the raw voltages in successively later channels. Since voltage is proportional to conductivity, and penetration increases with time, these are approximate maps of conductivity at successively greater depths for a flat-layered sequence. The swamp is underlain by glaciolacustrine deposits and the geophysical logs indicate a transition from a silty clay to a silt at about the same depth (16 m), so the assumption of flat layering in these deposits is probably valid. In channel 2, at early time, the data show a broad conductivity high across the swamp. This is due to the combined effect of low-level surface run-off from Pistol Dam, the Nickel refinery, and salt from the Ministry of Transport (MOT) buildings in surface waters, as well as elevated conductivity from the silty clay layer. This evolves in later time (channel 12) to a higher conductivity zone along the northwestern edge of the swamp. This represents the area of greatest conductivity-thickness product and the likely location of the plume at depth. Hole 104G was drilled to test this area. Due to thin ice the hole was not positioned on the peak of the high voltage area. No significant contamination was found in water samples from the basal aquifer in 104G and there was no significant borehole conductivity response. The reason for this absence of tailings water in the basal aquifer at this point is not known since preliminary results from DH105 and DH93, both south of 104G, both show tailings water. It is possible that 104G is just off the edge of the plume or that the plume is fingering around 104G. It is also possible that an apparent bedrock conductor that was located in later time along the northwest edge of the swamp may be interfering with the interpretation of the overburden conductivity. Additional deep holes would be necessary to resolve this issue and are beyond the scope of this work.

Figures H5 and H6 show, respectively, the interpreted conductivity and thickness of the upper silty clay layer. Higher conductivities at the northwest and northeast edges of the survey area are believed to be due to surface run-off from Pistol Dam and the MOT salt storage areas, respectively. The high conductivity over the south end of the survey area appears to be due to tailings water welling up from the deep aquifer, which is being forced up to surface at this point by the shallow bedrock to the south, and is apparent as red staining in the swamp.

Based on limited drill follow-up, the TEM work was not able to conclusively map a deep, thin, conductive plume under moderately conductive silty clays in the presence of bedrock conductors. This is a difficult target in complex environment but is probably typical of areas with lacustrine clay at surface with basal aquifers in more permeable deep units.

5.1.2 Borehole Surveys

Pistol Dam
A total of seven new holes were drilled into the Pistol plume and cased in plastic for borehole logging. The results are shown in Figures 5.1.2.1 to 5.1.2.6. In these figures the formation or bulk conductivity is the conductivity of the formation (soil with groundwater) as measured with the EM39. The fluid conductivity, as measured on groundwater samples, is shown as bars with width approximately equal to the width of the screened sampling interval; pH values of the water samples are given where available.

Compared to background conductivities between 1 mS/m and 20 mS/m most holes show some degree of contamination. Holes IN21G, IN30G, IN22G and IN81G form a line of holes along the axis of the plume. The results show a high-conductivity surface plume near the base of the dam (Pistol 21G), which evolves into separate surface and deeper plumes (Pistol 30G and 22G) in the basal aquifer, and, finally, a distinct deep plume in the basal aquifer (Pistol 81G). The high near-surface conductivity in Pistol 81G is due to salt from the nearby MOT road salt sheds. These results are consistent with the results of the University of Waterloo groundwater sampling program, as shown in section in Figure 5.1.3, as well as the water conductivity measurements shown on the logs. Note that the fluid conductivity is typically four times the bulk conductivity, as measured by the BHEM system. This is due to the resistive soil matrix and is discussed in more detail in Appendix C.

Borehole 104G was drilled to test a broad low-amplitude conductivity high located in the deepest part of the large swamp basin by the EM47 survey. This hole intersected a thin sandy basal aquifer but, as can be seen in the figure, there is no anomalous conductivity at depth. The strong anomaly at 18 m is due to a large pipe wrench that was dropped down the open 6" diameter hole. Subsequent work by the University of Waterloo group has detected tailings water in shallower holes along

the edge of the swamp to the south of this hole. These results indicate that the basal aquifer is not uniformly permeable and that the plume is moving through permeable channels in the basal aquifer.

The EM47 anomaly is probably due to the large thickness of moderately conductive clays and silts from 0 m to 17 m. This illustrates the difficulty of locating thin moderately conductive plumes under naturally conductive cover. It is possible that the main part of the plume is indicated by the deep conductive area located to the west of IN104G.

Borehole 92G shows moderate conductivities (30 mS/m) at surface, lower values from 5 to 11 m in depth, and moderate values (30 mS/m) from 11 m to the bottom of the hole. The higher near-surface conductivities are due to surface run-off from the nickel refinery, while the deeper conductivities are due to the tailings water in the basal aquifer identified by the University of Waterloo.

5.2   Levack Tailings

Site Description
Figure 5.2.1.1A is Ontario Geological Map P2428 (Dressler, 1981) reduced from 1:15,840 to 1:20,000 scale. This is a topographical and geological map of the Levack area with the tailings areas shown as light stippled areas. This map is used because it presents data on geology and mining activities (including tailings), as well as drainage, railines, powerlines, buildings, etc., all of which can be important in evaluating conductivity responses.

The Falconbridge tailings are confined to rock-bounded lakes of the Moose Lake drainage system in the southwest part of the map area. The Inco tailings are located to the north of the town of Levack in an elevated rock-bounded valley and are contained by large dams at the north and south limits. Most of the mines are located in the Moose Creek valley, which crosses the map sheet from northeast to southwest between the two tailings systems.

The INCO Levack tailings cover approximately 80 hectares. Tailings disposal at this site ceased in 1979 with the closure of the Levack mill but the site continues to be used for the discharge of mine water.

Surface drainage is generally to the south, with smaller streams feeding the Onaping River. Surface and presumably groundwater flow is confined to the rock-bounded valleys of the area, which are deep, and sand and gravel filled.

The Levack area was covered by the multifrequency AEM survey, which was reprocessed to produce apparent conductivity maps. This data is presented as a sample of one of the 35 1:20,000 included in the full Sudbury AEM survey. Such regional surveys are invaluable for establishing regional background values and

comparing conductivity values at different sites. The AEM data was ground truthed at selected locations at the INCO Levack tailings. The surface work confirmed the results of the AEM data on the ground and the drill hole geophysics and water analysis established the connection between the airborne and surface work and groundwater chemistry.

5.2.1   Airborne Surveys

AEM data was acquired at three frequencies and each frequency was reprocessed to produce a separate apparent conductivity map. Only the 4,000 Hz data is shown in Figure 5.2.1.1B. The 32,000 Hz data is the most sensitive to weak conductivities and could be consulted in specific areas but, because of its high sensitivity, the contrast between conductive areas and background values is reduced. The 900 Hz data is designed to penetrate conductive overburden to locate conductive bodies in bedrock. Hence, it does not respond well to the moderate conductivities typical of low-level groundwater contamination. It does, however, show the very conductive tailings areas.

In general, the 4,000 Hz airborne data showed that background conductivities in the Levack area are below 1 mS/m, with values over swamps and lakes not usually exceeding 10 mS/m. The principal source of conductivities in swamps and lakes are fine-grained clay sediments. Indicated conductivity over the tailings ponds themselves is over 1,000 mS/m. The low-conductivity background and high-conductivity sources are ideal for locating anomalous conductivity due to groundwater contamination.

The outstanding features of the conductivity map are the strong conductivity highs (greater than 1,000 mS/m) over the tailings areas and the graphitic slates in the southeast part of the map area. The high conductivity over the tailings is due to high total dissolved solids in the tailings water. These may be low pH, high sulphate, typical AMD where the tailings have been exposed to oxygen, or high pH, high sulphate, high calcium where the water is in its unoxidized state (tailings are limed before discharge, so unoxidized tailings are basic).

The high conductivity of the graphitic slate is due to electrical conduction by the graphitic component.

The AEM data show that the Falconbridge tailings are confined to the rock-bounded lake and drainage system. There is no large-scale contamination of groundwater beyond the limits of the tailings themselves and the Moose Lake drainage system.

The AEM data over the Inco tails clearly delimit the tailings area but also show moderate conductivity anomalies extending to the north under the North Dam and into the lake to the north, and to the south beneath the South Dam into the sand- and gravel-filled valley to south. These are due to tailings-derived water flowing in a sand and gravel aquifer that extends beneath the dams and the tailings. This flow is

apparent in a few iron, stained seeps in both areas. The airborne data show the essentially continuous nature of this conductive groundwater in the valley. They also show that these are the only directions of leakage from the tailings. The groundwater flow is confined to a narrow valley. This information immediately focuses follow-up plans into well defined areas, reducing sampling and monitoring costs as well as defining the approximate scope of future interception and treatment plans.

The low-conductivity area over the Town of Levack is an artifact of the data acquisition process. The helicopter is required to fly much higher than its normal survey altitude over towns, so that the system is essentially measuring the conductivity of air.

The other main area of anomalous conductivity is the Moose Creek valley, which contains most of the mine facilities. This is due to man-made features such as mine buildings, power lines, railroads, etc., sulphides in bedrock (the original target of the survey), sulphides in waste rock piles, as well as areas of groundwater contamination in the vicinity of the mines. Most of these areas have yet be followed up on the ground. In complex areas such as this, ground follow-up with small systems is essential to identify the various conductive sources.

Figure 5.2.1.2 shows an alternative presentation of the data that provides more information on the variation of conductivity with depth. The helicopter system acquires data at three separate frequencies simultaneously (900 Hz, 4,000 Hz and 32,000 Hz.). Since depth penetration is inversely proportional to frequency, the multifrequency data can be used to create approximate sections or pseudosections of conductivity versus depth along the survey line. These are called Sengpiel sections after the developer of the method (Sengpiel, 1986). The figure shows the Senpiel section from a single line that crosses the north end of the INCO tailings (centre of the figure) and the north-trending groundwater plume (left). The area of higher conductivity on the right of the figure is over the Moose Creek valley containing the mines and mine facilities and could be due to a number of sources.

Sengpiel sections were calculated for all the lines over the INCO tailings and stacked one above the other, as shown in Figure 5.2.1.3. This presentation shows in detail the horizontal and vertical conductivity variations over the tailings and the north and south groundwater plumes.

In addition to acquiring EM and magnetic data a colour video camera continuously records the ground surface directly under the helicopter. At 100 m line spacing and 80 m flight height this results in close to 100% video coverage of the survey area. The videos are delivered on completion of the survey and can be used for precise location of conductive features, as well as identification of surface features that may cause anomalous conductivity.

These data samples illustrate the wealth of information available from AEM surveys.

In fact, one of the biggest problems with a large AEM survey is absorbing the large amount of available data. The Sengpiel sections are an example of a system for producing approximate two-dimensional images of the subsurface from the data. Work is under way in the geophysical departments at Queen's University and the University of British Columbia to develop improved computer programs to directly image the subsurface 3D conductivity distribution from AEM data. These methods require large computer resources but should make the data much easier to work with and will stimulate the acquisition of broader band data (more frequencies) to improve the resolution of the images.

5.2.2   Surface Surveys
The airborne surveys in the vicinity of the INCO tailings were followed up with detailed ground surveys using the EM31 (1 m to 5 m depth penetration) and the EM34 (10 m to 40 m depth penetration) ground conductivity systems. The larger scale topographic map shown in Figure 5.2.2 shows the location of the survey lines as well as the location of the water sampling wells at the site. Most of these wells are multilevel plastic-cased piezometers. Water samples are taken at regular intervals and analyzed for major ions as well as a multielement ICP analysis for metals. To conform to existing grids in this area all horizontal distances were measured in feet.

The EM31 and EM34 data over the northern part of the tailings are shown plotted in profile form in Figures 5.2.2.1A and B. This data confirm the very high conductivities over the tailings themselves, the moderate but still highly anomalous conductivities over the groundwater plume below the north dam, and the very low background values. The rapid variations in the EM31 values within the conductive areas are due largely to topographic variations or the thickness of nonconductive fill. Because of the shallow depth-penetration of the system, the readings are quite sensitive to the height of the instrument above the water table.

At each station in the ground survey a total of five readings with different effective depths of penetration were taken with the EM31 and EM34. Inversions were carried out on selected lines to produce approximate conductivity versus depth sections. One such section from the line along the base of the north dam is shown in Figure 5.2.2.2. The general shape of the bedrock valley that contains the conductive groundwater is apparent in the section. This shape has been confirmed by seismic refraction surveying and drilling. The more erratic nature of the plot at depth is due to the loss of resolution at low conductivities and greater depths.

The EM data collected to the south of the south dam is shown in plan contour view in Figures 5.2.2.3 to 5.2.2.6.

The dam is located at the south end of the Levack tailings at the head of a long, narrow, sand- and gravel-filled valley. Background conductivity values for fresh water saturated sand and gravels in this area are 5 mS/m or less. Data have been

acquired from the dam to 800 m downstream. Data from all depth penetrations show a plume of higher conductivity extending down the valley.

Higher conductivity values (15 to 35 mS/m) in the shallow-penetrating data across Lines 470S to 1320S correlate with an area of surface seeps. Interpretation of geochemical data from the surface seeps indicates that the major source of the conductivity is sulphates derived from the tailings. The EM31 values are affected to some extent by topographic variations but the deeper penetrating readings taken with the EM34-20H (coil separation 20 m, horizontal dipoles) trace a relatively uniform plume of higher conductivity (10 to 15 mS/m) groundwater down the valley. This is consistent with the shape and location of the airborne conductivity anomaly but the conductivity values are somewhat lower. We believe this is largely due to an improvement in water quality between the 1987 airborne survey and the 1991 ground survey, due to flushing of the system with fresh water since the closure of the tailings.

The EM34-40H readings are lower again. This is probably due to penetration into the very low conductivity bedrock.

Ground EM surveys were extended down the Grassy Creek valley to the Onaping River. The purpose of this work was to trace the plume of tailings-derived water through the outskirts of the Town of Levack and determine where it flows into the Onaping River. Groundwork was necessary in this area since no airborne data were available over the town. By selecting suitable areas such as school yards, river frontage, etc., good-quality data was collected. In general, the readings were all very low (<5 mS/m), suggesting that the plume has moved to the east side of the valley under a developed area. This data will be used in support of river bottom conductivity surveys being carried out by AECL in the Onaping River.

Data from Lines 0+00 to 1070S were inverted to produce two-dimensional conductivity sections, as shown in Figures 5.2.2.7 to 5.2.2.9. These sections taken together give an approximate image of the geometry of the plume in three dimensions. The data set is a three-dimensional volume that can be sliced in any direction and contoured for presentation. Information on both the lateral and approximate vertical geometry of the plume can be obtained from this presentation and can be used to locate wells as well as determine approximate target depth for drilling and sampling.

5.2.3   Borehole Surveys
A total of 22 new water sampling wells was established in the vicinity of the Levack tailings at ten separate locations. Borehole surveys were conducted in the eight deep wells that were accessible, and are shown in Figures 5.2.3.1 to 5.2.3.8.

Holes T1, and G1 to G4 are located in the Grassy Creek valley tailings plume below the south dam. In general, they show moderate conductivity values (15-60 mS/m)

consistent with the surface conductivity values in this area. Surface peak values are expected to be somewhat less than borehole peak values because the surface systems average values over a much larger volume. These values are not high but are still quite anomalous compared to the 0 to 5 mS/m values obtained over clean water-saturated sand and gravels and bedrock in this area. Chemical analysis of water samples from these holes shows sulphate values between 400 mg/l and 800 mg/l and elevated pore fluid conductivity values as shown in the figures. This confirms that they have been moderately affected by tailings water.

Hole T1 was located as part of the overall tailings groundwater study and was the only hole planned below the South Dam. It was placed in the middle of the valley near a road where drill access was convenient, and not on the peak of the surface geophysical anomaly. Additional holes G1 to G4 were drilled as part of the MEND program and were designed to sample the conductivity plume, as defined by the geophysics, in more detail.

Hole T1, drilled to a depth of 15.2 m, lies approximately 400 feet south of the base of the South Dam.

The conductivity values are relatively low throughout the hole, generally in the 15-25 mS/m range. The hole appears to have missed the main body of seepage emanating from beneath the dam, which appears as a surface seep about 40 feet to the west of the hole. This is significant since even though this part of the valley is fairly narrow and appears to be filled with fairly uniform permeable material, the flow of tailings water is confined to a fairly narrow zone within the aquifer from beneath the dam to the drill hole at 5+00S. This confirms the results of the surface survey, which unexpectedly showed a very narrow and deep conductivity plume at the base of the dam. The drilling and seismic refraction surveys show high relief on the bedrock surface parallel to the axis of the valley. It is believed that the bedrock topography is strongly controlling the groundwater flow near the dam. Further down the valley the airborne and ground geophysics and the drilling show that the plume has broadened considerably.

At 9.5 m in depth an unusual conductivity signature is observed, consisting of a large negative spike followed immediately by a large positive spike, all within a 1 m wide zone. The anomaly was observed in both the downhole and uphole logs, thus ruling out an instrument or software problem. It is probably due to metal left in the hole during drilling operation, or to a sulphide boulder.

Hole G1, drilled to a depth of 5.5 m, is situated about 200 feet south of T1 and is the first in a fence of three holes drilled along Line 7+70S.

This hole was drilled only 5 m west of the main surface seepage site. Conductive tailings water (up to 65 mS/m) is detected at a depth of 1.3 m. The upper sections of the saturated zone (between 1.3 m and 2.8 m) display higher conductivities than the lower sections, possibly due to oxidation reactions that release H+ and change

the valence of the iron ions.

Hole G2 is located approximately 50 feet east of hole LEV-G1 along Line 7+70S and was drilled to a depth of 4.1 m.

The only noteworthy features in this hole are its shallow depth and the gradually increasing conductivity values with depth. The final depth is in good agreement with the seismic data, which indicate a depth to bedrock of approximately 6 m. The conductivity reaches a maximum value of 26 mS/m at the bottom of the hole, indicating only moderate contamination by tailings water.

Hole G3 is located approximately 120 feet east of hole LEV-G2 along Line 7+70S and was drilled to a depth of 18.1 m. Grassy Creek is located roughly 50 feet to the east.

Moderate conductivity in the 35-42 mS/m range is observed down to a depth of about 6.5 m where a sharp drop to the 20 mS/m range occurs (roughly coincident with a series of small gamma peaks). The conductivity rises again below 7 m depth, reaching a maximum of 40 mS/m near 13.5 m. A sudden drop in the conductivity below 13.5 m is coincident with the contact between a gravel till and an underlying sand unit that displays a high gamma signature.

The great depth of Hole G3 indicates that it was drilled close to the axis of a buried bedrock channel that runs along the east side of the upper valley. This channel may act as a conduit for tailings seepage.

Hole G4 is located on Line 13+20S, at 4+20E, and was drilled to a depth of 14.8 m. This hole was intended to provide information on groundwater conductivity outside the contaminated area. However, the moderate conductivity values (30-35 mS/m) observed through most of the hole indicate that the water has been moderately affected by tailings seepage (an AMD seepage spring occurs in an old gravel pit about 200 feet north of the hole).

A rising conductivity trend near the bottom of the hole (up to 40 mS/m) together with orange staining recorded in the soil log and groundwater chemistry (880 mg/l SO_4) confirm the flow of tailings water in the basal unit.

Figure 5.2.3.6 shows the borehole logs in borehole T5, which is located on the Levack tailings. This is apparent in the very high conductivities (up to 8,000 mS/m) observed in the top 9 m of the log. This represents the oxidized portion of the tailings, as indicated by the low pH (3.01) of the water sample from this depth. The zone from 9 m down to 17 m is still tailings but is unoxidized, as indicated by the pH value of 9.72 at 14 m. This zone is much less conductive as well, indicating lower total dissolved solids, as expected.

The very high conductivities in this hole are due to high TDS, principally SO_4 (15,000 mg/l at 5.5 m). The chemistry and borehole conductivity values confirm that the source of the high conductivities measured from surface and the air over the tailings is due to high TDS in the tailings water. As well, the conductivity log, which provides an essentially continuous record of conductivity between the water sample points, illustrates the rapid changes in conductivity and chemistry that are not well represented by the three water sample points.

The lower pH of 5.83 at the bottom of the hole may represent underflow of oxygenated water. The spikes in the gamma log at 2.5 m and 19 m are due to silt and/or clay layers at the top and bottom of the tailings. The tailings themselves show generally low gamma values. There is an increase in gamma values around 12.5 m. This is probably due to a change in the mined host rock type.

Drill hole T4 was located in fill and tailings near the west edge of the tailings and was drilled to a depth of 21.5 m. Conductivity and gamma profiles from this hole are displayed in Figure 5.2.3.7. The top 5 m of the hole passes through tailings (consisting mostly of low sulphide slimes) that display conductivities ranging from 75-100 mS/m. A large gamma peak at the top of the tailings is likely related to the very fine-grained material that has settled out of the mine water discharge. This material is intended to form a relatively impermeable "cap" over the exposed tailings surface. A smaller gamma peak occurs at the interface between oxidized and unoxidized tailings at 1.7 m.

The soils immediately below the tailings between 5 m and 8 m depth are unsaturated and display relatively low conductivities (around 20 mS/m). The water table is intersected at a depth of approximately 8 m and corresponds with a sharp rise in the conductivity, indicating that the pore water is contaminated. These conditions persist down to a depth of 17 m, with conductivities in the 45-60 mS/m range. A drop in the conductivity below 17 m corresponds with a sand and gravel till unit with a high gamma signature, indicating high clay content and low porosity. The till unit is probably acting as a barrier to the downward migration of the conductive tailings water at this location.

Trow hole 2, shown in Figure 5.2.3.8, is located at the base of the north dam in a plume of tailings-derived water that extends to the north into Pike lake. Higher borehole conductivity values are consistent with elevated surface and airborne readings at this site.

Below the water table at 10 m the conductivity log shows moderate conductivity values throughout the sand and gravel aquifer. These values are consistent with airborne and ground results. The source of the conductivity is acidic groundwater, as indicated by the low pHs.

Both the conductivity and gamma log show that the aquifer is not as uniform as

indicated by the stratigraphic log. In general, the gamma values are inversely correlated with the conductivity. High gamma and low conductivity indicate areas of higher clay content and presumably lower permeability. Low-gamma, high-conductivity areas correspond to areas of lower clay content and higher permeability.

The relationships between chemistry and conductivity in this hole are illustrated in the next two figures. Figure 5.2.3.9 shows the concentration of all significant ionic species. This is a characteristic AMD chemical signature with sulphate as the dominant species followed by iron and calcium.

Figure 5.2.3.10 shows the contribution that each ionic species makes to the total conductivity, as calculated from the chemical concentrations using the formulae given by McNeill (1980b). It is apparent that the conductivity, like the concentration, is dominated by the sulphate, iron and calcium ions. It is interesting to note that at this moderately low pH (4.28) the $H+$ ion makes a negligible contribution to the conductivity. However, due to the logarithmic nature of the pH measurement, the $H+$ concentration and its contribution to the conductivity increase rapidly with decreasing pH.

5.2.4   Repeat Ground EM Surveys
Figure 5.2.4 shows the repeat EM31 surveys on Line 1070S on the South Dam grid at Levack. It was expected that, due the closure of the Levack tailings in 1979 and the diversion of much of the surface water run-off from the tailings away from the Grassy Creek valley in 1992, the water quality in the valley would improve. This is apparent in the data, where conductivity values for all depth penetrations decreased steadily with time. This supports the less reliable comparison between the ground and airborne data, which suggested that ground conductivities in the Grassy Creek valley were decreasing with time.

The only repeat chemical results available, from January 7, 1993 and May 20, 1993, show decreases in pore fluid conductivity and sulphate of between 5% and 40% in all four holes in this area. So all the available data supports decreasing conductivity with time. The data from the ground and airborne surveys provide baseline information against which any future surveys, perhaps following remediation, can be compared.

5.3   Fault Lake Tailings
The Fault Lake tailings are located just north of the Town of Falconbridge and the main Falconbridge tailings area. The tailings were deposited in a large pothole in an extensive and thick sand and gravel plain. These tailings are no longer active. Falconbridge has undertaken hydrological studies of the site with the object of designing a permanent closure plan.

The reprocessing of the AEM data over the Levack area into apparent conductivity

maps, funded by the MEND program, demonstrated that the airborne conductivity maps were valuable tools for reconnaissance mapping of groundwater quality. On the basis of this work the INCO Environmental Control group proceeded with reprocessing and replotting of the entire Sudbury survey, a total of 35 map sheets. The Falconbridge area was covered by the survey and the excellent results in this area, and in particular over the Fault Lake tailings, encouraged us to bring this data into this study. As well, Falconbridge provided access to some excellent ground geophysical data (Geomar, 1991 and 1992) and groundwater chemistry in the vicinity of the south dam on the Fault Lake tailings. This data was supplemented with two holes drilled with MEND funding for BHEM surveys and groundwater sampling.

5.3.1 Airborne Surveys

The AEM conductivity results and topographic features are shown in Figure 5.3.1. The data clearly show an isolated area of very high conductivity (greater than 1,000 mS/m) directly over the tailings area and a well-defined plume of moderate conductivity (5 to 20 mS/m) extending below the south dam into a topographically low area to the south. This area drains into the main Falconbridge tailings located to the south of the map sheet. Background values in the area are of the order of 1 mS/m with slightly higher values over lakes and swamps.

The high conductivity area beside the road just south of Bailey's Corners is due to an MOT salt storage/snow dump site.

5.3.2 Surface Surveys

FEM surveys

Figures 5.3.2.1 to 5.3.2.4 (from Geomar, 1991) show the EM31 and EM34 surveys over a small area at the base of the south dam. The EM31 vertical dipole data (depth penetration 5 m) does not detect the plume at the base of the dam and just senses the top of it over lower ground at the south end of the survey grid.

The EM34 10 m separation data (depth penetration 5 m) just see the plume at the base of the dam, indicating that the top of the plume is located at about 5 m at this point. The EM34 20 m separation with horizontal dipole and vertical dipole (depth penetration 10 m and 20 m, respectively) shows increasing width and conductivity values (up to 14 mS/m), indicating depth extent to at least 20 m. This illustrates the need for deep-penetrating instruments in areas of deep permeable overburden.

This plume is coincident with the plume defined by the airborne data, but is much more precisely defined. The highest conductivity part of the plume is tightly confined, given the width of the dam and the apparent uniformity of the overburden, and could easily be missed by a limited drilling program. In general, except for large homogenous targets, ground surveys are required to locate drill locations.

Background values of about 1 mS/m are similar to the airborne results.

TEM surveys
The FEM data located the top and lateral extent of the plume but, due to their limited penetration, were not able to resolve the base of the plume. With bedrock as deep as 80 m in this area under sand and gravel, a determination of the base of the plume required a deeper penetrating system. A single line consisting of five stations was surveyed across the base of the south dam. The loop locations are shown in Figure 5.3.2.1 and the data are shown in Figure 5.3.2.5. The plume is clearly apparent in the resistivity low, centred on reading S3, with the lowest values at 0.02 msec. The data indicate a probable base to the plume, as evidenced by rise in resistivities around 0.06 msec to 0.07 msec in S3 and S4. The plateau in resistivities between 0.07 msec and 1.5 msec would correspond to more resistive overburden beneath the plume and the high resistivities at depth to bedrock.

An interpretation by Geomar is shown in Figure 5.3.2.6. This interpretation shows a discrete plume perched in the overburden with a maximum depth of about 20 m over a deep resistor at 70 m. The deep resistor has been identified with bedrock. One of the objects of the drill holes and BHEM at this location was to test this interpretation; however, due to water pressure problems (ground heave) penetration past 20 m was not possible with the rotary augur soil testing rig used.

The TEM interpretation is consistent with the FEM results and the available BHEM and water chemistry data. The principle benefit of the TEM data in this area is its large depth penetration compared to the FEM work.

5.3.3   Borehole Surveys

Two drill holes, F1 and F2, were targeted using the surface geophysical results. The geophysical and stratigraphic logs are shown in Figures 5.3.3.1 and 5.3.3.2.

Well F2 was drilled into the peak of the surface conductivity anomaly and F1 was drilled 30 m to the west on the flank of the plume.

The water table in both wells is located at about 6.5 m. The logs show a gradual increase to values of about 15 mS/m for F1 and 50 mS/m for F2 below 10 m. These results confirm the lateral conductivity distribution as indicated by the surface surveys. The surface values are low because of the dilution by the low conductivity unsaturated layer. The wells are located in an area where the surface surveys indicate depth to the top of the conductive zone to be between 5 m and 10 m, which is consistent with the borehole results.

Chemical analysis of water samples from 9, 18 and 24 m in F2 gave sulphate values of 717 mg/l, 1,240 mg/l and 174 mg/l, respectively, confirming that the source of the anomalous conductivity was tailings water.

It is interesting to note that the sulphate and pore fluid conductivity values from 24 m are about a third of the shallower values; however, there is no evidence of this decrease in the BHEM logs. Since the overburden is relatively uniform, such a large change should be obvious in the conductivity data; however, the values are constant to the bottom of the hole, suggesting that the plume extends to greater depth. The geophysical logs were run twice, once down and once up the hole, and repeated well. The main well is larger in diameter than the shorter auxiliary wells and there may have been some dilution of the sample. To resolve this problem it is recommended that the well be resampled. This was the only point in the study where groundwater chemistry and borehole geophysical logs were not well correlated.

5.4   IP/SP/Resistivity

Induced polarization and resistivity surveys were carried out along two lines and in one new drill hole (beside IN10) on the Copper Cliff tailings, as shown in plan view in Figure 5.4.1 and in section in 5.4.2 and 5.4.3. The two lines had been previously studied by the University of Waterloo and a number of shallow stratigraphic holes, together with groundwater monitoring wells, were available for correlation with the geophysics.

Different parts of the Copper Cliff tailings contain very different concentrations of sulphide, with values ranging from over 50% in the pyrrhotite storage areas to less than 1% in some areas. The lateral and vertical boundaries between different types of tailings is not always well known, particularly in older areas of the tailings. Since knowledge of the total volume of sulphide and the distribution of sulphides is important in predicting AMD production it was hoped that the IP data could provide some information on sulphide distribution in the tailings.

Drill hole control, as follows, was available along the lines. Sulphide content is weight % FeS equivalent.

Line	Station	Hole#	Average Sulphide	Comments
A	0S	IN13	3%	Depleted in sulphides to 0.7 m
	510S	IN10	<1%	
	1020S	IN11	1.5%	Depleted in sulphides to 1.7 m
	1409S	IN12	4%	Depleted in sulphides to 0.4 m; 30 cm of magnetite at 0.5 m
B	0S	IN14	7% est.	
	130S	IN15	7% est.	

Vertical profiles of sulphide content from shallow holes at IN11, 12 and 13 were available (Coggans, 1992) and are shown in Figure 5.4.4. These profiles show sulphide depletion in the top metre due to oxidation of sulphides. It is interesting to note that the maximum depth of oxidation in these and other holes is nowhere deeper than a few metres. Thus most of the sulphides in the tailings are unoxidized and should be a good target for IP. The apparent spike in FeS at the base of the oxidized zone is due to iron enrichment in iron oxide ferricretes.

No detailed logs from the holes along the B line, which is located in the more recent P area tailings, were available; however, typical sulphide values in this area, which postdates the closure of the Iron Ore Recovery Plant, are reported to be about 7%. (Blowes, personal communication 1993) .

Line A
This line starts in the M tailings area and extends from an area of moderate sulphide content of about 3% sulphides around Station 0 at IN13 into an area of very low sulphides (<1%) as indicated by IN10 at 510S, through low sulphides (1.5%) at IN11 to higher sulphides (4%) at IN12 in the M1 area. The 10 m dipole IP results correlate well with this expected variation, with values around 4 milliseconds (msec) of chargeability at 0, and values generally below 1 msec from 400S to 1140S. South of 1140S the line enters the M1 and is characterized by high and variable chargeability and very low resistivity (<1 ohm-m or greater than 1,000 mS/m). From 1480S to the top of the dam the data are characterized by high resistivities due to the lower water table and low chargeabilities. The low chargeabilities in the dam are expected since, in general, the dams are constructed with low sulphide tailings.

The IP data correlates well with the known distribution of sulphide, and it also provides a great deal of information between and below the holes. A few examples are discussed below.

It appears from the data that the low sulphide area around 500S (IN10) onlaps the

zone of higher sulphides at 0S (IN13). This is indicated by the higher chargeability values extending to depth to the south from 0S. The strong IP anomaly at 290S is due to a buried metal pipe at this location. Weak IP anomalies at 510S (IN10) and 1020S (IN11) are probably due to small vertical steel pipes used in the water sampling.

A well-defined moderate IP anomaly at depth at 860S indicates higher concentration of sulphides, or scrap metal at depth. The IP data alone cannot uniquely identify the source; however, the data can be used to accurately locate drill holes to test anomalous areas.

The high and variable IP results in the M1 area indicated a substantial volume of sulphides or buried metal. A weak IP response is also expected from the 30 cm of magnetite that was intersected in IN12. The very low resistivities (high conductivities) in this area indicate very high TDS.

Because the grain size in the tailings is relatively uniform and there is no interference from clays, the resistivity (or conductivity=1/resistivity) values should be directly proportional to TDS. Thus, the IP data in the absence of buried metal can be used to map the distribution of sulphides, and the resistivity data can map variations in TDS. It should be noted that variations in tailings water chemistry will have some effect on the resistivity as well. It is suggested that if correlation coefficients were established at sample wells then TDS could be mapped quantitatively.

Line B
The IP values along this line are generally higher as expected. Low IP values and high resistivities were recorded over the dam, which extends from 400S to the south end of the line.

The conductivity values are higher over the higher chargeability area, indicating higher concentrations of AMD associated with the sulphides. Based on the results of this work, it appears that surface IP and resistivity is a useful tool for mapping the distribution of sulphides and TDS in tailings.

Self Potential (SP)
SP data was acquired simultaneously with the IP/resistivity data using the Rx dipole only. The SP natural voltage has to be measured and cancelled out prior to the IP/resistivity measurement, and it is recorded automatically. Unfortunately, the surface dipole SP readings were noisy and did not repeat well. This is probably due to the short dipole lengths and short averaging times. It is recommended that future SP surveys be carried out independently of the other surveys so that longer stacking times and a pole-pole array can be used. The pole-pole array is a two-electrode system with a single fixed-reference electrode and a moving survey electrode. The voltage difference between the two electrodes is plotted at the position of the moving electrode.

Pole-pole SP data acquired by the McMaster University group is shown in Figure 5.4.6. The raw data were moderately noisy on a station-to-station scale and have been smoothed with a 2, 3, 7, 3, 2 weight averaging filter for the plot. A number of strong SP anomalies are apparent on a trend of rising voltages going from IN14, located on the tailings, to the base of the dam. The strongest are associated with the road, which is at the crest of the dam, and a rapidly rising response below the base of the dam. Since the tailings are a very large electrochemical cell, a large SP difference was expected between the top of the tailings (oxidizing) and the base (reduced). The anomaly at the dam crest may be related to the low-sulphide tails used in dam construction, and the lower water table. The IP and resistivity data show the dams to be very different, electrochemically, from the tailings. The small amount of data and the lack of downhole SP control on this line make it difficult to identify the sources of the SP anomalies. It is recommended that further surface SP surveys be done together with detailed downhole SP control, perhaps by pushing or hammering a electrode down through the electrochemically active zone (as suggested by Dr. Bill Morris). Such shallow vertical surveys, if acquired at a high enough density, may be more useful than the surface surveys since, for the surface survey, the electrodes are sitting on the surface of a conductor, which is an equipotential surface and the worst possible place to measure voltage differences. As well, surface readings are likely to be strongly affected by the surface conditions: wet versus dry, windblown sand versus revegetated soil, etc. The borehole SP data discussed below appear to give much more stable and reliable results.

Pyrrhotite Storage Area
To test the electrical surveys under extreme conditions a single short line was surveyed over a pyrrhotite storage area where the pyrrhotite content is over 50%. The results were quite surprising. Over the rocks that bound the shallow valley containing the pyrrhotite, the resistivities are high (up to 20,000 ohm-m) and the chargeabilities are low, as expected. At the edges of the pyrrhotite the IP values are highly anomalous, with peak values of +31 and -71. On the pyrrhotite, which extends from about 2+40S to 0+20S, the resistivities are very low (<1 ohm-m) as expected, but the chargeability values are also low, generally less than 2%.

It is believed that the low chargeability results are due to the extremely high pyrrhotite concentrations. The IP response is due to polarization by electrical current flowing from electrolytic conductors (electrolytes where current is carried by ions dissolved in groundwater) into sulphide grains with metallic conductivity. If the sulphide concentration is very high so that most sulphide grains are in contact with other sulphide grains then current will be transmitted directly through the sulphides without passing through the electrolyte that fills the pores. This would produce strong IP anomalies at the edges of the sulphides where essentially all the current crosses an electrolyte-sulphide boundary and little or no response over the sulphides would be observed.

Thus, high pyrrhotite areas will show up as strong IP anomalies when at least one pair of electrodes is outside the pyrrhotite. This will be the case for all hidden (buried) high pyrrhotite areas, therefore these will be detectable. The only problem will be for measurements directly on exposed high pyrrhotite; however, the areas are normally known or can be identified by surface sampling. It would be useful to carry out laboratory studies on pyrrhotite tailings mixtures to determine the variation of chargeability with sulphide content in more detail.

Drill Hole Results
The IP, SP and resistivity results from IN10G are shown in Figure 5.4.5. The detailed stratigraphy in this hole, including sulphide content, is not available yet, due to delays in laboratory analysis caused by the INCO production shutdown.

Resistivity values range from 12 to 18 ohm-m, gradually increasing with depth. This is consistent with the surface resistivity data.

The chargeabilities values range from 3 msec near surface to about 1.5 msec at depth with considerable small-scale variation. These values are slightly higher than the surface readings, which were mostly below 1 msec. This discrepancy is not large since the accuracy of the measurement is about 1 msec, but it is measurable and consistent. The reason for this difference in surface and borehole chargeability is the depletion of sulphides in the near surface layer, which is averaged with the surface layer in the surface data.

The variations in chargeability should reflect small changes in sulphide content through the section due to changes in processing or oxidation of sulphides at paleoweathering surfaces (previously exposed tailings surfaces).

The SP data show a decrease in electrical potential (voltage) with depth with respect to the surface electrode with a change in polarity at -2.0 m. This probably represents the change from the surface oxidizing environment to a reducing environment at depth. The total voltage difference from the surface to the bottom of the hole is about 0.2V. This is consistent with the view of the tailings as a giant unconfined battery, with metal in a reduced state (sulphides) in an electrolyte (dilute sulphuric acid), much like a car battery. It is interesting to speculate if any useful electrical power could be derived from such a system, perhaps to power treatment systems. Given the measured SP voltage and resistivities around 10 ohm-m, the vertical current flow at this location is about 1 milliamp per square metre. Extrapolating over the 32 square km of the tailings gives an total vertical current flow of about 32,000 amps. This is powered entirely by oxidation of sulphides and gives some idea of the scale of the electrochemical reaction; however, due to the widely dispersed nature of the system it is unlikely that the energy could be collected to do useful work.

The rate of change of SP with depth is also plotted. This is the voltage that would be

measured across a 0.5 m dipole downhole. The data show a rapid decrease in voltage just below the oxidized zone, with a relatively stable decrease, with occasional spikes, through the rest of the hole. The dSP/dZ spikes seem to correlate with IP lows, suggesting again that these may represent paleooxidation surfaces.

It is recommended that SP data be acquired in more detail through the electrochemically active zone from 0 m to 3 m for detailed correlation with downhole chemistry.

The borehole work confirms the picture, derived from the surface geophysical data and the shallow sampling, of a fairly uniform low-sulphide environment. More detailed correlation of sulphide with IP will be done when the final sulphide analysis from IN10G is available.

6.0   CONCLUSIONS AND RECOMMENDATIONS

Conclusions
Due to the low background conductivities and the high conductivities of AMD, electrical and electromagnetic geophysical methods work well in the Sudbury area. In this environment even small amounts of AMD in groundwater can be detected in first-time surveys.

In areas with more conductive (20-40 mS/m) clay soils, such as the Abitibi clay belt, subtle conductive features due to low levels of groundwater contamination will not be detectable in first-time surveys; however, with anomalous conductivities up to 100 mS/m at the base of the dams at Copper Cliff, similar AMD plumes should be detectable near their source in most Canadian environments. If soil types are not well known, test surveys to establish background values prior to undertaking large surveys are recommended. The use of background surveys carried out prior to development reduces the threshold of AMD detection in all areas and would be of particular advantage in areas of high and variable natural conductivity.

The work showed that conductivity measurements in boreholes could be related to groundwater conductivity and, hence, to TDS in groundwater. In turn, significant conductivity anomalies detected with surface and airborne surveys were correlated with AMD in the subsurface.

Airborne EM surveys with accurate positioning and closely spaced lines are an excellent tool for reconnaissance mapping of groundwater quality and providing regional background conductivity information. All airborne conductivity anomalies that have been followed up on the ground in this program and in similar site investigations at Sudbury have been confirmed. In general, ground surveys, with their improved horizontal and vertical resolution, are necessary to identify the sources of anomalous conductivity and to provide detailed information for drilling and sampling.

Airborne surveys processed to apparent conductivity colour maps provide an immediate visual image of regional conductivity and can be used to rapidly and inexpensively characterize large areas like the Sudbury basin, which would be impossible to cover in their entirety on the ground. Anomalous areas can be selected and arranged in order of priority for detailed ground follow-up. Airborne data should be correlated with detailed topographic maps to eliminate known conductive sources such as sulphides in bedrock, pipes, power lines, metal buildings, etc.

Borehole surveys provide a continuous record of the conductivity around a hole in real-time. The sample density is much higher than any practical downhole sampling, and can be used to interpolate results between sample points and to identify anomalous areas that may have been missed by the sample points. In general, well

water sample points are not optimally located. Downhole EM surveys in a hole prior to the installation of sampling points can be used to ensure that they are well located. For instance, a few sample points in a deep hole may miss a thin plume entirely and it is unlikely, in most cases, that sample points are located at the peak concentration of any confined plume. Repeat surveys can provide a detailed record of the variation of conductivity with time.

Limitations on the effectiveness of electrical and EM surveys may be imposed by man-made interference, topography, seasonal variations, and any combination of extreme depth, small size or low conductivity contrast of the target.

The work on the deep plume at Pistol showed that deep, thin plumes with only moderate conductivity contrast with their host may not be detectable with surface or airborne surveys. Developments in instrumentation and interpretation should improve detectability; however, there will always be thresholds of conductivity, size, thickness or combinations thereof below which features like plumes may be chemically definable but not detectable geophysically. Thus, in general, surface or airborne geophysics cannot be expected to detect all possible contamination.

Man-made interference from pipes, power lines, metal buildings, etc. is a potential problem in all geophysical surveys. The EM31 can take readings within 5 m of metallic objects and the EM34 within 20 m to 40 m depending on the mode (distance approximately equal to depth penetration). The effect of interference from powerlines varies, but readings can usually be taken within 20 m of smaller lines. Lines perpendicular to power lines (with the long axis of the instrument perpendicular to the lines) are less affected. In built-up industrial sites, such as a mine or mill, a good strategy is to survey the perimeter of the site to locate conductive groundwater moving off-site.

The Pistol site had powerlines, railines, pipelines, roads and buildings. Data were collected by selecting lines that minimized man-made interference, resulting in a non-rectangular and sparsely sampled grid. This complicates the data processing and interpretation but may be the only way to get data in built-up areas.

Topography must be taken into account when interpreting surface data, particularly for shallow depth penetrations. Local topographic highs will increase the depth to the water table, creating areas of apparently lower conductivity.

Seasonal variations, particularly in the shallower penetrating surveys, can be expected due to the reduction in conductivity with temperature in winter at shallow depths. Surveys designed to map very shallow conductivity variations should not be done in winter. On the other hand, suppression of shallow conductivity by cold can enhance the detectability of deeper conductivity variations.

All survey grids used for this work were tied to permanent markers so that they can

be accurately located and re-established if necessary for repeat surveys.

The IP/SP/resistivity surveys showed a good correlation between known sulphide concentrations in the tailings and IP values. Due to the uniform grain size of the tailings, resistivity values can be used to map TDS quantitatively. The combination of IP and resistivity can be used to study, in three dimensions, the relationship between sulphides and TDS, which should shed light on AMD generation and migration patterns. Buried metal interferes with all electrical measurements and may be a problem if tailings have been used as a scrap dump. On the other hand, geophysical methods, including the magnetic method, can be used to locate buried metal such as steel drums, etc., if desired.

Data have been presented in many different formats as appropriate to the area, data type, etc., but also to illustrate the variety of presentation formats available. Most of the contour data would normally be presented in colour, and was for many of the working copies; however, for ease of reproduction most contour plans have been rendered in black and white.

This work has concentrated on the acquisition and processing of various data sets to demonstrate applications to AMD data. There remains a great deal of detailed analysis and more quantitative correlations that could be done and that would contribute to understanding the relationships between physical properties and groundwater chemistry. The data presented here have been brought to the stage typical of a site investigation. Once the anomalous areas are defined, they are drilled to provide chemical data, and additional analysis of geophysical data may not be necessary. It is hoped, however, that some of the directions indicated in this work will be pursued further to provide better tools for characterizing AMD and other inorganic contaminants in the subsurface. In particular:

- better two- and three-dimensional imaging,
- using digital recording to acquire higher data densities and more data samples to provide better input to imaging systems and, ultimately, better resolution,
- quantitative correlation of chemistry with conductivity,
- larger scale repeat surveys to monitor the change of plumes with time,
- additional borehole logs to provide in situ density, porosity and, eventually, chemistry. Downhole nuclear probes using X-ray fluorescence or neutron activation are available now for mining and petroleum applications and nuclear magnetic resonance tools have been developed for large-diameter water wells, and
- develop a better understanding of the electrochemical processes active in tailings and IP and SP data with the object of providing data for predictive modelling of AMD from tailings.

Groundwater contamination by acid mine drainage has been identified by the

national Mine Environmental Neutral Drainage (MEND) program as the largest single environmental problem facing the Canadian mining industry. Geophysical methods, particularly electrical and electromagnetic methods, can, under suitable conditions, be used to quickly and inexpensively map the extent of groundwater contamination and the sulphide source of AMD.

It should be emphasized that geophysical methods should not be used in isolation. Because they do not uniquely identify the source of anomalies, and the accuracy of interpretations is often limited by data density, signal noise, or the equivalent signatures of different sources, they should only be used as a guide to drilling and sampling, not as a replacement.

In this program, we have focused on the geophysical methods that can be applied in remedial site investigations. This is appropriate as these are the sites requiring the most urgent attention. Geophysical methods also have a role to play in preventive site investigations designed to minimize future environmental problems. Surveys can be used to map permeable features such as sand and gravel channels or layers in clay soils, bedrock topography, faults in bedrock that may be permeable, sulphide concentrations in waste rock, dam foundation stability, lake bottom bathymmetry and stratigraphy, etc. Together with traditional geotechnical investigation techniques, pre-development geophysical surveys may reduce the need for remedial investigations in the future.

Recommendations - General
A general recommended sequence for the use of electrical or EM geophysical methods in AMD site investigations is given below. Not all steps are appropriate in all areas.

1) Determine expected natural background values from one or more of the following

      i) test surveys
      ii) soil type and natural groundwater conductivities
      iii) previous airborne or ground surveys

2) Estimate the expected conductivity response from contamination by

      i) test surveys or
      ii) calculating the conductivity response from contamination by the methods described in Geonics TN6 (McNeill, 1980b)

If the targets are detectable, then

3) Review AEM data if available. If the area is large or inaccessible acquire new AEM data.

4) Follow up anomalous areas with ground surveys using multiple depth penetrations.

5) Follow up areas of anomalous conductivity as defined by ground systems with drilling and sampling.

6) Log holes with borehole systems prior to locating sample points. Sample points can be located in anomalous areas, conductivity data can be used to interpolate water quality between sample points, and gamma logs can assist in mapping stratigraphy.

This sequence is an efficient search hierarchy that rapidly focuses more expensive follow-up methods on anomalous areas.

Studies should be integrated using geological, geotechnical, hydrological, geochemical and geophysical methods and data, as appropriate. Specialists often do not use data from other disciplines to its full effect. This may require the creation of multidisciplinary teams.

Large volumes of exploration geophysical, geochemical and geological drill hole data are usually available free of charge in the vicinity of mines, and can provide, among other things, valuable pre-development data. Corporate environmental groups should contact their exploration groups or exploration consultants to locate this data. As well, the two groups often have similar data processing and presentation requirements, and exploration groups can often supply state of the art processing and presentation expertise and equipment.

Data from the various disciplines should be entered and maintained in spatially linked databases suitable for input to image processing systems and geographical information systems (GIS).

Ground surveys
One of the most neglected aspects of ground work is positioning. Grids should be established accurately and tied to permanent markers so that drill holes can be accurately positioned and surveys can be duplicated in the future for monitoring purposes.

Data with multiple depth penetrations should be acquired, whenever possible, to provide vertical as well as horizontal resolution. These data are required for input to the existing and developing two- and three-dimensional imaging systems.

Borehole surveys
All holes drilled for groundwater sampling, geotechnical, etc. applications should be cased in 2" ID plastic. Even if a hole is not surveyed immediately, it is an invaluable future resource. At a cost of a few hundred dollars per hole, holes which cost

thousands of dollars are preserved and provide access for detailed geophysical logging in the future. EM conductivity surveys can provide detailed information on groundwater quality in geotechnical or other holes where no water sampling is done. Surveys in water monitoring holes can be used to locate optimum sample points and interpolate between sample points.

Gamma logs are recommended. They can be done at little additional cost and can provide valuable and detailed information on stratigraphy.

Airborne EM
Records should be searched for existing airborne data. Most mining areas in Canada have been flown several times by government and private interests. Old airborne and ground surveys can provide historical data.

Helicopter FEM data is preferable to most fixed wing TDEM data due to better positioning, higher frequencies and multiple coil orientations. New electronic positioning systems permit close line spacing. Detailed airborne surveys with line spacing of 10 m and sensor heights of 5 m have been flown recently for environmental applications (Nyquist, 1993). Such surveys approach the resolution of ground surveys.

AEM surveys are recommended for large or inaccessible areas. It is possible that repeated accurately positioned AEM surveys could be used to efficiently monitor many sites in an area on a regular basis.

Seismic surveys
Seismic refraction surveys should be considered whenever depth to bedrock is required. The tailings environment, uniform, fine grained, saturated sediments, is ideal for seismic surveys, and good data can be expected. Seismic reflection data may also be useful to map tailings stratigraphy and base of tailings. Very high resolution marine systems are available for ponds and lakes. These systems can be operated in very shallow water and even ponded to saturated soils if access is available.

Peter Pehme (Hyd-Eng Geophysics) - for BHEM and EM47 surveys at Pistol

Tony Sartorelli (Geo-physi-con Co. Ltd) - for inversion of FEM data

BIBLIOGRAPHY

Aerodat (1993)
  Hi res

Berrer, E. B., King, A. K. (1992)
  "Seismic refraction surveys of the Levack tailings", Unpublished internal INCO report

Blair, R. D., Cherry, J. A., Lim, T. P., Vivyurka, A. J. (1980)
  "Groundwater monitoring and contamination occurrence at an abandoned tailing area, Elliot Lake, Ont.", in First International Conference on Uranium Waste Proposal, AIME

Blowes, personal communication (1993)

Clark, M., A. (1991)
  "Locating fluid migration pathways in a high sulphide tailings pond using non-invasive methods", B.Sc. Thesis. McMaster University

Coggans, C.J. (1992)
  "Hydrogeology and geochemistry of the INCO Ltd. Copper Cliff, Ontario, mine tailings impoundments", M.Sc. Thesis, University of Waterloo

De Vos, K. J. (1992)
  Earth resistivity investigation of a plume of tailings derived groundwater, Copper Cliff, Ont. B.Sc. thesis, University of Waterloo

Dressler, B. O. (1981)
  Precambrian geology of Levack Twp., Sudbury District, OGS Preliminary map 2428

Filion, M. P., Sirois, L. L., Ferguson, K. (1990)
  "Acid Mine Drainage in Canada", CIM Bulletin, December 1990

Geomar Geophysics Ltd. (1991)
  "EM survey Falconbridge Sudbury operations Fault Lake, Falconbridge, Ontario", Prepared for Falconbridge Limited

Geomar Geophysics Ltd. (1992)
  "TEM survey Falconbridge Sudbury operations Fault Lake, Falconbridge, Ontario", Prepared for Falconbridge Limited

King, A., Pesowski, M. (1991)
"Environmental Applications of Surface Geophysics" Presented at the 93rd Annual General Meeting of the CIM, Vancouver

McNeill, J. D. (1980a)
Electrical Conductivity of Soils and Rocks. Geonics Ltd., Technical Paper TN-5. Mississauga, Ontario

McNeill, J. D. (1980b)
Electromagnetic terrain conductivity measurement at low induction numbers, Geonics Limited Technical Note TN-6

Nyquist, J.E., Doll, W.E., King, A.D, Holladay, A.D., Pellerin, L., Labson, V.F. (1993)
"Environmental characterization of the Oak Ridge Reservation using helicopter geophysics", International workshop on airborne EM methods, Tucson, Arizona

Ontario Geological Survey (1988)
"Airborne Electromagnetic and Total Intensity Survey, Timmins Area", by Geoterrex for Ontario Geological Survey

Pehme, P. E. (1981)
"Geophysical survey of the Nordic contamination plume". M.Sc. Thesis, University of Waterloo

Sartorelli, A. N., Pesowski, M. S., Wesselingh, L. G. (1990)
"Magnetic Induction Measurements in Support of Environmental Studies - Western Canada Examples" Presented at the 52 EAEG Meeting, Copenhagen

Sengpiel, K. P. (1986)
"Groundwater prospecting by multifrequency airborne electromagnetic techniques" in Airborne resistivity mapping, ed. G. J. Palacky, GSC paper 86-22, p.131-138

SELECTED REFERENCES

McNeill, J. D. (1988)
> Advances in Electromagnetic Methods for Groundwater Study presented at Proceedings of the Symposium on the Application of Geophysics to Engineering and Environmental Problems (SAGEEP), Golden, Colorado, March 1988

Pesowski, M. S. and King, A. R. (1989)
> Surface Geophysical Techniques for Investigation and Monitoring of Groundwater and Soil Contamination. Presented at the Prevention and Treatment of Groundwater and Soil Contamination in Petroleum Exploration and Production conference, Calgary, Alberta, May 1989

Robertson, W. D., Blowes, D. W., Cherry, J. A., Coggans, C., McGregor, R. J. (1992)
> "Hydrology and geochemistry of the INCO Copper Cliff mine tailings impoundment, Waterloo Centre for Groundwater Research, Unpublished

Telford, W. M., Geldhart, L. P., Sheriff, R. E., Keys, D. A. (1976)
> Applied Geophysics Cambridge University Press. New York

APPENDIX A

Geonics Technical Notes 5, 6 and 7

Technical Note TN-5

ELECTRICAL CONDUCTIVITY

OF

SOILS AND ROCKS

J.D. McNEILL

October, 1980

Table of Contents

I. INTRODUCTION

It was near the beginning of this century that Conrad Schlumberger first employed the technique of mapping sub-surface geology by injecting electrical currents into the ground and mapping the resulting potential field distribution. Since that time measurement of terrain resistivity has been applied to a variety of geological problems. A partial list of applications includes the determination of rock lithology and bedrock depth; the location and mapping of aggregate and clay deposits; mapping groundwater extent and salinity; detecting pollution plumes in groundwater; mapping areas of high ice content in permafrost regions; locating geothermal areas; mapping archaeological sites, etc.

In many instances resistivity mapping provides definite geological information; however there are also cases where the results are uninterpretable since the "geological noise" is too high. A limitation of resistivity surveying is that the actual value of terrain resistivity itself is seldom diagnostic. As a result of this ambiguity we generally examine the variations of resistivity, either laterally or with depth, to outline the geological features of interest. But a problem arises in that conventional surveys are time-consuming to carry out and the area actually surveyed is often smaller than one might wish in order to fully ascertain the background against which the anomalous feature is to be defined. Furthermore, although conventional resistivity techniques sense to a characteristic depth (determined by the interelectrode spacing) resistivity inhomogeneities much smaller than that depth can, if they are located near the potential electrodes, yield large errors in the measurement and thus a noisy survey profile.

For these reasons application of resistivity surveys to engineering problems is not as common as it might be, particularly in North America. Such surveys have achieved success in Europe and are used more routinely.

It was an awareness both of the potential of resistivity measurements for solving geological problems and equally of some of the drawbacks of conventional resistivity mapping which lead Geonics Limited to develop two new lines of instrumentation employing electromagnetic techniques to measure terrain conductivity. In the first of these a sinusoidally varying magnetic field electromagnetically induces currents in the ground in such a manner that their amplitude is linearly proportional to the terrain conductivity (reciprocal of resistivity). The magnitude of these currents is determined by measuring the magnetic field which they in turn generate. Through the use of electromagnetic techniques, ground contact is avoided and with these patented instruments it is possible to map terrain conductivity virtually as fast as the operator(s) can walk; furthermore the sample volume is averaged in such a manner as to yield excellent resolution in conductivity. Two instruments have been developed by Geonics to cover the range of depths generally useful for engineering geophysics: (i) the EM31, one-man portable, has an effective penetration depth of 6 meters and (ii) the EM34-3, two-man portable, has stepwise selectable depths from 7.5 meters to 60 meters.

In the second approach the current flowing in a loop situated on the ground is abruptly terminated, inducing eddy currents in the ground which diffuse away from the transmitter loop in a manner controlled by the ground conductivity. In this case the dispersal of the currents is determined by measuring the transient decay of their magnetic field. Based on this principle, the Geonics EM37 can be used to determine the electrical properties of the earth to depths of several hundred meters.

These devices are assisting in the solution of many geological problems. With the renewed interest in resistivity it has become apparent that there is a requirement for a short note which discusses, from the point of view of survey interpretation, the various factors that influence terrain resistivity. For example, typical questions raised include (1) When are gravels more resistive than finer material? (2) What is the influence of the depth to water table? (3) It rained heavily last week; will this affect the measurements? (4) What are typical resistivities for the following soil types?, etc., etc.

By describing the various factors that control the electrical conductivity/resistivity of soils and rocks under typical in-situ conditions this note will attempt to provide the technical background against which these questions can be answered and to thus give the operator greater confidence in his survey interpretation. The emphasis throughout this technical note is on those factors that influence the near-surface ground resistivity, particularly of soils.

The various topics are dealt with in the following sequence.

Section II: definition of conductivity & resistivity
Section III: description of relevant physical properties of soils and rocks
Section IV: relation of physical properties to the electrical conductivity
Section V: discussion of conventional resistivity measurements of soils in different climatic zones.

As mentioned above, this technical note is directed towards the user. Many readers will be familiar with the physical properties of soils and we ask their indulgence. None of the material on the electrical properties of soils is original; some has been taken verbatim from the references. However the compilation has been derived from many sources and we hope that it will prove useful.

II. RESISTIVITY/CONDUCTIVITY

Basically the electrical resistivity/conductivity of a substance is a measure of the difficulty/ease with which an electrical current can be made to flow through it. Suppose that we construct a tank with insulating sides and two conductive end plates as shown in Figure 1. The end plates are connected to a battery through an ammeter with which we measure the current flow through the sample. If the tank is empty there is of course no path by which the current can flow from one end plate to the other and the ammeter reads zero.

Suppose we fill the tank with a mixture of clean gravel and tap water. The ammeter will read a finite current and, depending on
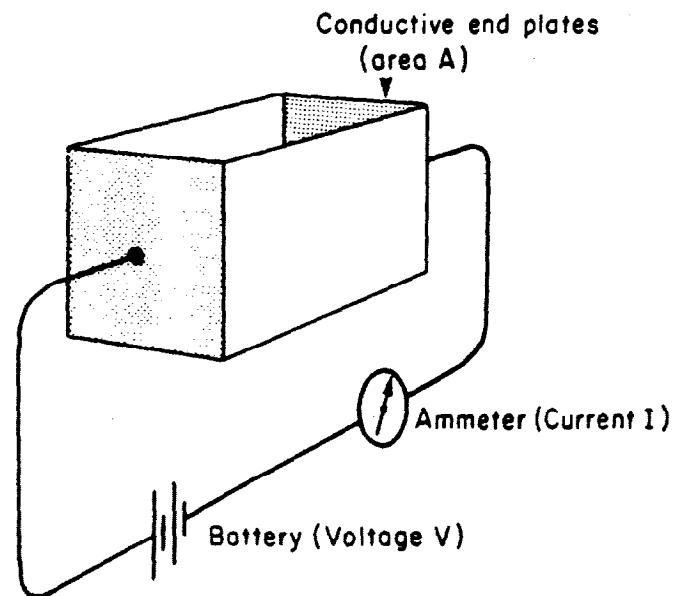
RESISTIVITY (ρ)

$$\rho = \frac{R A}{L} \text{ ohm-metres}$$

where $R = \frac{V}{I}$ ohms

CONDUCTIVITY (σ)

$$\sigma = \frac{G L}{A} \text{ mhos/meter}$$

where $G = \frac{I}{V}$ mhos

FIGURE 1. Resistivity/conductivity tank.

various parameters to be discussed in Section IV, might indicate a current flow of a few thousandths of an ampere i.e. a few milliamperes, for a voltage of one volt. If the ammeter reads two milliamperes the electrical resistance of the material in the tank, given by the ratio of the voltage divided by the current, is 500 ohms.

If we now fill a number of different rectangular tanks, of different dimensions, with the same mixture we would find that the electrical resistance is proportional to the length of the tank and inversely proportional to the area of the conductive plate electrodes. The constant of proportionality, a property of the mixture only, independent of the tank dimensions, is defined as the electrical resistivity. In the MKS system it has the units of ohm-meters and is the electrical resistance measured on a cubic sample whose dimensions are all one meter. In the CGS system of units the resistivity is defined as the resistance across two opposite faces of a cubic sample one centimeter on each side and the units are ohm-centimeters. From the defining relation we see that, given the resistivity in ohm-centimeters, we must divide by 100 in order to get the resistivity in ohm-meters.

Suppose that we empty our tank (now assumed to be one meter on a side) and fill it with a mixture of clay saturated with water. We might find that the ammeter read a few tenths of an ampere, perhaps as much as half an ampere. The resistance would then be two ohms, the resistivity two ohm-meters. The range of resistivities displayed by unconsolidated materials at temperate ambient temperatures usually lies between one ohm-meter and one thousand ohm-meters; the resistivity of rocks can vary from a few tens of ohm-meters to as high as 100,000 ohm-meters, discussed in further detail in Section IV.

The reciprocal of the electrical resistivity of our sample is defined as the electrical conductivity. In the MKS system the unit of conductivity is the mho per meter and a resistivity of one ohm-meter exhibits a conductivity of one mho per meter. 100 ohm-meters is equivalent to a conductivity of 0.01 mhos per meter, etc. The electromagnetic instruments actually measure terrain *conductivity* rather than *resistivity* and for this reason much of the remainder of this technical note will be concerned with the conductivity of various terrain materials rather than the resistivity.

It was stated above that a resistivity of 100 ohm-meters corresponds to a conductivity of 0.01 mhos per meter. To avoid the inconvenience of having zeros immediately following the decimal point all conductivities will be expressed in millimhos per meter: a conductivity of .01 mhos per meter corresponds to 10 millimhos per meter, etc. This has the advantage that the range of resistivities from 1 to 1,000 ohm-meters is covered by the range of conductivities from 1,000 to 1 millimho per meter and such numbers are easily handled. Table 1 lists the conversion from resistivity and conductivity in various units to conductivity in millimhos per meter.

In the experiments described above a direct current was employed. Had we used an alternating current and varied the frequency we might have discovered that the electrical properties of the sample varied with frequency. In reality soils and rocks are complex substances in which there are many (some poorly understood) mechanisms which govern the mode of current flow through the sample [1-5].

Fortunately, for materials with conductivity of the order of one to 1,000 millimhos per meter the electrical properties which control the current flow are relatively independent of frequency and the DC or low frequency conductivity measured with conventional resistivity equipment will be essentially the same as that measured using low frequency electromagnetic techniques.

Finally it should be noted that measurement of the electrical conductivity or resistivity of geological samples is, in reality, a very difficult procedure requiring much more complex equipment than the simple tank referred to above.

III. FACTORS AFFECTING TERRAIN CONDUCTIVITY

Most soil and rock minerals are electrical insulators of very high resistivity. However on rare occasions conductive minerals such as magnetite, specular hematite, carbon, graphite, pyrite and pyrrhotite occur in sufficient quantities in rocks to greatly increase their overall conductivity. This note assumes that such minerals are absent.

In general the conductivity is electrolytic and takes place through the moisture-filled pores and passages which are contained within the insulating matrix. The conductivity is therefore determined for both rocks and soils by

(1) porosity: shape and size of pores, number, size and shape of interconnecting passages
(2) the extent to which pores are filled by water i.e. the moisture content
(3) concentration of dissolved electrolytes in the contained moisture
(4) temperature and phase state of the porewater
(5) amount and composition of colloids

Since the constituents, structure, and included moisture of soil or rock are of great importance in determining the conductivity, this section will discuss the various physical and chemical properties in sufficient detail to illustrate how they affect the material conductivity.

III. 1. Soil Constituents

Soils consist basically of four components namely (i) mineral material (ii) organic material (iii) water and (iv) gases.

Figure 2 shows schematically the relative proportion of these components in an unsaturated loam soil (to be defined later). The illustration refers to a temperate zone soil; for humid region soils about 45% of the solid space may be occupied by clay minerals and 5% by organic matter.

The mineral fraction of a soil can be extremely variable, however some generalizations can be made based on grain size [6]:

sand size range – mostly quartz, small amounts of feldspar and mica present, all grains coated to some extent with iron and aluminum oxide (the rusty reddish-brown colour observed is due to the iron).

silt size range – quartz still dominant, less feldspar and mica than in the sand fraction, more iron and aluminum

TABLE 1. Resistivity conductivity unit conversion factors

mhos meter / 1000	⟶ millimhos meter
$\dfrac{1000}{\text{ohm-meters}}$	⟶ millimhos meter
$\dfrac{100,000}{\text{ohm-centimeters}}$	⟶ millimhos meter
$\dfrac{\text{cgs electrostatic units}}{9 \times 10^6}$	⟶ millimhos meter

Note: 1 Siemen (S) = 1 mho
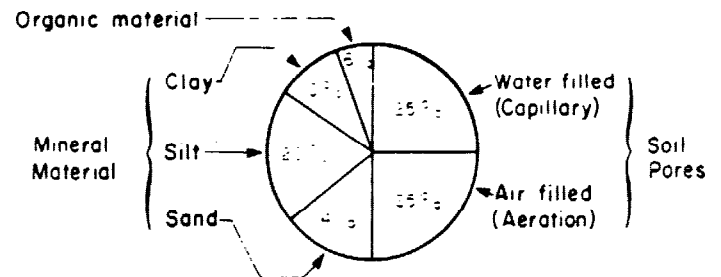
Organic material ⎯ ⎯ ⎯ ⎯

FIGURE 2. The volumetric composition of a loam soil when excess water has been removed. On a weight basis the percentage composition of the dry soil would be: organic matter 4%, clay 22%, silt 44% and sand 30% (after L.R. Webber [6]).
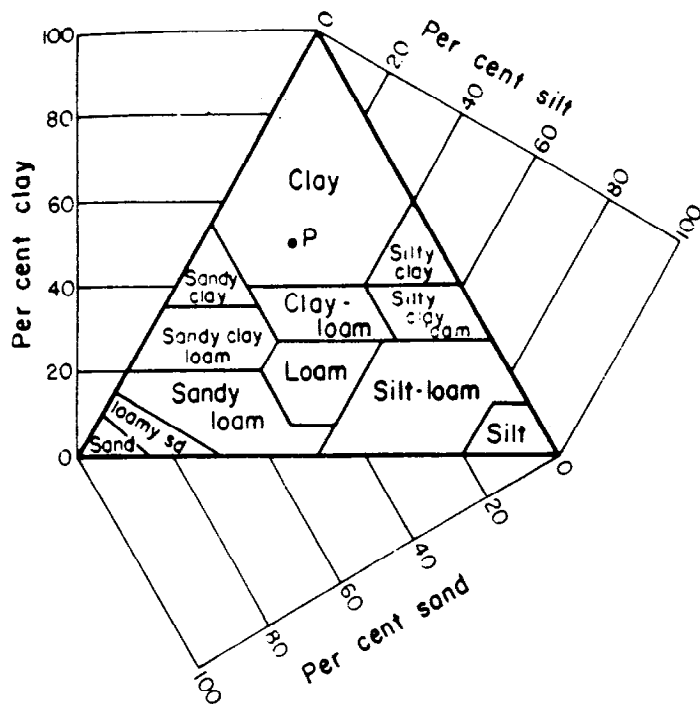
FIGURE 3. U.S. Department of Agriculture textural classification triangle with axes added. The point P represents a clay (soil) containing 50 per cent clay, 20 per cent silt, and 30 per cent sand (after D. Kirkham [7]).

TABLE 3. The cation exchange capacity (CEC) and colloid content of five soils of different textures (after L. R. Webber [6]).

Soil Texture	Organic Matter %	Clay %	CEC* me 100 g
Sand	1.7	7	6.3
Sandy loam	3.2	13.2	13.7
Loam	4.9	16.8	20.2
Silt loam	5.4	18.4	24.0
Clay loam	5.5	31.2	27.2

*The cation exchange capacity of a soil is expressed in terms of milliequivalents per 100 grams of soil (meq 100 g). A milliequivalent is defined as 1.0 milligram of hydrogen or the amount of any other element that will combine with or displace it. The milliequivalent weight of any element may be found as follows:

$$\frac{\text{atomic weight of element}}{\text{valence of element} \times 1000} = \text{milliequivalent weight}$$

oxides in the form of coatings due to the greater particle surface area on which the coatings may reside.

clay size range — finely divided quartz, feldspar, mica, iron and aluminum oxides, all of which appear in the coarser part of the clay fraction (0.002 millimeters - 0.001 millimeters in diameter); the finer part (less than 0.001 millimeters) is colloidal and consists mainly of layer silicates with smaller amounts of iron and aluminum oxides.

As indicated above soils are classified on the basis of texture or grain size independently of the mineralogical content of each particle size component. Sand is defined as particles with diameters between 0.05 millimeters and 2 millimeters, silt has diameters between 0.002 millimeters and 0.05 millimeters and clay has diameters less than 0.002 millimeters. Figure 3 shows the classification triangle for various types of soil and is useful as it allows an estimate of the clay content which often consists essentially of clay minerals which affect the soil conductivity.

The minerals in the sand and silt fractions of the soil are electrically neutral and are generally excellent insulators. Completely dry clay is also an insulator but the introduction of moisture changes the situation radically. Clay consists of microscopically fine particles

TABLE 2. Exchange capacity of common clays (after Keller and Frischknecht [5])

Clay	Exchange Capacity
Kaolinite	3 to 15 m-equiv 100 g
Halloysite . 2H$_2$O	5 to 10
Halloysite . 4H$_2$O	40 to 50
Montmorillonite	80 to 150
Illite	10 to 40
Vermiculite	100 to 150
Chlorite	10 to 40
Attapulgite	20 to 30

exhibiting a sheet-like structure, for which reason clays are often called "layer silicates". Composed of stable secondary minerals that have formed as a result of weathering of primary minerals such as feldspar, mica, etc. the particles are so fine-grained that they are described as micro-crystals.

Their crystalline structure is such that, as a result of crystal imperfections, the surface appears to be negatively charged [5]. During the formation of the clay through weathering, positive charges (cations) are adsorbed to the surface. These cations (typically Ca, Mg, H, K, Na, NH$_3$) are loosely held to the surface and can subsequently be exchanged for other cations or essentially go into solution should the clay be mixed with water. For this reason they are called exchangeable ions and the cation exchange capacity (CEC) of the soil is a measure of the number of cations that are required to neutralize the clay particle as a whole i.e. the weight of ions in milliequivalents adsorbed per 100 grams of clay.

The exchange capacities of some common clays are given in Table 2 and of some different soil textures in Table 3. It is seen from Table 3 that the cation exchange capacity increases with clay content and from Table 2 that this will depend on the type of clay.

Clay minerals are not the only materials which have cation exchange capacity; indeed any fine-grained mineral including quartz displays this property. The special significance of clay in this respect is that, because of the extremely small particle size, the surface area per unit volume of clay is very large and a great many ions are adsorbed. It will be seen in the next section that these adsorbed ions can contribute appreciably to the soil conductivity which thus becomes a function of the clay content.

The organic matter includes the remains of plant and animal life in the soil. The end products of decay accumulate as a blackish, finely-divided colloidal substance known as humus [6] which has large surface area per unit volume, takes up large amounts of water and can develop a negative electrical charge of varying intensity. Little is known of the effects of such colloidal characteristics on the electrical conductivity of humus but they may be significant.

The important influence of soil moisture on the electrical conductivity of soils is discussed at length in a later section.

The direct effect of soil gases on conductivity is negligible, however the indirect effect of CO$_2$ is important and is also described in a later section.

### III. 2. Formation of Soils [8] and Soil Profiles [9]

Soils are the result of mechanical, chemical, and biological weathering processes acting on surficial materials in such a way as to grossly alter their physical and chemical properties. In the process of decomposition of parent materials new and stable substances such as clay minerals and humic materials are formed.

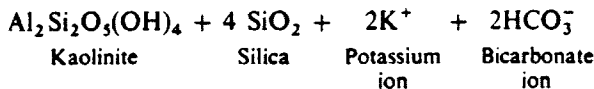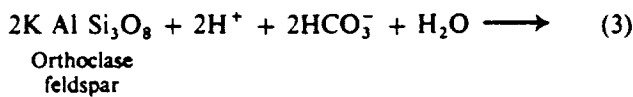As an example of the weathering process consider the chemical

weathering of orthoclase feldspar (an important constituent of granites and other intrusive rocks) to kaolinite, a clay. Atmospheric carbon dioxide is slightly soluble in water so as to form carbonic acid.

$$CO_2 + H_2O \rightleftharpoons H_2CO_3 \qquad (1)$$

$$\text{Carbon} \qquad \text{Water} \qquad \text{Carbonic}$$
$$\text{dioxide} \qquad\qquad\qquad \text{acid}$$
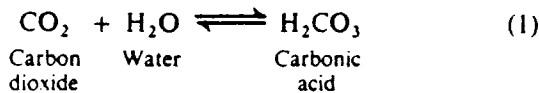
A small amount of the carbonic acid dissociates so as to produce a hydrogen ion and a bicarbonate ion

$$H_2CO_3 \rightleftharpoons H^+ + HCO_3^- \qquad (2)$$

$$\text{Hydrogen} \quad \text{Bicarbonate}$$
$$\text{ion} \qquad\quad \text{ion}$$
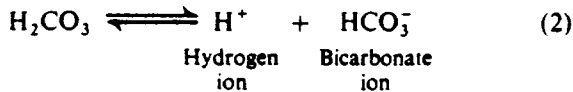
The bicarbonate ion and water combine with the feldspar to form kaolinite, dissolved silica, free potassium ions and free bicarbonate ions

$$2K\,Al\,Si_3O_8 + 2H^+ + 2HCO_3^- + H_2O \longrightarrow \qquad (3)$$

Orthoclase
feldspar

$$Al_2Si_2O_5(OH)_4 + 4\,SiO_2 + 2K^+ + 2HCO_3^-$$

Kaolinite   Silica   Potassium   Bicarbonate
ion   ion

The formula for kaolinite can also be written in the following manner

$$Al_2O_3 \cdot 2SiO_2 \cdot 2H_2O$$

to show that it consists of alumina, silica, and water.

These equations illustrate three important points: (i) The potassium and silica produced by dissolving the feldspar appear as dissolved material. Note that the potassium, converted to a potassium ion, goes into solution and may or may not be present depending on the drainage. (ii) Water is used up in the reaction; it is absorbed into the kaolinite structure. (iii) Hydrogen ions are used up in the reaction and the solution becomes more basic (i.e. less acidic) as the reaction proceeds. All of the reactions described herein affect the electrical properties of the soil by varying either the clay content or the ionic type and concentration in the soil water.

Now let us examine how various factors control this weathering process. The production of soil is a positive feedback process in that once a thin veneer of soil forms, the parent material weathers more rapidly, and more soil is formed. Suppose for example that we have a thin layer of soil on granite. This layer retains moisture which supplies both water that converts carbon dioxide to carbonic acid and water that is hydrated to form kaolinite. Other acids present in the soil contribute additional supplies of hydrogen ion to convert more feldspar to kaolinite as the equations indicate. Plant roots and the process of bacterial decay produce quantities of carbon dioxide to yield more carbonic acid (the amount of carbon dioxide in soil can be as much as ten times greater than that of rainwater, which makes soil water a particularly efficient dissolver of feldspars).

The speed of weathering is a function of climatic type since the rate at which chemical reactions proceed increases with temperature and, more importantly, biological process also proceed faster with higher temperature. Furthermore, since water is needed for the weathering reactions and vegetation grows more lushly in humid climates weathering is most intense in tropical climates which are wet and warm. The surface water resulting from rainfall percolates downwards through the soil, which is more or less permeable, and as it passes reacts chemically with minerals within the soil. The higher the rainfall the more water is available and the more the
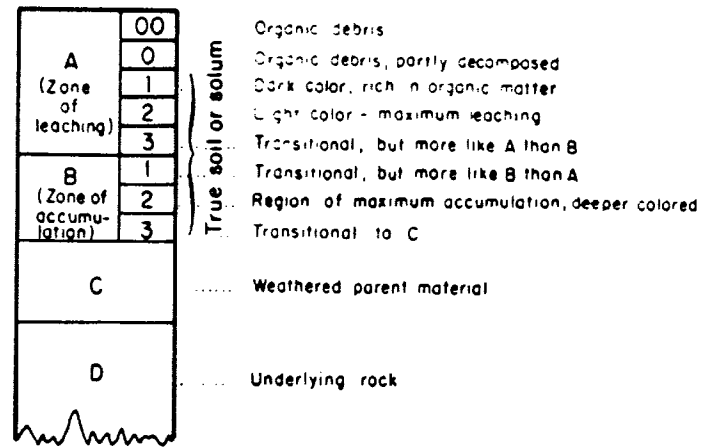
FIGURE 4. Normal or zonal soil profile (after G.B. Maxey [9]).

minerals will react with the undersaturated water. The longer the time the water percolates through, the more time it has to react chemically and again the higher the temperature, the faster the reaction rates.

As a result of these factors tropical soils tend to be thick. Well drained soils tend to be devoid of most unstable minerals. Arid soils contain a variety of minerals. The clay minerals which form are a function of temperature and humidity and there is a tendency for different clays to form in the various climatic belts [10].

As long as there is rainfall and the temperatures are not too low there is a tendency for soils to form a layered structure. In general three different regions or horizons are recognized as we move down through the soil profile, usually designated by the letters A, B, and C. These horizons can vary in thickness from a centimeter to several meters or tens of meters and differ in colour, texture, structure, and other properties.

The chief characteristics of a profile are illustrated in Figure 4. The A horizon, closest to the surface, is the most intensely weathered and has the soluble minerals leached out and most other minerals altered. This layer usually contains much humus, which contributes to its dark colour. Structurally it is friable, granular, or platey. When either friable or granular this horizon is permeable, much more so than the underlying B horizon which is generally a zone of clay accumulation, some of which was formed in-situ and some of which was transported downwards from the A zone by the soil water. The B horizon generally displays a vertical structure in widely or closely spaced joints and it is this horizon that exerts the greatest influence on water movement vertically downwards. When the clay is dry these joints allow rapid downwards movement but when the clay is wet it expands and can close the joints to make the layer impermeable, which may in turn cause the A horizon to become saturated for appreciable periods of time. The C horizon consists of less-weathered parent material and is usually relatively permeable [9].

This layering, with its relatively clay-free A horizon and clay-rich B horizon, greatly influences the vertical profile of electrical conductivity which will be seen to be a function of both clay and water content.

III. 3. Soil Moisture

It was noted at the beginning of this section that the electrical conductivity of soils and rocks was primarily electrolytic and took place through the moisture filled pores and passages which lie within the matrix of insulating minerals. For this reason a knowledge of the way in which soil moisture is distributed in typical terrain is important in understanding terrain conductivity.

When rainwater or irrigation falls on the surface of the soil a fraction runs off directly as surface runoff and the remainder percolates directly into the soil. A fraction of this moisture is retained by the soil, the remainder moves vertically downwards under the force

of gravity until it reaches the water table. In a soil moisture profile it is generally possible to distinguish four stages of moisture occurrence depending on the relative continuity of the moisture films across the soil grains [11] as shown in Figure 5. In the uppermost region we have the pendular state in which the pore space is largely filled with water vapour. The actual liquid water exists only in very small isolated rings around the grain contacts and a continuous path does not exist between the various moisture occurrences. At greater depth we have the funicular stage in which the pendular rings have coalesced to the point where the liquid films have just become continuous throughout the pore space and entirely enclose or encapsulate the vapour phase. Across the sample the moisture path is now continuous. Again further down, in the capillary stage, all pore spaces are occupied by liquid but the liquid pressure within the pores is less than the total pressure caused by gravity since capillary action within the fine pore spaces has caused the moisture to ascend into these pore spaces. Capillary rise, determined effectively by pore size and type, seldom exceeds several meters. Finally we arrive at the phreatic surface (water table) at which the atmospheric pressure is in equilibrium with the hydrostatic pressure. All pores within the phreatic surface are completely filled with liquid under hydrostatic pressure and this is the region of groundwater, also known as the zone of saturation. The three regions above the phreatic surface are collectively referred to as soil moisture, suspended water, vadose water, or zone of aeration.

Figure 5 also illustrates typically the fraction of pore space filled by liquid in the different zones.

A term that is often used in discussing the moisture content of soils is field capacity. Suppose that the water table is very deep below a surface soil of homogenous nature. After a heavy rainfall or irrigation the moisture content reaches a quasi-equilibrium condition in one to three days. As the water percolates down through the soil on its way to the water table capillary forces will retain a certain fraction of the moisture in the small pore spaces. This is the field

capacity and it is the moisture content of the soil after the gravitational water has been removed by deep seepage.

Note that in the event that we have a layered situation in which a soil with very fine pores overlies more granular material, both being far removed from the water table, moisture content of the upper layer will be many times that of the lower which, as will be seen later, affects the electrical conductivity.

Groundwater is free to move laterally with velocities ranging from a meter or more per day to less than a meter per year, depending on the hydraulic pressure differential and the permeability of the material. Table 4 illustrates the permeability of various materials in gallons per day per square foot of cross-section per foot of hydraulic head per lateral foot of distance. It is seen from the Table that for soil materials a factor of 10^{10} separates permeable from impermeable materials. The saturated hydraulic conductivity decreases with clay content, increasing compaction, and decreasing radius of the soil pores.

The laws of hydraulic movement of water produce a water table which in general is not horizontal and in fact is often a subdued version of the local topography, all other factors being equal. Two examples are shown in Figure 6: for the humid zone the moisture moves from topographic high regions down to the draining streams whereas in an arid zone the moisture moves downwards away from the streams.

The wide ranges of permeability greatly influence the final profile of the water table or phreatic zone sometimes leading, for example, to the occurrence of a perched water table as shown in Figure 7. Again such layering will be seen subsequently to influence the electrical properties.

It will be shown in Section IV that the electrical conductivity of soils and rocks depends on the porosity and on the degree to which the pores are filled with moisture. Figure 2 showed the volumetric composition of a loam soil from which the excess water has been removed i.e. the soil is undersaturated. We see that in this temperate zone example approximately 50% of the soil is occupied by either gas or capillary water. This division into about 50% solids is fairly typical of most soils.

If all of the moisture in a soil sample is removed by drying, the ratio of the empty volume to the total volume of the soil matrix is known as the soil porosity, a parameter that is relevant to the soil conductivity. Table 5 illustrates the porosity for a variety of typical terrain materials.
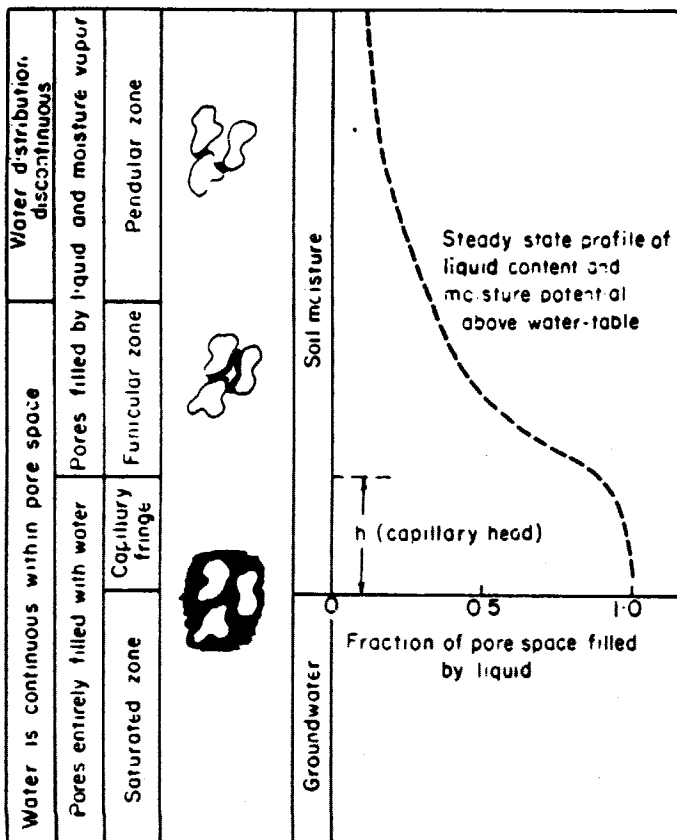
FIGURE 5. Liquid occurrence in soils (after P. Meyboom [11]).
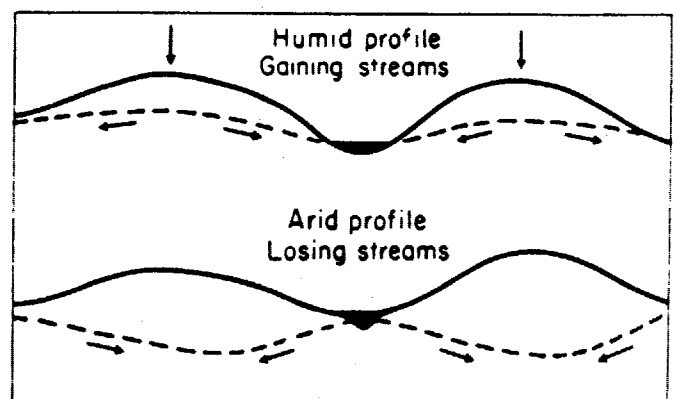
FIGURE 6. Profiles of water tables in arid and humid zones (after G. B. Maxey [9]).

ion	Mobility $(m^2$ sec V)
H⁺	36.2×10^{-8}
OH⁻	20.5×10^{-8}
SO₄⁻	8.3×10^{-8}
Na⁺	5.2×10^{-8}
Cl⁻	7.9×10^{-8}
K⁺	7.6×10^{-8}
NO₃⁻	7.4×10^{-8}
Li⁺	4.0×10^{-8}
HCO₃⁻	4.6×10^{-8}
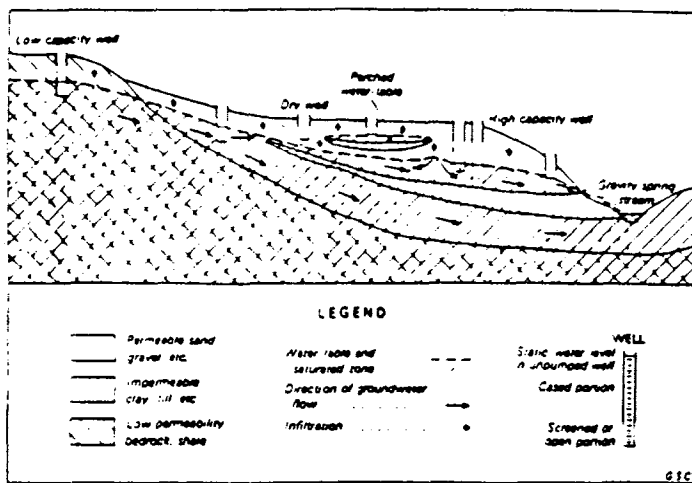
FIGURE 7. Water-table conditions - unconfined aquifers (after I.C. Brown [13]).

TABLE 5. Representative porosity ranges for sedimentary materials (after D. K. Todd [12])

Material	Porosity, %
Soils	50-60
Clay	45-55
Silt	40-50
Medium to coarse mixed sand	35-40
Uniform sand	30-40
Fine to medium mixed sand	30-35
Gravel	30-40
Gravel and sand	20-35
Sandstone	10-20
Shale	1-10
Limestone	1-10

Table 6 gives further data on porosity and also indicates the value of the ratio ρ_x (mixture resistivity) divided by ρ_1 (electrolyte resistivity) about which more will be said later in Sections IV and V.

It is obvious that the degree of compaction of a soil will affect the magnitude of the soil porosity.

IV. ELECTRICAL CONDUCTIVITY OF SOILS AND ROCKS

In Section III it was noted that the conductivity of soils and rocks was principally electrolytic. This section will discuss the parameters that determine the conductivity of electrolytes and the effects that arise when electrolytes are present in both clay-free and clay-rich soils and rocks.

IV. 1. Properties of Electrolytes

As an introduction suppose we empty our hypothetical tank of Section II and refill it with distilled water. The measured conductiv-

TABLE 6. Porosity of soils and rocks (after C. A. Helland [14])

Rock or Formation	Porosity	Ratio $\dfrac{\rho_x}{\rho_1}$
Igneous and metamorphic rocks	1- 2	100
Dense limestones and sandstones	2- 4	50 -100
Clays and sands in general	8-15	20 - 40
Porous clays, sands, sandstone, cellular limestones, and dolomites	15-40	3 - 20
Marl, loess, clay, and sandy soil	40-75	1.5- 4
Peat, diatomaceous earth	80-90	1.0- 1.5

ity is very low. If however a small amount of table salt (NaCl) is dissolved in the distilled water the conductivity increases substantially.

The conductivity of an electrolyte is proportional both to the total number of charge carriers (ions) in the solution and their velocity. In distilled water there are few ions and the conductivity is low. The dissolved sodium chloride molecules dissociate to form both positively charged sodium ions and negatively charged chloride ions which greatly increase the conductivity.

When a voltage is applied between the two end plates an electric field is established in the tank: the positively charged ions are attracted towards the negative plate, the negatively charged ions to the positive plate. The velocity of the ions is effectively controlled by the viscosity of the fluid. This velocity is slightly different for different ions since it depends upon their effective diameter, as illustrated in Table 7, where it can be seen that chloride ions move slightly more rapidly than the sodium ions.

In a sodium chloride solution the amount of current that flows, and therefore the electrical conductivity, is proportional to the sum of the number of sodium ions multiplied by their mobility (velocity per unit electric field) and the number of chloride ions multiplied by their mobility.

The further addition of different salts to our tank would increase the electrical conductivity independently of the presence of the sodium and chlorine ions as long as the concentrations remain reasonably dilute. The following equation is often used to calculate the approximate electrical conductivity in mhos per meter of a dilute solution of various salts at normal ambient temperatures:

$$\sigma = 96500[C_1M_1 + C_2M_2 + ...] = 96500 \sum C_iM_i \quad (4)$$

where C_i = no. of gram equivalent weights of ith ion per 10^6 cm³ of water

M_i = mobility of ith ion in meters per second per volt per meter.

For example, suppose that one gram of salt is dissolved in our tank which holds 10^6 cm³ of water. The atomic weight of sodium is 23, of chlorine is 35, so the atomic weight of sodium chloride is 23 + 35 = 58. Since we have introduced one gram of sodium chloride we have introduced

$\dfrac{23}{58}$ grams of sodium and $\dfrac{35}{58}$ grams of chlorine.

The gram equivalent weight of an ion is the atomic or molecular weight of the ion divided by its valence. In the case of both sodium and chlorine the valence is one so the gram equivalent weight of sodium is 23 grams, of chlorine 35 grams.

Then the number of gram equivalent weights of sodium per 10^6 cm³ of water is given by

$$C_{Na} = \frac{\text{weight of Na per } 10^6 \text{ cm}^3 \text{ H}_2\text{O}}{\text{gram equivalent weight}} = \frac{23\,58}{23} = \frac{1}{58}$$

and that for chlorine is given by

$$C_{Cl} = \frac{\text{weight of Cl per } 10^6 \text{ cm}^3 \text{ H}_2\text{O}}{\text{gram equivalent weight}} = \frac{35\,58}{35} = \frac{1}{58}$$

Using the data from Table 7 for the mobilities at 25° C we find that the conductivity for one gram of sodium chloride in 10^6 cm³ of water is given by

$$\sigma = 96500\left[\frac{1}{58} \times 5.2 \times 10^8 + \frac{1}{58} \times 7.9 \times 10^8\right]$$

$$= 0.00022 \text{ mho/m.} \quad (5)$$

The addition of only one part per million of sodium chloride by weight has produced the appreciable conductivity of 0.22 millimhos per meter.

The concentration of dissolved salts in natural groundwaters is substantially higher than one part per million, as a result of which their conductivity is much greater than 0.22 millimhos per meter. For example Table 8 illustrates the contribution of various ions to the measured conductivity of three of the Great Lakes. Lakes Erie and Huron which both occur in regions of Paleozoic carbonate rocks contain more dissolved salts than Lake Superior which is situated largely in Precambrian crystalline rocks, and this is reflected in the higher conductivities of the first two lakes. The bottom line of the table gives the measured conductivity: agreement with the calculated values using the above equations is good.

The following data from Heiland [14] illustrates typical values for the conductivity of various natural waters.

1. Meteoric waters, derived from precipitation: 1 to 30 millimhos per meter.
2. Surface waters (lakes, rivers) vary from 0.3 millimhos per meter for very pure water to as large as 10.000 millimhos per meter for salt lakes. Surface waters in districts of igneous rocks are estimated to range from 2 to 30 millimhos per meter; surface waters in areas of sedimentary rocks vary from 10 to 100 millimhos per meter (compare the Great Lakes above).
3. Soil waters (discharged into the atmosphere by evaporation) may be as large as 10.000 millimhos per meter but their average is around 10 millimhos per meter.
4. Normal groundwater in areas of igneous rock ranges from 6 to 30

millimhos per meter and in areas of sedimentary rocks to as large as 1.000 millimhos per meter.
5. Mine waters (copper, zinc, etc., sulfates) are of high conductivity, generally not less than 3.000 millimhos per meter.

The temperature dependence of the electrical conductivity of the electrolyte is almost entirely due to the temperature dependence of the viscosity of the liquid, which in turn directly affects the ionic mobility. The variation of either quantity with temperature is approximately linear over normal ambient temperatures. The temperature coefficient for a sodium chloride solution is 0.022 which value applies approximately to most other ions so that the electrolyte conductivity for a temperature other than 25°C is given by

$$\sigma(T) = \sigma(25°C)[1 + \beta(T - 25°)]$$

where $\beta = 2.2 \times 10^{-2}$ per °C

$$T = \text{temperature (°C) at which conductivity is to be calculated.}$$

A change of conductivity of 2.2% per degree centigrade implies that a change in temperature of 40°C will cause the conductivity to nearly double. The effect of temperature is illustrated in Figure 8 which shows calculated conductivity of four of the Great Lakes as a function of season.

The change of conductivity with temperature and therefore with season is not negligible and this applies equally well to ground conductivity over the normal range of ambient temperatures.

IV. 2. Conductivity of Saturated Clean (Clay-Free) Mixtures

We have examined how the electrical conductivity of the electrolyte in our tank varies with the concentration of dissolved salts and with temperature. Let us now start to fill the tank with perfectly insulating spheres of uniform radius (for example uniform pebbles). Assume for the time being that we can maintain these spheres uniformly dispersed throughout the solution. Since the spheres are insulating, the electrical current will find it more difficult to cross the tank and the conductivity will be reduced. A relationship was derived by Maxwell for the conductivity σ_x of a mixture consisting of a medium with conductivity σ_1 in which spherical grains of conduc-

TABLE 8. Conductivity of Great Lakes with contribution of the various ions (after L. H. Doherty [15])

Ion	Lake Erie	Lake Huron	Lake Superior
HCO₃	5.8	4.1	2.6
Ca	10.1	7.3	3.8
Mg	3.6	3.2	2.4
Na	1.8	0.6	0.2
Cl	3.9	1.2	0.2
SO₄	3.4	1.8	0.3
Calculated Conductivity (mmhos m)	28.6	18.2	9.5
Measured Conductivity (mmhos m)	26.7	18.2	8.4
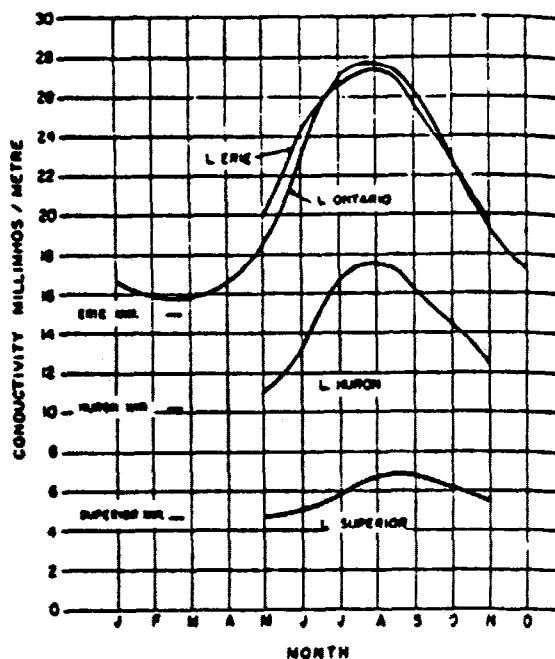
FIGURE 8. Seasonal variation of conductivity of Lakes Ontario, Erie, Huron and Superior (after L.H. Doherty [15]).

tivity σ_2 (here assumed to be zero) are imbedded in regular arrangement and in such a manner that their spacing is large compared with their radius [14]. Letting n be the porosity of the mixture (defined as the ratio of the volume of solution only, divided by the total volume of the solution including the spheres) Maxwell showed that the conductivity of the mixure was given by

$$\frac{\sigma_x}{\sigma_1} = \frac{2n}{3 - n} \qquad (7)$$

In Section II it was shown that the conductance of a current path is directly proportional to the cross-sectional area and inversely proportional to the length. The addition of insulating spheres to the tank tends to reduce the cross-sectional area available for current flow and to increase the effective length of the current paths, reducing the overall conductivity.

This dilute mixture does not resemble a soil so we continue to add insulating spheres until the tank is full. The condition for Maxwell's derivation, that the inter-particle distance be large compared with the particle radius, is invalid and the above equation can no longer be expected to apply. It turns out however that an almost equally simple empirical relationship called Archie's Law [5] is applicable to clean (i.e. clay-free) saturated mixtures. This equation is

$$\frac{\sigma_x}{\sigma_1} = n^m \qquad (8)$$

where n is the fractional porosity defined above and m is a constant. The reciprocal quantity ρ_x/ρ_1 is often called the formation factor (FF) of the rock or soil sample.

Originally derived from resistivity measurements on samples of consolidated porous rock, this equation also applies to a variety of unconsolidated materials. That such a simple law should give excellent results for a variety of both consolidated and unconsolidated materials with widely differing porosities is a surprise and indeed the underlying reasons for its success are not well understood [4]. It has been established [16] that in the case of marine sands the exponent m is dependent on the *shape* of the particles, increasing as they become less spherical (i.e. more platey) and that variations in the *size* of the particles and in the *dispersion* of sizes appear to have a very small effect.

Values of m are listed in Table 9 where it is seen that m varies from 1.2 for insulating spheres to 1.85 for very platey fragments of shell. Samples of natural sands have values in the range 1.4 to 1.6. The value of 1.85 for shell fragments is in good agreement with earlier measurements made on kaolinite particles and marine illite clays. This fact may or may not be significant for clays in normal soils depending on the extent to which ion exchange effects also contribute to the conductivity as discussed further on in this section.

Archie's Law for various exponents is plotted in Figure 9 along with Maxwell's Law. Over the range of porosities of most unconsolidated terrain materials (20% to 70% – see Tables 5 and 6) the different exponents do not greatly affect the mixture conductivity. Interestingly enough, Maxwell's Law gives excellent agreement with Archie's Law with exponent m = 1.3 over all ranges of porosity.

It would appear that for relatively clay-free substances located beneath the water table (so that the mixture is completely saturated) the primary matrix property measured through the electrical conductivity is the porosity of the matrix, essentially independent of the particle size or the particle size distribution. This explains why it is a relatively difficult matter using resistivity techniques to distinguish between sand and gravel. As long as the porosity is the same for both sand and gravel the resistivity or conductivity contrast may be quite small.

. Another point is that if the porosity is assumed to vary from 20% to 70% the conductivity of the mixture varies by a factor of approximately 8, depending somewhat on which value of exponent is

TABLE 9. The effect of particle shape on the FF n relation using artificial samples of decreasing sphericity. (after P. D. Jackson et al. [16])

Sample no.	Mean size ϕ*	Spread of sizes	Sphericity	Best fit Archie line FF = n^{-m} m ± 0.01
Spheres	0.38	0.17	1.0	1.20
Rounded sand	0.38	0.17	0.83	1.40
Shaley sand	0.50	0.34	0.78	1.52
Shell fragments	0.38	0.17	0.5	1.85

*ϕ = $-\log_2$ (diameter in mm).

adopted. Even in clean mixtures we do not expect a large range of conductivities and experimentally this has been confirmed.

Figure 9 is useful for the following type of calculation: in many glacial deposits gravel appears as pebbles (of the order of a few centimeters in diameter) dispersed throughout a mixture of finer relatively clean sand. How does the presence of this gravel modify the mixture conductivity? To obtain an approximate answer let us assume that the sand itself has a porosity of 30%. Using Archie's Law with m = 1.6 the electrical conductivity of the sand/water mixture will be 15% of the conductivity of the water. Assuming a water conductivity of 20 millimhos per meter gives a conductivity for the mixture of 3 millimhos per meter, a not uncommon value. We use this value in conjunction with Figure 9 to determine the effect of introducing pebbles into the mixture. If for example the pebbles occupy 50% of the volume the conductivity of the mixture will fall to one-third or approximately 1 millimho per meter, also a value that commonly occurs in actual practice. As will be seen later the addition of a relatively small amount of clay can increase these numbers by virtue of increasing the conductivity of the pore water but the relative values may well be similar.

IV. 3. Conductivity of Unsaturated Clean Mixtures

For Archie's Law to apply the material must be fully saturated with fluid. If the mixture is partially saturated the conductivites will be decreased since gas or air bubbles act as insulating particles to further impede the current flow. In the funicular stage of soil moisture the pendular rings have coalesced so that the liquid films are continuous throughout the pore space but only a fraction of the available pore space is filled with water. This moisture varies with time and temperature as a result of drainage, evaporation, and loss of water to plant roots.

In the event that the soil is partially desaturated the following approximate expression applies [5]

$$\frac{\sigma_x}{\sigma_1} = s^n \qquad (9)$$

where s is the fraction of total pore volume filled with electrolyte and n is a parameter experimentally determined to be approximately 2. This expression is equivalent to Archie's Law with m = 2 and indicates as seen from Figure 9 that if a small fraction of the total pore volume is filled with water the conductivity can be very low.

More recent work on soils has shown that the electrical conductivity varies as follows with moisture content when the soil is partially desaturated [17]

$$\sigma_x = \sigma_1 \theta(a\theta + b) + \sigma_s \qquad (10)$$

where θ is the volumetric water content (cm³ of water per cm³ of soil), a and b are constants which depend on the soil texture, and σ_s is a contribution from "surface conductivity" which will be discussed under Colloidal Conductivity. The values of the empirically determined constants a and b for a variety of soils are shown in
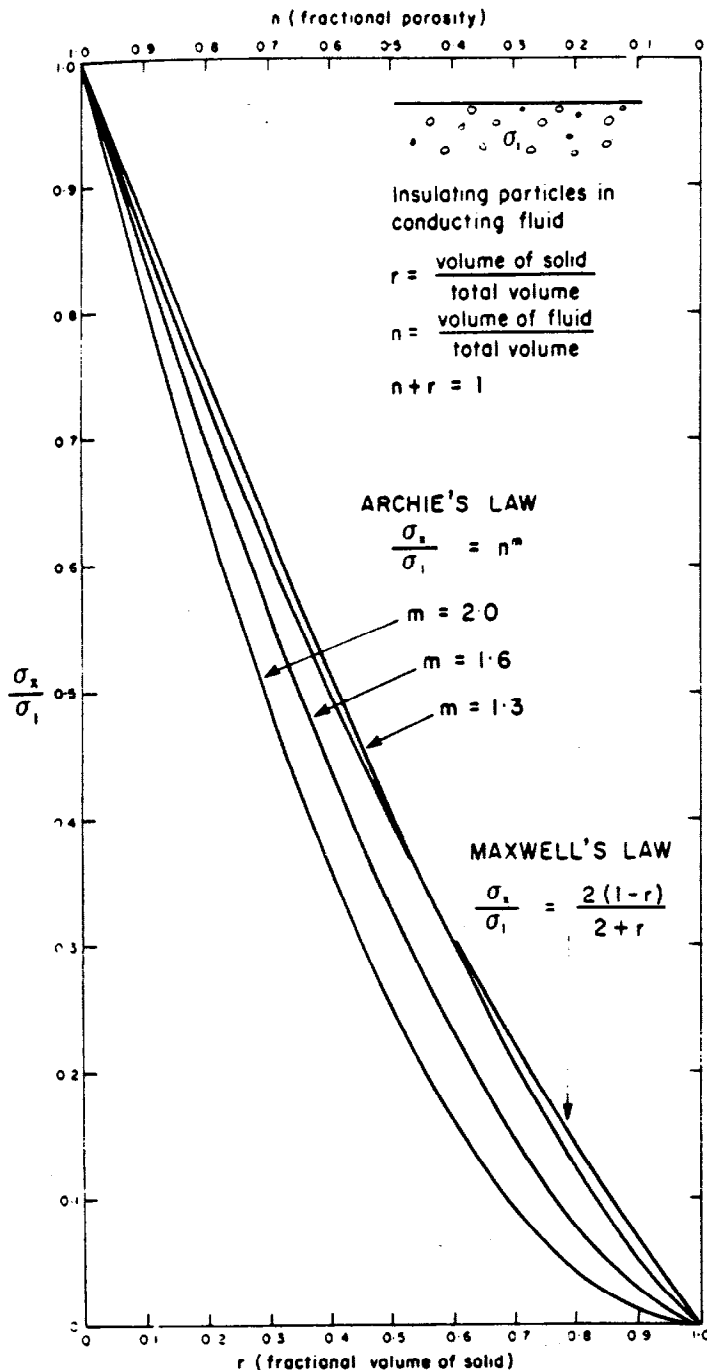
FIGURE 9. Graph of Archie's Law and Maxwell's Law.

The figure shows:

n (fractional porosity) on top axis, r (fractional volume of solid) on bottom axis, $\frac{\sigma_x}{\sigma_1}$ on vertical axis.

Insulating particles in conducting fluid

$$r = \frac{\text{volume of solid}}{\text{total volume}}$$

$$n = \frac{\text{volume of fluid}}{\text{total volume}}$$

$$n + r = 1$$

ARCHIE'S LAW

$$\frac{\sigma_x}{\sigma_1} = n^m$$

m = 2·0
m = 1·6
m = 1·3

MAXWELL'S LAW

$$\frac{\sigma_x}{\sigma_1} = \frac{2(1-r)}{2+r}$$

TABLE 10. Measured moisture content constants and surface conductivities (after J. D. Rhoades et al. [17])

Soil type	a	b	σ_s
			mmho cm
Pachappa fsl	1.382	−0.093	0.18
Indio vfsl	1.287	−0.116	0.25
Waukena l	1.403	−0.064	0.40
Domino cl	2.134	−0.245	0.40

increasing depth the conductivity rises rapidly as the moisture films become continuous. then more slowly as the available pore volume starts to fill. eventually saturating with complete filling of the pores. This situation will be rendered even more complex if the porosity itself is. as is often the case. a function of depth as suggested by the profile of Figure 4.

IV. 5. Colloidal Conductivity

It will be recalled that for clays the cation exchange capacity (CEC) was a measure of the number of ions adsorbed to the surface of clay particles. When the clay particles are immersed in a liquid there is evidence to show that these adsorbed ions can partially dissociate themselves from the clay particles and become available for ionic conductivity. Since the ion exchange capacity of clays can be great due to their large surface area many ions may be supplied for electrical conductivity; the addition of a small amount of clay to an otherwise clean mixture can substantially increase the electrical conductivity.

The addition of clay appears to affect the electrical conductivity of the mixture in two ways. Repeating equation (10)

$$\sigma_x = \sigma_1 \theta(a\theta + b) + \sigma_s \tag{10}$$

the added ions increase the value of σ_1 above the value that the porewater would have in the absence of the clay. Furthermore although dry clay is highly resistive. as soon as a thin layer of moisture (perhaps only a few molecules thick) surrounds the clay particles ion movement across the surface of the clay particle within the cloud of adsorbed ions may occur. This surface contribution to the conductivity. essentially independent of the moisture content. is the second term in the equation. It will be most significant at low moisture contents.

The contribution to σ_1 from clay content will be most evident for soils in which the porewater is relatively pure (and therefore has low conductivity) and will be least effective in soils having highly saline porewater. For either contribution we should expect that clays with higher CEC will produce more conductive soils and a comparison of Table 11 with Table 2 shows that this is the case

In summary. in areas where the soil porewater is not particularly saline the electrical properties of the soil may be strongly influenced by and indeed in some cases completely dominated by the amount and type of clay minerals present. The possible influence of clay materials should always be kept in mind. It is also possible that a similar effect arises as a result of the colloidal properties of humus which might be important in tropical climates where the humus layer is well leached and contains few clay minerals.

IV. 6. Effects of Freezing on Soil Conductivity

Suppose that we take our tank. filled with a clean sand/water mixture. and start to lower the temperature. The electrical conductivity of the mixture will decrease in exactly the same way that the conductivity of the electrolyte does. When the temperature reaches 0°C the water freezes and since the conductivity of ice is extremely low the conductivity of the mixture falls essentially to zero.

Now suppose that in addition to the sand some clay is introduced to the mixture and the temperature is again reduced. As the temperature passes through 0°C some of the water freezes: however the

Table 10 from which it is seen that except for very low moisture the relationship is essentially a square law with mosture content.

It has been suggested by Rhoades et al [17] that it might be possible to estimate the values of σ_s. a. and b on the basis of soil texture and mineralogy and. given a measurement of the bulk soil conductivity and the moisture content. to determine the conductivity of the fluid and thus salinity.

IV. 4. Electrical Layering Arising from Soil Moisture

From the preceding paragraphs we observe that. even if the soil material is physically homogeneous. for example consists of clean well-sorted silt. as soon as we introduce soil moisture of finite electrical conductivity we have established a medium in which the electrical conducvitity can vary strongly with depth. Near surface where the moisture content is low the conductivity is also low. With

Topographic location	Sample no.	Moisture (%)	Conductivity (mmho m)	Clastic material (%)	Clay fraction (%)	Clay type(s) (%)
Uplands	1	42	16.0	21	79	100% kaolinite
Uplands	2	46	1.2	42	58	100% kaolinite
Uplands	3	25	1.0	5	95	100% kaolinite
Lowlands	4	21	65.0	66	34	100% montmorillonite
Lowlands	5	32	169.0	39	61	60% montmorillonite 40% kaolinite
Lowlands	6	25	269.0	15	85	90% montmorillonite 10% kaolinite

electrical field of the adsorbed ions on the clay particles locally orients the neaby water molecules to prevent their freezing [17]. Furthermore as the solvent freezes there is a tendency for the impurity ions to stay within the liquid fraction and the actual electrical conductivity of the remaining liquid water increases with decreasing temperature. The net result is that mixtures containing clay or silts tend to have an electrical conductivity which decreases relatively slowly with temperature as the temperature passes through 0°C and indeed to retain a moderate conductivity even at temperatures well below freezing as illustrated in Figure 10.
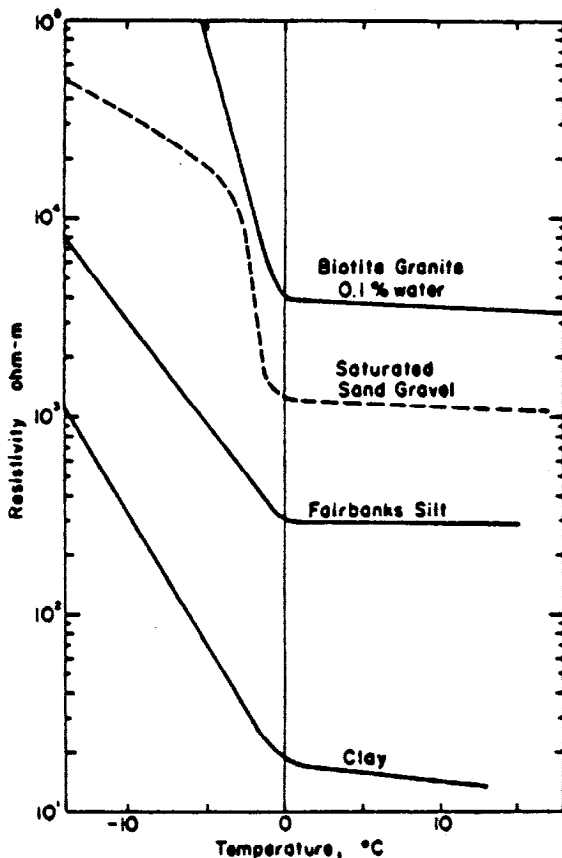
FIGURE 10. Resistivities for several soils and one rock type as a function of temperature (after Hoekstra and McNeill [20]).

IV. 7. Electrical Properties of Rocks

As with unconsolidated materials the matrix of most water-bearing rocks is insulating and the electrical conductivity is also electrolytic. A major difference between unconsolidated sediments and rocks lies in the types of pore geometries. For example in sedimentary rocks the porosity is generally inter-granular and consists of voids still remaining from the compaction process. In igneous rocks the porosity of the rock itself may be extremely small, however moisture circulates through fractures in the rock which are the result of mechanical breakage. These cracks are called joints and may be sufficiently large and/or numerous that their presence completely dominates the electrical conductivity. Such jointing may also play a major role in the conductivity of the more impermeable sedimentary rocks. When large joints are present the local conductivity may be expected to vary strongly with position. A third form of porosity which may not make a major contribution to electrical conductivity as normally measured is vugular porosity. It consists of cavities (as might be caused by solutions circulating in limestone) interconnected by small pores which dominate the D.C. electrical behavior. It should be noted that in the case of electromagnetic excitation of currents direct electrical (ohmic) inter-cavity connection is not necessary and appreciable response to this excitation may come from the fluid in each cavity separately.

Table 12 illustrates normal porosity for various rock types. It is seen that the total porosity can be very small, of the order of a few percent, and we would therefore expect, particularly for unfractured Precambrian igneous rocks and high-ranking metamorphosed rocks, the electrical conductivity to be very low, as is generally the case. On the other hand shales may be relatively porous and in addition the conductivity of the pore water may be high as a result of ion exchange effects. For this reason shales can be as conductive as 30 to 40 millimhos per meter and in some cases even higher.

Since in general the porosities are smaller for consolidated materials and furthermore at this end of the scale the various exponents in Archie's Law have a large effect, it is difficult to predict the electrical properties of any given rock type.

There is another feature which occurs in sedimentary rocks and which is of importance in determining their electrical characteristics. Being depositional in nature these rocks are layered and the electrical conductivity perpendicular to the bedding planes may be less than the conductivity parallel to the planes.

This feature is illustrated in Table 13 which lists the coefficient of anisotropy for various layered rocks. The coefficient is defined in Figure 11.

Another type of rock conductor called a structural conductor [21] occurs as a result of fracturing and is often linear in shape. Such conductors arise in the interior of faults, shear zones, contact frac-

TABLE 12. Normal ranges in porosity for rocks (after Keller and Frischknecht [5])

Rock type	Intergranular porosity (%)	Joint porosity (%)	Vugular porosity* (%)
Paleozoic sandstones and shale	5–30	0–1	0
Paleozoic limestones	2–10	0–2	0
Paleozoic clastic volcanics	5–30	0–2	0
Post Paleozoic sandstones and shale	10–40	0	0
Post-Paleozoic limestones	4–20	0–2	0
Post-Paleozoic clastic volcanics	10–60	0	0
Precambrian sediments and low-rank metamorphosed sediments	1–8	0–2	0
Precambrian igneous rocks and high-rank metamorphic rocks	0–2	0–2	0
More recent igneous rocks	0–10	0–2	0

*Vugular porosity accounts for an appreciable total porosity only in rare cases.

TABLE 13. Coefficients of anisotropy for layered rock (after Keller and Frischknecht [5])

Rock type	Coefficient of anisotropy
Volcanic tuff, Eocene and younger, from Nevada	1.10–1.20
Alluvium, thick sections from the southwestern United States	1.02–1.10
Interbedded limestones and limey shales from northeastern Colorado	2.0 –3.0
Interbedded anhydrite and shale, northeastern Colorado	4.0 –7.5
Massive shale beds	1.01–1.05
Interbedded shale and sandstone	1.05–1.15
Baked shale or low-rank slate	1.10–1.60
Slates	1.40–2.25
Bitumenous coal and mudstone	1.7 –2.6
Anthracite coal and associated rocks	2.0 –2.6
Graphitic slate	2.0 –2.8

ture zones. etc., where the rock material has been ground into small particles which allows increased circulation of groundwater resulting in enhanced weathering to produce clay minerals. Structural conductors occur in a wide range of sizes.

V. EXAMPLES OF CONVENTIONAL MEASUREMENTS OF SOIL AND ROCK RESISTIVITIES

The material in this section gives a broad indication as to the range of resistivity or conductivity which might be encountered in various terrain materials in various climatic zones. Extreme caution must be exercised in employing these values for anything other than a rough guide as to anticipated survey results.

As an introduction Table 14 illustrates the resistivities of igneous and metamorphic rocks as given by Telford et al [22]. Table 15 lists resistivities of sediments from the same source. Table 6, from Heiland [14], lists the ratio ρ_x/ρ_0 as defined in Section IV for various consolidated and unconsolidated materials.

V. 1. Temperate Zones
Table 16 records the ranges of resistivity compiled for different terrain materials from a variety of survey and laboratory measurements. from Culley et al [23].

Table 17 from Sellman et al [24] shows survey data over different soil types made with three different measurement techniques (i) radio-frequency magneto-telluric at approximately 300 kHz. (ii)
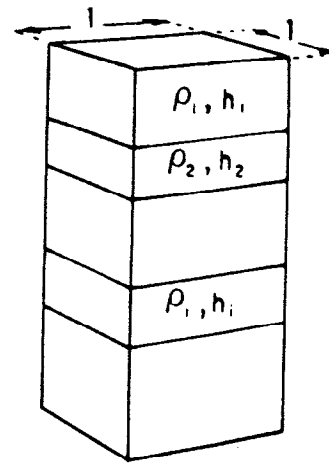
FIGURE 11. Definition of coefficient of anisotropy (λ) for layered sediments (after Keller and Frischknecht [5]).

$$\rho_i = \frac{\Sigma(\rho h)}{\Sigma h}$$

$$\rho_i = \frac{\Sigma h}{\Sigma(h_i/\rho)}$$

$$\lambda = \left(\frac{\rho_i}{\rho_i}\right)^{\frac{1}{2}}$$

low-frequency magnetically induced currents using dipole transmitter and receiver at 10 kHz. and (iii) standard Wenner array at DC. The measured resistivities are relatively independent of the method of measurement: the general trend of increasing resistivity with particle size should be noted.

A complete set of measurements by Smith-Rose [25] on a variety of soils from different depths, with different moisture contents. and measured at various frequencies. shows that at the lower frequencies (i.e. between 1 and 100 kHz) the conductivity of soils is essentially independent of frequency. At higher frequencies the conductivity rises and the increase in conductivity is generally greatest for the most poorly conducting samples. The results of his laboratory measurements on soil samples taken from various parts of England are illustrated in Table 18 and profiles of conductivity with depth

TABLE 14. Resistivities of igneous and metamorphic rocks (after W. M. Telford et al. [22])

Rock type	Resistivity range (Ωm)
Granite	3×10^2–10^6
Granite porphyry	4.5×10^3 (wet)–1.3×10^6 (dry)
Feldspar porphyry	4×10^3 (wet)
Albite	3×10^2 (wet)–3.3×10^3 (dry)
Syenite	10^2–10^6
Diorite	10^4–10^5
Diorite porphyry	1.9×10^3 (wet)–2.8×10^4 (dry)
Porphyrite	10–5×10^4 (wet)–3.3×10^3 (dry)
Carbonatized porphyry	2.5×10^3 (wet)–6×10^4 (dry)
Quartz porphyry	3×10^2–9×10^5
Quartz diorite	2×10^4–2×10^6 (wet)–1.8×10^6 (dry)
Porphyry (various)	60–10^4
Dacite	2×10^4 (wet)
Andesite	4.5×10^4 (wet)–1.7×10^2 (dry)
Diabase porphyry	10^3 (wet)–1.7×10^5 (dry)
Diabase (various)	20–5×10^7
Lavas	10^2–5×10^4
Gabbro	10^3–10^6
Basalt	10–1.3×10^7 (dry)
Olivine norite	10^3–6×10^4 (wet)
Peridotite	3×10^3 (wet)–6.5×10^3 (dry)
Hornfels	8×10^3 (wet)–6×10^7 (dry)
Schists (calcareous and mica)	20–10^4
Tuffs	2×10^3 (wet)–10^5 (dry)
Graphite schist	10–10^2
Slates (various)	6×10^2–4×10^7
Gneiss (various)	6.8×10^4 (wet)–3×10^6 (dry)
Marble	10^2–2.5×10^8 (dry)
Skarn	2.5×10^2 (wet)–2.5×10^8 (dry)
Quartzites (various)	10–2×10^8

TABLE 15. Resistivities of sediments (after W. M. Telford et al. [22])

Rock type	Resistivity range (Ωm)
Consolidated shales	$20-2 \times 10^3$
Argillites	$10-8 \times 10^2$
Conglomerates	$2 \times 10^3 - 10^4$
Sandstones	$1-6.4 \times 10^8$
Limestones	$50-10^7$
Dolomite	$3.5 \times 10^2 - 5 \times 10^3$
Unconsolidated wet clay	20
Marls	3–70
Clays	1–100
Alluvium and sands	10–800
Oil sands	4–800

TABLE 16. Resistivity ranges for various terrain materials (after Culley et al. [23])
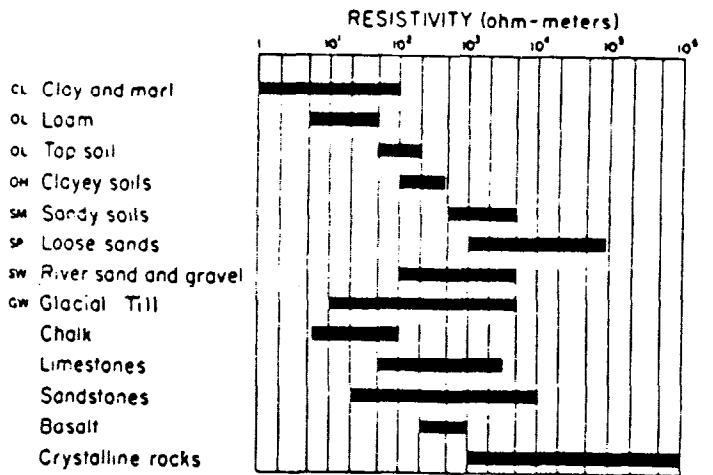
from these measurements are shown in Figure 12. It is seen from Table 18 that the soil type varies rapidly with depth, as does the soil moisture content; both of these influence the conductivity profiles. Smith-Rose concludes that clays have the highest conductivities, greater than 10 millimhos per meter, loams and chalks are of the order or 10 millimhos per meter and sandy or gritty soils are appreciably less. He also points out that a diurnal temperature range of 20°C at the surface of the soil represents a temperature change of approximately 1.4°C at a depth of one foot. Measurements made on a soil sample at 1.2 MHz as a function of moisture content by weight show a conductivity that increases approximately as the square of the moisture content.

V. 2. Tropical Humid Zones [26]

The examples given above have been taken from temperate zone soils and seem to be fairly representative. In the case of soils occurring in tropical humid climates (annual temperatures of the order of 25°C; annual precipitation of greater than a meter, generally falling during a part of the year) the weathering can be very deep. Indeed, unweathered parent rock may not occur until 30 meters in flat country, 60 meters in hilly country and in rare occasions depths

TABLE 17. Apparent resistivity data obtained for various material types using three measuring techniques (after Sellman et al. [24])
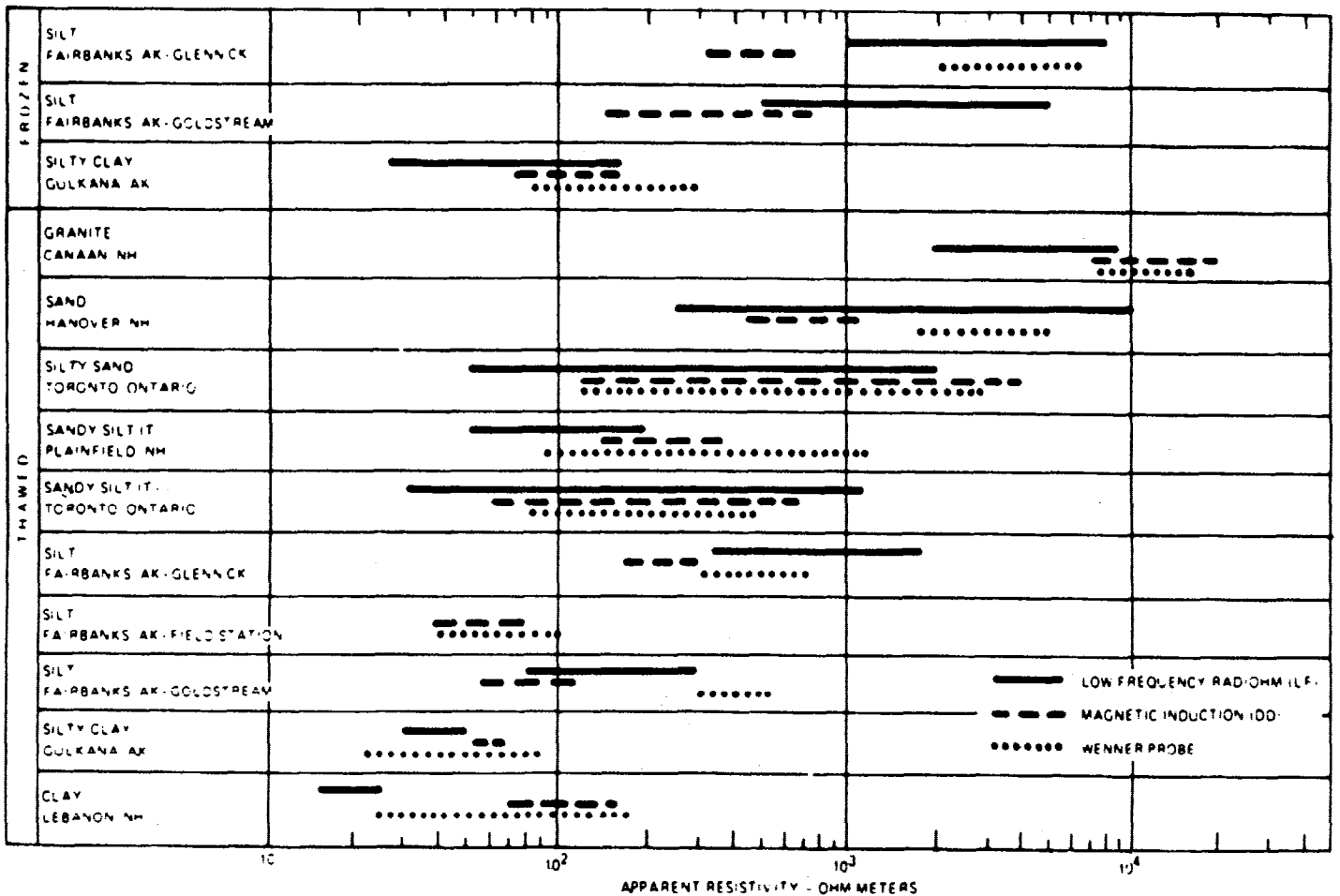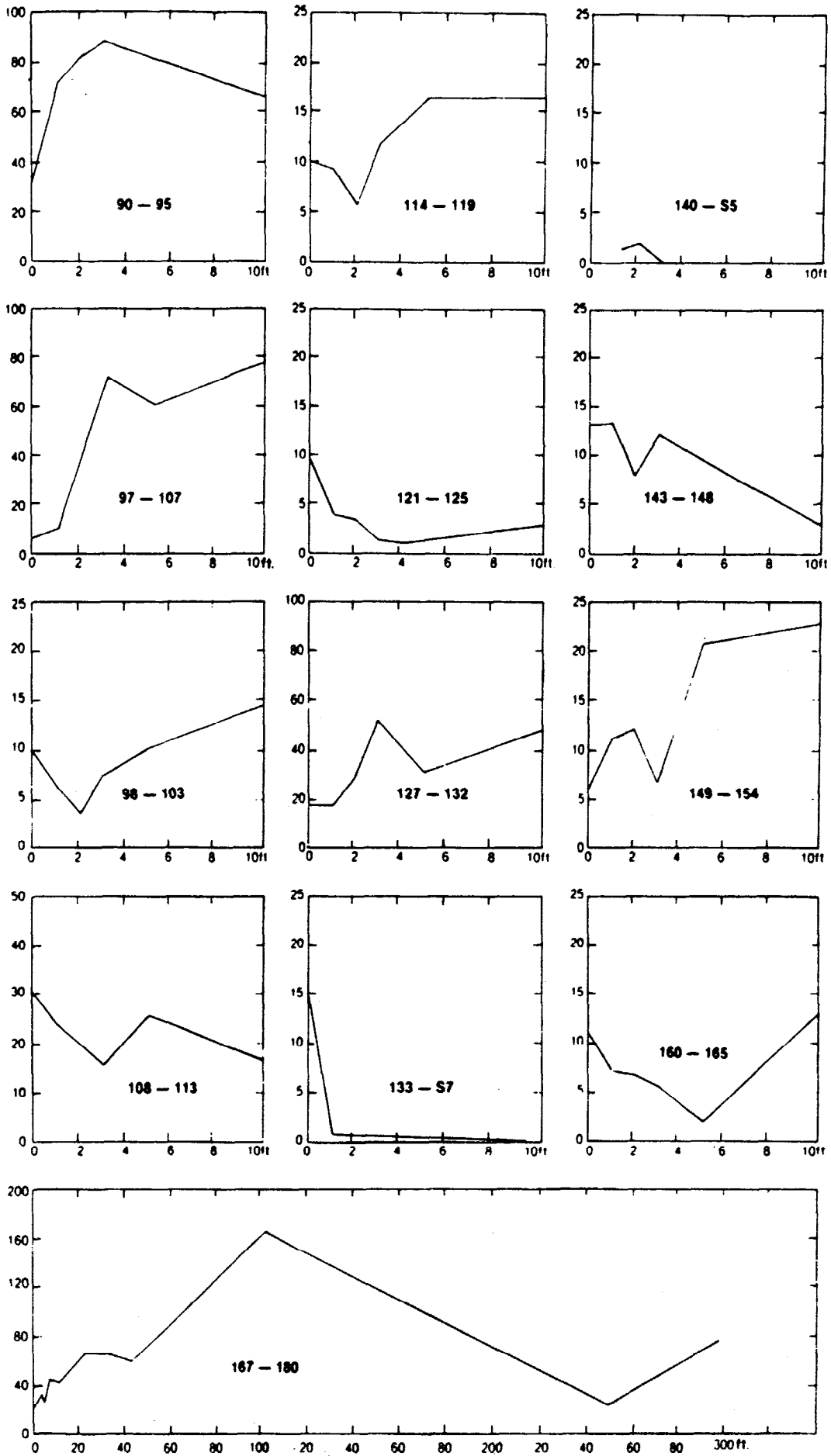
FIGURE 12. Plots of conductivity (mmhos/m) versus depth (feet) for data in Table 18.

Sample No.	Site	Geological classification	Depth	Description of sample	Moisture content	Conductivity at 20 C Millimho m	
						1 kHz	100 kHz
			ft.		per cent		
90	Rugby Radio	Lower lias	Surface	Dark fibrous loam	60	33	38
92	Station (1)		1	Loam and clay	33	72	78
93			2	Clay and sand	26	83	89
94			3	Blue clay	25	89	100
95			10	Blue clay	23	67	72
97	Rugby Radio	Lower lias	Surface	Loam	22	6.1	7.2
104	Station (2)		1	Loam and clay	13	9.4	9.4
105			3	Blue clay	27	72	83
106			5	Clay and sand	21	61	61
107			10	Blue clay	25	78	89
98	Baldock, Herts	Chalk	Surface	Fibrous loam	21	9.4	10.0
99	(P.O. Receiving Station)		1	Chalky loam	21	6.1	6.1
100			2	Chalk	24	8.1	2.9
101			3	Chalk	27	7.2	7.8
102			5	Chalk	26	10.1	15.6
103			10	Chalk	27	14.4	15.6
108	Tatsfield, Kent	Upper greensand	Surface	Fibrous loam	37	30	38
109	(B.B.C. Receiving Station)		1	Brown, sandy clay	11	24	27
110			2	Brown sand	15	20	22
111			3	Light brown sand	13	15.6	10.7
112			5	Light brown sand	20	26	26
113			10	Yellow sand	15	16.7	19
114	Brookmans Park, Herts	London clay	Surface	Fibrous loam	19	10.0	10.6
115	(London Regional Station)		1	Stony loam	18	9.4	10.0
116			2	Light sandy clay	22	5.6	7.2
117			3	Sandy clay	22	12.2	13.3
118			5	Sandy clay	21	16.7	18.8
119			8 to 10	Clay and shingle	10	16.7	17.8
121	Daventry	Upper lias	Surface	Fibrous loam	28	9.4	10.6
122	Northants		1	Sandy loam	16	3.8	3.8
123			2	Brown sand	14	3.2	3.2
124			3	Brown sand	5.0	1.1	1.2
126			5	Sand and sandstone	8.5	0.8	1.0
125			10	Sand and sandstone	24	2.9	3.7
127	Washford Cross, Somerset	Red Marls	Surface	Reddish-brown loam	23	16.7	18.9
128	(West Regional Station)		1	Reddish-brown clay	20	16.7	18.9
130			2	Reddish-brown clay	18	28.9	31
129			3	Reddish-brown clay	21	52	54
131			5	Reddish-brown clay	19	31	34
132			10	Reddish-brown clay	15	48	50
133	Brendon Hills, Somerset	Devonian	Surface	Black fibrous loam	210	14.4	16.7
134			1	Loam and slate	9.0	0.3	0.3
135			2	Loam and slate	9.0	0.2	0.2
136			3	Loam and slate	8.0	0.1	0.1
137			5	Loam and slate	5.5	0.0	0.0
S.7			10	Slate	—	0.0	0.0
140	Merrivale, Dartmoor, Devon	Granite	1	Gritty loam	18	1.3	1.3
141			2	Gritty loam	13	1.6	1.6
S.1			3 to 10	Granite	—	0.0	0.1
S.2			3 to 10	Granite	—	0.0	0.1
S.5			3 to 10	Granite	—	0.0	0.0
139	Dousland, Dartmoor, Devon	Devonian	Surface	Loam	47	6.1	6.7
142			1	Dark brown loam	41	2.7	2.7
S.4			Below 1	Slate	—	0.0	0.0
S.6			Below 1	Granite	—	0.0	0.0
143	Moorside, Edge, Yorks	Millstone grit	Surface	Fibrous loam	130	13.3	17.8
144	(North Regional Station)		1	Dark grey clay	60	13.3	15.6
145			2	Dark grey clay	35	7.8	10.6
146			3	Dark grey clay	39	12.2	16.7
147			5	Dark grey clay	19	9.4	11.1
148			10	Yellow and grey clay	15	3.4	3.7
149	Westerglen, Falkirk	Boulder clay	Surface	Fibrous loam	38	6.1	7.2
150	(Scottish Regional Station)		1	Fibrous loam	30	11.1	11.1
151			2	Clay and loam	19	12.2	12.2
152			3	Dark grit and clay	18	6.7	7.8
153			5	Dark grit and clay	18	21	24
154			10	Dark grit and clay	15	23	26

(continued over)

TABLE 18. (concluded)

Sample No.	Site	Geological classification	Depth ft.	Description of sample	Moisture content per cent	Conductivity at 20 C Millimho/m 1 kHz	100 kHz
160	Teddington, Middlesex	London	Surface	Fibrous loam	26	11.1	12.2
161	(N.P.L.)	clay	1	Sandy loam	20	7.2	7.8
162			2	Sandy loam	13	6.7	7.2
163			3	Fine gravel	6.5	5.6	6.7
164			5	Coarse gravel	2.9	1.9	2.0
166			7	Fine sand	2.6	1.6	1.6
165			10	Sand and shingle	20	13.3	15.6
167	Wychbold, Droitwich	Red Marls	1	Red clay and loam	15	16.7	20
168	(Midland Regional Station)		2	Red clay	13	34	32
169			3	Red clay	14	23	24
170			5	Red clay and stones	15	43	51
171			10	Red clay and stones	21	41	44
172			20	Red clay suspension	31	67	78
173			30	Red clay suspension	41	67	78
174			40	Red clay suspension	25	61	72
175			50	Red clay	27	78	83
176			100	Grey clay and salt	28	177	233
177			150	Red clay and salt	27	—	—
178			200	Red clay and salt	24	—	—
179			250	Red clay and salt	22	24	26
180			300	Red clay and salt	31	7?	89

of 250 meters have been observed. The resulting soils are red to yellow, soft with a high clay content, and with a specific gravity approximately one-half of that of the parent rock. Compared with the soils of temperate climates they are thick, humus poor, permeable, and have a high clay-silt ratio. Although the clay content is high this is somewhat compensated for by the fact that in well drained soils the clays are kaolinitic and the cation exchange capacity is less than in temperate zones (see Table 11). Iron-rich concretionary horizons called laterites form as a result of reprecipitation. These are hard, permeable, and if dry are usually very resistive.

The nature and the extent of the soil formation is a function of the rock type, texture, jointing, surface relief, vegetation, water-table, and micro-climate. For example, the relative absence of silt is due to the fact that fine-grained rocks weather faster than coarse-grained rocks; the abundance of clay results from the fact that it is a stable mineral.

An excellent series of measurements of the electrical properties of the weathered zones in tropical climates has been carried out by Palacky and Kadekaru in Brazil [27]. The measurements were done with conventional resistivity techniques and many soundings were taken. The results gave good agreement with a three-layered earth model and are summarized in Table 19. In general a resistive soil, relatively thin, is situated on top of a thick quite conductive weathered zone, in turn situated on the relatively resistive parent rock.

V. 3. Tropical Arid Zones

It is in tropical arid zones that the most conductive soils are encountered. As for humid zones the weathered layer can be many tens of meters in thickness, however in arid climates this material often contains a high salt concentration due to evaporation. Whereas the surface materials are usually dry, possibly lateritic, and resistive, deeper material may approach resistivities of the order of 1 ohm-meter. Furthermore substantial lateral variations of resistivity are not uncommon.

In the humid tropical zones referred to above the conductivity of the intermediate zone was due to the presence of an abundance of colloidal particles with moderate ion exchange capacities: abundant rainfall means that drainage patterns are well established and soil salts have long since been leached into major river channels and

TABLE 19. Tropical resistivity profiles (after Palacky and Kadekaru [27])

	Site	Soil Thickness (meters)	Soil Resistivity (ohm-meters)	Weathered Zone Thickness (meters)	Weathered Zone Resistivity (ohm-meters)	Bedrock Type	Bedrock Resistivity (ohm-meters)
Humid Tropical	Nova Lima	5-10	2000-15000	20-80	50-100	schists	∞
					200-400	granodiorite	∞
	Canabrava	5	90	3-18	15-27	basic	∞
		5	360	12-30	3-12	ultrabasic	∞
	Santa Fe	3	11000-18000	35	80-100	dunite	∞
	Quatipuro	0-1	200	15-35	10-30	phyllites	∞
			300-700	3-8	35-20	serpentinites	> 300
Arid Tropical	Santa Luz	-		3-5	65	granite	910
		1	120	10-20	13	basic volcanic	∞
	Curaça	-		6-10	20-35	amphibolites	1200
				15-20	80-130	gneiss	2000

19

TABLE 20. Diagnostic criteria for distinguishing between unaffected soil sites and encroaching and developed saline seeps (after Rhoades and Halvorson [28])

Site type	Salt content	Water content	Soil electrical conductivity
Unaffected	Low, increasing with depth	Low, increasing with depth	Low, increasing with depth
Encroaching saline seep	Low, increasing to a peak at a relatively shallow depth, then decreasing with further depth	Moist surface, becoming wet with depth	Intermediate, increasing to a peak at a relatively shallow depth, then decreasing with further depth
Developed saline seep	High, decreasing with depth	Relatively uniformly wet to the water table	High, decreasing with depth

thence into the oceans. In hot arid climates drainage patterns are poorly established and drainage basins may have no outlet to permanent streams. Salt-bearing waters drain from topographically high regions into lower areas where the water evaporates, leaving a high residual salt content, largely a reflection of the imperfect drainage channels.

The occasional addition of water might be due either to precipitation or irrigation. In the cultivated dry land soils of the northern Great Plains the near surface (plant root-zone) is leached with essentially pure water derived from rain and snow melt during the wet months. Rhoades and Halvorson [28] discuss how this results in a soil salinity concentration which increases with depth. However during the summer months when a saline water table in this climate is situated within approximately one meter from the surface an upwards flow of moisture is caused by evaporation at the soil surface and transpiration within the root zone. This upwards flow reverses the original leaching which transported salts downwards and causes them to ascend so that a concentration peak can form in the soil salinity profile. The soils can remain excessively wet as a result of the hygroscopic nature of the salts and because the salts reduce the effective use of water by plants via evapo-transpiration. Rhoades defines such a condition as a "saline seep" and notes that it can form without the water table actually emerging at the surface. As this seep develops the peak in the soil salinity profile moves upwards until it finally appears at or near the surface as indicated in Table 20 which illustrates the various conditions that can exist in a region which sees seasonal precipitation followed by seasonal drought. Figure 13 illustrates vertical profiles of resistivity versus depth as determined by an expanding Wenner array for the three conditions described in Table 20.

For saline soils, the contribution to conductivity from salt concentration generally outweighs that from cation exchange capacity and the conductivity is relatively independent of clay content.

The effect of weathered-zone salinity is probably at its worst in western Australia where the zone is often 100 meters in thickness and has been known to exceed 300 meters. Hygroscopic salts maintain soil moisture at levels substantially above the water table and resistivities of the order of 1 ohm-meter have been observed. Large lateral variations result from the imperfect drainage patterns: slight changes in surface topography often show up as large changes in subsurface conductivity. A lateritic hard pan is not unusual on the surface. This layer is extremely resistive and completes the complexity and difficulty of making conventional electrical measurements in this environment.

V. 4. Arctic Zones

Finally we turn our attention to arctic regions in which permafrost is a major consideration. It should be noted that the definition of permafrost requires only that the mean annual temperature of the ground be less than 0°C for several years; the definition is completely independent of the nature of the material, the amount of moisture, and indeed whether or not the moisture is frozen. In
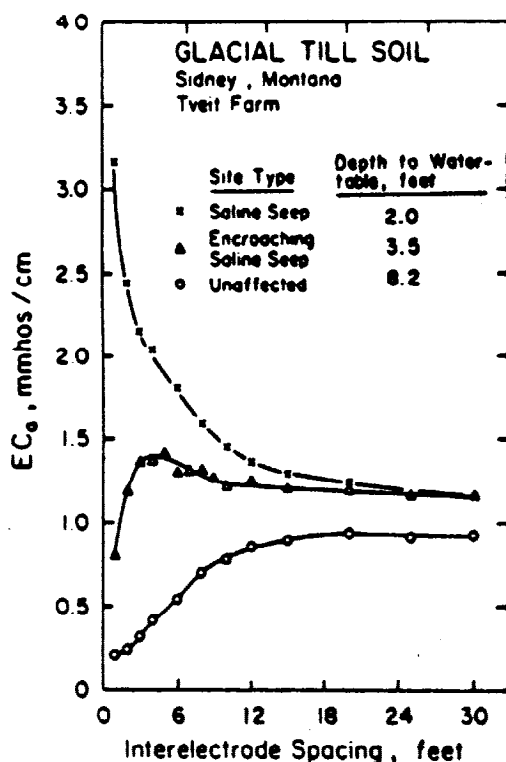
FIGURE 13. Relation between soil electrical conductivity, EC_a, and interelectrode spacing for a saline seep, an encroaching saline-seep site, and an unaffected site for glacial till-clay loam soil near Sidney, Montana (after Rhoades and Halvorson [28]).
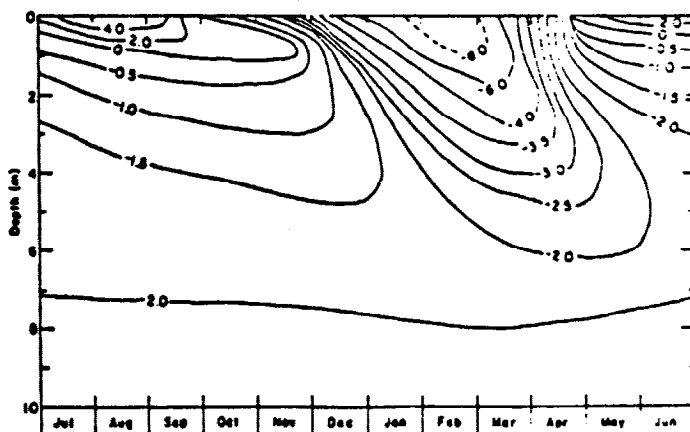
FIGURE 14. Vertical and temporal temperature variations – contoured in °C (after Arcone et al [29]).
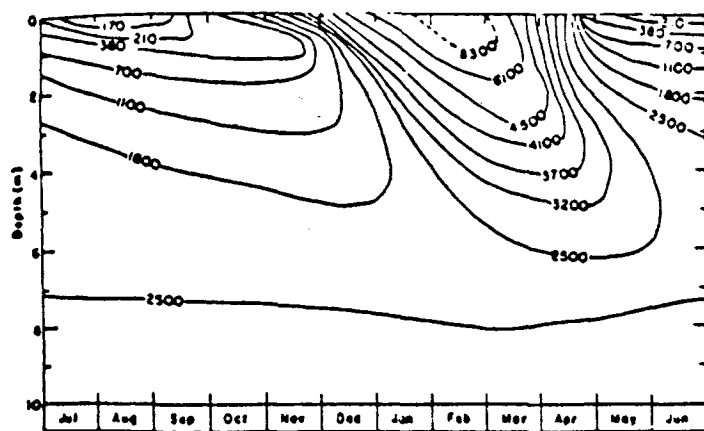
FIGURE 15. Computed vertical and temporal resistivity variations from data of Figure 14 – contoured in ohm-meters (after Arcone et al [29]).

northern climates we find that mineralogy, porosity, free water content, and ionic concentration within the free water are important resistivity factors as they are for temperate zones. In permafrost regions we have the additional complexity that small changes in temperature of the ground near 0°C may exert a large influence on terrain conductivity. The effect depends on the nature of the material and also the moisture content since as we have seen earlier even at temperatures substantially below 0°C considerable moisture may remain unfrozen in the case of clays whereas in the case of coarser material virtually all will be frozen. In short, ice content is a complicated function of many variables.

As an example of electrical layering arising due to temperature only consider Figure 14 which illustrates annual variations in ground temperature recorded near Fairbanks, Alaska. The region is in a discontinuous permafrost zone and subsurface material consists primarily of perennially frozen organic silt containing a varying amount of ground ice. From laboratory measurements on saturated organic silt to determine the variation of electrical resistivity with temperature, a plot of electrical resistivity with depth and time was derived [23] and is shown in Figure 15. We see from this figure that a resistivity range of 50 to 1 can occur as a result of temperature changes alone.

In the discontinuous zone of permafrost subsurface temperatures are subtly influenced by many variables and even in ground which is
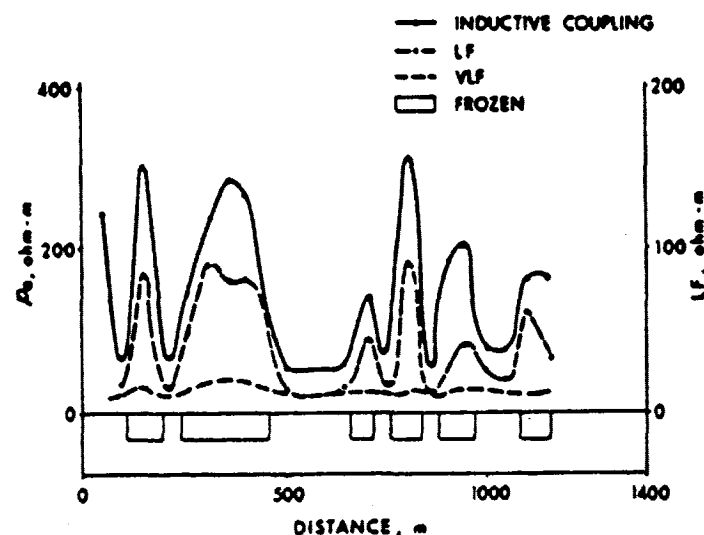
laterally uniform insofar as material type is concerned lateral temperature variations can bring about large changes in electrical resistivity as shown in Figure 16 where the survey traverse was taken over glacial lake basin sediments. The frozen areas outlined on the figure were derived from resistivity measurements and confirmed by drilling [24].

VI. SUMMARY

In this technical note we have discussed the concept of terrain conductivity, examined some of the properties of soils and rocks that affect their conductivity, and reviewed some measurements on typical terrain materials under a variety of climatic conditions.

To summarize, terrain conductivity is usually determined by one or more of the following parameters:

(1) clay content, clay type
(2) moisture profile with depth
(3) moisture salinity
(4) moisture temperature

Of these the most complex is usually the moisture profile, by which is meant the way in which (i) the porosity, (ii) the extent to which the pores are filled with water, and, (iii) the number, size and shape of interconnecting passages all vary with depth. The moisture profile is affected by material type (directly influencing porosity etc., or indirectly influencing permeability and water table location), topography (influencing the water table location), compaction (influencing porosity), and season (rates of precipitation, evaporation).

It is evident that many parameters may affect the ground conductivity. Fortunately at any given location relatively few are usually dominant however the survey interpreter should be aware of the possible alternatives. It is hoped that this brief treatment will be useful in assessing those parameters that are influential in the survey area and will thereby lead to a more accurate interpretation of survey data.

The bibliography gives a good indication of current interest in the electrical properties of rocks and soils and the curious reader will find much valuable material in the cited references.

BIBLIOGRAPHY

[1] Olhoeft, G.R. (1975) "Electrical Properties of Rocks". The Physics and Chemistry of Rocks and Minerals. pp 261-278. J. Wiley and Sons. N.Y.

[2] Olhoeft, G.R. (1977) "Electrical Properties of Natural Clay Permafrost". Can. J. Earth Sciences (14) pp 16-24.

[3] Ward, S.H., Fraser, D.C. (1967) "Conduction of Electricity in Rocks". Ch. 2. Mining Geophysics Vol. II. Society of Exploration Geophysicists, Tulsa, Oklahoma.

[4] Madden, T.R. (1976) "Random Networks and Mixing Laws". Geophysics (41, No. 6A) pp 1104-1125.

[5] Keller, G.V., Frischknecht, F.C. (1966) "Electrical Methods in Geophysical Prospecting". Ch. 1. Pergamon Press, N.Y.

[6] L.R. Webber, Ed. "Ontario Soils". Publication 492, Ministry of Agriculture and Food. Province of Ontario. Canada.

[7] Kirkham, D. (1964) "Soil Physics". Handbook of Applied Hydrology. Ch. 5. Chow, V.T., Ed. McGraw Hill, N.Y.

[8] Press, F., Siever, R. (1978) "Earth". Ch. 4. W.H. Freeman & Co., San Francisco.

[9] Maxey, G.B. (1964) "Hydrogeology". Handbook of Applied Hydrology. Ch. 4. Chow, V.T., Ed. McGraw Hill, N.Y.

[10] Millot, G. (1979) "Clay". Scientific American (240), 4, pp 109-118.

[11] Meyboom, P. (1967) "Hydrogeology". Groundwater in Canada. Ch. 2. Brown, I.C., Ed. Geol. Surv. Canada. Econ. Geol. Rept. 24.

[12] Todd, D.K. (1964) "Groundwater". Handbook of Applied Hydrology. Ch. 13. Chow, V.T. Ed. McGraw Hill, N.Y.

[13] Brown, I.C. (1967) "Introduction". Groundwater in Canada. Ch. 1. Brown, I.C., Ed., Geol. Surv. Canada. Econ. Geol. Rept. 24

[14] Heiland, C.A. (1968) "Geophysical Exploration". Ch. 10. Hafner Publishing Co. N.Y.

[15] Doherty, L.H. (1963) "Electrical Conductivity of the Great Lakes". J. Res. Natl. Bur. Stds. (67D), pp 765-771..

[16] Jackson, P.D., Taylor Smith, D., Stanford, P.N. (1978) "Resistivity –

FIGURE 16. Results of the apparent resistivity measured with VLF (18.6 kHz), LF (375 kHz) radiohm and a magnetic induction instrument (EM31) over a section of shallow discontinuous permafrost (after P. Hoekstra [30]).

Porosity – Particle Shape Relationships for Marine Sands". Geophysics (43) pp 1250–1268.

[17] Rhoades, J.D.; Raats, P.A.C.; Prather, R.S. (1976) "Effects of Liquid-Phase Electrical Conductivity, Water Content, and Surface Conductivity on Bulk Soil Electrical Conductivity". Soil Sci. Soc. of America Jour. (40) pp 651–665.

[18] Walker, J.W.; Hulse, W.H.; Eckart, D.W. (1973) "Observations of the Electrical Conductivity of the Tropical Soils of Western Puerto Rico". Geol. Soc. Amer. Bull. (84) pp 1743–1752.

[19] Olhoeft, G.R. Private Communication.

[20] Hoekstra, P.; McNeill, J.D. (1973) "Electromagnetic Probing of Permafrost". Proc. Second Intl. Conference on Permafrost. Yakutsk, USSR. pp 517–526.

[21] Grant, F.S.; West, G.F. (1965) "Interpretation Theory in Applied Geophysics". Ch. 13. McGraw Hill, N.Y.

[22] Telford, W.M.; Geldart, L.P.; Sheriff, R.E.; Keys, D.A. (1976) Applied Geophysics Ch. 5. Cambridge Univ. Press, N.Y.

[23] Culley, R.W.; Jagodits, F.L.; Middleton, R.S. (1975) "E-Phase System for Detection of Buried Granular Deposits. Symposium on Modern Innovations in Subsurface Exploration". 54th Annual Meeting of Transportation Research Board.

[24] Sellmann, P.V.; Arcone, S.A.; Delaney, A. (1976) "Preliminary Evaluation of New LF Radiowave and Magnetic Induction Resistivity Units – Over Permafrost Terrain". Natl. Res. Council Canada Tech. Mem. 119. Proc. Symposium on Permafrost Geophysics. 12 Oct.

[25] Smith-Rose, R.L. (1934) "Electrical Measurements on Soil with Alternating Currents". Proc IEE No. 75 pp 221–237.

[26] Meillon, J.J. (1978) "Economic Geology and Tropical Weathering". Can. Inst. Mining and Metallurgy (CIM) Bulletin, July, pp 61–69.

[27] Palacky, G.J.; Kadekaru, K. (1979) "Effect of Tropical Weathering on Electrical and Electromagnetic Measurements". Geophysics (44) pp 69–88.

[28] Rhoades, J.D.; Halvorson, A.D. (1977) "Electrical Conductivity Methods for Detecting and Delineating Saline Seeps and Measuring Salinity in Northern Great Plains Soils". Agricultural Research Service Dept. ARS W-42 U.S. Dept. of Agriculture. Western Region.

[29] Arcone, S.A.; Sellman, P.; Delaney, A. (1979) "Effects of Seasonal Changes and Ground Ice on Electromagnetic Surveys of Permafrost". USA CRREL Report. U.S.A. Cold Regions Research & Engineering Labs. Hanover, New Hampshire, U.S.A.

[30] Hoekstra, P. (1978) "Electromagnetic Methods for Mapping Shallow Permafrost". Geophysics (43) pp 782–787.

REFERENCES NOT CITED BUT USEFUL

[31] Morley, L.W., Ed. (1967) "Mining and Groundwater Geophysics". Geological Survey of Canada. Econ. Geol. Dept. No. 26.

[32] Wilcox, S.W. (1944) "Sand and Gravel Prospecting by the Earth Resistivity Method". Geophysics (9) pp 36–45.

[33] Kelly, S.F. (1962) "Geophysical Exploration for Water by Electrical Resistivity". Jour. New England Water Works Assoc. (76) pp 118–189.

Technical Note TN-6

ELECTROMAGNETIC TERRAIN

CONDUCTIVITY MEASUREMENT

at

LOW INDUCTION NUMBERS

JD McNEILL

October, 1980

Table of Contents

I. INTRODUCTION

The measurement of terrain resistivity to map geology has been utilized for over half a century. Several shortcomings, however, have prevented this technique from being widely accepted for engineering purposes. The first of these is that conventional galvanic resistivity surveys require a relatively large amount of manpower to execute and are thus expensive. Secondly, the actual value of resistivity itself is seldom diagnostic; it is the lateral or vertical variations of resistivity which form the basis of any interpretation. However the high cost of resistivity surveying generally means that fewer measurements are made than would be desirable, with the result that either (i) the survey area is not made large enough to establish a reasonable background against which the anomalous areas are to be delineated or (ii) the anomalous area itself is obscure and lacks definition.

An additional problem inherent to conventional resistivity techniques is that although the effective depth of exploration is determined by the selected inter-electrode spacing, resistive inhomogeneities which are small compared to this depth but which are located near the potential electrodes can cause a significant error in the measurement. Such fluctuations in the measured results are truly geological "noise" because it is not possible to determine the physical size, resistivity contrast, or location of the source. As a result of such inhomogeneities resistivity profiles carried out at constant interelectrode spacing tend to be noisy, limiting the resolution in resistivity that can be achieved, even though the instrumentation itself is capable of producing much higher accuracy.

It was an awareness of both the advantages of resistivity for engineering geophysical surveys and the disadvantages of conventional resistivity techniques that led Geonics Limited to examine the possibility of employing electromagnetic (inductive) techniques as an alternative for resistivity surveys. With the development of the EM31 and the EM34-3 it is now possible to map terrain conductivity virtually as fast as the operator(s) can walk; furthermore the sample volume is averaged in such a manner as to yield unexcelled resolution in conductivity.

These patented instruments have been designed to cover the range of depths generally useful for engineering geophysics; the EM31, one-man portable, has an effective depth of approximately 6 meters and the EM34-3, two-man portable, has stepwise selectable depths from 7.5 meters to a maximum of 60 meters.

Typical applications for the EM31 and EM34-3 instrumentation are:
  (i) Delineating regions of permafrost (frozen pore water)
  (ii) Locating gravel
  (iii) Extending known gravel deposits
  (iv) Mapping saline intrusions
  (v) Detecting cavities in carbonate rocks
  (vi) Mapping pollution plumes in groundwater
  (vii) Mapped bedrock topography
  (viii) Mapping terrain conductivity for electrical grounding
  (ix) General geological mapping (soil types, fault and fracture zones, etc.)
  (x) Archaeological exploration
  (xi) Locating pipes (EM31) and metallic-type conductors

This technical note describes both the principles and the instrumentation employed to measure terrain conductivity using electromagnetic techniques at low induction numbers. For a detailed discussion of the concept of terrain resistivity/conductivity and of the various factors that control this parameter the reader is referred to Geonics Limited Technical Note "Electrical Conductivity of Soils and Rocks".

II. PRINCIPLE OF OPERATION

The application of electromagnetic techniques to the measurement of terrain resistivity, or more properly, conductivity* is not

*Conductivity is preferred with inductive techniques since the response is generally proportional to conductivity and inversely proportional to resistivity.
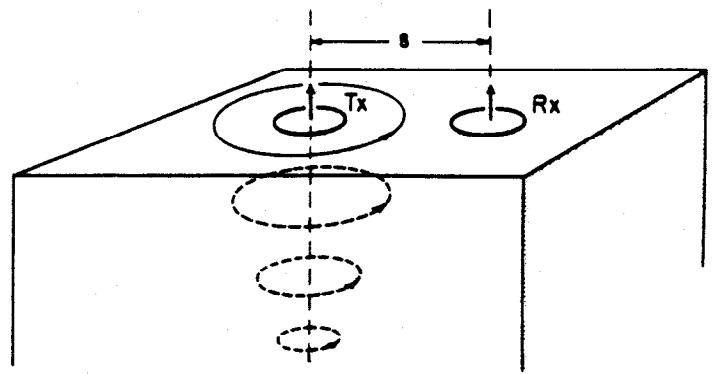
FIGURE 1. Induced current flow (homogeneous halfspace).

new and excellent descriptions of this technique are given in the literature [1], [2].

Consider Figure 1 in which a transmitter coil Tx energized with an alternating current at an audio frequency, is placed on the earth (assumed uniform) and a receiver coil Rx is located a short distance s away. The time-varying magnetic field arising from the alternating current in the transmitter coil induces very small currents in the earth. These currents generate a secondary magnetic field H_s which is sensed, together with the primary field, H_p, by the receiver coil.

In general this secondary magnetic field is a complicated function of the intercoil spacing s, the operating frequency, f, and the ground conductivity σ. Under certain constraints, technically defined as "operation at low values of induction number" (and discussed in detail in the appendix) the secondary magnetic field is a very simple function of these variables. These constraints are incorporated in the design of the EM31 and EM34-3 whence the secondary magnetic field is shown to be:

$$\frac{H_s}{H_p} \simeq \frac{i\omega\mu_o\sigma s^2}{4} \qquad (1)$$

where H_s = secondary magnetic field at the receiver coil
  H_p = primary magnetic field at the receiver coil
  ω = $2\pi f$
  f = frequency (Hz)
  μ_o = permeability of free space
  σ = ground conductivity (mho/m)
  s = intercoil spacing (m)
  i = $\sqrt{-1}$

The ratio of the secondary to the primary magnetic field is now linearly proportional to the terrain conductivity, a fact which makes it possible to construct a direct-reading, linear terrain conductivity meter by simply measuring this ratio. Given H_s/H_p the apparent conductivity indicated by the instrument is defined from equation (1) as

$$\sigma_a = \frac{4}{\omega\mu_o s^2}\left(\frac{H_s}{H_p}\right) \qquad (2)$$

The MKS units of conductivity are the mho (Siemen) per meter or, more conveniently, the millimho per meter.

III. INSTRUMENTATION

The EM31 (shown in Figure 2) has an intercoil spacing of 3.7 meters, which yields an effective depth of exploration of about 6 meters. The instrument can also be operated on its side, in which
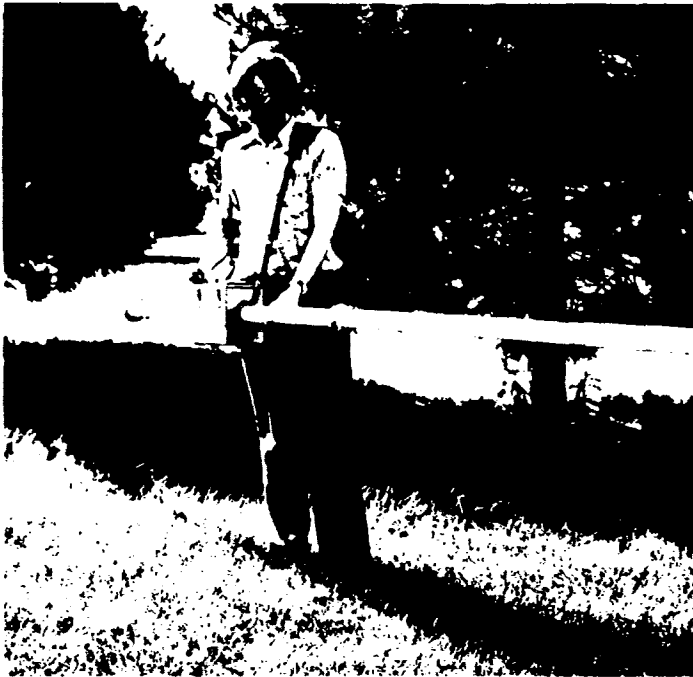
FIGURE 2. EM31 in field operation.

TABLE 1. Exploration depths for EM34-3 at various intercoil spacings

Intercoil Spacing (meters)	Exploration Depth (meters)	
	Horizontal Dipoles	Vertical Dipoles
10	7.5	15
20	15	30
40	30	60

To measure terrain conductivity the transmitter operator stops at the measurement station; the receiver operator moves the receiver coil backwards or forwards until his meter indicates correct intercoil spacing and he reads the terrain conductivity from a second meter. The procedure takes 10 to 20 seconds. The coils are normally carried with their planes vertical (horizontal dipole mode) since in this configuration the measurement is relatively insensitive to misalignment of the coils. In the event that the greater depth of penetration resulting when the two coils are in the vertical dipole mode is desired, more care must be taken with intercoil alignment. Because of the relatively short intercoil spacing correct alignment is usually not difficult to achieve.

Both instruments are calibrated to read terrain conductivity in millimhos per meter. To convert these readings to resistivity (in ohmmeters) one simply divides them into 1,000, i.e. 50 millimhos per meter is the equivalent of 20 ohmmeters.

case as will be seen in Section IV., the effective depth of exploration is reduced to approximately 3 meters. The instrument is one-man portable and can be used either in "station-by-station" mode or read continuously. The presence of layering in the earth can be detected by raising the instrument and noting the readings as a function of instrument height. If the earth is two-layered the conductivity of both layers and the upper layer thickness can be resolved.

The EM34-3 which is two-man portable has the two coils flexibly connected (Figure 3). The intercoil spacing is measured electronically so that the receiver operator simply reads a meter to accurately set the coils to the correct spacing, which can be 10, 20, or 40 meters so as to directly vary the effective depth of exploration as shown in Table 1.

IV. SURVEY TECHNIQUES AND INTERPRETATION

For either the EM31 or EM34-3 it can be shown that in a homogeneous or horizontally stratified earth the current flow is entirely horizontal. Furthermore under the constraints by which the instruments are designed the current flow at any point in the ground is independent of the current flow at any other point since the magnetic coupling between all current loops is negligible. Finally, under these constraints the depth of penetration is limited only by the intercoil spacing. We say that the depth of penetration is "source" or "geometry" limited rather than "skin depth" limited since it is now controlled by the fall-off with distance of the dipolar transmitter field. For this reason all dimensions are normalized with respect to the intercoil spacing in subsequent sections of this technical note.

IV. 1. Instrumental Response as a Function of Depth (Homogeneous Halfspace)

Consider a homogeneous halfspace on the surface of which is located an EM31 or an EM34-3 transmitter as shown in Figure 4. Fixing our attention on a thin layer of thickness dz at depth z (where z is the depth divided by the intercoil spacing s) it is possible to calculate the secondary magnetic field in the receiver coil arising from all of the current flow within this or any other horizontal thin layer. One can thus construct the function $\phi_V(z)$ shown in Figure 4 which describes the relative contribution to the secondary magnetic field arising from a thin layer at any depth z. We see from this figure that material located at a depth of approximately $0.4s$ gives maximum contribution to the secondary magnetic field but that material at a depth of $1.5s$ still contributes significantly. It is interesting to note that the ground at zero depth, i.e. the near surface material,

FIGURE 3. EM34-3 in field operation.
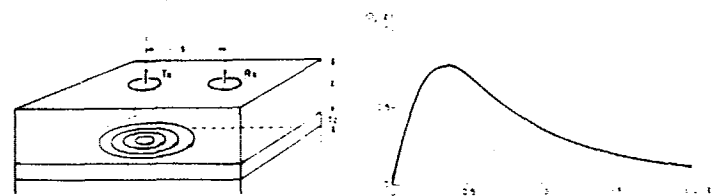
FIGURE 4. Relative response versus depth for vertical dipoles. $\phi_V(z)$ is the relative contribution to H_s from material in a thin layer dz located at (normalized) depth z.
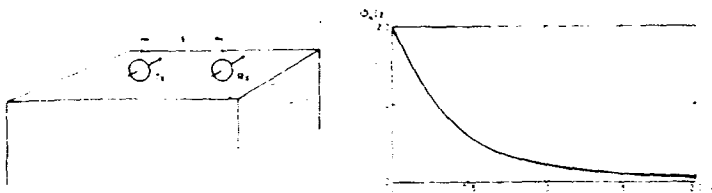
FIGURE 5. Relative response versus depth for horizontal dipoles

makes a very small contribution to the secondary magnetic field and therefore this coil configuration is insensitive to changes in near surface conductivity.

Figure 5 illustrates the function of Figure 4 for the case of both transmitter and receiver dipoles horizontal coplanar rather than vertical coplanar. For the coil configuration of Figure 5 (commonly used for the EM34-3 since it is less critical to intercoil alignment) the relative contribution from material near-surface is large and the response falls off monotonically with depth.

A comparison of the function ϕ for both coil configurations in Figure 6 emphasizes the different manner in which they respond to material at different depths. The difference is important since either instrument can be rolled over so that the vertical dipole transmitter/receiver geometry becomes a horizontal dipole transmitter/receiver geometry and vice versa. As will be seen later, this feature is useful in diagnosing and defining a layered earth. The figure also shows that for regions greater than one intercoil spacing in depth the vertical transmitter/receiver dipole gives approximately twice the relative contribution of the horizontal transmitter/receiver dipole.

To summarize, with either horizontal or vertical transmitter/receiver dipole orientation it is possible to construct a function which gives the relative response to the secondary magnetic field at the receiver from a thin layer of ground at any depth. That this is possible arises from the fact that (i) all current flow is horizontal and (ii) all current loops are independent of all other current loops. It should be noted that it is not possible to construct such functions for conventional resistivity techniques.

Finally, since as shown in Section II the definition of apparent conductivity is given in terms of the secondary magnetic field at the receiver, the functions in Figure 6 also give the relative contribution
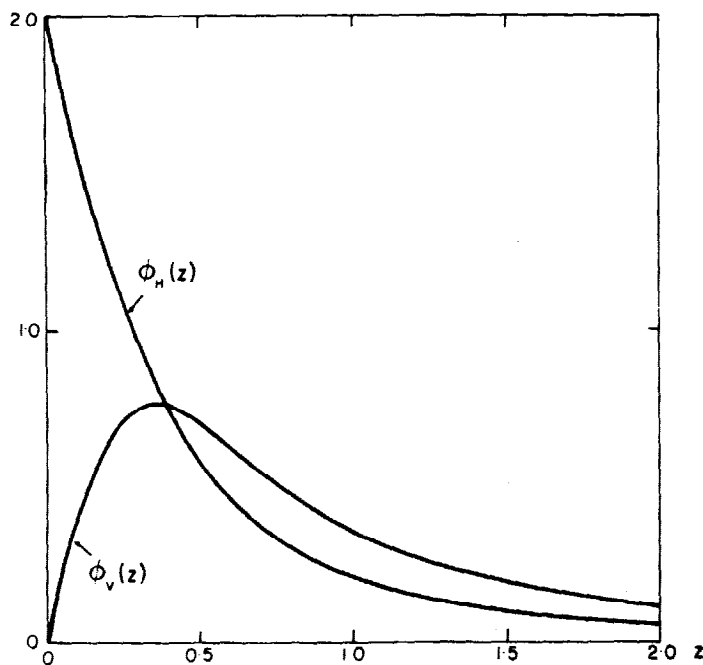
from material at different depths to the *apparent conductivity* indicated by the instrument meter. The integral of either function from zero to infinity gives the total secondary magnetic field at the receiver coil from a homogeneous halfspace which is directly related to the electrical conductivity of the halfspace by equation (1). It is therefore possible to state with great precision the relative influence of material at different depths to the indicated apparent conductivity.

IV. 2. Multi-Layered Earth Response

The functions shown in Figure 6 are useful for describing the relative sensitivity of either of the two coil configurations to material at various depths. However a function derived from them is more useful for performing calculations. It is defined as the relative contribution to the secondary magnetic field or apparent conductivity from all material below a depth z and is given by

$$R_V(z) = \int_z^\infty \phi_V(z)dz \qquad (3)$$

Called the cumulative response, this function is illustrated in Figure 7 for vertical coplanar transmitter/receiver dipoles. The figure shows, for example, that for this configuration all material below a depth of two intercoil spacings yields a relative contribution of approximately 0.25 (i.e. 25%) to the secondary magnetic field at the receiver coil.

Suppose now that our homogeneous halfspace has a conductivity of 20 millimhos per meter (50 ohmmeters). The equipment having been calibrated according to equation (2), the output meter indicates 20 millimhos per meter. From Figure 7 we observed that the material below two intercoil spacings contributed 25% to the secondary magnetic field and therefore 25% to the indicated meter reading. Suppose that we replace this deep material with an infinitely resistive (zero conductivity) substance. Since we have reduced to zero the 25% that this material contributed to the meter reading the new reading will be 75% of 20, or 15 millimhos per meter. Conversely, if we leave all of the material below two intercoil spacings at 20

FIGURE 6. Comparison of relative responses for vertical and horizontal dipoles.

$R_V(z)$
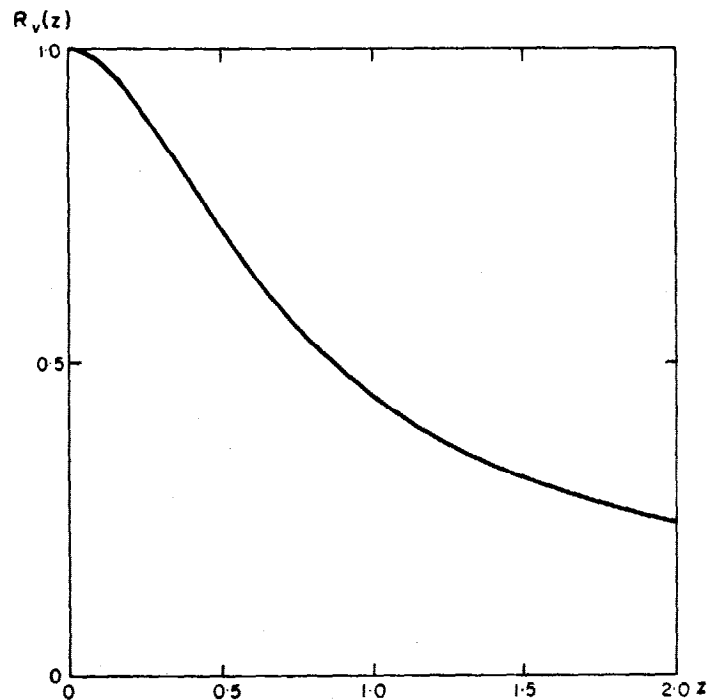
FIGURE 7. Cumulative response versus depth for vertical dipoles. $R_V(z)$ is the relative contribution to H_s from all material below a (normalized) depth z.

7
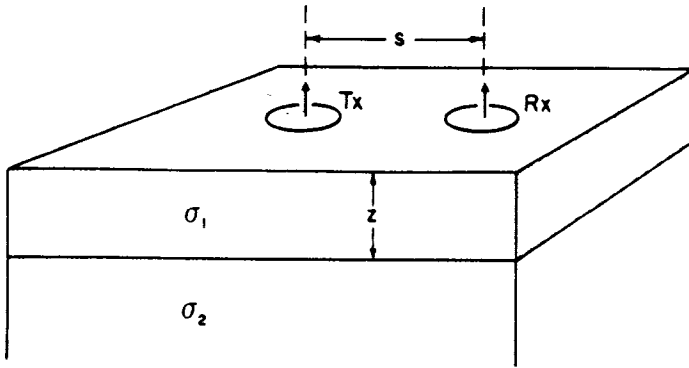
FIGURE 8. Two layer earth model.

millimhos per meter but make all material above two intercoil spacings infinitely resistive the meter reading will fall from the original 20 millimhos per meter for the homogeneous half space to 5 millimhos per meter, since, if all of the material below two intercoil spacings contributed 25% of the meter reading, all of the material above two intercoil spacings must contribute 75%; when removed the meter reading becomes 0.25 × 20 or 5 millimhos per meter.

From this example we see that there is a simple way to calculate the instrument reading on an arbitrarily layered earth as long as the intercoil spacing is much less than the skin depth in all of the layers. We simply add the contribution from each layer independently, weighted according to its conductivity and depth according to Figure 7. For example assume that we have a two-layer case as shown in Figure 8. The contribution from the upper layer is given by

$$\sigma_a = \sigma_1[1 - R_V(z)] \tag{4a}$$

since all of the material below zero depth yields a relative contribution of unity or 100% to the meter reading. Conversely all of the material in the lower layer adds a contribution given by

$$\sigma_a = \sigma_2 R_V(z) \tag{4b}$$

and the actual instrument reading will therefore be the sum of these two quantities

$$\sigma_a = \sigma_1[1 - R_V(z)] + \sigma_2 R_V(z) \tag{5}$$

If the earth is three-layered as shown in Figure 9 the same procedure is employed to determine the instrumental response. In this example the calculations are performed for different middle layer thicknesses.

$\sigma_1 = 20\,mS/m$ z_1 $z_1 = 0.5$

z_2 $z_2 = 1.0,\ 1.5$

$\sigma_2 = 2\,mS/m$

$\sigma_1 = 20\,mS/m$
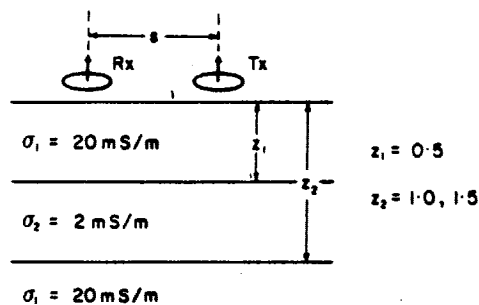
$\sigma_a = \sigma_1[1-R(z_1)] + \sigma_2[R(z_1)-R(z_2)] + \sigma_3 R(z_2)$

$z_2 = 1.0,\quad \sigma_a = 20[1-0.70] + 2[0.70-0.44] + 20 \times 0.44 = 15.3\,mmho/m$

$z_2 = 1.5,\quad \sigma_a = 20[1-0.70] + 2[0.70-0.32] + 20 \times 0.32 = 13.2\,mmho/m$

FIGURE 9. Calculation of response to three layer earth – center layer thickness varying.

The ease with which such calculations are performed facilitates survey preparation and interpretation. It is sometimes possible to make advance estimates of the electrical properties of the materials to be encountered during a survey or, alternatively, once on-site the operator can obtain the same information from sample measurements of the different materials. The procedures outlined above are then employed to estimate the apparent conductivity measured under various terrain conditions. Examples of such calculations for the EM31 are shown in Figure 10. As is seen in the appendix the algebraic expressions for $\phi(z)$ and $R(z)$ are very simple and are easily programmed on hand held calculators.

In Figure 10 the vertical dimensions are greatly exaggerated with respect to the horizontal dimensions. The question arises as to what degree of lateral uniformity is required before the earth can be considered as horizontally stratified or homogeneous. Survey experience indicates that if the ground conductivity does not significantly vary with horizontal distance within a radius of one intercoil spacing from the instrument the ground can be considered to be laterally uniform.

The above discussion referred to the use of vertical transmitter/receiver dipoles; it is equally possible to construct a cumulative response function for the horizontal coplanar dipole configuration and Figure 11 illustrates this function for both coil configurations. A comparison of the two curves illustrates that the vertical dipole mode of operation has approximately twice the effective exploration depth of the horizontal dipole mode.

IV. 3. Comparison with Conventional Resistivity Techniques

Many readers will be familiar with the two-layer curves employed to interpret data from conventional resistivity surveys using a Wenner array of four equally spaced electrodes. Using the techniques described in the previous section it is a simple matter to calculate two-layer curves for the electromagnetic technique; Figure 12 shows such curves for both the vertical and horizontal dipole configurations superimposed on standard Wenner curves. The general shape is similar but there are marked differences in detail. For vertical coplanar transmitter/receiver dipoles we see that when the substrate is the more resistive the response of the two systems is similar; however when the substrate is the more conductive the electromagnetic technique sees deeper in that the influence of the substrate, for a given conductivity contrast, is felt at smaller intercoil spacing than inter-electrode spacing. This is a general characteristic of electromagnetic systems which prefer to look through an insulator to a conductor rather than through a conductor to an insulator.

For the horizontal dipole configuration if the lower layer is the more resistive the effective exploration depth of the inductive technique is slightly less than the Wenner array; however, once again, in the case where the lower layer is the more conductive the exploration depth of the inductive technique is substantially greater.

IV. 4. Resolution of Two-Layered Earth by Varying Intercoil Spacing

The principal advantage of the inductive electromagnetic technique over conventional resistivity lies in the speed and accuracy with which lateral changes of terrain conductivity can be measured. However this technique can also be used to measure the vertical variation of conductivity by expanding the intercoil spacing in a manner analogous to that in which the electrode spacing is expanded in conventional resistivity sounding techniques. The current state-of-the-art, however, is such that relatively few intercoil spacings can be employed; for example the EM34-3 can be operated with an intercoil spacing of 10, 20 or 40 meters. This feature is somewhat mitigated by the fact that the instruments can be used in either the vertical or horizontal dipole modes which, as shown in a previous section, exhibit different sensitivity to various depths thus yielding more information than would be available by simply using three spacings with one coil orientation.

To interpret a two-layer geometry the two-layer curves for both dipole configurations are superimposed on a common plot as shown

CROSS-SECTIONS

BURIED RIVER VALLEY

Till $\sigma_1 = 8\,mmho/m$

Shale $\sigma_2 = 40\,mmho/m$

Z_1
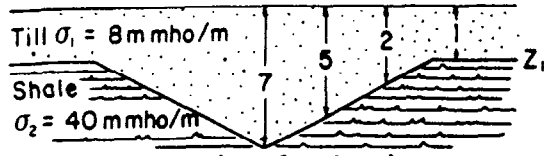
$$\frac{\sigma_a}{\sigma_1} = 1 - R(Z_1) + k_2 R(Z_1)$$

$$k_2 = \frac{\sigma_2}{\sigma_1} = \frac{40}{8} = 5$$

Z_1 (m)	σ_a (mmho/m)
1	32·6
2	26·9
5	18·6
7	16·0

BEDROCK HIGH

Muskeg 30 mmho/m

Bedrock 0·1 mmho/m
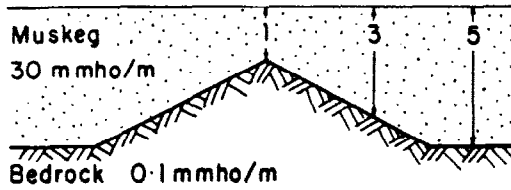
$$\frac{\sigma_a}{\sigma_1} = 1 - R(Z_1) + k_2 R(Z_1)$$

$$k_2 = \frac{\sigma_2}{\sigma_1} = \frac{0·1}{30} = 0·0033$$

Z_1 (m)	σ_a (mmho/m)
1	6·9
3	15·9
5	20·1

GRAVEL DEPOSIT

A   B   C   D

Till 10 m mho/m

Gravel 1 mmho/m
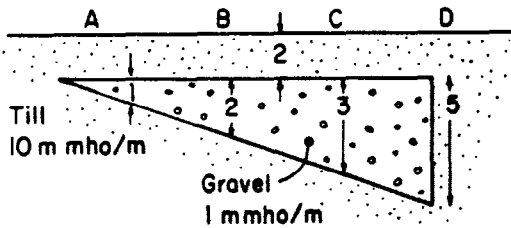
$$\frac{\sigma_a}{\sigma_1} = 1 - R(Z_1) + k_2[R(Z_1) - R(Z_2)] + k_3 R(Z_2)$$

$$k_2 = \frac{\sigma_2}{\sigma_1} = \frac{1}{10} = 0·10$$

$$k_3 = \frac{\sigma_3}{\sigma_1} = 1·00$$

station	σ_a (mmho/m)
A	8·9
B	8·2
C	7·7
D	6·9

FIGURE 10. EM31 calculated response across various geological features, using R (Z) corrected for instrument operation at waist (1 meter) height. Coil separation s = 3.67 meters.
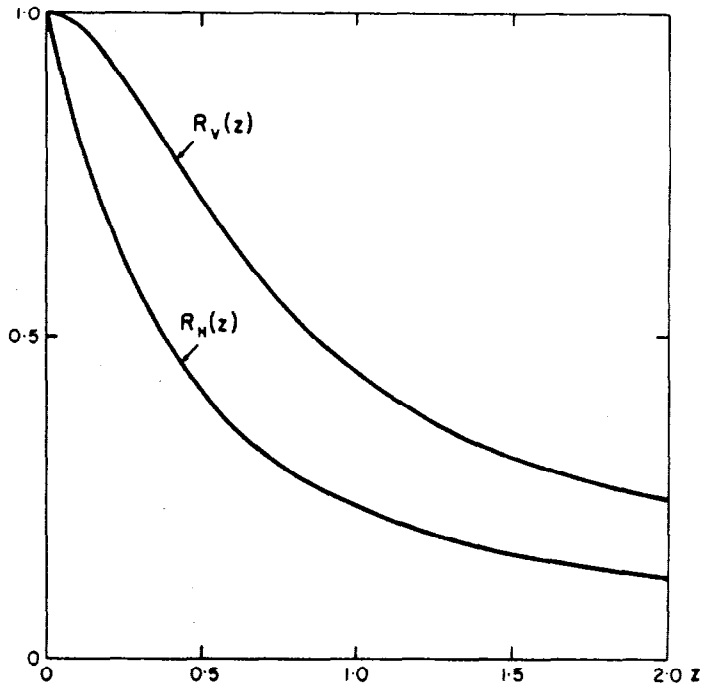
FIGURE 11. Cumulative response versus depth for vertical and horizontal dipoles.
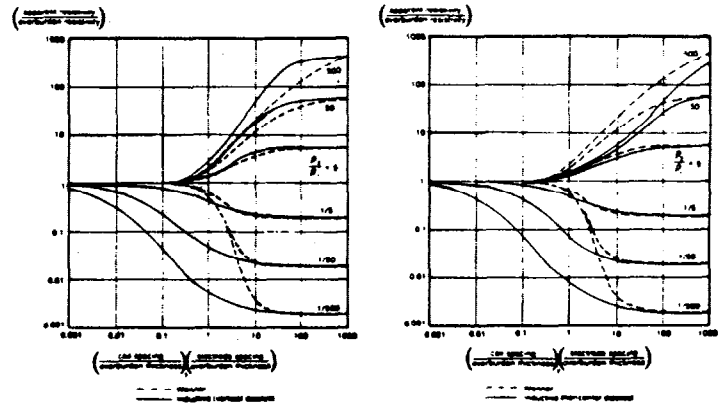
FIGURE 12. Comparison of Wenner array and inductive electromagnetic sounding curves for a two layer earth.
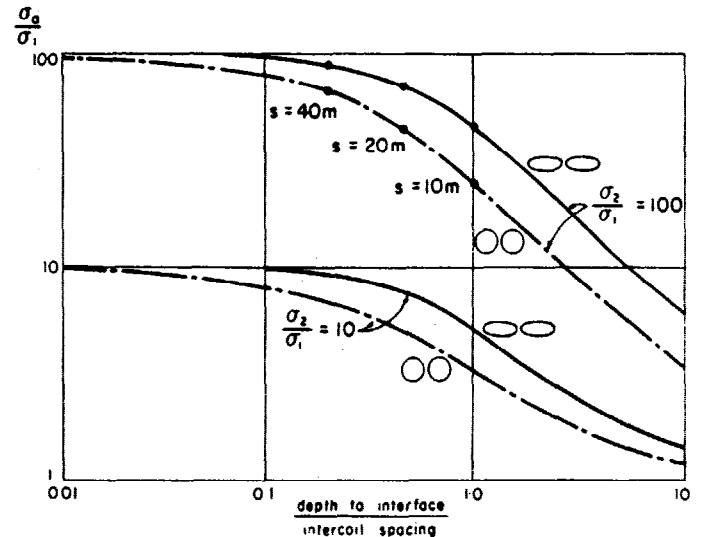
FIGURE 13. Two layer earth response curves (σ_2/σ_1 = 10,100; intercoil spacing varied). Dots indicate typical survey results.

9

in Figure 13. The six data points obtained by making measurements with two coil orientations and three intercoil spacings are plotted to the same scale on a piece of transparent paper and are translated vertically and horizontally on the two-layer curves to ascertain whether a satisfactory fit can be achieved. In the event that such a fit can be made. the earth does exhibit two-layer characteristics and the values of conductivity for both layers and the thickness of the upper layer are directly read off.

IV. 5. Resolution of Two-Layered Earth by Varying Instrument Height

In the case of the EM31 the intercoil spacing is rigidly fixed so that the technique described above is not available to analyse a layered earth. It is. however. possible to raise the instrument above the ground. measuring the apparent conductivity as a function of instrument height for both the vertical and horizontal dipole configurations. This has the effect of shifting the response curves of Figure 6 upwards through the various regions of the earth and the variation of apparent conductivity with height is therefore of diagnostic value in determining the nature of any layering. It is a straightforward matter to calculate the response of the instrument as a function of height for various two-layered earth geometries and typical curves are shown in Figure 14b. To use the curves one simply plots the measured apparent conductivity versus height for both coil configurations on a piece of transparent paper to the same scale as Figure

(a)

(b)

(c) Case history .....

Interpreted results $t_1 = 1m$, $\sigma_1 = 0.30\, m\, mho/m$

$\sigma_2 = 30\, m\, mho/m$
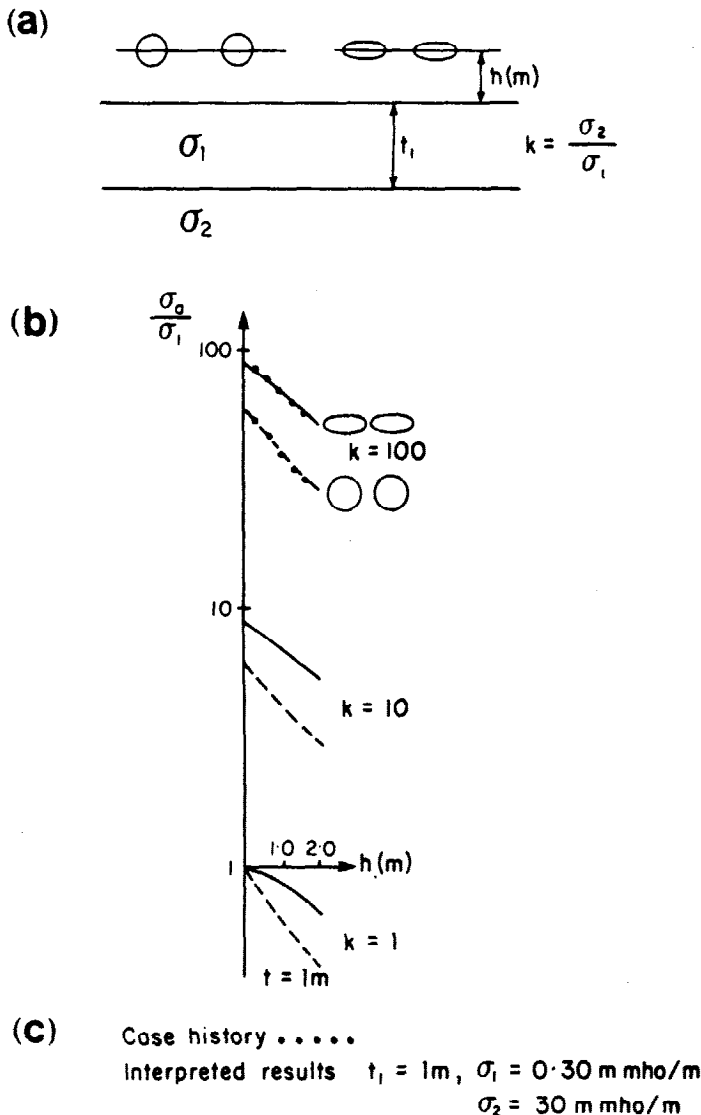
FIGURE 14. Two layer earth response curves $(\sigma_2/\sigma_1 = 1, 10, 100$: instrument height varied). Dots are actual survey results.

14b and shifts the plotted data vertically until good agreement is achieved with one of the curves. whereupon the two conductivities and the upper layer thickness are immediately determined as in the illustrated case history of Figure 14c.

In the event that the conductivity of either one of the two layers is known to be much less than the other. so that its contribution to the meter reading is negligible. it is simply necessary to lay the instrument on the ground. take a reading. lay it on its side. take a second reading. and from these two values one can immediately calculate the conductivity of the more conductive layer and the thickness of the upper layer.

V. ADVANTAGES AND DISADVANTAGES OF INDUCTIVE TERRAIN CONDUCTIVITY MEASUREMENTS

V. 1. Advantages

The advantages of the use of inductive electromagnetic techniques to measure terrain conductivity are as follows:

(i) *Excellent resolution in conductivity*. It was stated in Section I that a problem with conventional resistivity was that the presence of localized resistivity inhomogeneities near the potential electrodes caused large errors. If we examine the current flow in a homogeneous halfspace for the inductive technique described herein we realize that in the vicinity of the transmitter the current density is very high and we might expect the presence of a conductive inhomogeneity located here to have a large effect. However where the current density is high. the radius of the current loops is small and their distance from the receiver coil large. so that these loops do not couple well magnetically with the receiver. The effect of changing this current by varying the local conductivity is consequently negligible. The lateral extent of the volume of earth whose conductivity is sensed by the inductive technique is approximately the same as the vertical depth. The result is that small changes in conductivity. for example of the order of 5% or 10%. are easily and accurately measured.

(ii) *No current injection problems*. Since currents are magnetically induced in the earth. current injection problems encountered with conventional resistivity in materials such as gravel. bedrock. permafrost. snow and ice. etc.. are not encountered with this type of instrumentation.

(iii) *Simple multi-layered earth calculations*. This matter is dealt with at length in Section IV.

(iv) *Easy. rapid measurements*. A problem with the conventional Wenner array is that in order to survey to an effective depth a the array must be 3a in length and the total length of wire required 4a. used in four sections. This presents many opportunities for snagging and breaking the wire. Furthermore each measurement requires insertion of four electrodes and relatively careful measurement of the inter-electrode spacing. These features are avoided with the inductive electromagnetic techniques and it is no exaggeration to say that a survey can often be carried out five to ten times faster using this technique. Indeed with either the EM31 or the EM34-3 it is usually possible under average terrain conditions to survey 5 to 7 line-kilometers a day with a station spacing of 25 or 50 meters.

V. 2. Disadvantages

As with all geophysical instruments. there are some limitations and disadvantages to the use of inductive electromagnetic techniques and these are as follows:

(i) *Limited dynamic range (1 – 1000 mmhos per meter)*. At low values of terrain conductivity it becomes difficult to magnetically induce sufficient current in the ground to produce a detectable magnetic field at the receiver coil. Conversely at high values of conductivity the quadrature component of the received magnetic field is no longer linearly proportional to terrain conductivity as is shown in the appendix.

(ii) *Setting and maintaining the instrument zero*. Ideally in order to set the zero the instrument would be suspended in free space

and the zero set there. The more acceptable alternative is to search out a region of very resistive ground, to accurately measure its conductivity using conventional techniques, and to set the instrumental zero at that location. This is the procedure which is actually followed.

It is necessary that this zero be accurately maintained over long periods of time and over the wide variations of temperature encountered during geophysical survey in various parts of the world. This produces tight constraints on the circuitry, with the result that the zero may be in error by up to ±0.2 mmhos per meter. Such an error would be negligible over the usual range of terrain conductivities; however in the event that measurements are being made on highly resistive ground the zero error can become significant.

(iii) *Limited Vertical Sounding Capability*. In theory it is possible to use a system such as the EM34-3 at a continuum of intercoil spacings to yield more information about electrical layering in the ground. To achieve a wide variety of inter-electrode spacings with conventional resistivity equipment is simple; in the case of the inductive electromagnetic technique the rapid fall-off of the magnetic field from the dipole transmitter introduces a serious dynamic range problem. In due course there will undoubtedly be instrumentation with a wider variety of spacings at the expense of additional complexity.

VI. CASE HISTORIES

This section describes several case histories obtained with the EM31 and the EM34. The surveys (i) illustrate the resolution in conductivity that can be achieved, (ii) compare the results obtained with conventional resistivity and (iii) illustrate the use of the latter for locating sand, gravel and conductive minerals, determining bedrock topography (including locating a buried river channel) and mapping the pollution plume from a land-fill site. In some cases the indicated conductivity has been converted to resistivity to facilitate comparison with conventional resistivity survey results.

Case History #1

Location: Mississauga, Ontario
Instrument: EM31
Application: Illustrates resolution and repeatability of EM31

For this case history a Rustrak chart recorder was used to monitor the output of an EM31. A line of length 200 meters was traversed in a field in both easterly and westerly directions. Figure 15 demon-
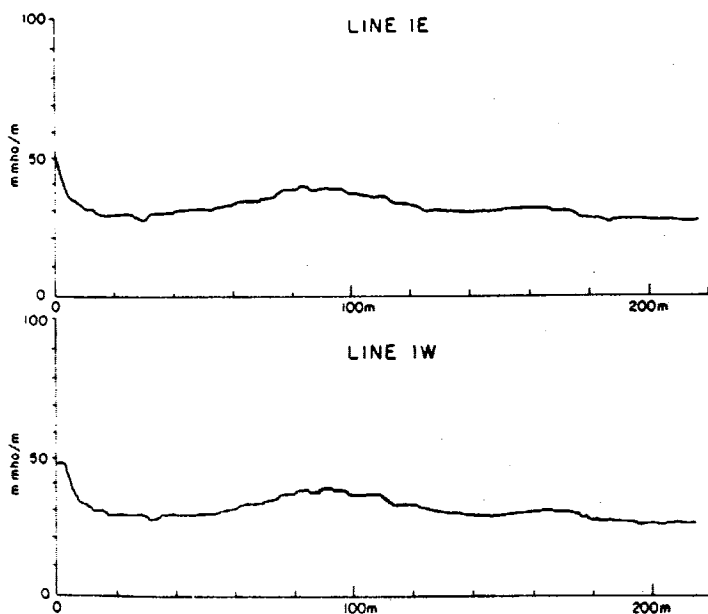
FIGURE 15.
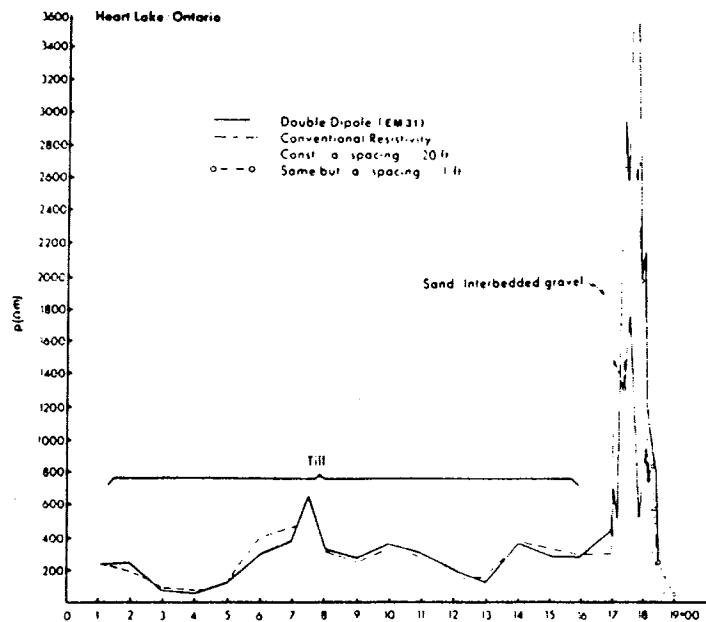
FIGURE 16.   Test survey line – Heart Lake, Ont.

strates that the instrument is resolving conductivity changes of less than 1 mmho/m (1% of full scale deflection) and that the repeatability is of the same order. In fact the repeatability is limited in this case by the resolving power of the chart recorder itself. It should furthermore be noted that the instrument is detecting spatial changes in conductivity of a few meters in length – compatible with the intercoil spacing of 3.7 meters.

Case History #2

Location: Hearth Lake, Ontario
Instruments: EM31
                      Conventional resistivity apparatus
Application: Location of sand/gravel
                      Comparison of EM31 and conventional resistivity

In this survey a line 1900 ft. (580 meters) in length was surveyed with a measurement interval of 100 ft. (30 meters). The survey area was generally located on a buried esker, however the last few survey stations, 17 + 00 to 19 + 00, traversed a region of exposed sand and gravel (often occurring in the form of concretions) and over this portion of the line measurements were made every 10 ft. (3.0 meters).

The conventional resistivity profile was carried out using a Wenner array with an a spacing of 20 ft. (6.1 meters) except between stations 17 + 00 and 19 + 00 where the a spacing was reduced to 1 ft. (0.30 meters).

In general the correlation between the two sets of data is excellent, and demonstrates the ability of the EM31 to generate good quantitative data even in regions of low conductivity. Over the esker the EM31 was actually read continuously down the line – the data was recorded only at the 100 ft. intervals, with the exception of the reading at station 7 + 50 which was also recorded since it was noted that a conductivity low occurred there. Such an anomaly was, of course, missed by the conventional resistivity where measurements were only made every 100 ft.

Both sets of data become rather erratic between stations 17 + 00 and 19 + 00 as a result of the very rapid lateral changes in resistivity arising from the concreted material referred to above.

Case History #3

Location: Cavendish, Ontario.
Instrument: EM31
Application: Location of metallic type conductors

This survey line, of length 2000 ft. (610 meters), is located at a site
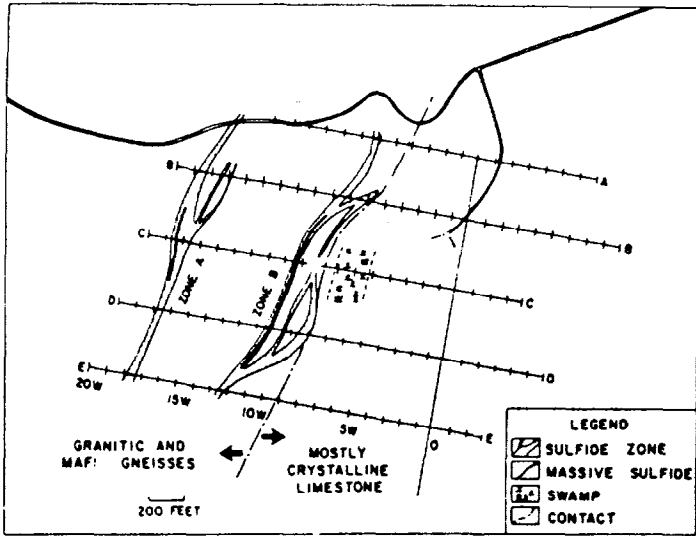
FIGURE 17. Geologic map of the Cavendish test site and the grid of traverse lines used in geophysical studies (after Ward et al [3]).
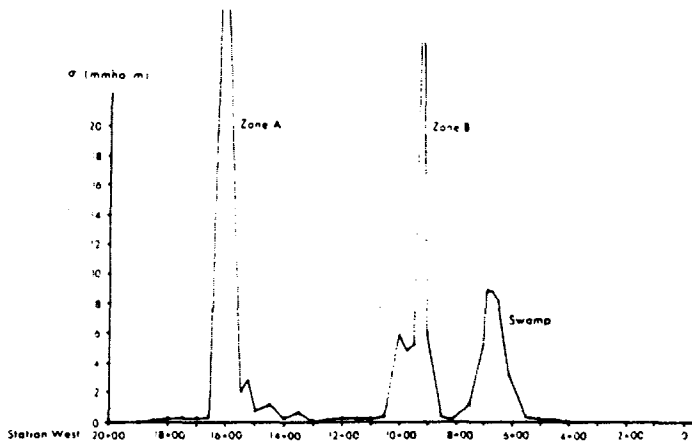
FIGURE 18. EM31 survey of Cavendish test range Line 'C'.

FIGURE 19. EM31 and EM34 survey line over preglacial river valley, Mississauga, Ontario.

in Ontario which is often used by Canadian instrumentation manufacturers to test new electromagnetic geophysical equipment. The survey, along line C, illustrates response from both the swamp and the two zones of metallic mineralization. Although measurements were only taken every 50 ft. (15 meters) both zones are well delineated and when such high responses are encountered localization to within a few meters is quickly and easily carried out.

Inasmuch as the EM31 and EM34-3 were designed to map terrain conductivity at the conductivity levels encountered in typical soils both instruments are extremely sensitive electromagnetic detectors. For example on the most sensitive scale, full scale deflection for the EM31 is 800 ppm of the primary magnetic field and for the EM34-3 it is 3800 ppm. Such sensitivity makes either instrument useful for detecting metallic type conductors at what are very low conductivity levels by normal standards.

Case History #4

Location: Mississauga, Ontario
Instruments: EM31, EM34
Application: Determination of bedrock topography

Total line length for this survey was 8400 ft. (2600 meters) and measurements were made every 100 ft. (30 meters) with both the EM31 and the EM34 – an earlier version of the EM34-3 which had two intercoil spacings vis. 100 ft. (30 meters) and 50 ft. (15 meters). The survey was performed to outline the cross-sectional profile of a

buried preglacial river valley whose existence had been suggested from water-well data. At either intercoil spacing the time required for the EM34 profile was 1-1/2 hours, resulting in approximately one survey measurement per minute – including the time to walk the 100 feet between measurement stations. The time taken for the subsequent EM31 survey was similar.

Typical bedrock conductivity in the area is approximately 30 mmho/m, whereas an average value for the conductivity of the infilling glacial till is of the order of 8 to 12 mmho/m. Thus the EM34 at either intercoil spacing yields approximately 30 mmho/m at the valley edges where the overburden is thin and 12 to 14 mmho/m at the valley centre. The EM31 yields values of 14 to 18 mmho/m at the valley edges (slightly affected by the presence of bedrock) and approximately 10 mmho/m at the valley centre. The interpreted depth of the valley, based on the model shown in the figure, is approximately 120 feet (36 meters) which is in reasonable agreement with the water-well data value of 150 feet (45 meters), bearing in mind that the three sets of data show that a two-layer model is an over simplification.

The conductivity high which occurs between stations 32 and 38 results from a very large pile of waste furnace ash lying on the surface.

Case History #5

Location: Camp Borden, Ontario
Instruments: EM31, EM34
Conventional resistivity apparatus
Application: Mapping groundwater salinity
Comparison of EM34 and conventional resistivity

Geophysical surveys were carried out over a sanitary landfill site using, in addition to other instruments, an EM31, EM34 and conventional resistivity [4]. The survey results in the accompanying figures illustrate the good agreement between these techniques and also indicate the reduction in survey time achieved using inductive electromagnetic techniques. Particularly interesting are the vertical variations in resistivity as shown by the EM31 at 3.7 m intercoil spacing and the EM34 at 15 and 30 m spacing.

VII. SUMMARY

This technical note describes in detail the principles of mapping the electrical conductivity of the ground using magnetically induced
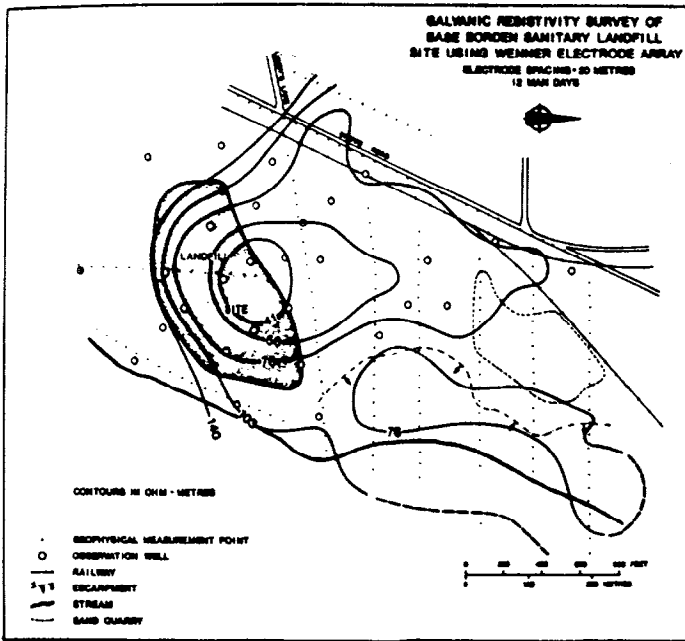
FIGURE 20(a).
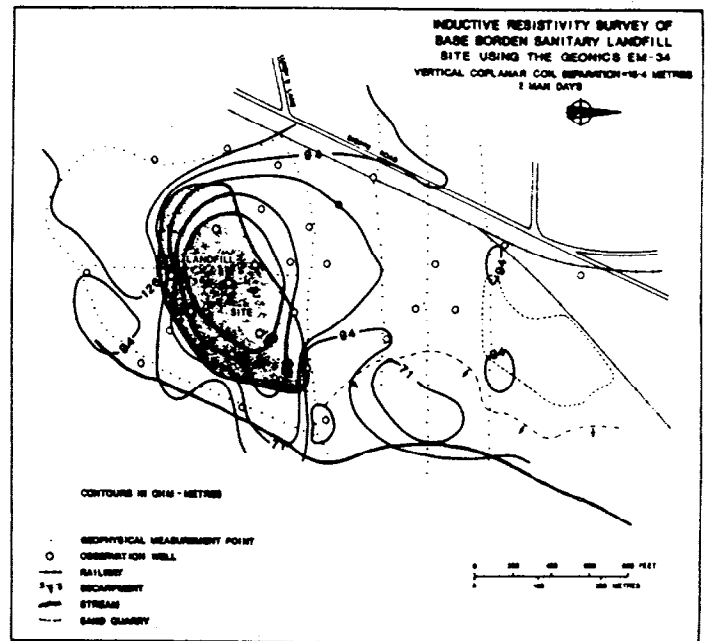
FIGURE 20(c).
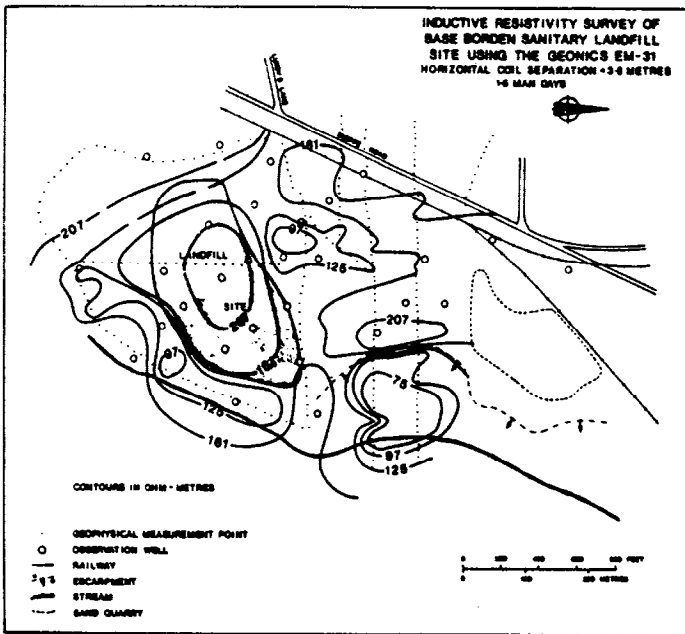
FIGURE 20(b).
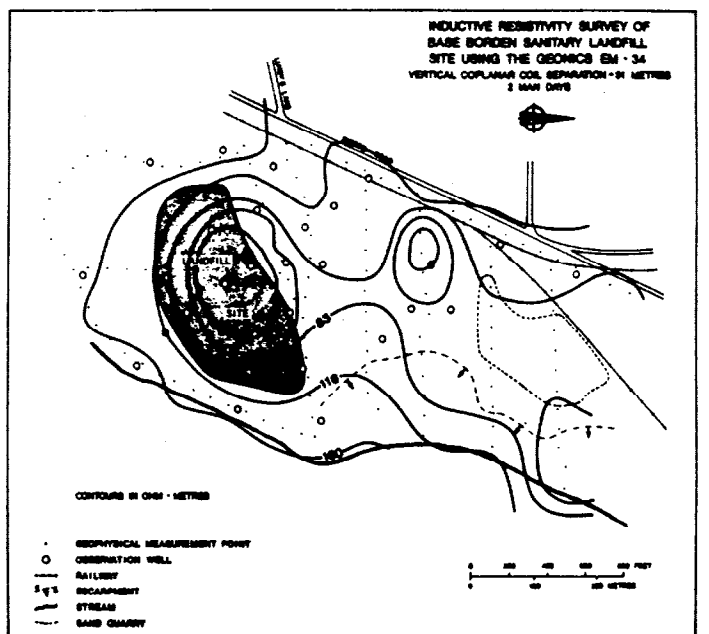
FIGURE 20(d).

currents at low frequencies. It has been shown that certain advantages can be derived from working at low values of induction number. Amongst these are excellent resolution in conductivity, a substantial reduction in man-hours necessary to carry out a conductivity survey and a simplification in the calculation of layered earth response.

Two points should be kept constantly in mind when performing surveys of this type to map geology. The first is that these instruments map only the electrical conductivity. If the conductivity does not vary significantly with the geological environment, or if parameters other than the geology also influence the conductivity, the survey results may be difficult to interpret.

The second point is that measurement of terrain conductivity, like any other geophysical measurement, must begin and end with geology. Such measurements are only an aid to help visualize geological conditions which cannot be seen. It is always necessary to interpret

geophysical data against known geology from out-crops, boreholes, or any other such "bench marks". Geophysical measurements can be very effective by allowing interpolation between such sources, or extrapolation away from them. However in every case knowledge derived from geophysical measurements must be eventually reconfirmed against known geological conditions.

BIBLIOGRAPHY

(1) Keller, G.V., Frischknecht, F.C. Electrical Methods in Geophysical Prospecting. Pergamon Press 1966.

(2) Wait, J.R. 1962. A Note on the Electromagnetic Response of a Stratified Earth. Geophysics V.27. pp 382-85.

(3) Ward, S.H.; Pridmore, D.F.; Rijol, Glenn W.E. Multispectral Electromagnetic Exploration for Sulphides. Geophysics Vol. 39 No. 5 p. 666. 1974.

(4) Survey carried out by Dr. J. Greenhouse, University of Waterloo, Waterloo, Ontario.
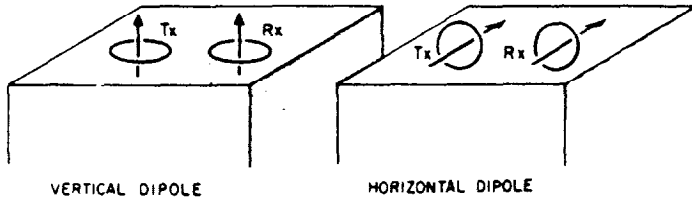
FIGURE A1. Vertical and horizontal dipole coil configurations.

APPENDIX: Theory of Operation at Low Induction Numbers

Consider the two coil configurations shown in Figure A1. In each case the transmitter coil is energized with alternating current at a frequency f Hertz. The measured quantity is the ratio of the secondary magnetic field H_s at the receiver when both coils are lying on the surface of the homogeneous half-space of conductivity σ to the primary magnetic field H_p in the absence of the half-space (i.e. as if the coils were in free space). The spacing between the coils is s meters.

The field ratios for vertical and horizontal dipole configurations are given by equations (1) and (2) respectively.

$$\left(\frac{H_s}{H_p}\right)_v = \frac{2}{(\gamma s)^2} \{9 - [9 + 9\gamma s + 4(\gamma s)^2 + (\gamma s)^3] e^{-\gamma s}\} \quad (1)$$

$$\left(\frac{H_s}{H_p}\right)_H = 2\left[1 - \frac{3}{(\gamma s)^2} + [3 + 3\gamma s + (\gamma s)^2] \frac{e^{-\gamma s}}{(\gamma s)^2}\right] \quad (2)$$

where $\gamma = \sqrt{i\omega\mu_0\sigma}$
$\omega = 2\pi f$
f = frequency (Hz)
μ_0 = permeability of free space
$i = \sqrt{-1}$.

These expressions are complicated functions of the variable γs which is in turn a reasonably complicated (complex) function of frequency and conductivity. However, as will be shown below, under certain conditions they can be greatly simplified.

A well known characteristic of a homogeneous half-space is the electrical skin depth δ, which is defined as the distance in the half-space that a propagating plane wave has travelled when its amplitude has been attenuated to $1/e$ of the amplitude at the surface. The skin depth is given by

$$\delta = \sqrt{\frac{2}{\omega\mu_0\sigma}} = \frac{\sqrt{2i}}{\gamma} \quad (3)$$

and therefore

$$\gamma s = \sqrt{2i}\,\frac{s}{\delta} \quad (4)$$

The ratio s/δ, the intercoil spacing divided by the skin depth, is defined as the induction number B, whereupon

$$\gamma s = \sqrt{2i}\, B \quad (5)$$

Now if B is much less than unity (ie $\gamma s \ll 1$) it is a simple matter to show that the field ratios of equations (1) and (2) reduce to the simple expression

$$\left(\frac{H_s}{H_p}\right)_v \simeq \left(\frac{H_s}{H_p}\right)_H \simeq \frac{iB^2}{2} = \frac{i\omega\mu_0\sigma s^2}{4} \quad (6)$$

which is the equation given in Section II.

The magnitude of the secondary magnetic field is now directly proportional to the ground conductivity and the phase of the secondary magnetic field leads the primary magnetic field by 90°.
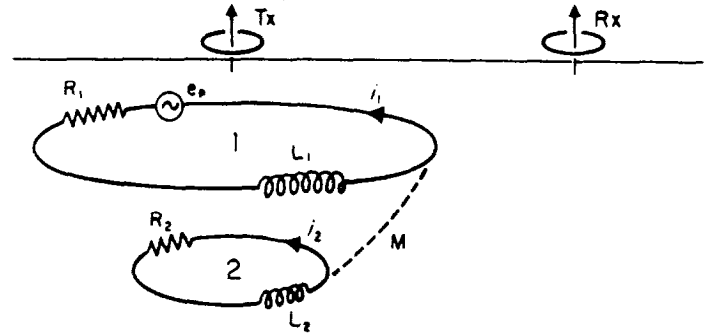
FIGURE AII. Electrical model for vertical dipoles.

To make B much less than unity we see that we must make s very much less than δ and thus

$$\omega \ll \frac{2}{\mu_0\sigma s^2} \quad (7)$$

That is, having decided on a value for s (which fixes the effective depth of penetration under the condition $B \ll 1$), the maximum probable ground conductivity is estimated and the operating frequency is chosen so that equation (7) is always satisfied.

The apparent conductivity which the instrument reads is then defined by

$$\sigma_a = \frac{4}{\omega\mu_0 s^2} \left(\frac{H_s}{H_p}\right)_{\substack{\text{quadrature} \\ \text{component}}} \quad (8)$$

To examine the reasons for this simplification let us focus our attention on the vertical dipole coil configuration shown in Figure AII since symmetry makes this configuration the simplest to understand.

Consider current loop 1. The primary emf e_p causing this current to flow is given (through Faraday's law) by the time rate of change of the primary magnetic flux from the transmitter through this loop. Three impedances cause the current to be limited. These arise from (i) the electrical resistance R_1 of the loop, (ii) the fact that the current i_1 generates its own magnetic field which causes a time-varying secondary magnetic flux through the loop (self-inductance, L_1), and (iii) the fact that all other current loops such as i_2 generate their own magnetic fields which in turn cause a time-varying magnetic flux to link with loop 1 (mutual-inductance, M).

The equivalent circuit for this configuration is easily derived from elementary circuit theory with the result shown in Figure AIII.

The complex impedance Z incorporates all of the affects of magnetic coupling between current loop 1 and any other current loop 2. We see from this expression that Z can be made arbitrarily small by reducing $\omega = 2\pi f$, the operating frequency. When Z is thus
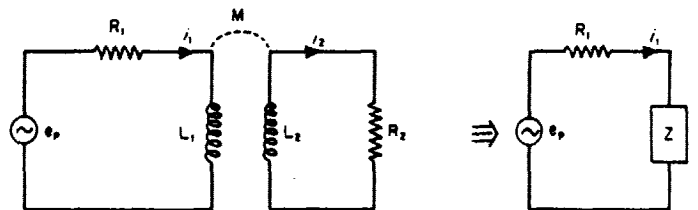
$$Z = i\omega L_1 + \frac{\omega^2 M^2}{R_2 + i\omega L_2}$$

$$i_1 = \frac{e_p}{R_1 + Z}$$

FIGURE AIII. Equivalent circuit for model of Figure AII.

made much smaller than R_1 the current flow in loop 1 is simply given by

$$i_1 = \frac{e_p}{R_1} = \frac{i\omega\phi_p}{R_1} = i\omega\phi_p G_1 \qquad (9)$$

where ϕ_p = primary flux linking loop 1
G_1 = conductance of loop $1(G_1 = 1/R_1)$
$i = \sqrt{-1}$

We see that the magnitude of the current is linearly proportional to the loop conductance and furthermore that the phase of the current leads the primary flux by 90°. Since the secondary magnetic field at the receiver from current i_1 is in phase with and directly proportional to i_1 it too will be directly proportional to G and will lead the primary flux by 90°. Thus

$$\left(\frac{H_s}{H_p}\right) \propto i\omega G_1 \qquad (10)$$

which has the same dependence on frequency and conductance as equation (6). We infer therefore, that the condition $B \ll 1$ is equivalent to stating that for all current loops that affect the receiver output the operating frequency is so low that we can ignore any magnetic coupling between the loops. Thus the current that flows in any loop is (i) completely independent of the current that flows in any other loop since they are not magnetically coupled and (ii) is only a function of the primary magnetic flux linking that loop and of the local ground conductivity.

The lack of interaction between current loops is of great importance in simplifying the data reduction procedures. Of equally great significance is the fact that for any value of B and for any orientation of a magnetic dipole (or indeed of any magnetic source) over either a uniform halfspace or a horizontally stratified earth it can be shown that all current flow is horizontal. That this is the case for a vertical dipole is easy to see from symmetry; for a horizontal dipole it is less evident but equally true. Thus, in a horizontally layered earth no current crosses an interface which is fortunate since, if it did, changing either of the conductivities would, by virtue of refraction of the current, change the direction of the current as it flowed from one medium to the other.

If no current flow crosses an interface and if there is no magnetic coupling between current loops, changing the conductivity of any one of the layers of a horizontally stratified earth will not alter the geometry of the current flow. Varying the conductivity of any layer will proportionately vary only the magnitude of the current in that layer. To calculate the resultant magnetic field at the surface of a horizontally layered earth it is simply necessary to calculate the independent contribution from each layer, which is a function of its depth and conductivity, and to sum all the contributions.

The functions $\phi(z)$ and $R(z)$ discussed in Section II define the relative influence of current flow as a function of depth. Their derivation is involved and will not be given here. The resultant
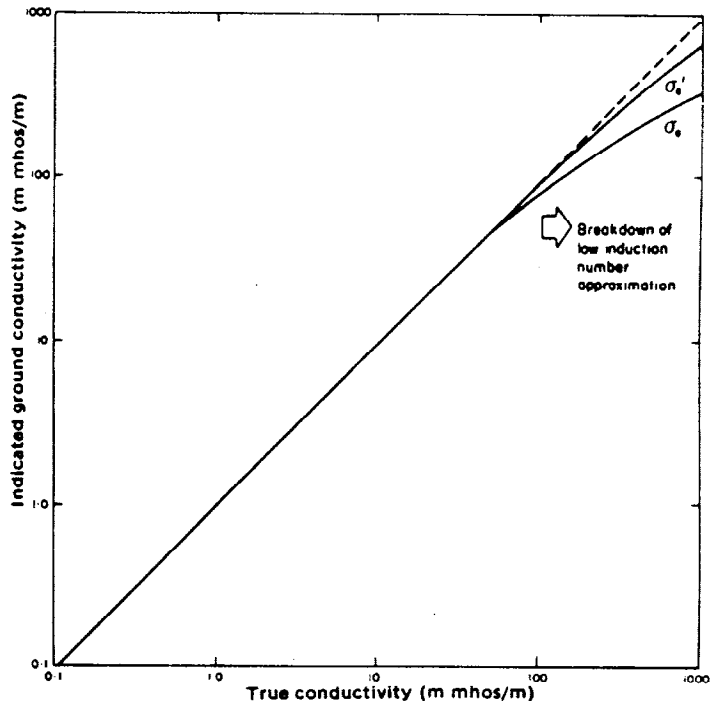
FIGURE AIV. Plot of indicated conductivity for EM31 versus true (homogeneous half-space) conductivity for both vertical (σ_a) and horizontal (σ_a') dipoles.

expressions are, however, simple and easily programmed into hand calculators:

$$\phi_V(z) = \frac{4z}{(4z^2 + 1)^{3/2}} \qquad (11)$$

$$\phi_H(z) = 2 - \frac{4z}{(4z^2 + 1)^{1/2}} \qquad (12)$$

$$R_V(z) = \frac{1}{(4z^2 + 1)^{1/2}} \qquad (13)$$

$$R_H(z) = (4z^2 + 1)^{1/2} - 2z \qquad (14)$$

where z is the depth divided by the intercoil spacing.

Finally it should be noted that for a given frequency and intercoil spacing as the terrain conductivity increases the approximation of equation (6) eventually breaks down and the instrumental output is no longer proportional to terrain conductivity. This effect is illustrated in Figure AIV. which plots apparent (indicated) conductivity against true (homogeneous halfspace) conductivity for both vertical and horizontal transmitter/receiver dipoles for the operating parameters of the EM31. As would be expected the horizontal dipoles exhibit linearity to greater values of conductivity as a result of the reduced depth of penetration in this configuration.

Technical Note TN-7

APPLICATIONS OF

TRANSIENT ELECTROMAGNETIC

TECHNIQUES

JD McNEILL

October, 1980

Table of Contents

INTRODUCTION

The ever increasing requirements for greater depth of exploration, improved rejection of conductive overburden or host-rock response and enhanced definition of potential ore-bearing structures all demand the application of large scale transient electromagnetic methods with their inherent ability to generate highly diagnostic data.

Furthermore it is not generally realized that transient electromagnetic techniques lend themselves very well to general geological mapping. Thus, in addition to their employment for the direct detection of conductive ores, they can also be used in the relatively resistive environments that often occur when prospecting for aggregates or aquifers, or when measuring the depth to bedrock or the thickness of permafrost. Indeed transient electromagnetic techniques are one of the "unconventional" methods employed in Russia for exploration for oil.

This short technical note reviews certain aspects of transient techniques which are not well covered in the literature. In the first section a brief outline of the nature of the transient response is followed by a short description of a typical large transient system, after which the reasons for certain design features are summarized. The next section illustrates the response calculated for several theoretical models and discusses the difference between confined and unbounded conductors. The last section considers several popular misconceptions about transient techniques and considers some merits and deficiencies.

The author wishes to acknowledge that much of the material in Section III either originated with or was supplied by Dr. Alex Kaufman of the Colorado School of Mines. More importantly the author wishes to express his gratitude for the many hours spent discussing electromagnetic techniques with Dr. Kaufman, whose insight is invariably illuminating.

SYSTEM CONSIDERATIONS

A procedure commonly utilized for ground exploration using transient techniques is to lay a large loop (as shown in Fig. 1) in the vicinity of the area to be examined. A steady current is caused to flow in the loop for a sufficiently long time to allow turn-on transients in the ground to dissipate. The quiescent current is then sharply terminated in a controlled fashion; for example the current turn-off may be a linear-ramp waveform (Fig. 2a). In accord with Faraday's Law rapid reduction of the transmitter current, and thus also of the transmitter primary magnetic field, induces an electromotive force (emf) in nearby conductors. The magnitude of this emf is proportional to the time rate-of-change of the primary magnetic field at the conductor. For this reason it is desirable to reduce a large transmitter current to zero in a short time so as to achieve a large emf of short duration (Fig. 2b). This emf causes eddy currents to flow in the conductor with a characteristic decay which is a function of the conductivity, size, and shape of the conductor. The decaying currents generate a proportional (secondary) magnetic field (Fig. 2c), the time rate-of-change of which is measured by a receiver coil.

Analysis of the nature of the transient decay is carried out by sampling the amplitude at numerous intervals of time (and over many cycles of the transmitter pulse so as to enhance the signal-to-noise ratio). A typical system block diagram is illustrated in Fig. 3.
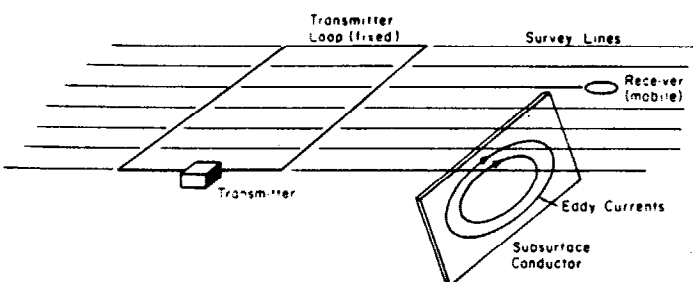
The survey output is an accurate knowledge of the three spatial components of the time-derivative of the secondary magnetic field as a function of position on the earth's surface and from this data much information can usually be derived about a survey target.

In order to appreciate certain system constraints, suppose for simplicity that the target is a wire loop having resistance and inductance as shown in Fig. 4. The transmitter primary magnetic field coupling with the loop generates a flux which is caused to rapidly decrease from a steady state value ϕ_p to zero within a time Δt which is much less than the time constant of the loop (defined as L/R). The emf generated in the loop is given by $\phi_p/\Delta t$ and from simple circuit theory the current can be shown to be

$$i(t) = \frac{\phi_p}{L} e^{-t/\tau}$$
$$\text{where } \tau = \frac{L}{R} \tag{1}$$

The secondary magnetic field is proportional at all times to i(t).

Note that the initial amplitude of both the current and the secondary magnetic field at t = 0 is independent of the ring resistance. Since by definition the inductance of the loop is the flux per unit current, we are not surprised to see that the initial current is given by ϕ_p/L i.e. it is exactly that value required to make the total flux through the loop equal to the value that existed just before transmitter turn-off.

The receiver-coil output voltage is proportional to the time rate-of-change of the secondary magnetic field and is therefore of the form

$$e_0 \propto \frac{1}{\tau} e^{-t/\tau} \tag{2}$$

We see from this expression that conductive targets (i.e. those having a small value of resistance and thus a large value of τ) yield signals with small initial amplitude that, however, decay relatively slowly. Signals from poorly conducting targets (large resistance) have high initial amplitude and decay rapidly. Typical decay times for orebodies range from as small as 100–200 μsec to as high as 10–20 msec and thus cover a factor of approximately one hundred in

FIGURE 1. Survey configuration.
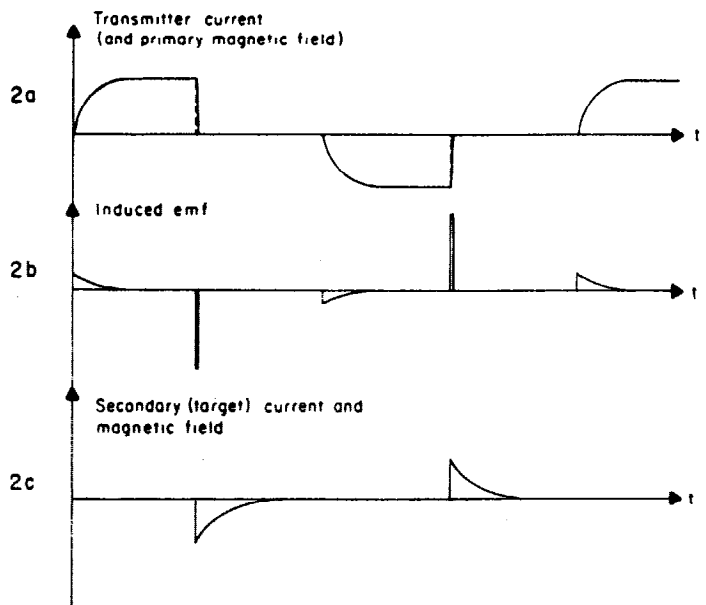
FIGURE 2. System waveforms.
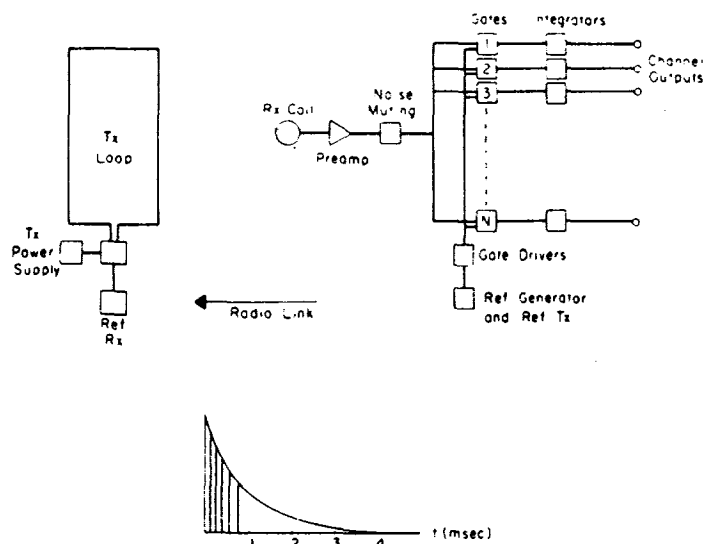
FIGURE 3. Block diagram and typical transient (showing initial gates).

time. In order to accurately resolve this range of transient decays, measurements must be made at a large number of time intervals. Furthermore at the initial portion of the transient decay the receiver output voltage varies rapidly with time, particularly for small values of r. For this reason the sampling "gates", particularly the earlier ones, must be of short duration so as to avoid distortion of the signal resulting from appreciable changes in the signal amplitude during the sampling period. Since the transients obtained in actual practice can be quite complex the only way to ensure low distortion is to employ a large number of narrow gates.

As equation (2) indicates the initial amplitude of the transient decay can also vary by a factor of one-hundred arising simply from the variation of r; target size, depth, etc., can easily account for another factor of one hundred, so it is most important that transient measuring systems have a very large dynamic range to handle the wide variety of signals that will occur in the field.

It was assumed above that the turn-off time of the transmitter pulse was much shorter than the characteristic decay time of the targets to be measured. In the event that this condition is not met for targets exhibiting exponential decay with low values of r the amplitude of the response will be less than that given in equation (2). Thus the response from poor conductors will be suppressed when compared with that from good conductors. Such suppression might be an advantage in a system designed to search only for better conductors but it is a definite disadvantage in a system designed to (i) search for all types of conductors and (ii) additionally map geology since in this application it materially complicates the data interpretation. For these reasons it is important to maintain the transmitter turn-off time as short as possible.

Finally it should be noted that by their very nature transient systems are broadband. A Fourier analysis of the emf induced in the
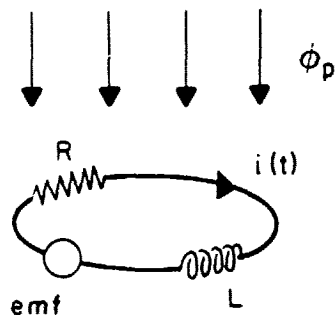
target (Fig. 2b) shows that odd-harmonic components exist from the basic pulse repetition-frequency (typically from 3 to 30 Hz) up to a value determined by the duration of the transmitter turn-off time; for example a 200 μsec turn-off puts significant excitation to frequencies of many kHz. This multi-spectral excitation is very desirable for obtaining detailed information about the target spectral response, however an accompanying disadvantage is that the receiver, being broadband, is susceptible to external noise and interference. In fixed-frequency systems, where the primary field is carefully cancelled out, the system noise is usually determined by errors in this cancellation and a point is soon reached where increases in transmitter dipole moment do not increase the signal-to-noise ratio. The situation is quite different for transient systems in which measurement is made during the transmitter off-time: for such systems the effective exploration depth is often set by external noise and the availability of a large transmitter loop with a high value of transmitter current becomes of great importance. Other techniques such as synchronization of the system to power-line frequencies so as to avoid having the system output oscillating at the powerline frequency and "spherics" noise-limiters also help reduce the sensitivity to external noise and interference and increase the exploration depth.

TARGET RESPONSES

I Confined Targets

As our first example of a target response consider the case of a conducting sphere which, for the sake of simplicity, we will assume to be in a region of uniform magnetic field which is suddenly terminated at time $t = 0$. The sphere, of radius a and conductivity σ, is shown in Fig. 5.

At the instant after termination of the primary field (called the early-time) currents immediately flow on the surface of the sphere with a distribution that exactly maintains the original uniform magnetic field within the sphere. The current distribution at this time (indicated in Fig. 6a) is independent of the conductivity of the sphere and we say that we are in the high-frequency limit since the current distribution is that which would flow if the sphere were located in a very high-frequency alternating (uniform) magnetic field. The definition of high-frequency in this case is such that the electrical skin-depth in the sphere material

$$\delta = \left(\frac{2}{\mu\sigma\omega}\right)^{1.2} \tag{3}$$

where $\mu = 4\pi \times 10^{-7}$ h/m
$\omega = 2\pi f$
$f = $ frequency (Hz)

is much less than the sphere radius.

At time $t = 0^+$ the primary field has disappeared and for all further time the distribution of circulating currents within the sphere is governed solely by their interaction with their own magnetic field.

FIGURE 4. Wire loop target.
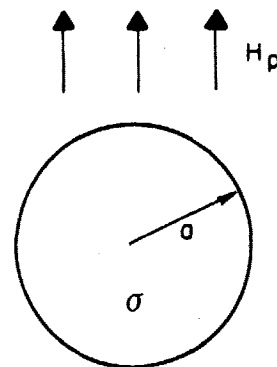
FIGURE 5. Sphere target.

6
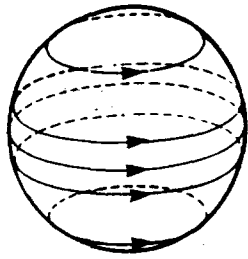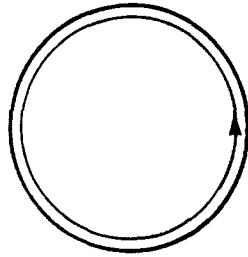
(a) Early time

(b) Early time
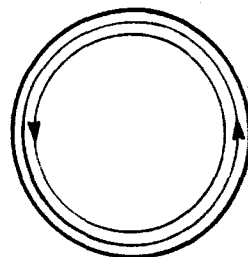
(c) Intermediate time
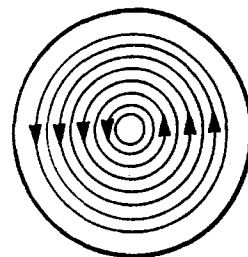
(d) Late time

FIGURE 6. Sphere currents at various times (a – surface currents; b–d – equatorial/plane currents).

Consider then Fig. 6b which shows in section the current flow in the equatorial plane of the sphere at t = 0⁺. The current, as mentioned above, is concentrated at the edge of the sphere. Virtually immediately, however, the amplitude of the current commences to decrease as a result of ohmic losses in the conductive sphere material. The local magnetic field from the current also decreases and (again through Faraday's Law) this decrease induces an emf which causes new current to flow, as shown in Fig. 6c. This process continues, with the result that the current flow moves inward with the passage of time. We say that the current diffuses radially inwards, although at no time is there actually a radial component of current flow – we are simply seeing the interaction of currents and their magnetic field in a conductive body.

The period of time during which the actual current distribution is in motion is called the "intermediate-time". During this period the external magnetic field associated with the moving and decreasing currents decays rapidly with time. A stage is reached, however, where the current distribution becomes invariant with time, with the form indicated in Fig. 6d. Close to the sphere centre the current density increases linearly with radial distance, becoming relatively uniformly distributed at one-half the radius, and decreasing slightly towards the edge. This period of time is called the "late-time"; the inductance and resistance associated with each current ring have stabilized and from this time onwards both the currents and their associated external magnetic field commence to decay exponentially with a time-constant given by

$$\tau = \frac{\sigma\mu a^2}{\pi^2} \tag{4}$$

A plot of the distribution of current with time is shown in Fig. 7 and the time derivative of the external magnetic field is shown in Fig. 8.

We see that measurement of the transient decay or its derivative yields useful diagnostic information about the electrical properties of the target. The late stage of the decay commences at a value of t/τ = 0.5 (characteristic of a sphere) and determination of τ gives a value for σa^2.

Furthermore, measurement of the transient response at various locations in the vicinity of the target (made simpler by the absence of the primary field) additionally yields information as to the sphere
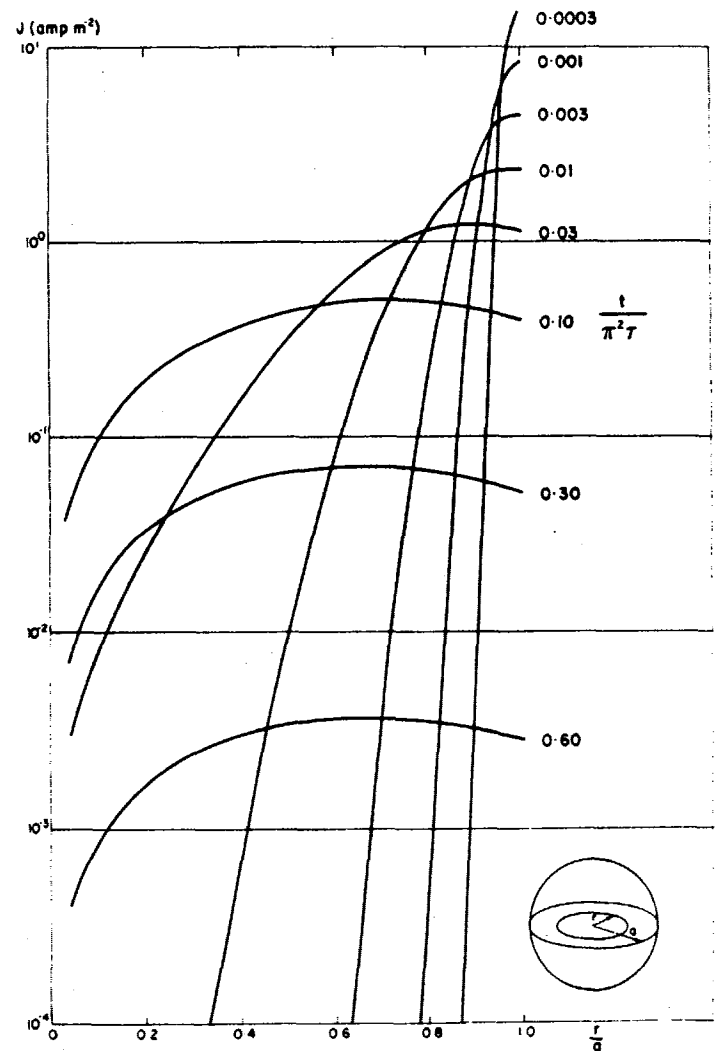
FIGURE 7. Radial distribution of sphere currents.

7
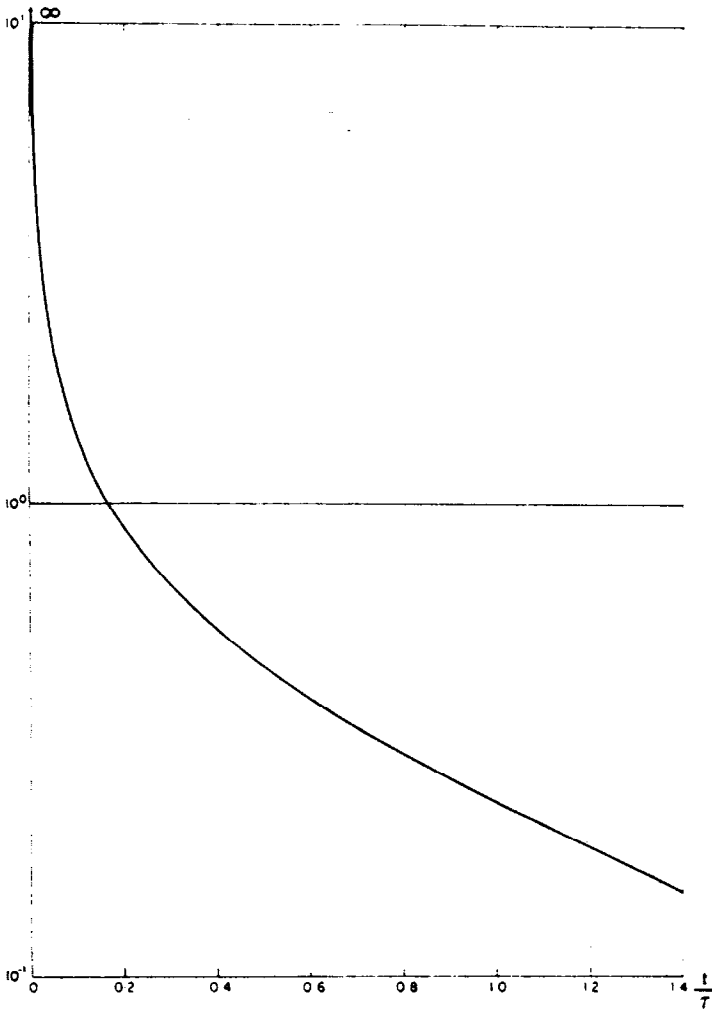
FIGURE 8. Time derivative of sphere secondary magnetic field.

FIGURE 10. Dependence of spheroid time-constant on eccentricity.

radius and depth. This is particularly true of the early channels since, as we have seen above, the early current flow is independent of the sphere conductivity and dependent only on its geometry. Our sphere is an example of an isolated conductor, i.e. a confined target surrounded by an insulator. The significance of this point is that for any confined conductor at early times the current distribution is a function of time and the overall decay is not exponential; there is however always some stage of time after which the current distribution becomes invariant with time and the decay becomes exponential at a rate determined by the shape, size, and conductivity of the body.

A second model that is useful is the oblate spheroid shown in Fig 9. Again we assume that the energizing field is uniform (a condition that, as we shall see later, is usually not too restrictive). As for the case of the sphere immediately after removal of the primary field surface currents, concentrated on the surface, flow so as to maintain the internal magnetic field at the value of the original (uniform)

FIGURE 9. Oblate spheroid.

inducing field. These currents diffuse radially inwards for a period of time which depends essentially on σ and a, after which the current distribution is no longer a function of time and the currents and external magnetic field decay exponentially with a characteristic time-constant.

More specifically the late-time commences at approximately (1)

$$\frac{d}{a} \simeq 1.5 \qquad (5)$$

$$\text{where } d = 2\pi\left(\frac{2t}{\mu\sigma}\right)^{1/2} \qquad (6)$$

The quantity d is a characteristic diffusion distance which gives the position of the current at time t and about which more will be said later. This quantity is the transient analogue of the skin-depth defined in equation (3).

Combining equations (5) and (6) we see that the late-time is given by

$$t_l = \frac{1.5^2\mu a^2\sigma}{8\pi^2} = 3.6 \times 10^{-8}a^2\sigma \qquad (7)$$

and is a function of σ and a^2 but not b.

The transient decay time-constant is given by (1)

$$\tau = \frac{\mu Sa}{q} \qquad (8)$$

where $S = 2\sigma b$ (the conductivity-thickness product)

and the function q(a/b) is plotted in Fig. 10. From this figure we see that for the larger values of eccentricity a/b the value of q is approximately 8 and the time-constant is therefore determined essentially by S and a as shown by equation (8). Furthermore subject to the assumption of the constancy of q, equations (7) and (8) can be combined to yield

$$\frac{t_l}{\tau} = 0.11\frac{a}{b}, \quad \frac{a}{b} > 4 \qquad (9)$$

to give the aspect-ratio of the body. This equation shows that a highly eccentric spheroid exhibits a late time which is comparable to or larger than its time-constant.

An eccentric oblate spheroid resembles massive sulphide orebodies, making this model useful in exploration for such deposits. As an example assume that the conductivity of the ore material is 2 mhos per meter, the radius a is 150 m and the thickness 2b is 20 m. Then the conductivity-thickness product s is 40 mhos, late-time begins at $t_l = 1.5$ msec and the decay time-constant is 0.94 msec. Such values are quite typical.

It was mentioned above that the assumption of a uniform primary field was not usually too restrictive. Consider again the case of a

$$T = \frac{\mu S \sigma}{2q\left(\frac{a}{b}\right)}, \quad \text{where } S = 2\sigma b$$
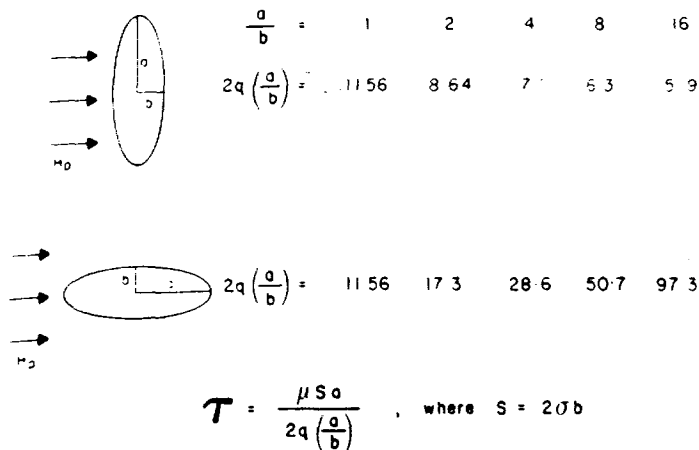
FIGURE 11. Time constant – infinite elliptical cylinder.

sphere excited by a uniform magnetic field. As is well known the resulting external magnetic field distribution arising from the sphere currents at any instant of time is that of a magnetic dipole located at the centre of the sphere. It is this apparent dipole moment which decays, initially faster than exponentially, then exponentially.

If now the sphere is excited by means of an adjacent magnetic dipole rather than a uniform magnetic field higher order multipoles are also induced. The strength of each multipole is a function of the distance (in terms of the sphere radius) of the inducing dipole from the sphere. Fortunately (i) the higher order multipole fields decrease more rapidly than the dipole field with measurement distance from the sphere and (ii) the higher order multipoles also decay more rapidly in time than the dipole (2). For these reasons, as long as both the inducing dipole and the receiver coil are further than approximately two sphere radii from the sphere centre those currents in the sphere (or indeed, any compact target) causing the secondary field sensed by the receiver coil will be essentially the same as if the inducing field were uniform by the time that the late-time condition has arrived; a very useful result!

Another phenomenon that will be observed occurs if an eccentric target such as the spheroid is subject to a primary field at an oblique angle. The inducing field can be resolved into components along each axis a and b. The late-stage time-constant for currents circulating about the b axis is however greater than the time-constant for currents circulating about the a axis. The result is a decaying dipole whose axis changes direction with time, eventually pointing in the direction that corresponds to the largest time-constant and thus largest projected area, independently of the orientation of the inducing dipole. Conversely a target exhibiting spherical symmetry generates a dipole moment that is always aligned with the primary field direction at the target.

This effect can be deduced from Fig. 11 which gives the time-constants for an infinite elliptical cylinder oriented so as to be both parallel and perpendicular to a uniform primary magnetic field (3). It is seen that for reasonably eccentric cylinders there is an order of magnitude difference in the late-time decay rate. Although this example assumes a uniform inducing field it can also be shown (4) that the time-constants listed in the figure are approximately correct for magnetic dipole excitation as long as both the source and observation point are located a distance of several times a from the target.
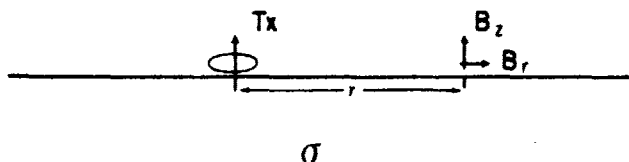
FIGURE 12. Homogeneous half-space.
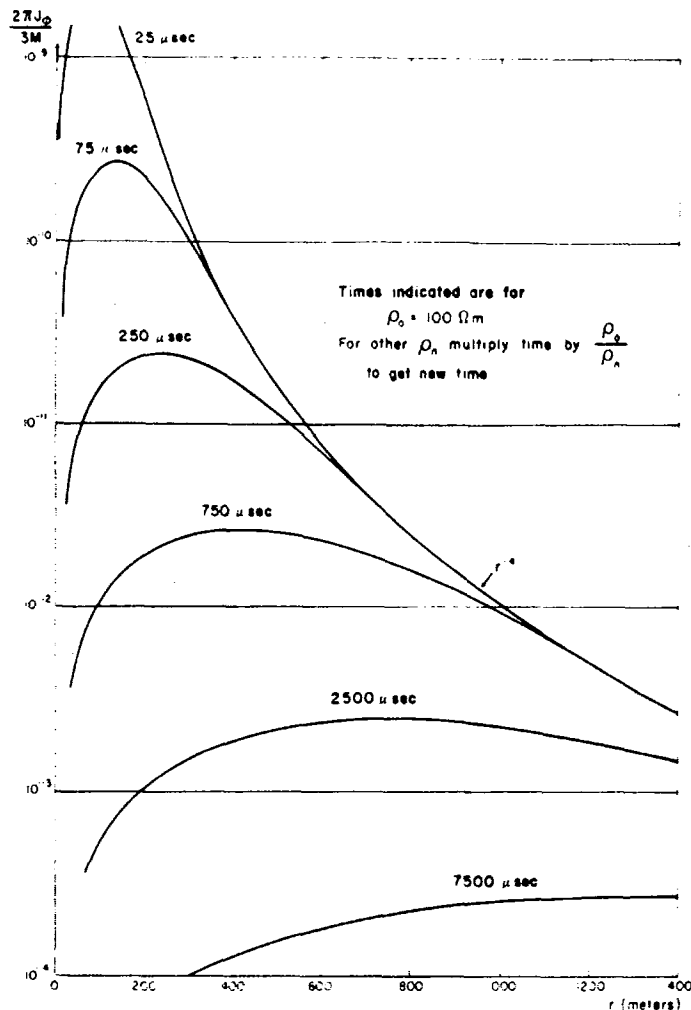
FIGURE 13. Current density – surface homogeneous half-space.

II Homogeneous Half-space

Consider a vertical magnetic dipole transmitter located on a homogeneous half-space as shown in Fig. 12. At time t = 0 the inducing dipole moment is reduced instantly to zero. Immediately* a surface current flows, distributed in such a manner as to maintain the magnetic field everywhere at the value that existed before turn-off: such a surface current flow decreases as r^{-4} with distance from the transmitter.

Near the transmitter the surface current starts to diffuse into the homogeneous half-space, whereas the current at great distance maintains the value dictated by the r^{-4} fall-off as illustrated in Fig. 13. The net effect as time progresses is that, due to the deficiency of current near the transmitter, the current appears to have moved out and down as a diffusing ring. The real cause of this effect is the relative decay of the current at the apparent trailing edge of the ring. Such a current distribution was recently described by Nabighian (5) whose results are shown in Fig. 14.

The magnitude of the surface current induced at time t = 0⁻ is not a function of the conductivity. However the apparent velocity with which the ring expands away from the transmitter is inversely proportional to the conductivity as indicated on Fig. 13.

It is useful to plot the radial position of the surface current maximum as a function of time for various resistivities (Fig. 15) since a comparison of Figs. (13) and (14) shows that the position of this maximum also accurately locates the radial distance of the subsur-

---

*It should be noted that only diffusion effects are of any significance at the intervals of time that are commonly used for geophysical measurements (the quasi-stationary approximation). Wave propagation effects which occur much earlier have long since disappeared.
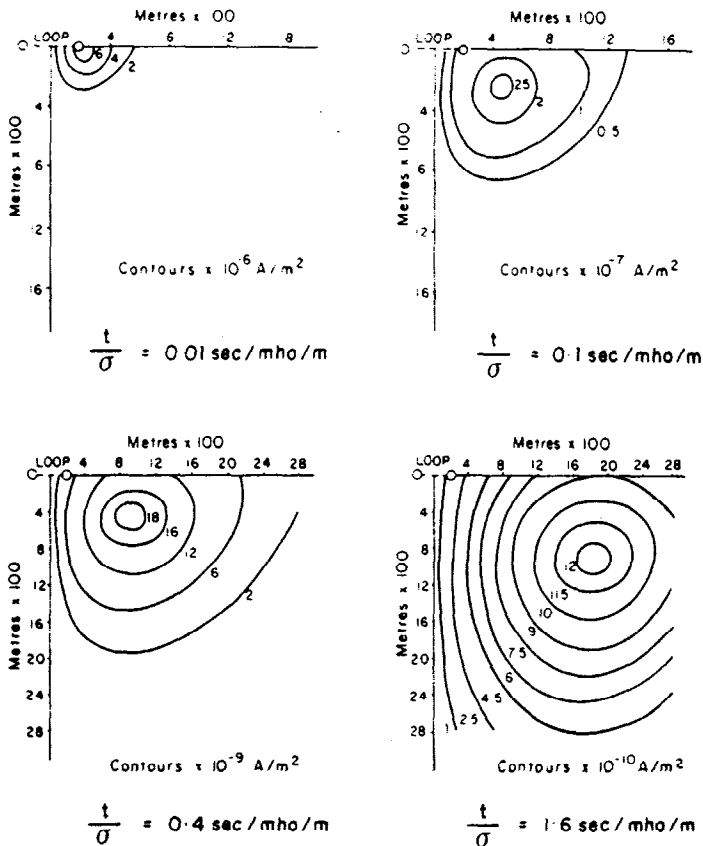
FIGURE 14. Computed contours of current density passing through loop centre (loop has dimensions 400 × 800 m (5)).

face current maximum. The location of the surface current maximum is proportional to

$$d = 2\pi\left(\frac{2t}{\mu\sigma}\right)^{1/2} \tag{6}$$

the characteristic diffusion length discussed in the previous section. The peak can be shown to be located at

$$r_{max} \simeq \frac{d}{5.2} \tag{10}$$

The significance of the diffusion distance d arises from the fact that it enables us to visualize the location of the maximum current density at any instant of time.

Since the location of the surface current maximum increases as $t^{1/2}$ the apparent velocity varies as $t^{-1/2}$. Initially the wave expands rapidly but as time passes the velocity decreases to a small value. The ring diameter becomes practically self-limiting. This feature is of practical importance because at the resistivities encountered in most ore materials (less than 1 Ωm) Fig. 15 shows that the current maximum travels at most a few tens of meters in any reasonable length of time. In conductive materials diffusion is a slow process; it is this fact that accounts for the relatively long time required for currents to stabilize in a confined conductor as demonstrated for the spheroid example above.

The magnetic field arising from a ring current is schematically illustrated in Fig. 16. The actual calculated magnetic field components arising on the surface (for the current distribution at 75 μsec in Fig. 13) are shown in Fig. 17 along with the current distribution. At large distance, much greater than the radius of the effective current loop, the vertical magnetic field still decreases as r^{-3} since the surface current at the large distance maintains the magnetic field at
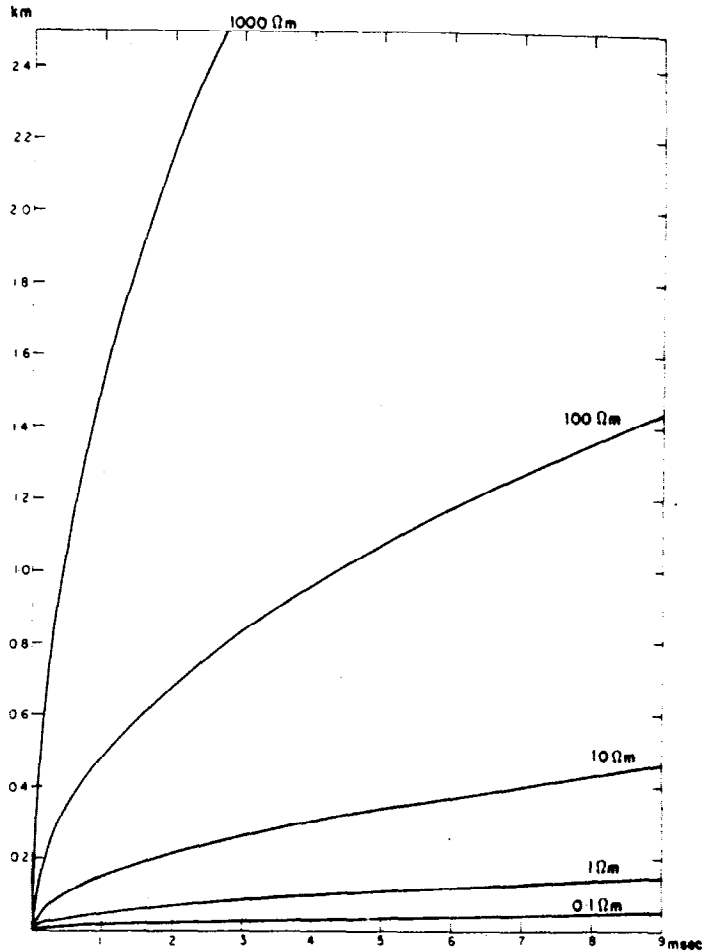
FIGURE 15. Location of surface current maximum—homogeneous half-space.

the value before transmitter current shut-off. At distances close to the transmitter the newly developed absence of current (recall that the original current density fell off as r^{-4}, so was very large near the transmitter) causes the vertical component of the magnetic field to be negative since all the current contributing to the field component now resides at relatively large radial distance. In a small region near the transmitter the vertical magnetic field is not a function of position in agreement with the well-known result for the invariance of the vertical magnetic field near the centre of a loop, illustrated in Fig. 16.

As time increases the current ring diffuses outwards and downwards; the vertical magnetic field for various times is shown in Fig. 18. When the current has moved out an appreciable distance from the transmitter location, there is a larger region where the vertical magnetic field is not a function of position, as indicated on the figure. This time is defined as the late-stage and is, of course, a function of the transmitter-receiver spacing since the current must have moved

FIGURE 16. Magnetic field above current ring.
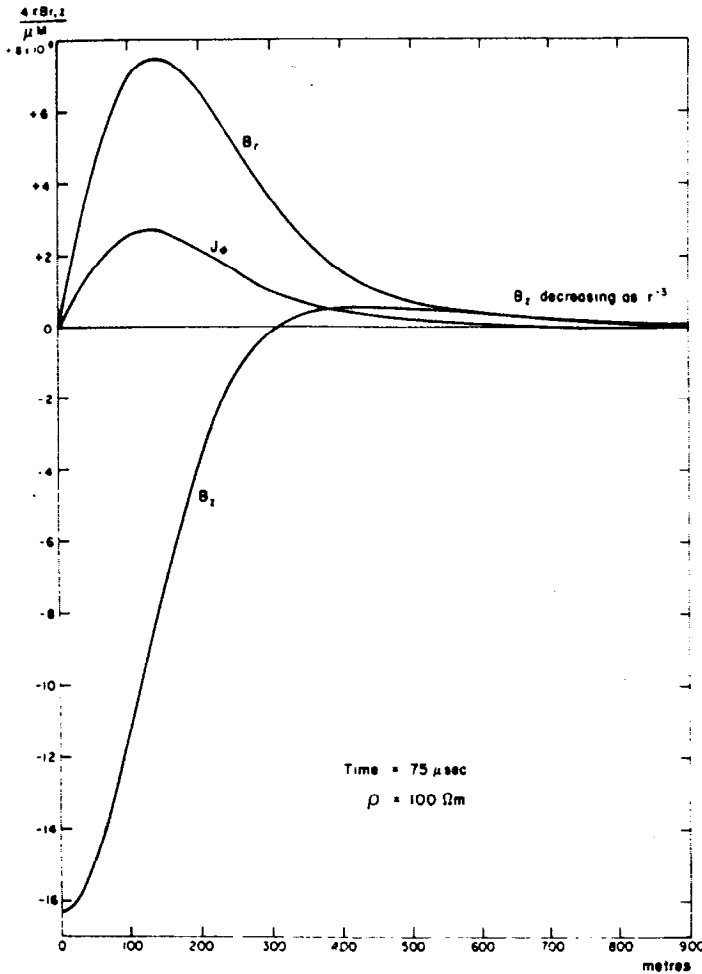
FIGURE 17. Magnetic field components at surface of homogeneous half-space.
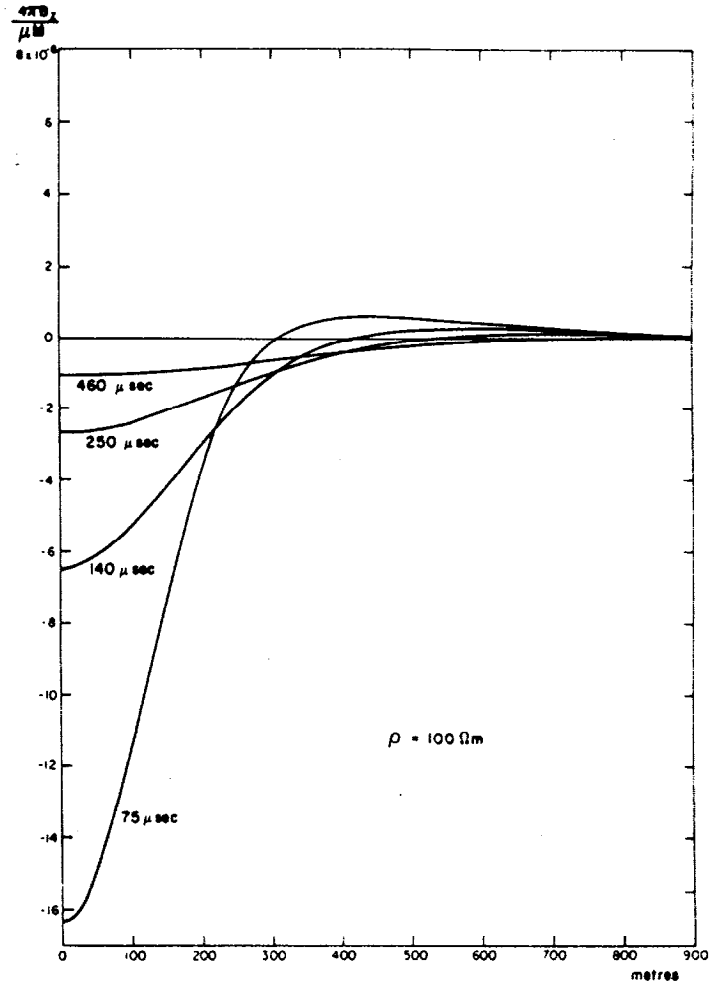
FIGURE 18. Vertical magnetic field component at surface of homogeneous half-space.

a large distance compared to this spacing. Late-time is usually considered to have commenced when

$$\frac{d}{r} > 10 \qquad (11)$$

where r = Tx/Rx spacing
and d is defined in equation (6)

At such late-times a considerable simplification occurs in the expressions for the magnetic field components; they become (6)

$$B_r \simeq \frac{\mu M}{4\pi r^3} \frac{r^4}{32t^2} (\mu\sigma)^2 \qquad (12)$$

$$\text{and } B_z \simeq \frac{\mu M}{4\pi r^3} \frac{2r^3}{15\pi^{1/2}} \frac{(\mu\sigma)^{3/2}}{t^{3/2}} \qquad (13)$$

where M = transmitter dipole moment

These equations are the basis of what the Russians call "transient sounding in the near-zone" for determining the electrical conductivity (resistivity) of the ground. It is evident that measurement of either B_r or B_z as a function of time will permit the determination of σ. Several features suggest measurement of the vertical field component; (i) at late-times both this component and its time derivative are larger with the result that the measurement is relatively insensitive to receiver coil misorientation. (ii) The magnitude of this com-

ponent is not a function of the distance r between the measurement station and the transmitter dipole. The reason for this has been discussed above and is clear from Figs. (16) and (18). (iii) This component and its derivative decrease more slowly with time in the late stage. (iv) Although this component is proportional to $\sigma^{3/2}$ whereas the radial component is proportional to σ^2, the vertical component still offers adequate resolution of small changes in terrain conductivity.

Since we are making our measurements with a coil it is the time derivatives which are of importance; they are given by

$$\frac{\partial B_r}{\partial t} \simeq \frac{-\mu Mr}{64\pi} \frac{(\mu\sigma)^2}{t^3} \qquad (14)$$

$$\text{and } \frac{\partial B_z}{\partial t} \simeq \frac{\mu M}{20\pi^{3/2}} \frac{(\mu\sigma)^{3/2}}{t^{5/2}} \qquad (15)$$

The voltage induced in a horizontal receiver coil decays as $t^{-5/2}$, characteristic of a uniform half-space. In distinction with the earlier case of confined conductors no insulating barrier now exists to contain the currents; they diffuse without limit. The response is no longer exponential.

It should be kept in mind that the functional dependency of either field component on the terrain conductivity arises only because the apparent velocity of the diffusing current is related to the conductivity. The actual magnitude of the initial current is, as stated earlier, dependent only on the transmitter dipole moment and is independent of the ground conductivity.

11
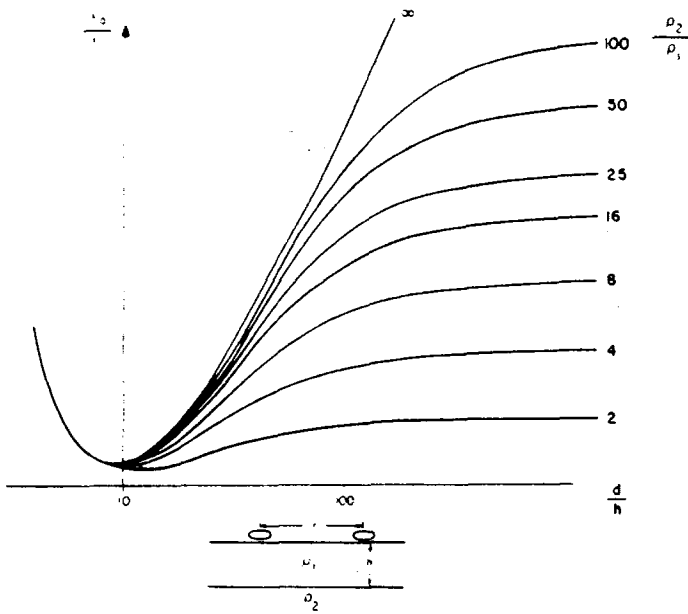
FIGURE 19(a). Two layer curves.

$$\frac{\rho_2}{\rho_1} > 1, \quad \frac{r}{h} = 1$$

$$\frac{\rho_2}{\rho_1} < 1, \quad \frac{r}{h} = 1$$
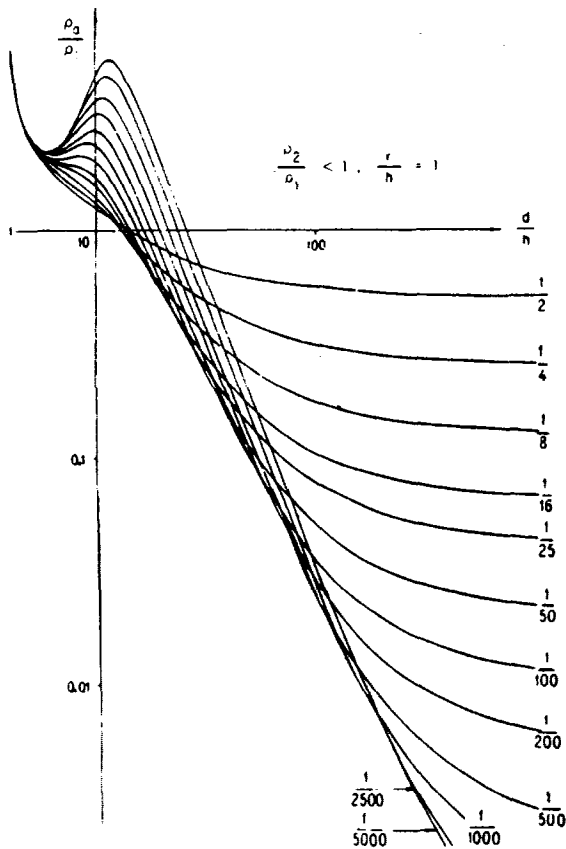
FIGURE 19(b). Two layer curves

Equation (15) suggests the possibility of inversion so that the apparent resistivity as a function of time is defined by

$$\rho_a(t) \triangleq \frac{\mu}{4\pi t}\left(\frac{2\mu M}{5tB_z}\right)^{2/3} \tag{16}$$

If now measurements are made of B_z for late values of time and the values substituted into equation (16) the apparent resistivity so defined should not be a function of time, indicating the presence of a uniform half-space.

III Layered Earth

Suppose, however, that the earth is not uniform but consists of a layer of resistivity ρ_1 and thickness h overlying a substrate of resistivity ρ_2. It is evident that at sufficiently early time the diffusing current will be situated entirely in the upper medium and measurements of the field components will be diagnostic of that medium. Conversely at much later times the currents will be predominantly in the substrate and measurements of the magnetic field components will substantially reflect its characteristics. The behaviour at intermediate time will be diagnostic of the thickness of the upper layer.

Many calculations for a layered earth have been carried out by the Russians. Typical results are shown in Figs. (19a) and (19b) where it is seen that for both a relatively insulating or conducting substrate the apparent resistivity defined in equation (16) is a well-behaved and diagnostic feature of the electrical properties. Such curves, which are also available for a three-layered earth, are used in a fashion completely analogous to the use of master curves for conventional resistivity. One simply plots the calculated values of $\rho_a(t)$ (derived from the measured values of B_z and t) against $t^{1/2}$ (the abcissa of the curves is given in terms of d/h where d is defined in equation (6) and h is the upper-layer thickness) on log-log paper to the same scale as the curves and shifts the plotted data until agreement is achieved, whereupon ρ_1, ρ_2, and h can be calculated.

Some important features of this technique are as follows:

(i) in our earlier discussion it was noted that for a uniform half-space the measured apparent resistivity was independent of the intercoil spacing r as long as care was taken to ensure that the measurements were made at the late-stage of the transient decay (which time was governed by the resistivity). Similarly, in the case of a two-layered earth the response should be independent of the intercoil spacing as long as the same condition holds for the upper-layer resistivity. That this is essentially the case is shown by a comparison of Fig. (19a) and Fig. (20) where the major difference is seen to occur at early values of d/h.

(ii) Fig. (20), which illustrates the two layered response when the intercoil spacing is only one-quarter of the upper-layer thickness, clearly indicates that it is possible, using transient techniques, to sound to a distance which is much greater (four times, in this case)

$$\frac{\rho_2}{\rho_1} > 1, \quad \frac{r}{h} = \frac{1}{4}$$
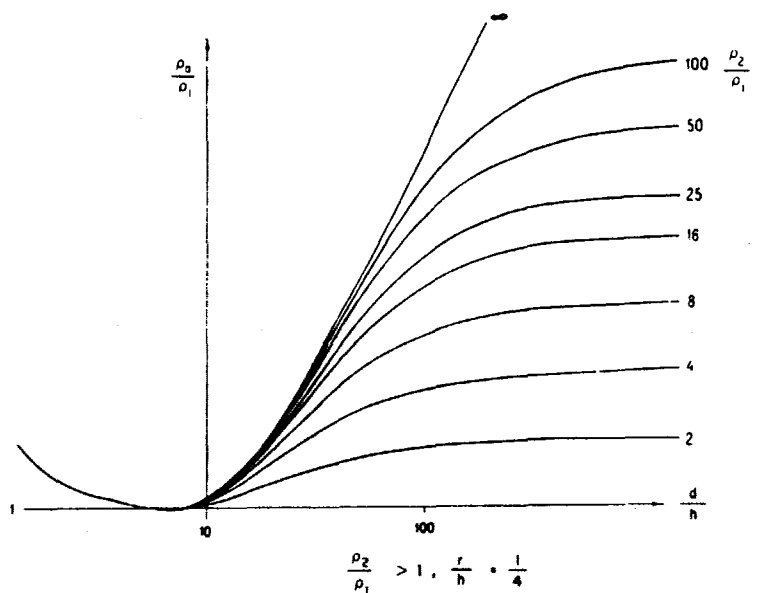
FIGURE 20. Two layer curves.

than the intercoil spacing. This contrasts very favourably with conventional resistivity techniques where it is necessary to expand an array to be several times the upper-layer thickness in order to fully resolve it.

(iii) The master curves shown in Fig. (19–20) were derived under the assumption of an infinitely fast turn-off of the transmitter current. In order to avoid performing a convolution the actual transmitter waveform should approximate this condition.

(iv) With conventional resistivity techniques one expands the array size from a value which is substantially less than the upper-layer thickness to a value much greater than the thickness in order to resolve it. In electromagnetic frequency-domain sounding it is necessary to analogously adjust the frequency from a value such that the skin-depth (defined in equation (3)) also varies from much less than to much greater than the upper-layer thickness. Since the skin-depth is inversely proportional to the square-root of the frequency this means that a large frequency range is necessary to adequately resolve the layer. The analogy for transient electromagnetic techniques is evident from Figs. (19–20) when it is realized that d is proportional to the square-root of time. In order to see the entire behaviour of the two-layered transient, measurement must be made over two decades of time and the time range must have been selected to correspond to the upper-layer diffusion thickness ($d/h \approx 30$) at mid-range. Obviously this is not always possible and one often ends up working with a limited portion of the appropriate curve. Many useful techniques are given in the Russian literature for this situation and it is for this reason that it is of great importance to make accurate measurements over the limited range of the transient decay which in turn requires (a) the use of many narrow gates so as to ensure good time-resolution and avoid distortion, (b) that such gates cover a wide range of time and (c) to employ transmitters with large dipole moment so as to keep the signal-to-noise ratio as high as possible in view of the desirable narrow gate-widths.

(v) Finally, calculation of the late-stage behaviour when the two layers consist of a conductor over an insulator shows that the amplitude of the transient decay is proportional to the cube of the conductivity-thickness product of the upper layer, permitting accurate resolution of small changes in the thickness. This feature is of considerable significance in mapping the depth to an insulating basement through a sedimentary column. It is also significant that, for the case of either a uniform half-space or a horizontally stratified earth, current flow in transient sounding is always horizontal (in distinction to conventional resistivity techniques) so that anisotropy in the resistivity of horizontally layered sedimentary rocks is not a significant problem.

IV Thin Sheets

As is usually the case a thin sheet is defined as being so thin that there is no variation in current flow across the thickness of the sheet. In the case of sinusoidal excitation this means that the sheet thickness must be a small fraction of the skin depth in the sheet material; analogously for transient techniques sufficient time must have elapsed so that the current density is uniform throughout the cross-section of the sheet. With this constraint satisfied let us examine the behaviour of a vertical dipole transmitter located on the surface of such an (infinite) horizontal thin sheet. It can be shown that the current flow is given as a function of distance r from the transmitter and time by

$$J = \frac{3M}{\pi} \frac{1}{r^3} \frac{m}{(1 + 4m^2)^{5/2}} \quad (17)$$

where J = current density (amps/m)

$$m = \frac{t}{\mu Sr}$$

S = sheet conductance (mhos)
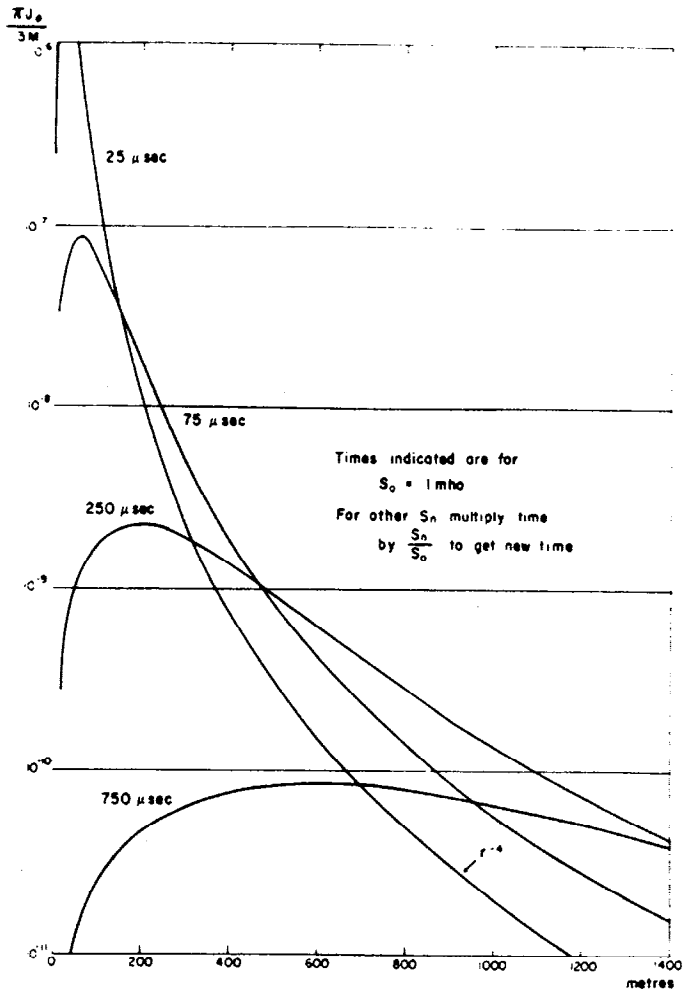
FIGURE 21. Current density – horizontal thin sheet.

Behaviour of this function, illustrated in Fig. 21, is similar to that of the homogeneous half-space; for any time t the current initially increases with distance from the transmitter, reaches a maximum and then decreases as r^{-4} (the dependence required to maintain the magnetic field at the value before current shut-off). Once again the initially induced current density is not a function of S, the conductivity-thickness product. Sheets with different values of S exhibit the same behaviour as long as the time scale is modified as indicated in Fig. 21.

By setting the derivative of equation (17) equal to zero it is a simple matter to solve for the location of maximum current-density as a function of time. The result is

$$t_{max} = \mu S r_{max} \quad (18)$$

Conversely there is an effective velocity defined as

$$v = \frac{r_{max}}{t} = \frac{1}{\mu S} \quad (19)$$

The position of maximum current moves out linearly with time (in distinction with the homogeneous half-space where it moved out as the square-root of time) and the effective velocity is determined by the conductivity-thickness product S. Calculation of the velocity for typical values of orebody conductances shows that once again it is quite low – for example at 100 mhos the velocity is 8 meters per msec.

A further difference between the homogeneous half-space and the thin sheet is that for the former immediately after turn-off the
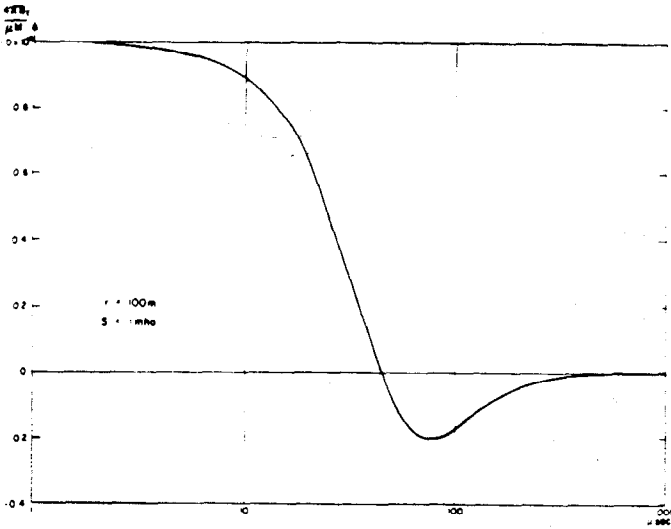
FIGURE 22. Vertical magnetic field component at surface of horizontal thin sheet.

FIGURE 24. Vertical magnetic field component above horizontal thin sheet.

surface currents at any point r fell off as r^{-4}; the current stayed at this value until the current ring passed underneath, after which time the current decreased monotonically to zero. In the case of the thin sheet at any location r the current initially increases, reaches a maximum value at the time given by equation (18), and then falls monotonically to zero.

The magnetic field components arising from the diffusing current ring also have the same general characteristics as those for the homogeneous half-space. For example Fig. 22 shows the vertical component of the magnetic field as a function of time. At short values of time the magnetic field is maintained at the value before turn-off. Since the primary field has been terminated this magnetic field arises solely from the currents flowing in the sheet. With the passage of time the deficiency of current between the transmitter and the observation point causes the vertical component to decrease, become zero and change polarity as the effective current moves beneath and passes beyond the observation point.

Again defining the late-time as that taken by the current to diffuse to a radial distance much greater than that of the observation point it can be shown that the vertical magnetic field and its time derivative are given at late-times by

$$B_z \simeq \frac{MS^3\mu^4}{16\pi t^3} \qquad (20)$$

$$\text{and } \dot{B}_z \simeq \frac{-3MS^3\mu^4}{16\pi t^4} \qquad (21)$$

Again the current wave diffuses without limit and the response is not exponential. Since for the thin sheet the current diffuses outwards at a faster rate (relatively) then for the homogeneous half-space the

FIGURE 23. Thin sheet.

secondary magnetic field (and its time-derivative) decrease much more rapidly with time.

Measurement of the time-derivative of the vertical magnetic field at late-time yields S directly and it should be noted that the transient response of a thin sheet is singularly sensitive to the conductivity-thickness product being proportional to S^3.

Finally consider the situation where the vertical dipole is elevated to a height h above a (horizontal) thin sheet as shown in Fig. 23. In this case it can be shown that

$$B_z = \frac{\mu M}{4\pi r^3} \frac{1 - 8(\alpha t + H)^2}{[1 + 4(\alpha t + H)^2]^{5/2}} \qquad (22)$$

$$\text{and } \dot{B}_z = \frac{-\mu M}{4\pi r^3} \frac{4\alpha(\alpha t + H)[9 - 24(\alpha t + H)^2]}{[1 + 4(\alpha t + H)^2]^{7/2}} \qquad (23)$$

$$\text{where } \alpha = \frac{1}{\mu Sr}, \ H = \frac{h}{r} \qquad (24)$$

The behaviour of the vertical component of the magnetic field is shown in Fig. 24. The affect of raising the transmitter and receiver dipoles above the sheet (i) reduces the initial amplitude of the vertical magnetic field and (ii) as seen from equation (22) linearly shifts the time scale by an amount $t_h = \mu Sh$; an event (such as the zero crossing) which happened at time t_o when both dipoles were located on the surface of the sheet now happens at time $t = t_o - t_h$.

The same translation occurs for the time derivative of the vertical magnetic field, which is illustrated in Fig. 25.

One would expect that, for dipoles raised above the sheet, at late-times the response will be the same as if the dipoles were on the sheet if by definition the current ring at such time is radially much further than the receiver distance and receiver/transmitter height. From equations (22) and (23)

$$\text{if } \frac{t}{\mu S} \gg h, \frac{t}{\mu S} \gg r \qquad (25)$$

$$B_z \simeq \frac{M}{16\pi} \frac{\mu^4 S^3}{t^3} \qquad (26)$$

$$\text{and } \dot{B}_z \simeq \frac{-3M}{16\pi} \frac{\mu^4 S^3}{t^4} \qquad (27)$$

Neither quantity is a function of h and the expressions are indeed the same as for both dipoles located on the thin sheet.
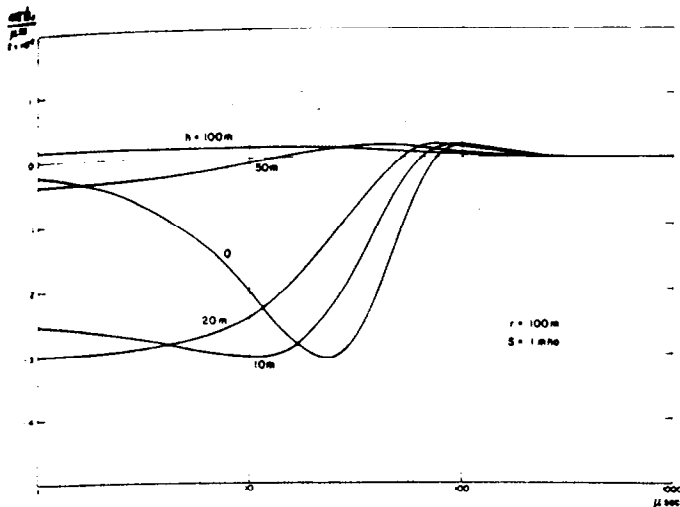
FIGURE 25. Derivative of vertical magnetic field above horizontal thin sheet.

Given S from such a measurement of $\dot{B}_z$ and knowing both r and t_0 (the time of the zero crossing of $\dot{B}_z$) it can be shown from equation (23) that h, the depth to the sheet, is given by

$$h = 0.6124r - \frac{t_0}{\mu S} \qquad (28)$$

In order for the crossover to occur it is obvious that r must be chosen so that the right-hand side of this equation is positive and in general r is chosen to be as large as possible. This ensures, for given h and S, that the crossover occurs at realistically large values of time, particularly necessary for low values of S which cause the current ring to move out at great radial velocity.

V Further Comments

This concludes our discussion of typical models and their responses. It is seen that much information can be derived from transient measurements.

It has perhaps been noted that no mention was made of the semi-infinite vertical thin sheet so popular with horizontal loop systems. Because of the large transmitter loop size used with large transient systems it is less likely that targets whose dimensions are infinite compared with those of the transmitter loop will occur and a more valuable target model is the very oblate spheroid discussed earlier.

SOME MERITS AND DEFICIENCIES OF TRANSIENT ELECTROMAGNETIC TECHNIQUES

One sometimes hears that transient measurements are essentially quadrature-phase determinations since measurement is made in the absence of the primary field. Although it is true that targets which exhibit in-phase response only (such as non-conductive bodies with $\mu > \mu_0$) also yield no response after termination of the primary field it will be shown below that in general the transient method is responsive to both the in-phase and quadrature-phase components of the target response.

Furthermore one hears that since transient and multi-spectral frequency-domain responses are related through the Fourier transform such techniques are equivalent. Whilst theoretically correct this statement ignores the important influence of the major source of noise for each technique, the net result of which is that very often they are not in a practical sense equivalent and transient techniques can offer a major advantage.

Consider the transmitter current waveform in Fig. 26a. This
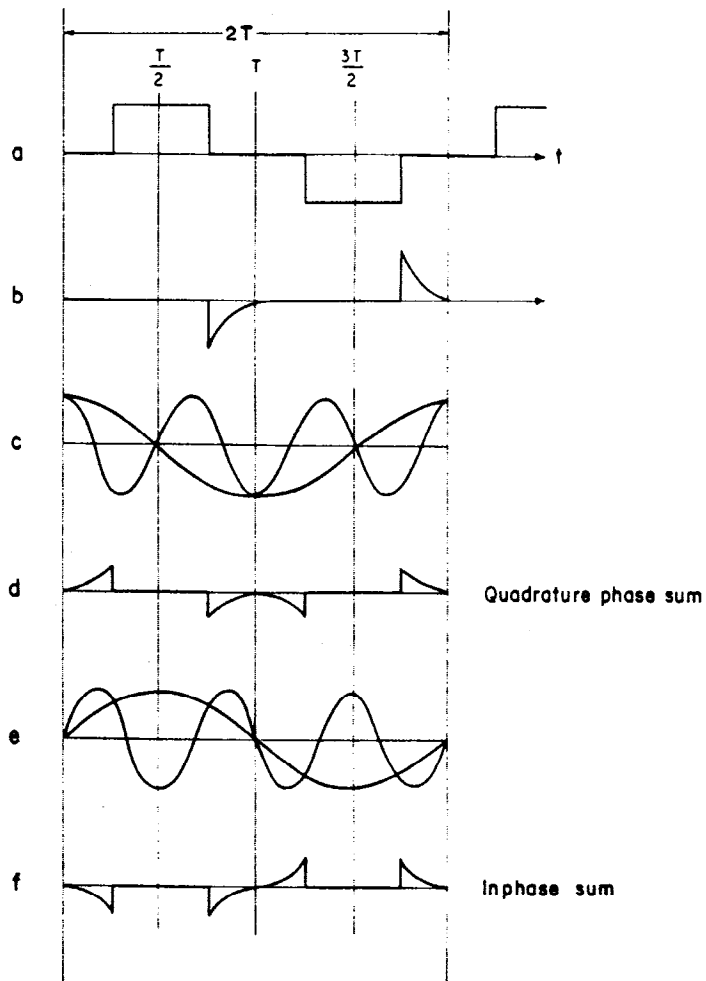
FIGURE 26. Synthesis of transient response.

waveform is easily shown to be the Fourier sum of a fundamental and an infinite series of *odd* harmonics

$$f(t) = \sum_{n=1}^{\infty} \sin\left(\frac{n\pi}{2}\right) \frac{\sin\left(\frac{n\pi}{4}\right)}{\frac{n\pi}{4}} \sin n\omega t \qquad (29)$$

Each of these frequencies excites the target which we assume to have an exponential decay with time-constant which is short compared with one-quarter of the period of the fundamental (thus ensuring both in-phase and quadrature-phase response). The receiver gates out the transients which occur during the transmitter on-time; those which remain for processing are shown in Fig. 26b. Since these transients arise from the transmitter excitation it must also be possible to synthesize this waveform from an infinite series of odd harmonics. The question arises as to whether there will be only cosine terms (quadrature-phase) or both cosine and sine (in-phase) terms in this series.

Consider a series of cosines at fundamental and odd harmonic frequencies, an example of the first two terms of which is shown in Fig. 26c. Examination of this figure shows that, as long as only the odd harmonics are present, the infinite sum of such harmonics (at arbitrary amplitudes) must exhibit even symmetry about T. Consider further the interval from 0 to T. Within this interval odd symmetry must be exhibited about T/2. Likewise in the interval T to 2T odd symmetry must be exhibited about 3T/2. The synthesized waveform shown in Fig. 26d satisfies these requirements.

Consider next a series of odd harmonic sine terms, the first two

15

terms of which are shown in Fig. 26e. Their infinite sum must exhibit odd symmetry about T and, in the smaller intervals, even symmetry about T/2 and 3T/2. Such a synthesized waveform is shown in Fig. 26f. Now in the interval 0 to T/4 the response shown in Fig. 26b is zero. Therefore within this interval the waveforms shown in Fig. 26d and Fig. 26f must be everywhere equal, since their sum is everywhere zero. Furthermore the waveforms shown in Fig. 26d and Fig. 26f between 3T/4 and T/4, 7T/8 and 2T must be everywhere the same. If the in-phase response were everywhere zero the quadrature-phase would have to be zero as well. Evidently the quadrature and in-phase components are equally important in synthesizing the final waveform.

Transient systems are definitely not quadrature-phase systems; they generally respond about equally to the in-phase and quadrature-phase components from the target.

In fact the principal advantage of the transient electromagnetic system is that it allows measurement of many of the in-phase characteristics of the response of a target in the absence of the primary field. To understand the significance of in-phase measurement we refer to a recent article by Kaufman (7) in which he asserts that the most diagnostic exploration system is the one which is the most sensitive to small changes in conductivity, ie. has a response which is proportional to conductivity raised to a high power. He reviews the fact that conventional (DC) resistivity surveys respond functionally to conductivity contrasts as

$$
\frac{\left(1 - \dfrac{\sigma_t}{\sigma_b}\right)}{\left(1 + \dfrac{2\sigma_t}{\sigma_b}\right)} \tag{30}
$$

where σ_t = target conductivity
σ_b = background conductivity

which function is insensitive to changes in conductivity at medium or high conductivity contrasts. Such systems are therefore inherently not diagnostic.

Turning to frequency-domain methods he shows that at low frequencies where both the in-phase and quadrature-phase response are increasing with target conductivity the quadrature-phase component responds linearly to conductivity variations. This is an improvement over conventional resistivity but better can be achieved with the in-phase component, for in this case at low frequencies the system response is of the order σ^2. In-phase measurements are truly more diagnostic but this advantage is seldom fully realized since the major source of noise in such measurements results from inadvertent changes in the inter-coil spacing. Since the in-phase component arising directly from the transmitter is proportional to r^{-3} (where r is the intercoil spacing) small changes in this spacing have a large effect on the signal-to-noise ratio. Such noise is completely absent in the case of transient systems in which measurement is made in the absence of the primary field. Yet they are still, as we have seen above, sensitive to the in-phase components. We should therefore expect such systems to be able to take full advantage of the diagnostic value of the in-phase components and this is indeed the case.

As our first example consider the infinite horizontal thin sheet referred to earlier. At low frequencies it can be shown that the quadrature-phase component is proportional to S. Conversely the in-phase component is proportional to S^2 and as we have seen, the transient response is proportional to S^3. Obviously in the context of the last paragraph the transient response is the most diagnostic. A less-than-obvious advantage of transient systems lies in the way in which the in-phase and quadrature-phase components of the target response are effectively synthesized to make the final transient waveform.

Kaufman continues to explore the relative merits of various electromagnetic techniques for the exploration picture shown in Fig. 27. A large, shallow, moderately conductive bounded overburden

$\sigma_2 > \sigma_1$
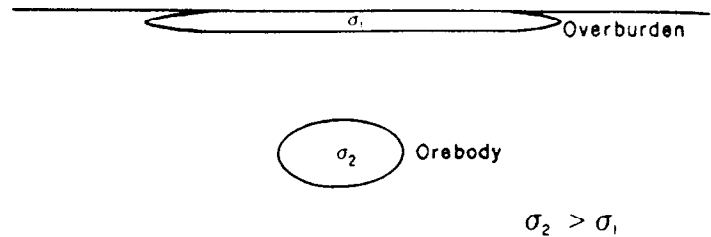
FIGURE 27. Orebody beneath conductive overburden.

overlies a deep, small, but intrinsically more conductive target. As a result of its proximity to both the transmitter and receiver the overburden yields a large response to quadrature-phase systems, even though not particularly conductive.

The situation is substantially improved for the case of in-phase measurements since the influence of conductivity (relative to proximity) is enhanced. However such improvement requires that instrumental noise be of low order (optimally less than the response from the overburden).

The ultimate performance is achieved by the use of transient techniques. The early-time response from the overburden can be very large but if the decay rate is faster than that of the orebody one simply has to wait a sufficient length of time for the masking effects of the overburden to disappear and the orebody to appear. The only requirement is that the transient decay of the orebody be slower than that of the overburden so that the latter eventually disappears. Unfortunately by the time that this happens the response from the orebody may be so low as to be undetectable against the system noise. But the noise in this case is external (man-made interference, spherics) and there is always one way to overcome it – brute force, ie. a large high-powered transmitter.

In the case of in-phase systems increases in transmitter power have no effect – both the signals and the noise linearly increase with transmitter dipole moment. For transient systems the signal-to-noise ratio is almost invariably linearly related to transmitter power. The higher the power (ie. the higher the primary inducing magnetic field) the longer one can afford to wait for the various effects (overburden, etc.) to sort themselves out. In the case of bounded conductors with adequate transmitter power everything comes to he who waits!

A disadvantage of transient systems is that by virtue of being broadband they are sensitive to noise and interference of the type referred to above. For this reason a large transmitter dipole moment is desirable and since resonant techniques are not available with pulses the transmitters tend to be heavy and the transmitter loops of large area. For this reason it is not currently possible to make a system that is truly portable in the sense of a conventional horizontal loop system.

In the example just given it was assumed that the "geological noise" also consisted of a confined conductor so that the response was exponential with time. Consider now the situation where the target (in this example, a sphere) is imbedded below the transmitter in a conductive host-rock at a depth z (Fig. 28). The same loop is also used as the receiver coil. At early times, before the diffusing current arrives at the location of the target the secondary fields will be entirely those of the homogeneous half-space as described in the previous section. As the diffusing current approaches the target the changing magnetic field of the current ring generates the eddy-current flow in the target (the transmitter has long since been shut off). During this time there is a good deal of electromagnetic coupling between the ring and the target. As time progresses the current ring diffuses onwards and the currents in the (presumed relatively conductive) target commence to decay and later to diffuse outwards into the conductive half-space. At still later times the currents from the target will have dissipated to zero and once again the measured secondary fields will be essentially those of the homogeneous half-space (an exponential decay is much faster than $t^{-3/2}$).

It can be shown (8) that, for targets of such a size, location, and

Tx - Rx Loop

Orebody

$\dfrac{E_i + E_o}{E_o}$

$\dfrac{z}{a} = 2 , \dfrac{r}{a} = 2$

$\dfrac{\sigma_i}{\sigma_e}$

1024
512
256
128
64
25
8

$\dfrac{d_i}{a}$
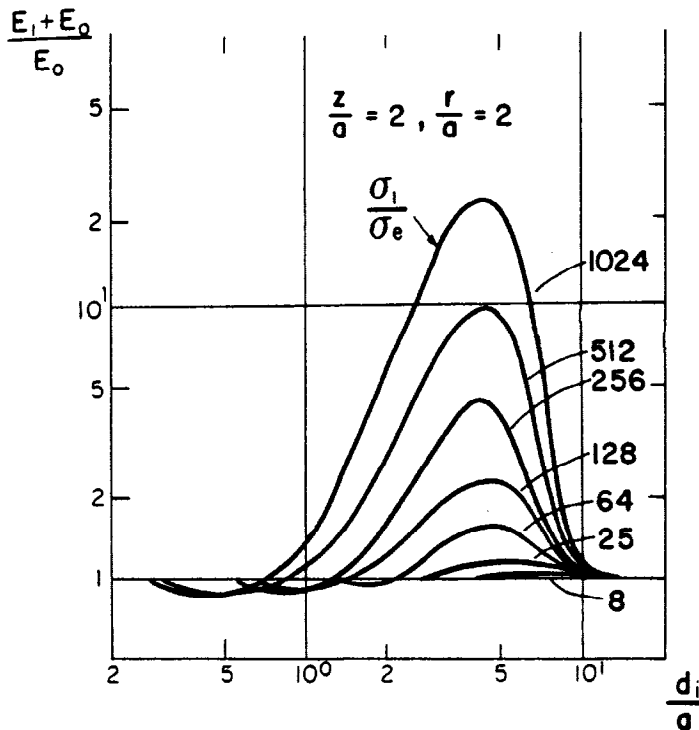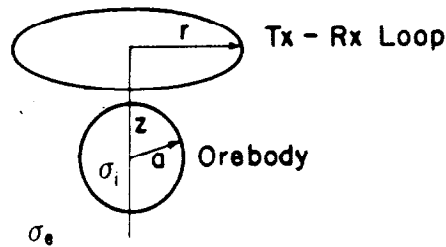
FIGURE 28. Combined response from orebody and conductive host rock (8).

geometry as to give a reasonably large response compared to the homogeneous half-space, there is an interval of time during which (i) the response of the orebody and the half-space are relatively un-coupled – ie. the total response is essentially the sum of the two individual responses, and (ii) the response from the target is exponential with the free space time-constant so that measurements made during this time are diagnostic of the target. An example of such a response is shown in Fig. 28. The quantity plotted as a function of d_i/a is the ratio of the total emf induced in the loop when both target and half-space are present to the emf when just the half-space is present. The figure clearly indicates the "window" during which measurements are quite sensitive to the target parameters, as well as the early and late-time behaviour referred to above.

Similar calculations carried out for conventional multi-spectral frequency-domain systems show that the quadrature-phase response does not exhibit the type of behaviour shown in Fig. 28 (now as a function of frequency) whereas the in-phase response does exhibit analogous characteristics to the transient response. Once again the advantage of the transient technique is that it permits virtually noise-free (assuming no limit to the transmitter dipole moment) measurements of the essential features of the in-phase response.

An interesting effect can occur if the current ring actually impinges on the target. Consider again Fig. 1 which shows a sheet conductor now assumed to be embedded in a homogeneous half space of conductivity σ_e. At early times such that d_e/r is small (r is now the distance to the target) the magnetic field at the target remains exactly as it was before shut-off. The only current flow that occurs in the vicinity of the target is the surface current that flows on the surface above it. With the passage of time the current ring diffuses outward with the result that the changing magnetic field from the moving current causes induced eddy currents within the target. Two situations can occur: (i) the target is located sufficiently far from the path of the diffusing current ring at all times so that the only significant effect in the target is the induced eddy currents arising from the changing magnetic field or (ii) the target may actually be in the path of the diffusing current in which case the current will be substantially distorted as it envelopes the target. This is an example of what has recently been called "current gathering". It is obviously a question of degree since there is always some conductive interaction between the diffusing current and the target. Measurements made of the magnetic field or its time derivative on the surface above the target will be additionally affected by current gathering.

Finally having accepted the fact that the transmitter loop of a transient system, particularly a high-powered one, is rather large there is another major advantage associated with such systems which is the high degree of flexibility that is available in exploring the geometrical aspects of the target response. With complete freedom one moves the receiver about, making three-axis measurements of the time derivative of the *target* response only, rather than of a complicated vector function of both the transmitter (primary) magnetic field and the target response.

An obvious extension of this freedom applies to borehole geophysics. In conventional frequency-domain methods lowering the sonde down a borehole accurately depicts the fall-off with distance of the primary magnetic field with, occasionally, a small anomaly superimposed on the large primary signal. With transient techniques there is nothing – unless an anomaly.

SUMMARY

Transient electromagnetic techniques offer significant advantages over multi-spectral frequency-domain measurements. The latter have been well treated in the literature; relatively little information is available about transient responses. It is hoped that this technical note will help to rectify the unbalance.

BIBLIOGRAPHY

(1) Kaufman, A. 1978. Frequency and transient responses of electromagnetic field created by currents in confined conductors. Geophysics V. 43, pp 1002-1010

(2) Nabighian, M.N. 1970. Quasi-static transient response of a conducting permeable sphere in a dipolar field. Geophysics V. 35. pp 303-309

(3) Kaufman, A. 1979. Personal communication

(4) Kaufman, A. 1979. Personal communication

(5) Nabighian, M.N. 1979. Quasi-static transient response of a conducting half-space – An approximate representation. Geophysics V. 44. pp 1700-1705

(6) Kaufman, A. 1977. The theoretical basis of transient sounding in the near zone. Translation published by Resource Geophysics and Geochemistry Division. Geological Survey of Canada.

(7) Kaufman, A. 1978. Resolving capabilities of the inductive methods of electroprospecting. Geophysics V. 43 pp 1392-1398

(8) Kaufman, A. 1980. The influence of currents in the host-rock on secondary electromagnetic fields in inductive prospecting. Paper submitted to Geophysics.

APPENDIX B

Equipment Specifications

ONE MAN
CONTINUOUS READING
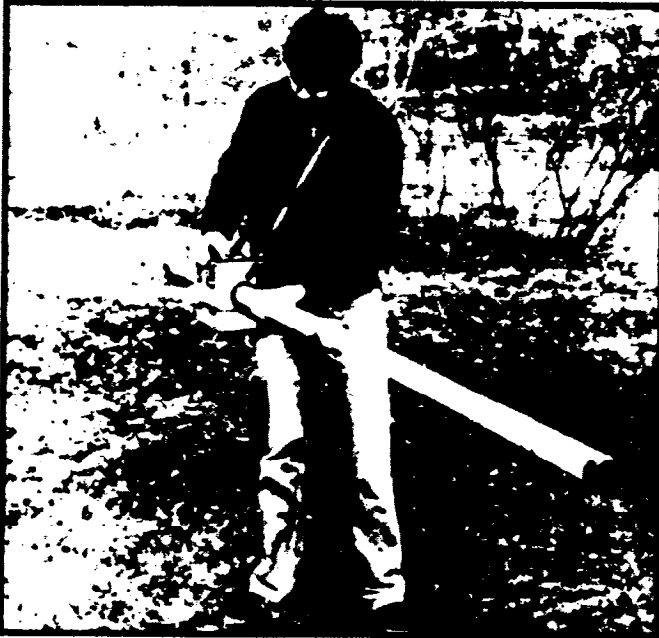
EM31

The Geonics EM31 maps geology or groundwater contaminant plumes by measuring terrain conductivity without electrodes or ground contact, using a patented electromagnetic inductive technique. The instrument reads directly in millisiemens per meter.

Using the inductive method, surveys are readily carried out in all regions including those of high surface resistivity such as sand, gravel, and asphalt. The effective depth of exploration is about six meters, making it ideal for many geotechnical and groundwater contaminant surveys. Important advantages of the EM31 over conventional resistivity methods are the speed with which surveys can be conducted, the precision with which small changes in conductivity can be measured and the continuous readout while traversing the survey area. The EM31 now provides an output of both the quadrature-phase (conductivity) and inphase components which can be recorded simultaneously on the DL55 digital data recorder. The inphase component is especially useful for detecting shallow ore bodies and, in waste site surveys, for searching for buried metal drums, pipes, and other ferrous and non-ferrous metallic debris.

With the capability of simultaneously mapping contaminant plumes and buried metal the EM31 is the ideal tool for site assessment surveys.

Specifications

MEASURED QUANTITY	Apparent conductivity of the ground in milliSiemens per meter (mS/m)
	Inphase response in parts per thousand (ppt) of secondary to primary magnetic field
PRIMARY FIELD SOURCE	Self-contained dipole transmitter
SENSOR	Self-contained dipole receiver
INTERCOIL SPACING	3.66 meters
OPERATING FREQUENCY	9.8 kHz
POWER SUPPLY	8 disposable alkaline 'C' cells (approx. 20 hrs life continuous use)
CONDUCTIVITY RANGES	3, 10, 30, 100, 300, 1000 mS/m
MEASUREMENT PRECISION	±2% of full scale
MEASURMENT ACCURACY	±5% at 20 mS/m
NOISE LEVELS	0.1 mS/m, 0.03 ppt

DIMENSIONS		
	Boom	• 4.0 meters extended • 1.4 meters stored
	Console	24 x 20 x 18 cm
	Shipping Case	145 x 38 x 23 cm
WEIGHT	Instrument	11 kg
	Shipping	26 kg

TWO MAN
VARIABLE DEPTH

EM34-3

Operating on the same principles as the EM31, the EM34-3 is designed to achieve much greater depth of exploration and also yields more information about the vertical conductivity structure by varying the intercoil spacing.

Simple operation, fast survey speed and straight-forward data interpretation make the EM34-3 a versatile and cost-effective tool for the engineering geophysicist. The instrument has been particularly successful in mapping deeper groundwater contaminant plumes and in groundwater exploration.

The underlying principle of operation of this patented non-contacting method of measuring terrain conductivity is such that the depth of penetration is independent of terrain conductivity and is determined solely by the intercoil spacing and coil orientation. The EM34-3 can be used at three intercoil spacings of 10, 20 or 40 meters, to yield depth of exploration of approximately 7.5, 15 and 30 meters in the vertical coplanar mode (shown above) and 15, 30 or 60 meters in the horizontal coplanar mode.

For surveys in regions of particularly high cultural and atmospheric noise the high powered EM34-3XL reduces the noise at the 40 m spacing by a factor of 10 and at the 10 m and 20 m spacing by a factor of 4.

Like the EM31, the EM34-3 comes complete with a connector for the DL55 digital data recorder.

Specifications

MEASURED QUANTITY	Apparent conductivity of the ground in mS/m	
PRIMARY FIELD SOURCE	Self-contained dipole transmitter	
SENSOR	Self-contained dipole receiver	
REFERENCE CABLE	Lightweight, 2 wire shielded cable	
INTERCOIL SPACING & OPERATING FREQUENCY	• 10 meters at 6.4 kHz • 20 meters at 1.6 kHz • 40 meters at 0.4 kHz	
POWER SUPPLY	Transmitter Receiver	8 disposable or rechargeable 'D' cells 8 disposable or rechargeable 'C' cells
CONDUCTIVITY RANGES	3, 10, 30, 100, 300, mS/m	
MEASUREMENT PRECISION	±2% of full scale deflection	
MEASURMENT ACCURACY	±5% at 20 mS/m	
NOISE LEVELS	0.2 mS/m (can be greater in regions of high power line interference)	
DIMENSIONS	Receiver Console	19.5 x 13.5 x 26 cm
	Transmitter Console	15 x 8 x 26 cm
	Coils	63 cm diameter
WEIGHT	Receiver Console	3.1 kg
	Receiver Coil	5.6 kg
	Transmitter Console	3.0 kg
	Transmitter Coil	8.8 kg
	Shipping	43 kg

NEAR SURFACE CONDUCTIVITY
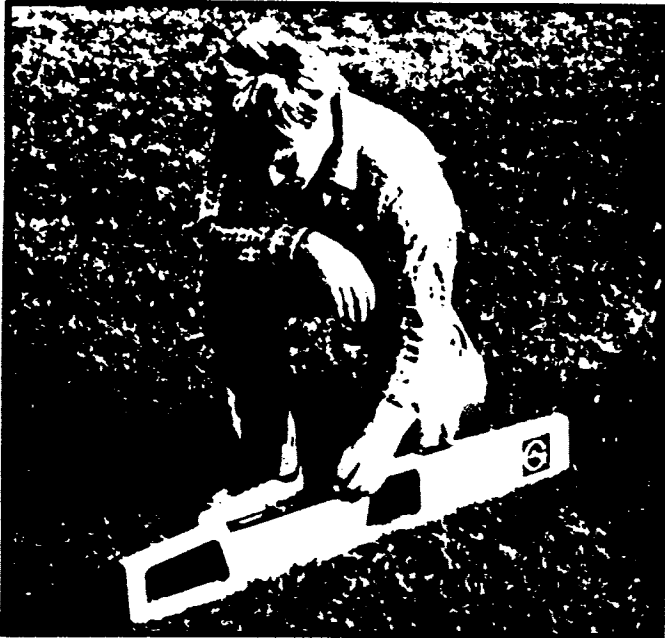
EM38

Designed to be particularly useful for agricultural surveys for soil salinity, the EM38 can cover large areas quickly without ground electrodes. Based on the same patented principles as the other Geonics Ground Conductivity Meters, the EM38 provides depths of exploration of 1.5 meters in the vertical dipole mode (shown above) and 0.75 meters in the horizontal dipole mode.

Very lightweight and only one meter long, the EM38 provides rapid surveys with excellent lateral resolution. Measurement is normally made by placing this instrument on the ground and noting or recording the meter reading. However, it is also possible to mount the EM38 on a wooden sled which is towed at walking speed across the ground while data is recorded essentially continuously (about every 0.3 m) using the DL55 digital data recorder. In this mode of operation 3000 data points can be measured easily in one hour to provide extremely dense data acquisition.

To further enhance the mapping potential of the EM38, measurement can also be made of the magnetic susceptibility of resistive soils.

In addition to agricultural applications the EM38 has proven very useful in other areas such as general geotechnical mapping and archaeology.

The EM38 comes complete with a connector for the DL55 digital data recorder.

Specifications

MEASURED QUANTITY	Apparent conductivity of the ground in mS/m
	Inphase response in parts per thousand (ppt) of secondary to primary magnetic field
PRIMARY FIELD SOURCE	Self-contained dipole transmitter
SENSOR	Self-contained dipole receiver
INTERCOIL SPACING	1 meter
OPERATING FREQUENCY	14.6 kHz
POWER SUPPLY	9V Transistor Radio Battery (e.g. Mallory MN1604)
CONDUCTIVITY RANGES	100, 1000 mS/m (4 digit digital meter)
MEASUREMENT PRECISION	±0.1% of full scale deflection
BATTERY LIFE	30 hours continuous for MN1604
DIMENSIONS	103 x 12 x 2.5 cm
WEIGHT	Instrument 2.5 kg
	Shipping 9 kg

BOREHOLE CONDUCTIVITY

EM39 Conductivity Logger

The EM39 provides measurement of the electrical conductivity of the soil and rock surrounding a borehole or monitoring well, using an inductive electromagnetic technique. The unit employs coaxial coil geometry with an intercoil spacing of 50 cm to provide a substantial radius of exploration into the host material while maintaining excellent vertical resolution; measurement is unaffected by conductive borehole fluid in the monitoring well or by the presence of plastic casing. The instrument operates to a depth of 200 meters.

The combination of a large conductivity range, high sensitivity and very low noise and drift, allows accurate measurement of subsurface conditions for groundwater contamination monitoring, for ground water and mineral exploration, and for geothermal and general geotechnical applications.

Operation of the system is enhanced by use of a motorized winch and analogue or DL55 digital data recorder. An opto-electronic counter at the tripod head triggers either data storage system at selectable depth increments so that measurement is unaffected by cranking speed.

Specifications

MEASURED QUANTITY	Apparent conductivity in mS/m	
PRIMARY FIELD SOURCE	Self-contained dipole transmitter	
SENSOR	Self-contained dipole receiver	
INTERCOIL SPACING	50 cm	
OPERATING FREQUENCY	39.2 kHz	
CONDUCTIVITY RANGES	30, 100, 300, 1000, 3000 mS/m	
DEPTH	100 meters (200 meter cable optional)	
MEASUREMENT PRECISION	2% of full scale	
MEASURMENT ACCURACY	5% at 30 mS/m	
NOISE LEVEL	<0.5 mS/m	
POWER SUPPLY	10 disposable "D" cells, or 12 VDC external power source	
DIMENSIONS	Probe	3.6 cm diameter, 133 cm length
	Console	37 x 13 x 38 cm
WEIGHT	Probe	2.2 kg
	Console	4.3 kg
	Shipping	90 kg (2 boxes)

GAMMA 39 Gamma Ray Logger

The EM39 induction conductivity logger has been designed to permit rapid, accurate measurement of groundwater contamination in the earth or rock surrounding monitoring wells since most inorganic contaminants enhance terrain conductivity due to increased concentration of total dissolved solids (TDS). Certain clays also increase the electrical conductivity; to resolve this ambiguity Geonics has introduced the Gamma 39 probe. This sensor, which measures the level of naturally occuring gamma radiation in the monitoring well, generally reflects the clay content of the surrounding material. Thus, conductivity highs with coincident gamma ray highs often indicate enhanced clay content, whereas conducitivy highs not associated with a gamma-ray high can be expected to be due to enhanced TDS in the groundwater.

Like the conductivity probe, the gamma-ray probe is unaffected by plastic casing in the well. It requires no special licences, can be used anywhere, is relatively fast to operate, and can, of course, also be employed to detect radioactive wastes in the ground.

The EM39 console and cable mate interchangeably with either the conductivity or gamma-ray probe to provide a lightweight, stand-alone exploration or contamination monitoring package.

Specifications

MEASURED QUANTITY	Naturally occuring gamma-radiation, in counts/second	
SENSOR	Thallium-activated sodium iodide crystal	
COUNTS RANGE	100, 300, 1000 counts/second	
DEPTH	100 meters (200 meters cable optional)	
MEASUREMENT PRECISION	one count/second	
POWER SUPPLY	10 disposable 'D' cells, or 12 VDC external power source	
DIMENSIONS	Probe	3.6 cm diameter, 100 cm length
	Console	37 x 13 x 38 cm
WEIGHT	Probe	1.6 kg
	Console	uses EM39 console

DL55 DIGITAL DATA RECORDER

The DL55 digital data recorder is a hand-held, programmable recorder that can be used with any of the Geonics Ground Conductivity Meters. Because Geonics uses a separate data recorder, an EM31 owner who decides to use an EM34-3 only needs to buy the inexpensive program modules to update his DL55 recorder for operation with the EM34-3. The DL55 is particularly useful with the EM31 since it automatically records both conductivity and inphase responses; with either the EM31 or EM38 it offers the facility of continuous data recording as the operator walks the survey line.

The DL55 comes complete with all programs necessary to dump the recorder into an IBM compatible computer, to edit the data, and to plot the data in stacked profile form. Contouring programs (line and colour) are also available.

Specifications

STORAGE	3000 two-channel records	
A/D RESOLUTION	12 bits	
DIMENSIONS	20 x 11.5 x 6.5 cm	
WEIGHT	Instrument	1.5 kg

VLF EM
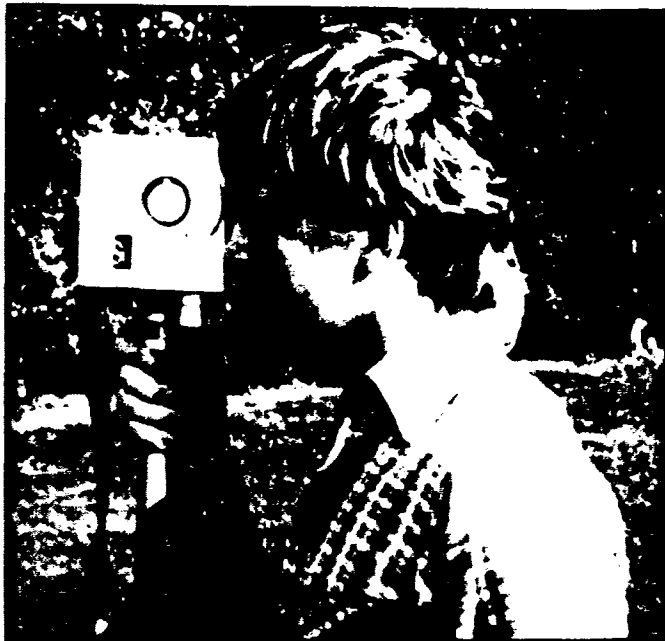
EM16

Probably the most popular and widely used electromagnetic instrument, the EM16 VLF receiver makes the ideal reconnaissance tool for mapping geological structure. This can be attributed to its field reliability, operational simplicity, compactness and mutual compatibility with other reconnaissance instruments such as portable magnetometers and radiometric detectors.

The VLF method of EM surveying, pioneered by Geonics, has proven to be a simple economical means of mapping geological structure and fault tracing. The applications are many and varied, ranging from direct detection of massive sulphide conductors, the indirect detection of precious metals and radioactive deposits, and mapping groundwater contamination in fracture zones.

FEATURES
- The EM16 measures the quadphase as well as the inphase secondary field. This has the advantage of providing an additional piece of data for more comprehensive interpretation and also allows a more accurate determination of the tilt angle.

- The secondary fields are measured as a ratio to the primary field making the measurement independent of absolute field strength.

Specifications

MEASURED QUANTITY	Inphase and quadphase components of vertical magnetic field as a percentage of horizontal primary field. (i.e. tangent of the tilt angle and ellipticity)	
SENSITIVITY	Inphase	± 150%
	Quadphase	± 40%
RESOLUTION	± 1%	
OUTPUT	Nulling by audio tone. Inphase indication from mechanical inclinometer and quadphase from a graduated dial.	
OPERATING FREQUENCY	15-30 kHz VLF Radio Band. Station selection done by means of plug-in units.	
OPERATING CONTROLS	On/Off switch, battery test push button, station selector switch, audio volume control, quadrature dial, inclinometer.	
POWER SUPPLY	6 disposable 'AA' cells	
DIMENSIONS	53 x 21.5 x 28 cm	
WEIGHT	Instrument	1.8 kg
	Shipping	8.35 kg
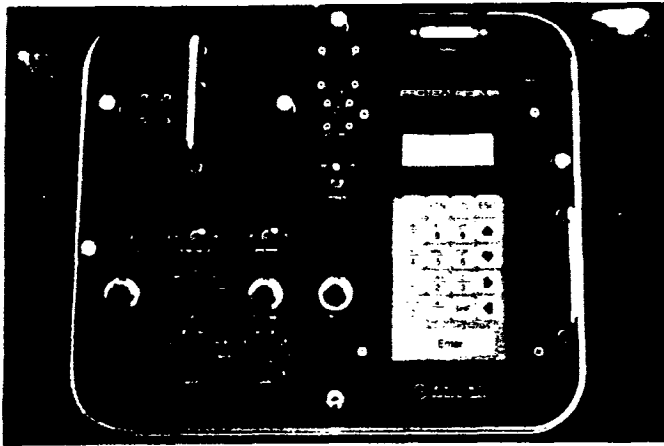
PROTEM RECEIVER

There are new insights in the employment of electromagnetic exploration systems. Large loop Turam-type systems have greatest depth of exploration in resistive bedrock. However in conductive bedrock this configuration generates a large half-space response, which makes detection of deep targets difficult, and a large galvanic current component (current gathering), which can make target differentiation on the basis of conductivity, shape, orientation, etc., less precise. Conversely a moving-transmitter configuration, with small transmitter loop in close proximity to the target, provides shallower exploration depth but reduced half-space response and enhances vortex current response with respect to galvanic current response. Good spatial resolution, now a fundamental requirement of the mineral exploration industry, can be provided only by using a moving-transmitter survey configuration with very short intercoil spacing (a few tens of meters).

Ground electromagnetic systems are routinely employed for general geological mapping such as in the search for fresh water aquifers in bedrock fractures and for mapping the shape and extent of groundwater contamination plumes. Mapping requires that calibration and stability of modern EM systems be very precise.

Recognition of these developments led Geonics Limited to create the extremely flexible PROTEM time-domain ground electromagnetic system in which the basic PROTEM receiver is used with a suite of transmitters. Using either cable reference or crystal synchronization this lightweight, multi-channel receiver operates at any of five switch-selectable base frequencies, ranging from 3 Hz to 315 Hz, with twenty logarithmically-spaced time gates at each base frequency. For example, at 315 Hz the first gate (of width 2 μsec) is located at the very early time of 6.9 μsec and the last at 707 μsec. At 75 Hz the gates extend from 49 μsec to 2.9 msec (an extended version of the Barringer INPUT ⁿ system gates) and at base frequencies of 30, 7.5 and 3 Hz the gate locations are the same as for the well known EM37-3. Four interchangeable receiver coils are used with the PROTEM receiver; the 315 Hz coil has bandwidth of 850 kHz, indicating the enormous spectral range covered by the system.

Specifications

NO. OF CHANNELS	3 (multiplexed)
MEASURED QUANTITY	Time rate of decay of magnetic flux along 3 axes
SENSORS	Different air and ferrite - cored, coils, depending on the application
REPETITION RATE (Base Frequency)	• 3 Hz, 7.5 Hz, 30 Hz, 75 Hz, or 315 Hz in countries using 60 Hz power line frequency
	• 2.5 Hz, 6.25 Hz, 25 Hz, 62.5 Hz or 262.5 Hz in countries using 50 Hz power line frequency
TIME GATES	20 geometrically spaced time gates for each base frequency gives range from 6 μs to 80 ms
SYNCHRONIZATION	• Reference cable • High stability quartz crystal (optional)
INTEGRATION TIME	17 5 msec and 70 msec
STORAGE	Solid state memory with capacity for 740 data sets. (Optional memory for up to 2,960 data sets available).
DISPLAY	4 lines x 16 character alphanumeric LCD
DATA TRANSFER	Standard RS232 communication port
RECEIVER BATTERY	12 volts rechargeable battery for 16 hours continuous operation. (8 hours with crystal synchronization).
RECEIVER SIZE	34 x 38 x 27 cm
RECEIVER WEIGHT	13 kg
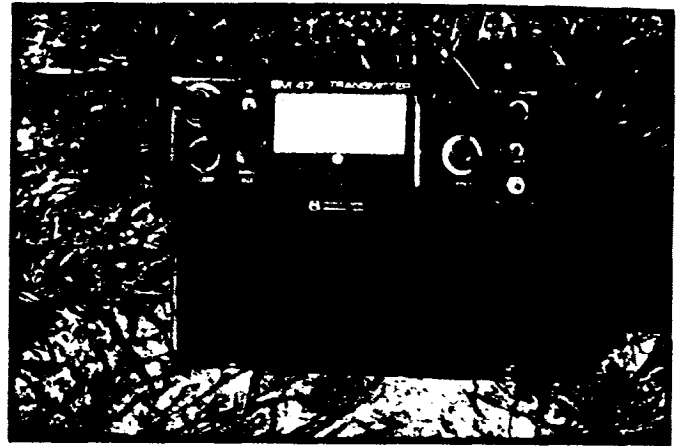
TEM47 TRANSMITTER

Three interchangeable transmitters – TEM47, TEM57 and TEM37 – are used with the PROTEM receiver to make up different PROTEM systems for various applications such as mineral exploration, structural mapping, resistivity sounding, etc.

The fastest transmitter, the TEM47, is a small, lightweight, battery operated transmitter. When used in the PROTEM 47/P (profiling) mode it supplies 3 amps to an 8 turn, 5 m x 5 m moving transmitter loop to provide a dipole moment of 600 amp-m². With base frequency of 75 Hz and 20 gates from 49 μsec to 2.9 msec this configuration is optimal for Slingram (horizontal loop) surveys for mineral exploration to shallow depths, and for groundwater exploration in bedrock fractures. Electrical sounding is performed simultaneously with the search for dike-like targets.

The TEM47 transmitter can also be used in the PROTEM 47/S (sounding) mode to drive 3 amps into a 40 m x 40 m, single turn loop with a linear ramp turnoff time of only 2.5 μsec, for very shallow sounding. Maximum transmitter output is 3 amps into a single turn, 100 m x 100 m loop. The PROTEM 47/S mode, designed for shallow sounding in the 5 m to 150 m depth range, is ideally suited for many geotechnical applications.

The TEM47 transmitter uses a reference cable to achieve the high synchronization accuracy required for shallow sounding.

Specifications

CURRENT WAVEFORM	Bipolar rectangular current with 50% duty cycle
REPETITION RATE	• 30 Hz, 75 Hz or 315 Hz in countries using 60 Hz power line frequency
	• 25 Hz, 62.5 Hz or 262.5 Hz in countries using 50 Hz power line frequency
TURN-OFF TIME	Very fast linear turn-off 2.5 μs at 2 amps into 40 m x 40 m loop. Faster in smaller loop.
TRANSMITTER LOOP	• Any dimension from 5 m x 5 m to 100 m x 100 m maximum at 3 amps.
	• Multiple-turns loop possible.
OUTPUT VOLTAGE	0 to 9 volts continuously variable
POWER SOURCE	Internal 12 volts rechargeable battery
BATTERY LIFE	5 hours continuous operation at 2A output current
TRANSMITTER SIZE	10.5 x 24 x 32 cm
TRANSMITTER WEIGHT	5.3 kg

ELREC 6

MULTI CHANNEL IP FOR MINING EXPLORATION

ELREC 6 SAMPLING MODES
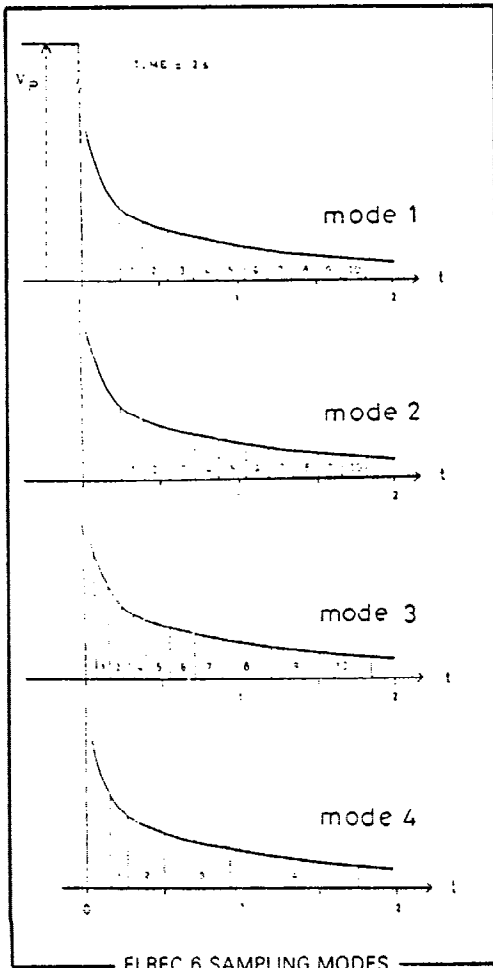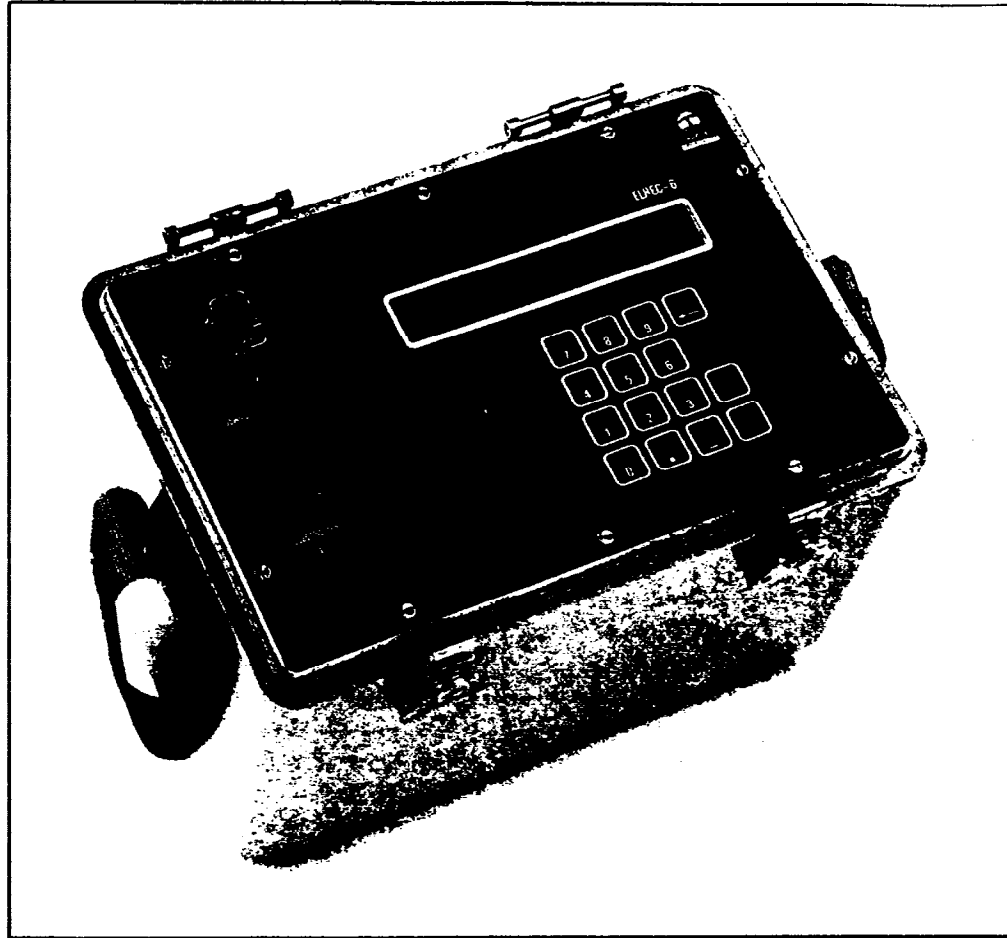
Backed by the success of ELREC and ELREC 2, **BRGM INSTRUMENTS** introduces **ELREC 6,** a six channel multiwindow Time Domain Induced Polarization receiver.

The **six channels** permit to measure six receiver dipoles, which provides a high efficiency in the field, specially when used with the multidipole cable.

IP decay curves may be analysed by various types of sampling : up to **10 windows** are available, with arithmetic or logarithmic widths, preset or programmable. This multiwindow analysis provides a high accuracy in the definition of the decay curve.

Measurements are made very easy through a fully automatic measuring process : self test and calibration, autosynchronization and resynchronization at each cycle, continuous tracking of SP including linear drift correction, automatic gain selection, digital stacking for noise reduction, and fully documented displays are controlled by the microprocessor

to ensure the highest accuracy and reliability of the results.

The operator can select various reading options regarding the parameters which are displayed : display of **Running** or **Cumulative** average values for monitoring the noise; display of **Normalized** or **True** chargeability values for referring or not to a standard decay curve; during the measurement possibility of simultaneously displaying the average chargeabilities of the six dipoles, or their standard deviations, or the primary voltage, average chargeability and standard deviation of each dipole.

The internal memory can store eighteen hundred measurements; a serial link permits to transfer the data to a printer for listing the results or to a microcomputer for storing, plotting and interpreting the data.

SPECIFICATIONS

- 6 input channels.
- up to 10 chargeability windows:
  Mode 1 : 10 preset arithmetic windows.
  Mode 2 : 10 programmable arithmetic windows (delaytime and window width).
  Mode 3 : 10 preset logarithmic windows.
  Mode 4 : 3 to 6 preset logarithmic windows.
- signal waveform : symmetrical time domain (ON+, OFF, ON-, OFF) with a pulse duration of 1, 2, 4 or 8 s. input impedance : 10 Mohm.
- input overvoltage protection up to 1 000 Volts.
- input voltage range
  - each dipole : 8 V maximum.
  - sum of voltages dipoles 2 to 6 : 12 V maximum.
- overload indication.
- automatic gain ranging.
- automatic stacking, automatic SP bucking (-1 V to +1 V) with linear drift correction up to 1 mV/s.
- sampling rate : 10 ms.
- 50 and 60 Hz power line rejection greater than 100 dB.
- accuracy in synchronization : 10 ms.
- common mode rejection : 86 dB (for Rs = 0).
- primary voltage
  - resolution : 10 μV.
  - accuracy typ. 0.3%; max 1%.
- chargeability
  - resolution : 1mV/V for Vp>10 mV.
    0.1 mV/V for Vp>100 mV.
  - accuracy typ. 0.6%; max 2% for Vp>10 mV.
- display of primary voltage, partial and average chargeabilities, standard deviation of primary voltage and of average chargeability, computation of apparent resistivity (dipole dipole, pole dipole, gradient, VES, ...).
- battery test : manual and automatic before each measurement.
- grounding resistance measurement from 0.1 to 128 kohm.
- memory capacity : about 1 800 measurements.
- RS 232 C link to transfer the data to printers or microcomputers; transfer rates : 300 to 19 200 bauds.
- a remote control is provided, as an option, in order to drive the unit through a microcomputer.

GENERAL FEATURES

- dimensions : 30 x 20 x 20 cm (12 x 8 x 8 inch).
- weight : 7.5 kg (17 lb.).
- operating temperature range : -40°C to +70°. The above mentioned specifications are given over the entire temperature range.
- storage temperature range : -40°C to +85°C.
- power supply : six 1.5 V D size alkaline dry cells (20 hours of operation at 20°C).

FREQUENCY MODE OPTION

An analysis of the measurements in the Frequency Domain is provided as an option, through a Fourier Transform Computation of either a Frequency Domain Waveform (ON+, ON-) or a Time Domain Waveform (ON+, OFF, ON-, OFF), and a pulse duration of 1, 2, 4 or 8 sec.
The parameters measured are the amplitudes of the fundamental and of the first six odd harmonics (3RD to 13TH), the frequency effects and relative phases of the harmonics with respect to the fundamental, and the standard deviations of these parameters. Due to the large amount of data gathered, the capacity of the internal memory is reduced by fifty percent in the frequency mode.
Both types of data measurements (Time and Frequency domains) can be carried out and stored alternatively in the memory, to give to **ELREC 6** receiver the highest versatility.

IPT-1

Variable Frequency, Time Domain and Phase IP Transmitter

- **Reliable:** Backed by twenty years experience in the design and worldwide operation of induced polarization and resistivity equipment

- **Versatile:** Can be used for resistivity, variable frequency IP, time domain IP or phase angle IP measurements

- **Stable:** Excellent current regulation

- **Lightweight, portable**

- **Wide selection of power sources**

- **Low cost**

Transmitter Configurations

	for Variable Frequency and Time Domain IP		for Phase and Spectral IP	
Timing Options	Internal A Model Timing Board	Internal B Model Timing Board	External Precision Clock Module	External Isolated Cable Drive
Console		IPT-1 Console		
Power Modules	BPS-1 Low Power Dry Cell Battery Module	BPS-2 Medium Power Rechargeable Battery Module	AC 3000 Standard Transformer Module	AC 3003 Extended Frequency Transformer Module
Motor Generators		MG-1 1 KVA	MG-2 2 KVA	MG-3 3 KVA

PHOENIX GEOPHYSICS LIMITED

Geophysical Consulting and Contracting, Instrument Manufacture, Sale and Lease.

Motor Generators

There are three motor generators, differing in weight and power, which can be used with the transformer power modules. All three supply three phase, 400 Hz (350 to 600 Hz), 60V (45V to 80V). The voltage is regulated by feedback from the transmitter.

MG - 1: This lightweight unit is designed for easy portability in areas of moderately high resistivity. It is well suited for massive sulfide exploration in Northern Canada, Europe and Asia, as well as general IP and resistivity surveys in rugged, mountainous areas around the world. The motor is a 4-cycle Briggs and Stratton which produces 3 HP at 3600 rpm. The dimensions of the unit, including packframe, are 40 x 45 x 60 (16 x 18 x 24 in). Total weight is 25 kg (55 lb).

MG - 2: 2KVA motor generator. This versatile unit is adequate for the vast majority of IP and resistivity surveys conducted worldwide. It is light enough to be carried by one man, yet powerful enough for most survey requirements. The motor is a 4-cycle Briggs and Stratton which produces 5 HP at 3600 rpm. The dimensions of the unit, including packframe, are 40 x 45 x 60 cm (16 x 18 x 24 in). Total weight is 34 kg (75 lb).
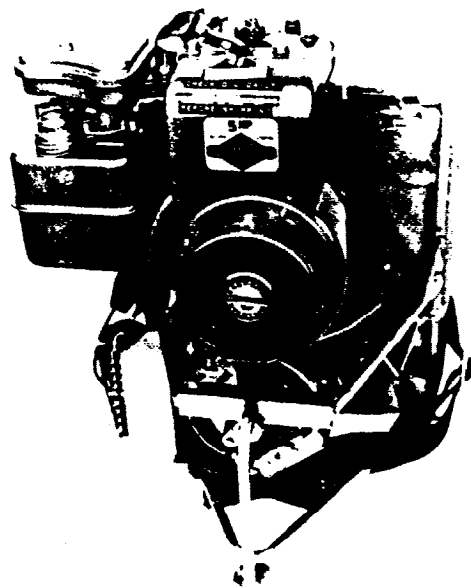
MG - 3: 3KVA motor generator. This two-man portable unit is designed for surveys in areas which require additional power. The motor is a 4-cycle Briggs and Stratton which produces 8 HP at 3600 rpm. The unit is mounted in a square frame with dimensions 40 x 48 x 75 cm (16 x 19 x 29 in). Total weight is 55 kg (120 lb).
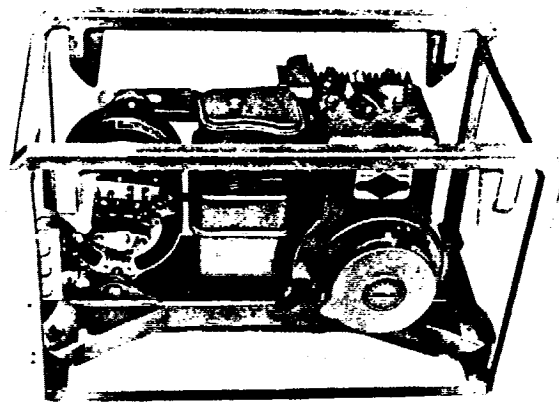
APPENDIX C

Conductivity in the Earth

APPENDIX C

ELECTRICAL CONDUCTIVITY IN THE EARTH

For more quantitative work, surface conductivity measurements, when inverted to three-dimensional conductivity measurements, can be used to extrapolate the chemistry as measured on water samples between holes. To extract more quantitative information from the geophysical data we need to examine the relationships between measured bulk conductivity, pore fluid conductivity and chemistry.

The average or bulk electrical conductivity of the earth is determined by the conductivity of the fluid in the pore spaces, the conductivity of the soil or rock matrix, the pore fluid volume (porosity), the connections between the pores (permeability) and the temperature.

For clean (clay-free) saturated soil or rock the bulk conductivity can be approximated using an empirical relationship known as Archie's law (Archie, 1942) as follows:

$$\frac{\sigma_b}{\sigma_f} = n^m$$

where

σ_b = the bulk conductivity
σ_f = the pore fluid conductivity
n = the fractional porosity
m = an empirical constant

This formula assumes that the soil or rock matrix is perfectly resistive.

The empirical constant m varies from 1.2 for perfectly spherical grains to 1.85 for platy, flat grains with natural sands having values in the range 1.4 to 1.6. Figure C1 shows the value of $\frac{\sigma_b}{\sigma_f}$ for m = 1.6. Clean sand, with a typical porosity of 30%, has a $\frac{\sigma_b}{\sigma_f}$ ratio of 0.13 indicating that the bulk conductivity is only 13% of the fluid conductivity or equivalently the fluid conductivity is 7.7 times the bulk conductivity. The actual conductivities as measured in boreholes at 32 sample points in this study are shown in Figure C2. In this case, the fluid conductivity was measured on water samples and the bulk conductivity was measured with a downhole EM system. The best fit linear relationship yields a value of 4.03 for the ratio of fluid to bulk conductivity.

The value of this ratio is important because it provides one link in the chain for calculating TDS in the pore fluid from measured conductivity.
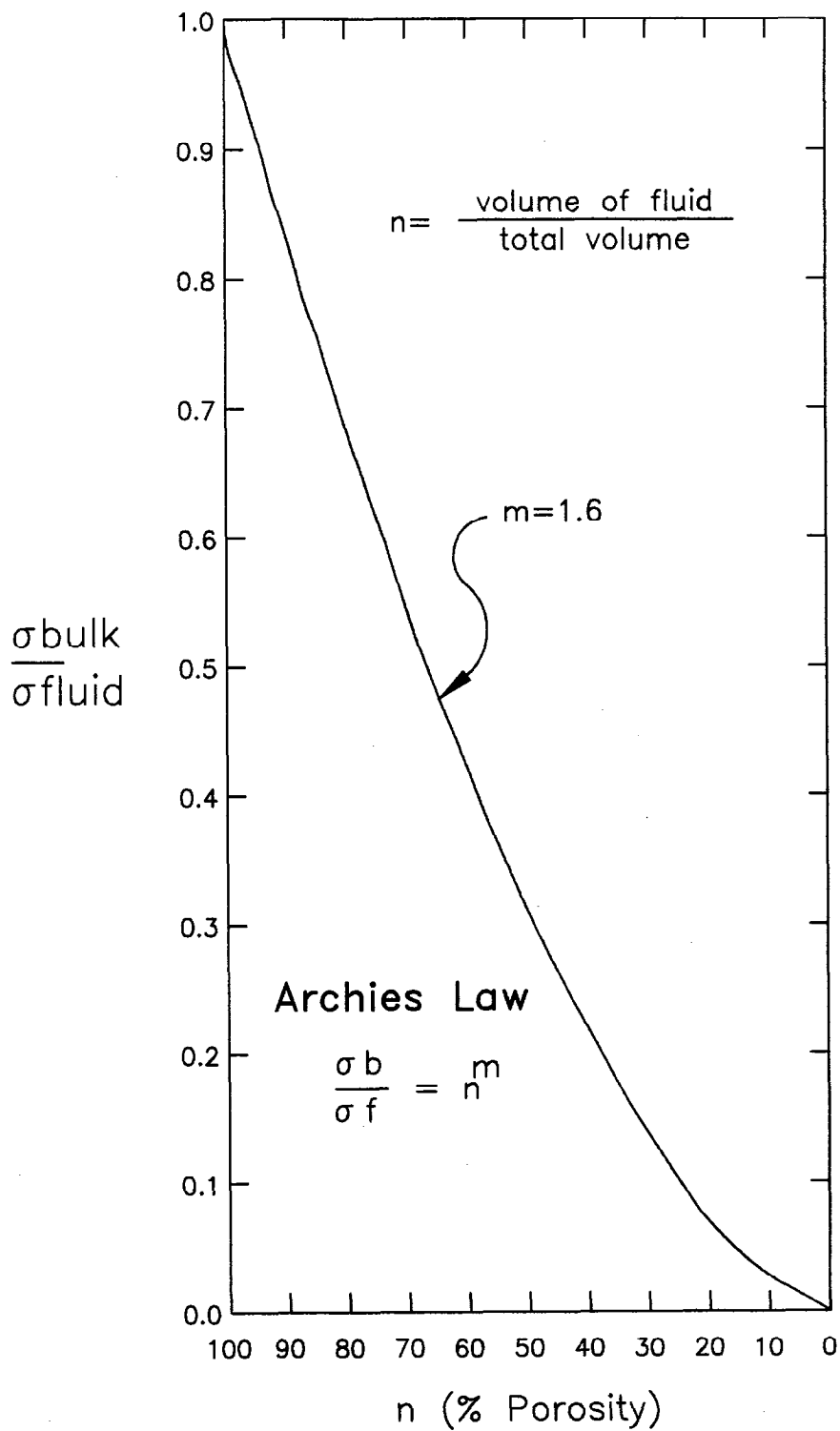
Graph of Archies Law

(from Geonics, 1980a)
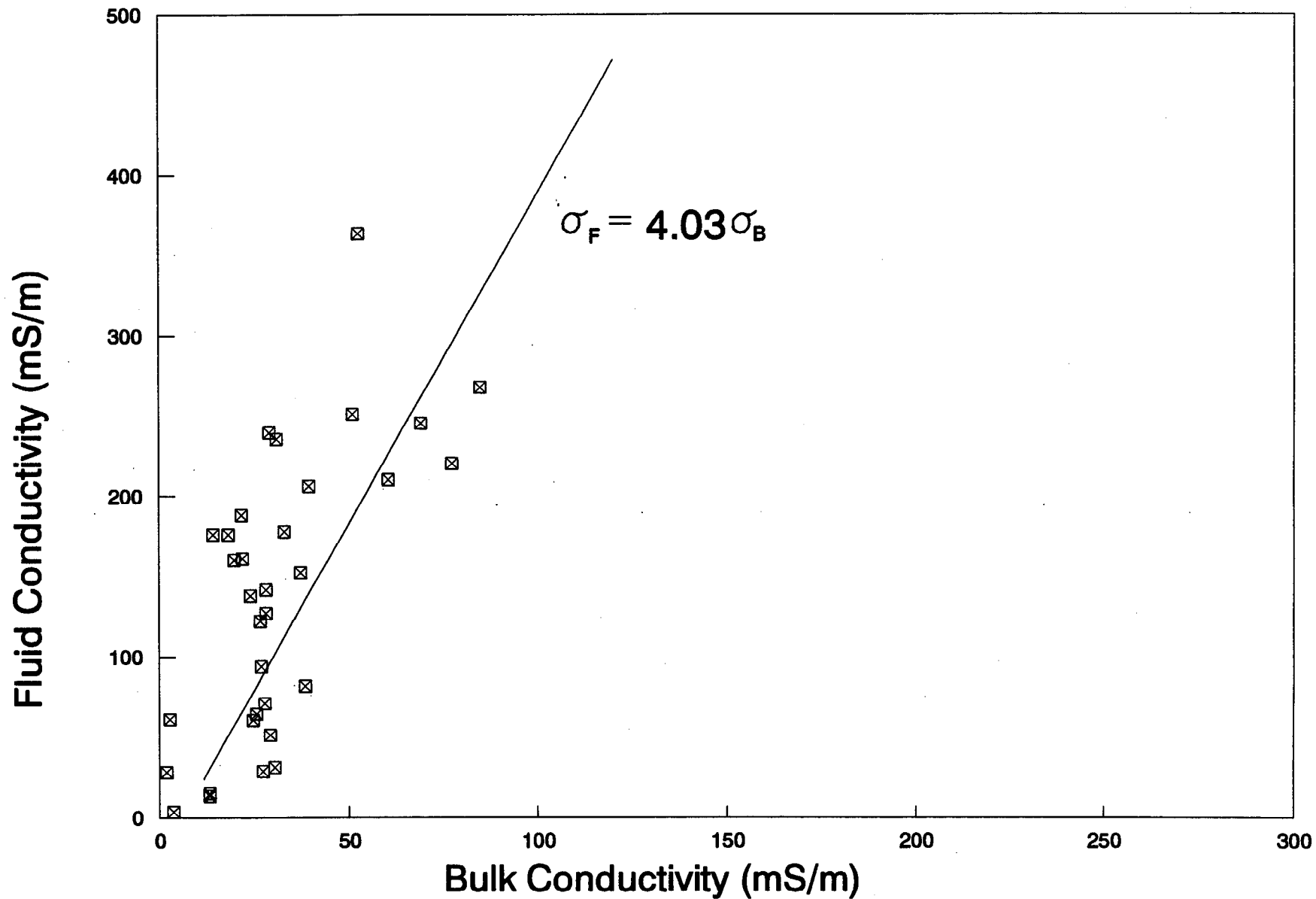
FIGURE C1

FLUID CONDUCTIVITY VS. BULK CONDUCTIVITY

FIGURE C2

The difference between the theoretical and observed ratios could be due to a number of factors including variations in porosity, clay content, sampling procedures, temperature and lack of absolute calibration between the BHEM bulk conductivity measuring system and the portable conductivity meters used to measure pore fluid conductivity.

To investigate the variation in this ratio systematically, it is recommended that:

i) porosity be measured in holes either on samples or with geophysical porosity logs;

ii) clay content be measured in holes either on samples or with other geophysical logs (gamma, etc.);

iii) BHEM system and the conductivity meters be calibrated by immersing the BHEM probe in waters of varying conductivity (lakes, tailings ponds, treatment ponds, etc.) and simultaneously measuring the water conductivity with the conductivity meter; and

iv) temperature be measured and corrected for if necessary.

The reduction in bulk conductivity with respect to the fluid conductivity is important as it can substantially reduce the detectability of conductive areas by electrical or EM methods which rely on conductivity contrasts. In clean soils (clay-free) the relative reduction in bulk conductivity is the same for all conductivities so the conductivity contrast and detectability (to the noise level of the system) is preserved. However, in most areas, there is some clay in the soil which produces a low background conductivity below which conductivity variations due to changes in pore fluid conductivity cannot be detected.

Archie's law describes the relationship between bulk and pore fluid conductivity. To complete the link between bulk conductivity and chemistry it is necessary to establish the relationship between fluid conductivity and chemistry.

TN5 (Geonics 1980a) gives an equation for calculating conductivity in reasonably dilute solutions.

$$\sigma = 96500[C_1M_1 + C_2M_2 + ...] = 96500\Sigma C_1M_1$$

Where C_1 = no. of gram equivalent weights of
i^{th} ion per 10^6 cm^3 of water
M_1 = mobility of the ith ion in metres per
second per volt per metre

Table C1 gives an expanded list of mobilities of all the ions likely to be involved in AMD. These were calculated from equivalent conductances given in Dobos (1975).

The factors for converting conductivity to concentration for individual ionic species can be derived from this equation. Freeze and Cherry (Freeze et al., 1979) give an approximate multiplication factor of 6.5 for converting from conductivity in mS/m to TDS in mg/l. Table C1 shows that there is considerable variation in this factor for different ions

and provides exact conversion factors (at 25 degrees C) for each ionic species. Chemistry cannot be derived from conductivity, but if the relative proportions of the different ionic species are known from sampling, these factors can be used together with the measured bulk conductivity to interpolate chemistry between sample points.

The inverse of these factors can be used to calculate total fluid conductivity from chemistry. Of course, it is necessary to include the temperature correction, given in TN5, of 2.2% increase in conductivity per degree C for accuracy.

In summary, pore fluid conductivity can be calculated from bulk conductivity using Archie's law if the porosity is known and a suitable exponent m has been established. In the absence of any chemical data, TDS can be estimated from fluid conductivity using the approximate value from Freeze and Cherry. Given:

  i)   a 3D model of the relative abundances of the different ionic species based on interpolation between water sample points,
  ii)   a 3D model of porosity based on porosity measurements in drill holes and geological modelling, and
  iii) three-dimensional bulk conductivity data from inversion of surface data with borehole control, then

the concentration of the different ionic species can be estimated in three dimensions between sample locations, provided the main source of the conductivity is due to groundwater and not to clays.

BIBLIOGRAPHY

Archie, G.E. (1942)
  "The electrical resistivity log as an aid in determining some resevoir characteristics",
  Trans. A.I.M.E. 146, p. 54-62

Dobos, D. (1975)
  "Electrochemical data", Elsevier, New York

Freeze, R.A., Cherry, J.A. (1979)
  "Groundwater", Prentice Hall

Common Geophysical Methods

METHOD	PHYSICAL PROPERTY
Electrical - Galvanic	Conductivity/Resistivity
- Electromagnetic	Conductivity/Resistivity
- Induced Polarization	Chargeability or Polarization (Low Frequency)
Radiometric	Radiation
Magnetic	Magnetic Susceptibility or Magnetization
Seismic	Acoustic Velocity and/or Density
Radar	Dielectric Constant
Thermal	Temperature
Gravity	Density

TABLE 1

TABLE 2

Instrument	Coil Spacing	Coil Orientation and Height	System Abbreviation	Effective Depth of Penetration
EM31	3.66 m	Horizontal dipoles on ground	EM31HG	2 m
EM31	3.66 m	Vertical dipoles at hip level	EM31VH	4 m
EM31	3.66 m	Vertical dipoles on ground	EM31VG	5 m
EM34	20 m	Horizontal dipoles on ground	EM34/20H	12 m
EM34	40 m	Horizontal dipoles on ground	EM34/40H	24 m
EM34	40 m	Vertical dipoles on ground	EM34/40V	48 m
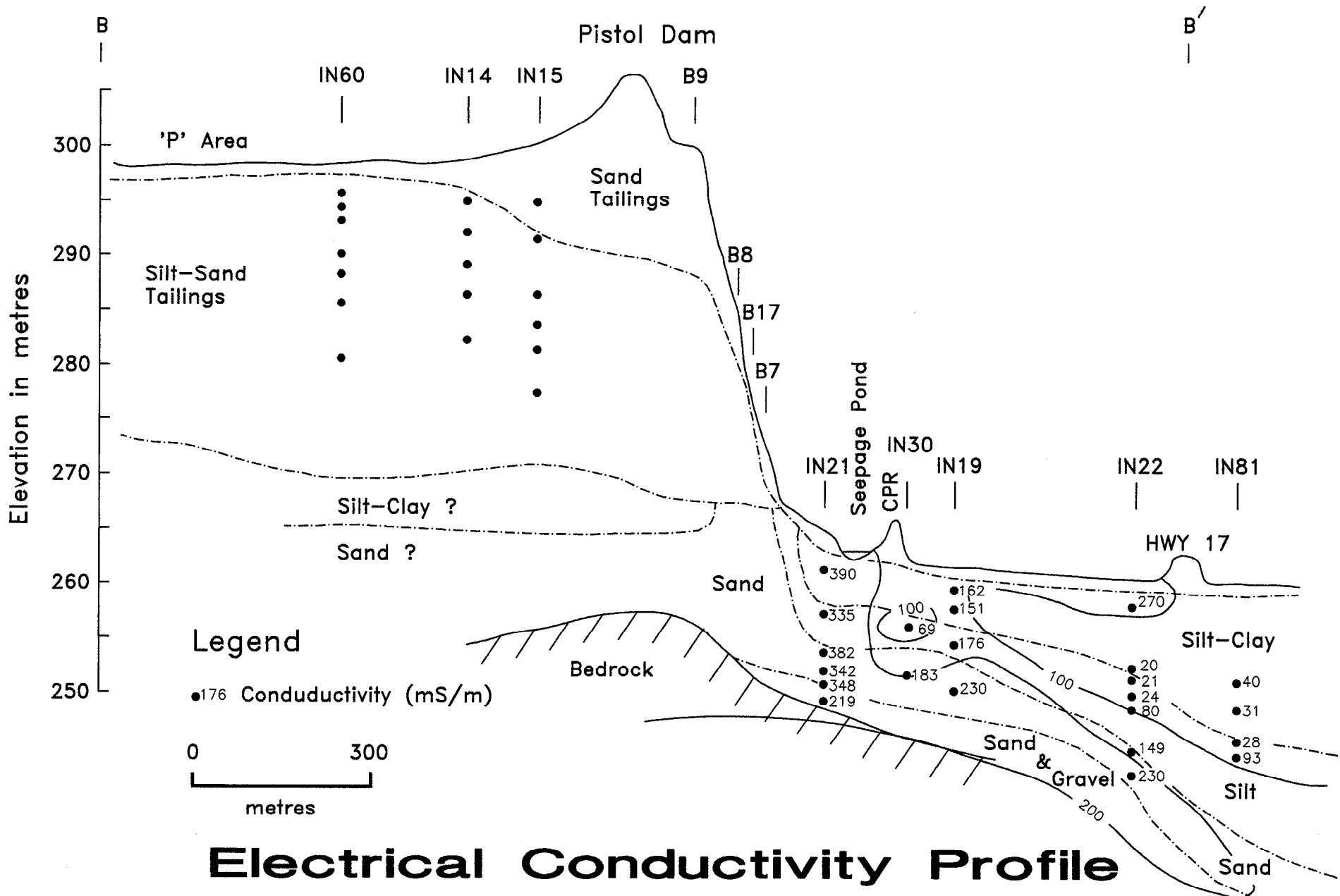
**Electrical Conductivity Profile
Section B (Robertson et al. 1992)**

FIGURE 5.1.3

LEGEND

■	TAILINGS
▓	TAILINGS WATER
—	ROADS
⊥⊥⊥	TAILINGS

INCO Tailings

LOT 9
CON 3

Falconbridge Tailings

Moose Lake System

Town of Levack
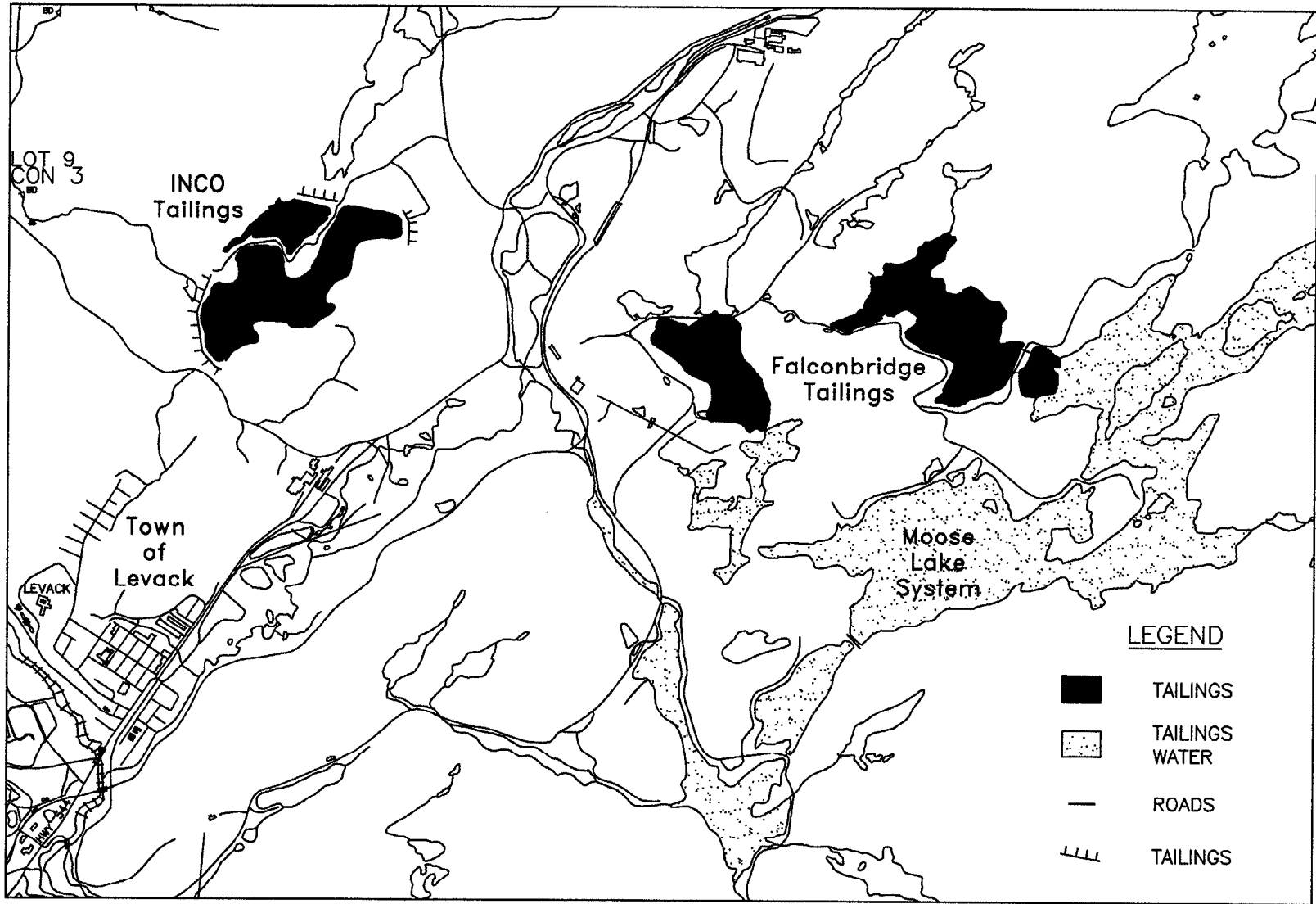
LEVACK

Levack Area Tailings
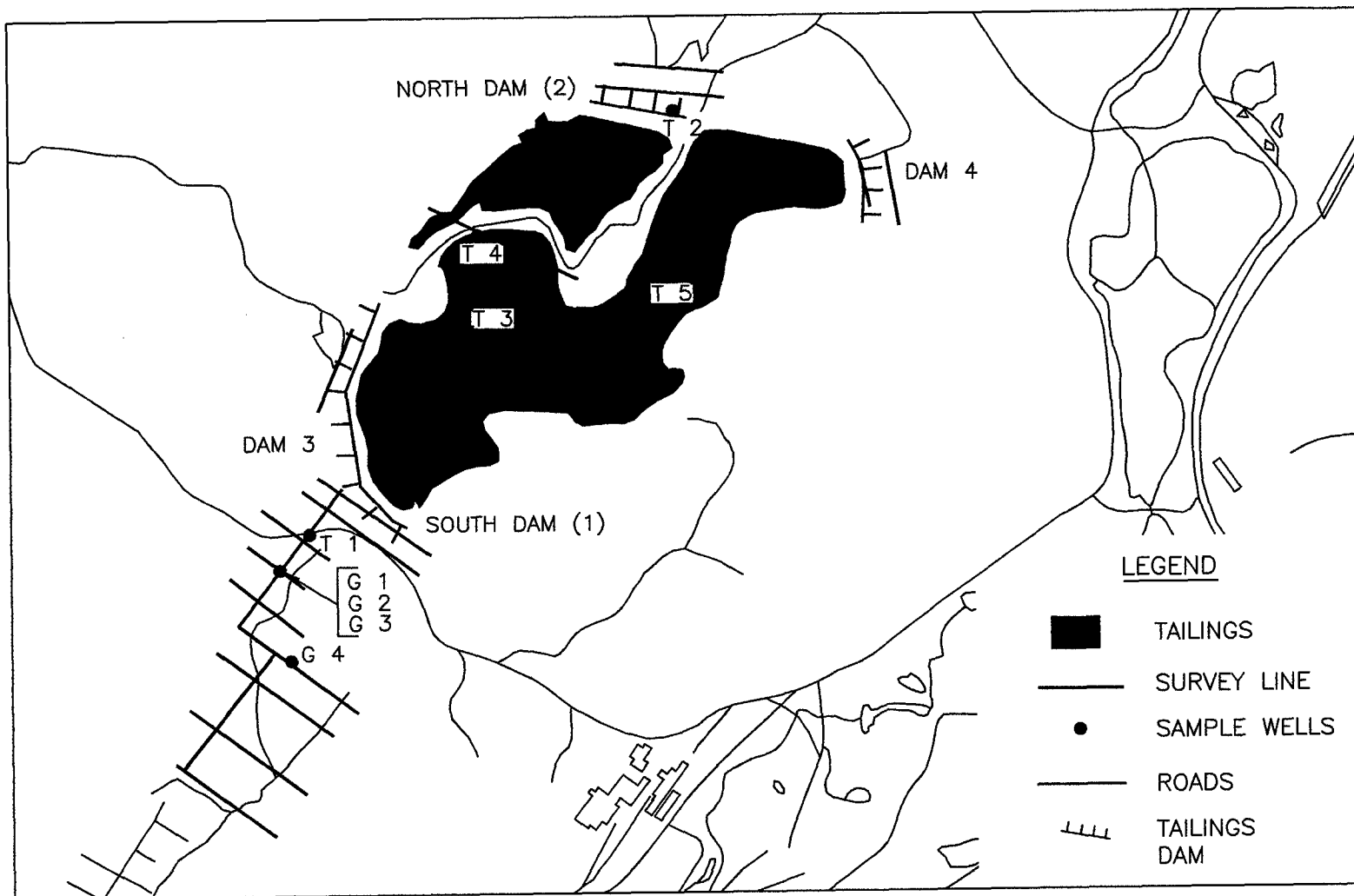
FIGURE 5.2.1

INCO Levack Tailings

FIGURE 5.2.2
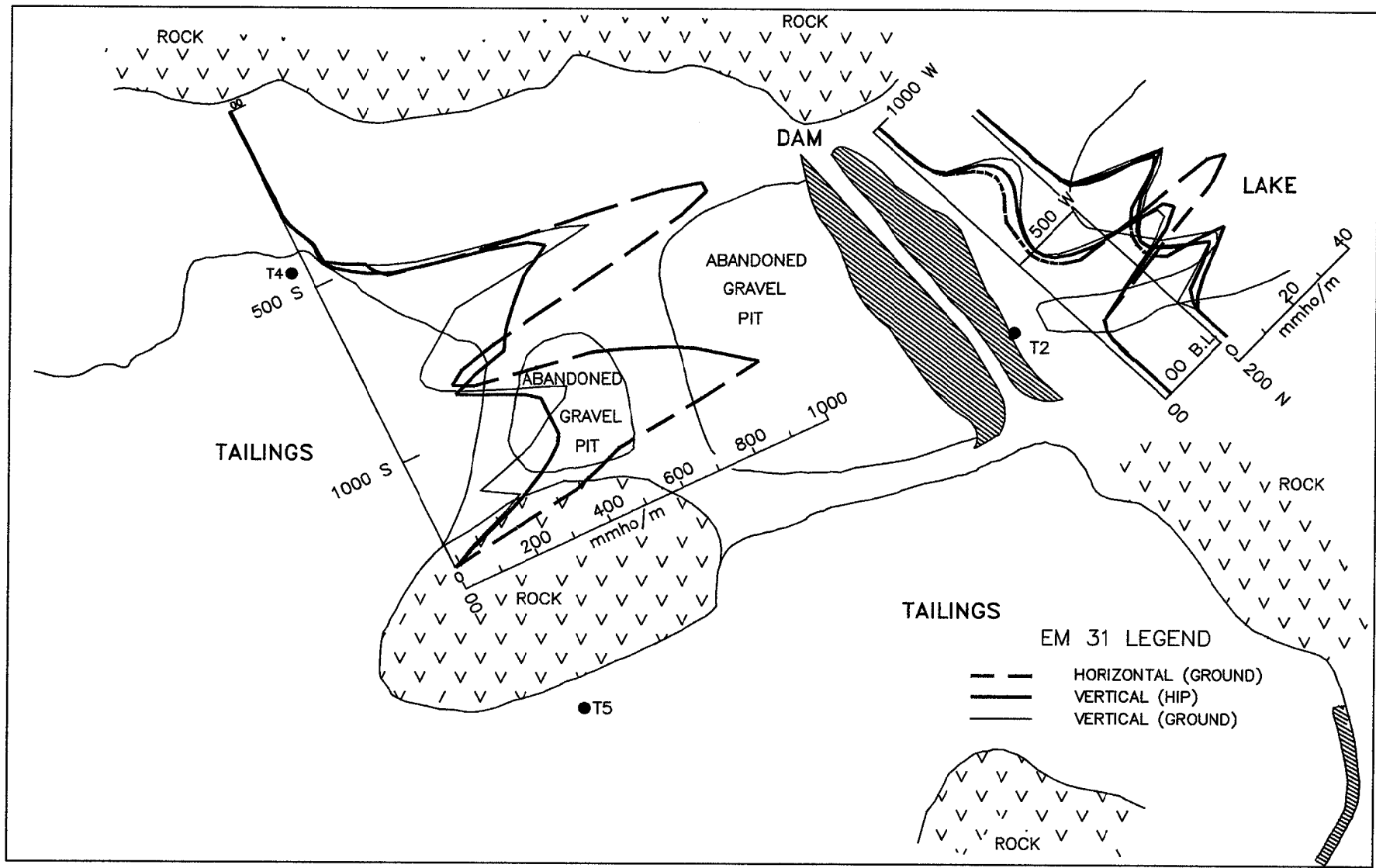
North Dam Profiles - EM31

FIGURE 5.2.2.1A

ROCK

ROCK

DAM

1000 W

500 W

LAKE

T4●

ABANDONED
GRAVEL
PIT

●T2

00 10 20

0

mmho/m

00

200 N

ABANDONED
GRAVEL
PIT

TAILINGS

ROCK

V V V V V V V V V V ROCK

TAILINGS

●T5

EM 34 LEGEND

——————— 20H
- - - - - - - - - 40H

ROCK

North Dam Profiles - EM34

FIGURE 5.2.2.1B

Natural Conductivity of Soils

FIGURE 2.1

SPECIFIC CONDUCTANCE
(per unit charge)
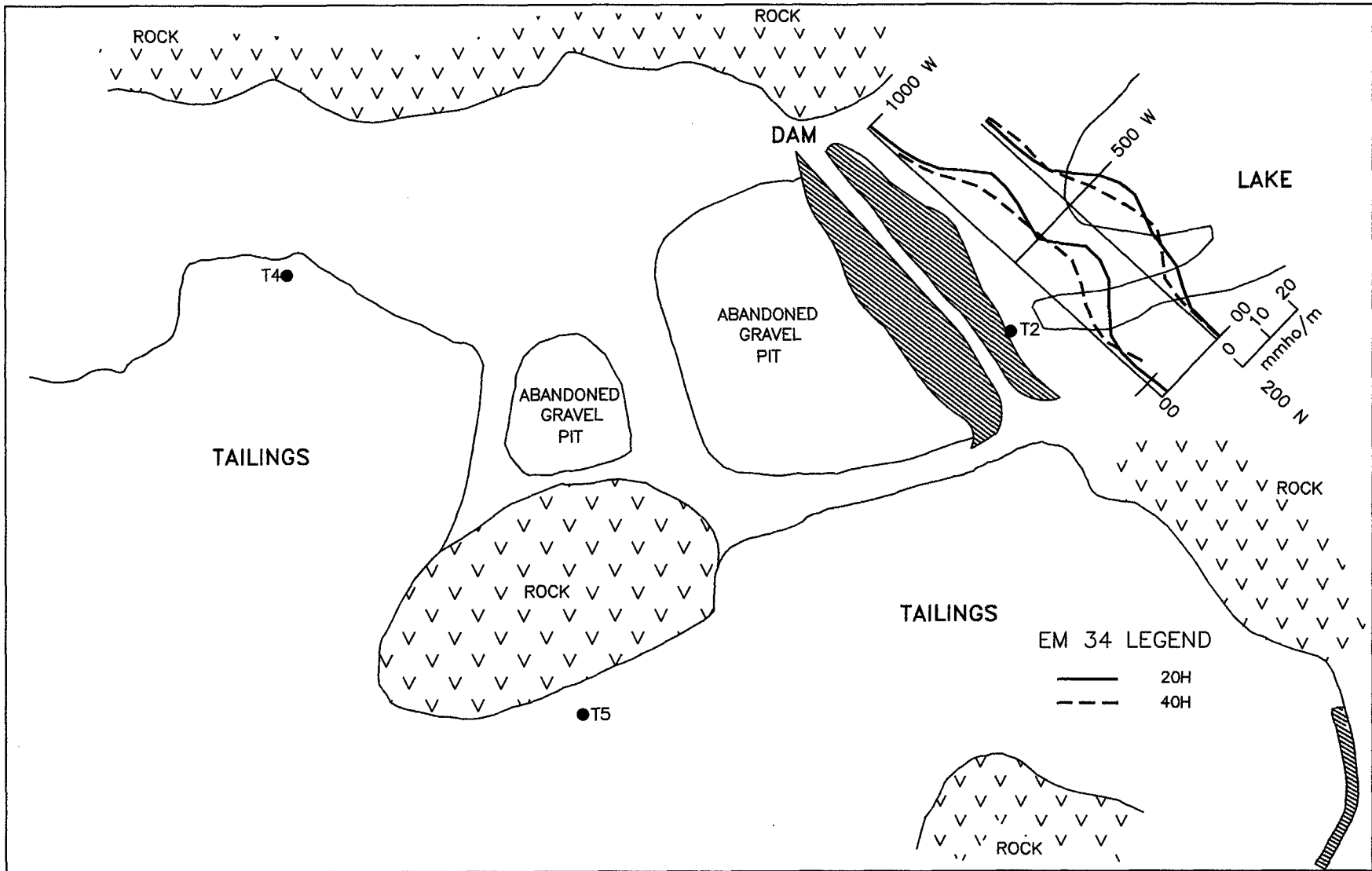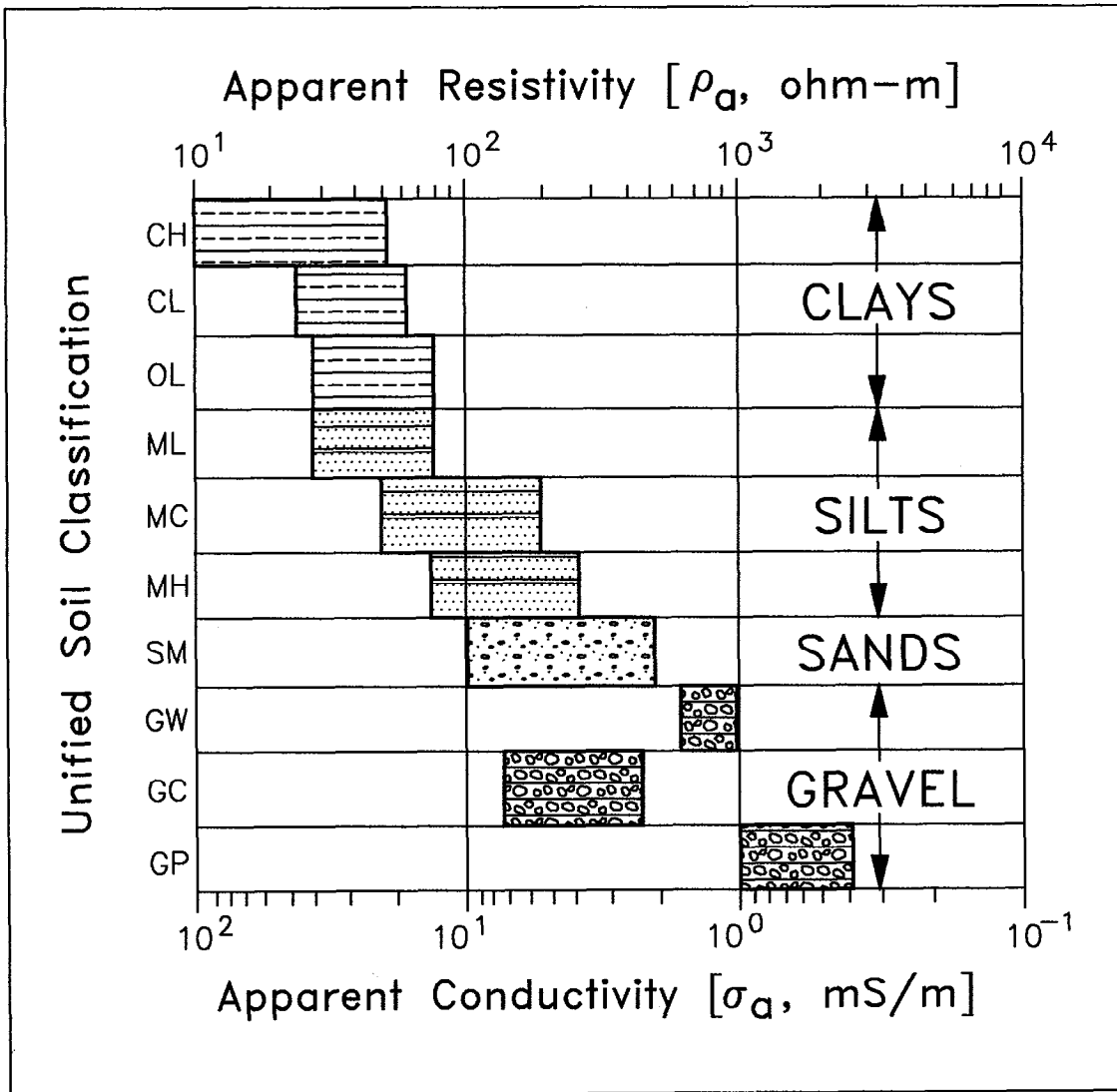
Major Ions
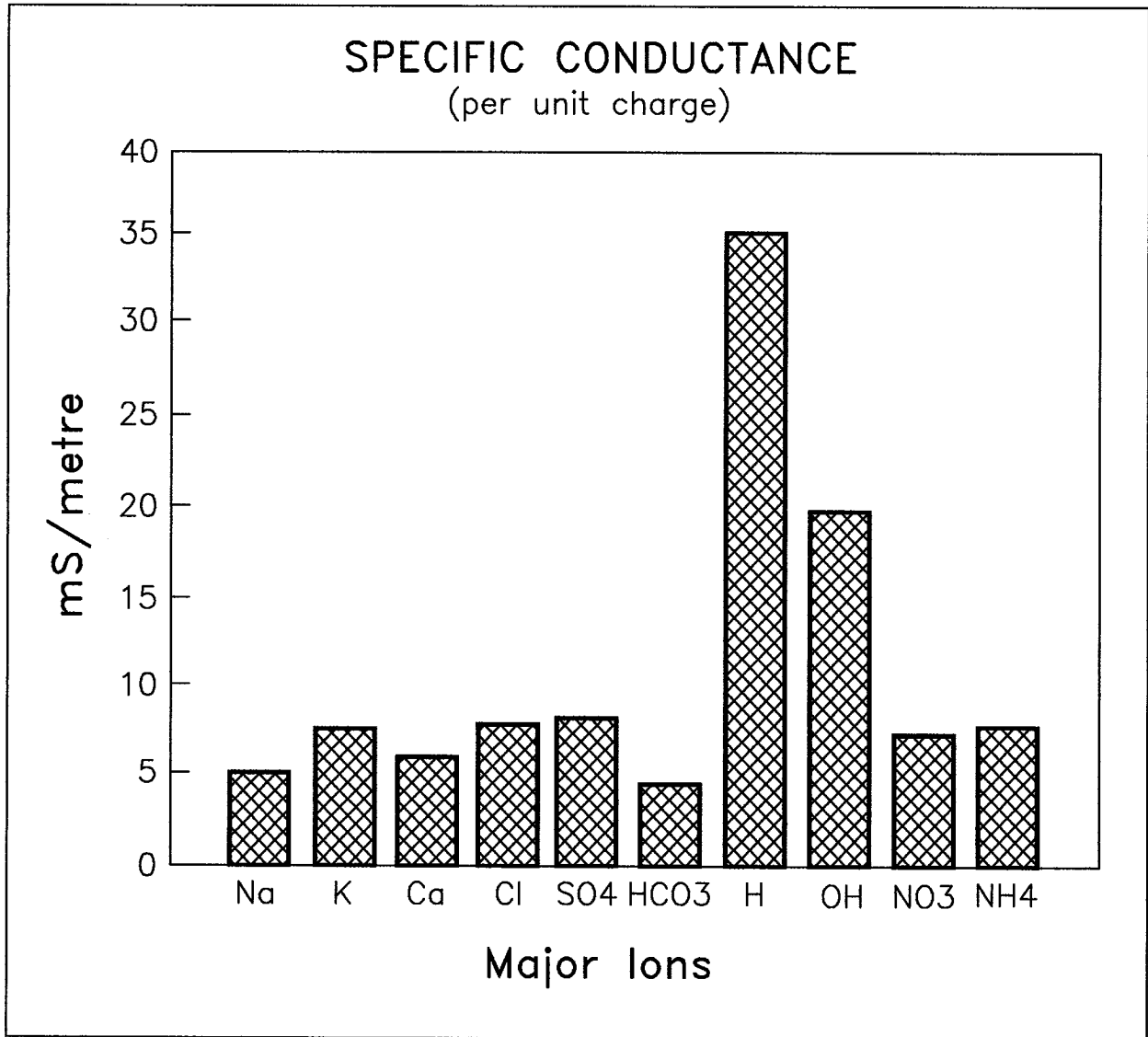
**Conductivity Contribution
of Specific
Groundwater Ions**

FIGURE 2.2
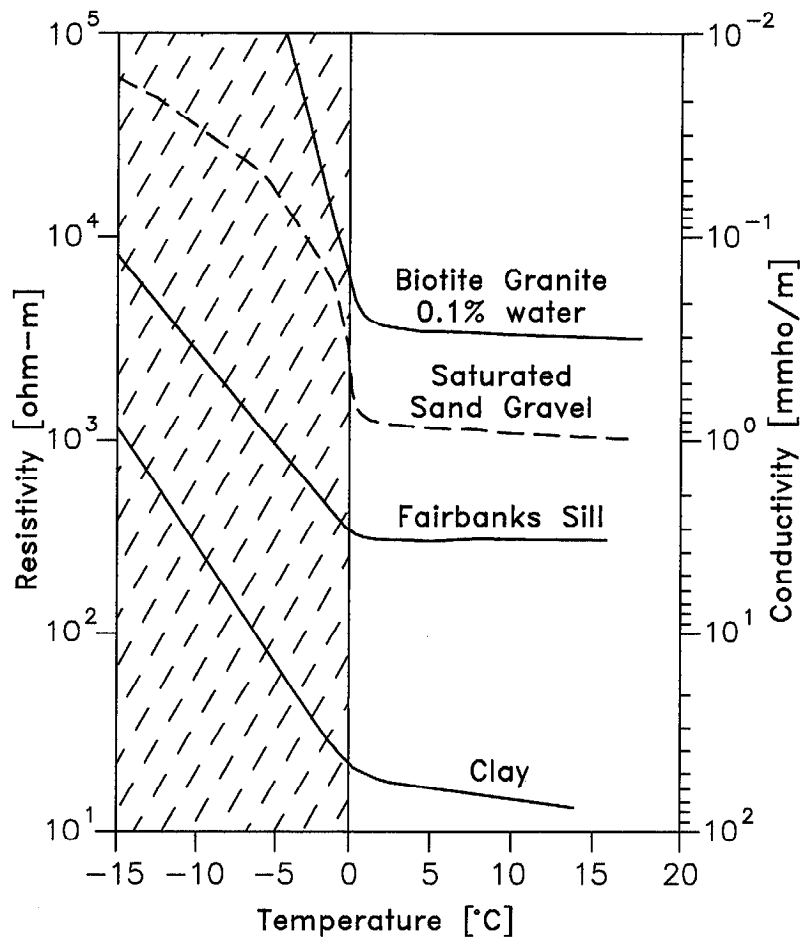
a: TEMPERATURE – CONDUCTIVITY RELATIONS
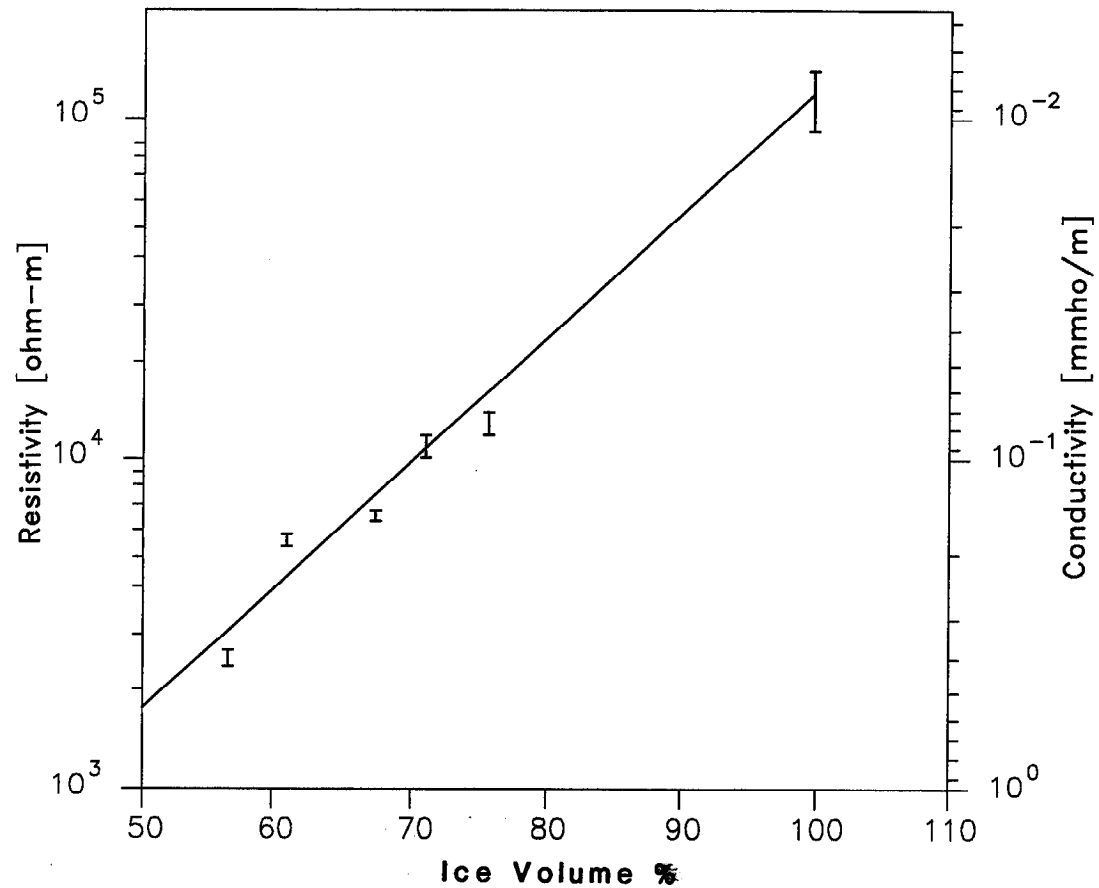
b: ICE CONTENT – CONDUCTIVITY

Conductivity Variation with Temperature and Ice Content

(HOEKSTRA and McNEILL, 1973)

FIGURE 2.3

Tailings

Profile B

M8

M10

2

12 M11 Ditch M15

Creek

Buckles

6 M13

M14
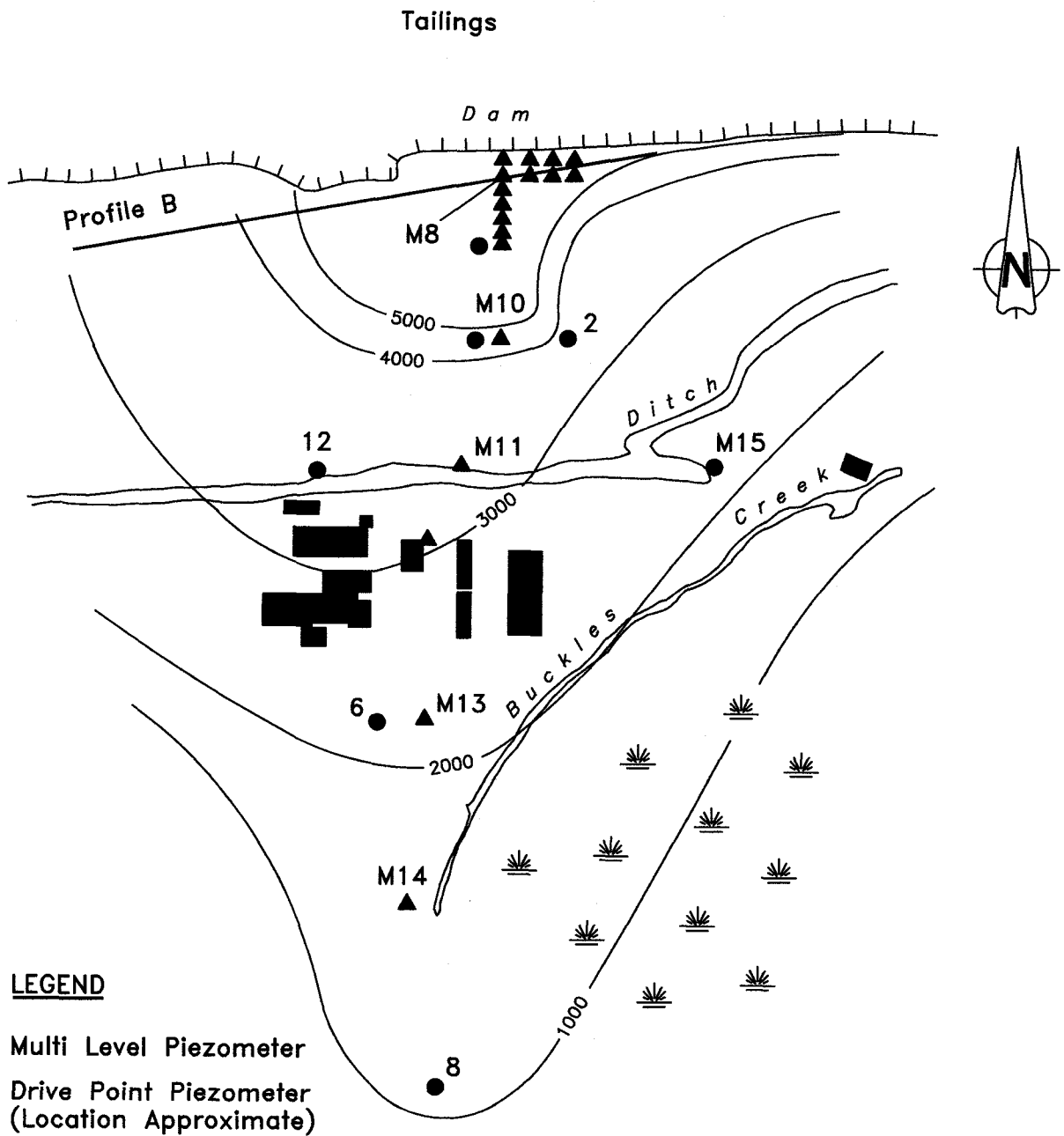
LEGEND

▲ Multi Level Piezometer

● Drive Point Piezometer
(Location Approximate)

8

Sulphate in Groundwater (mg/l)

Contour Locations
Approximate
(After Pehme, 1981)

0   50

m
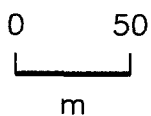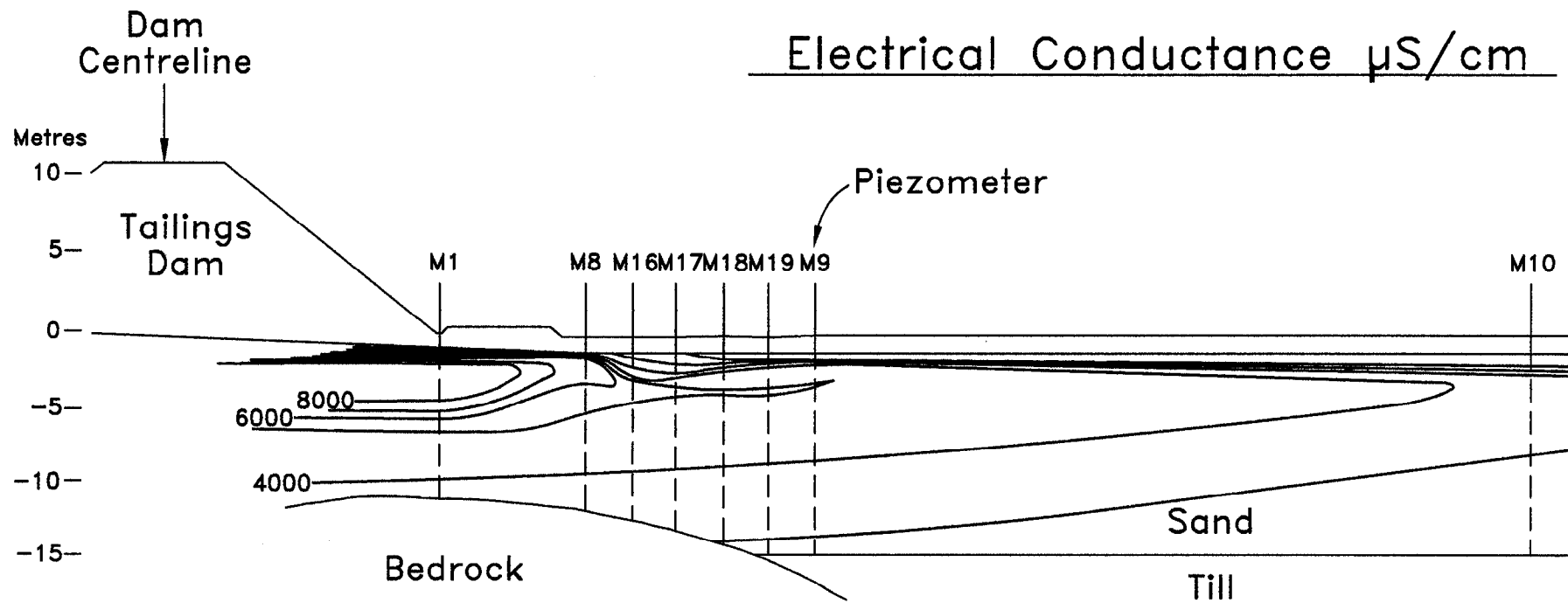
FIGURE 2.4

Groundwater Conductivity

After Blair et al (1980)

FIGURE 2.5A
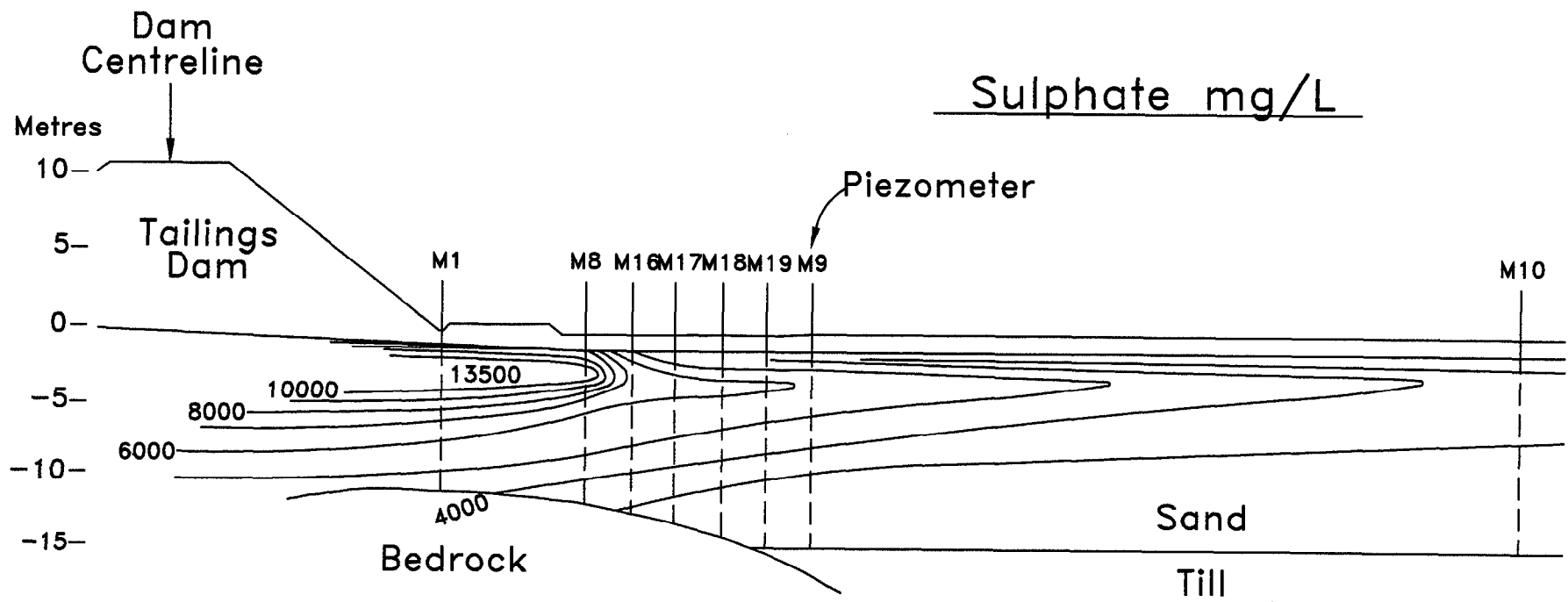
Sulphate in Groundwater

After Blair et al (1980)
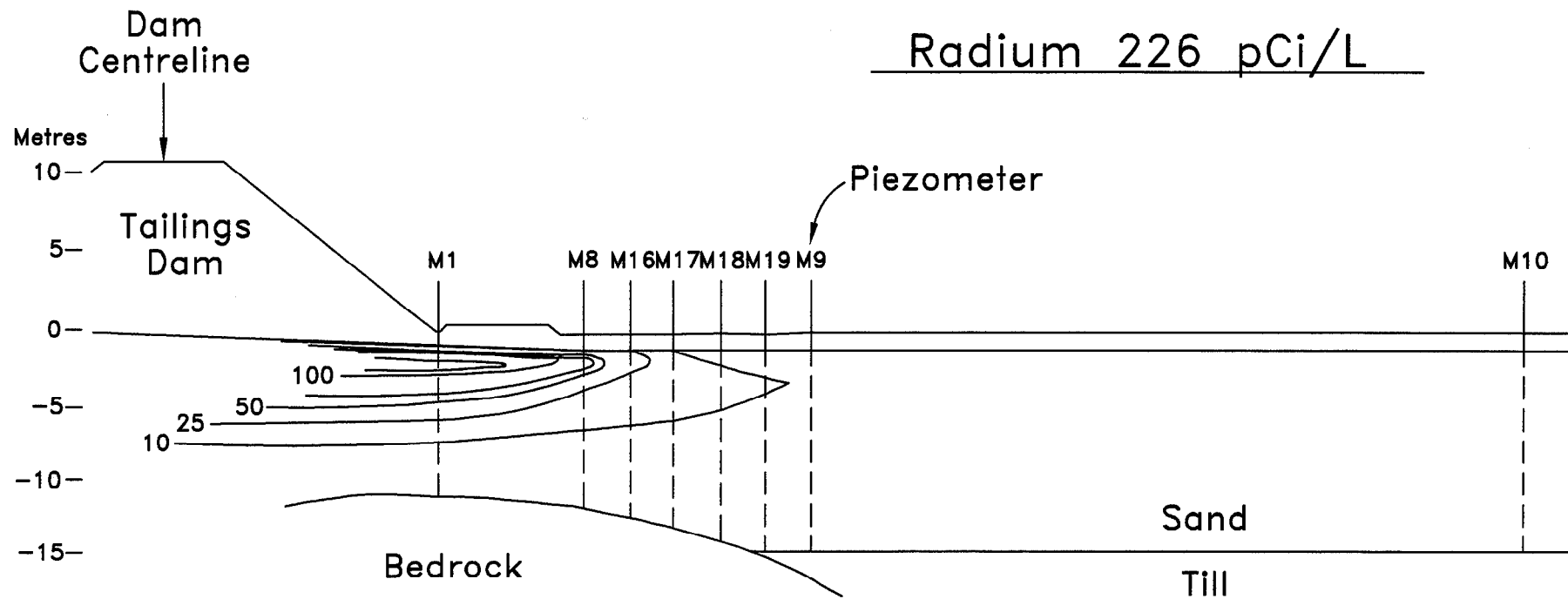
FIGURE 2.5B

Radium in Groundwater

After Blair et al (1980)

FIGURE 2.5C
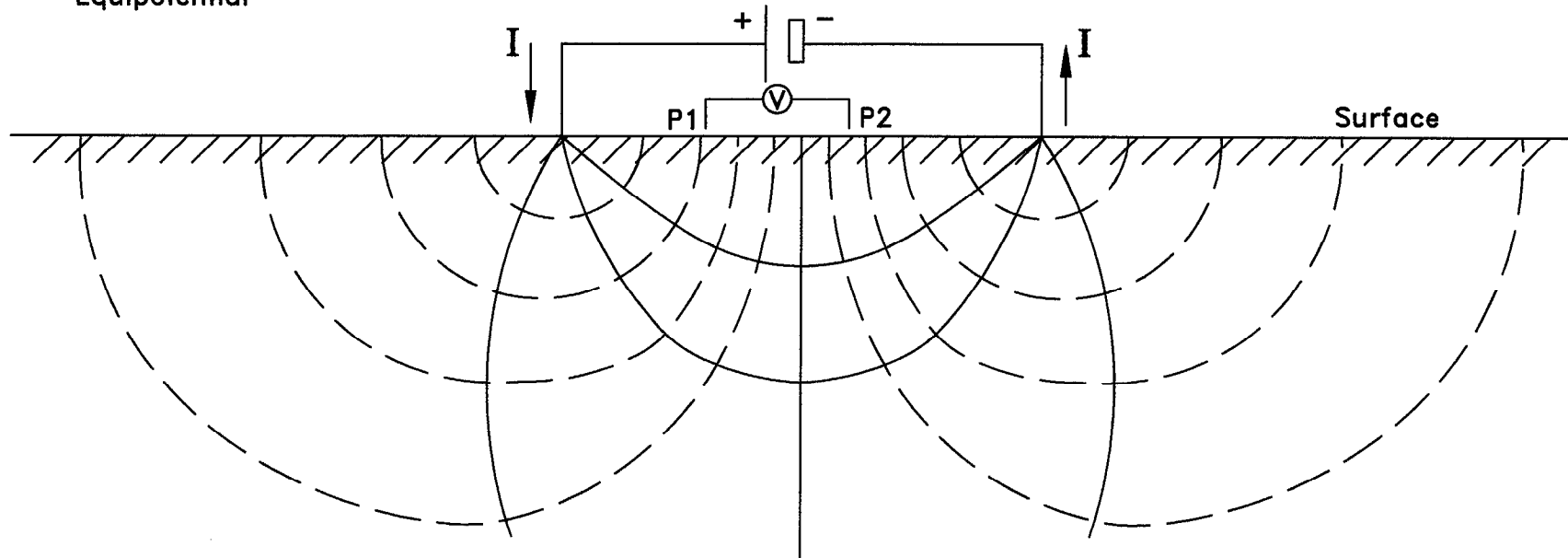
DC Resistivity Measurements

Equipotential and Current Flow Lines
for Two Point Sources Of Current

(After Dobrin, 1960)

FIGURE 2.6
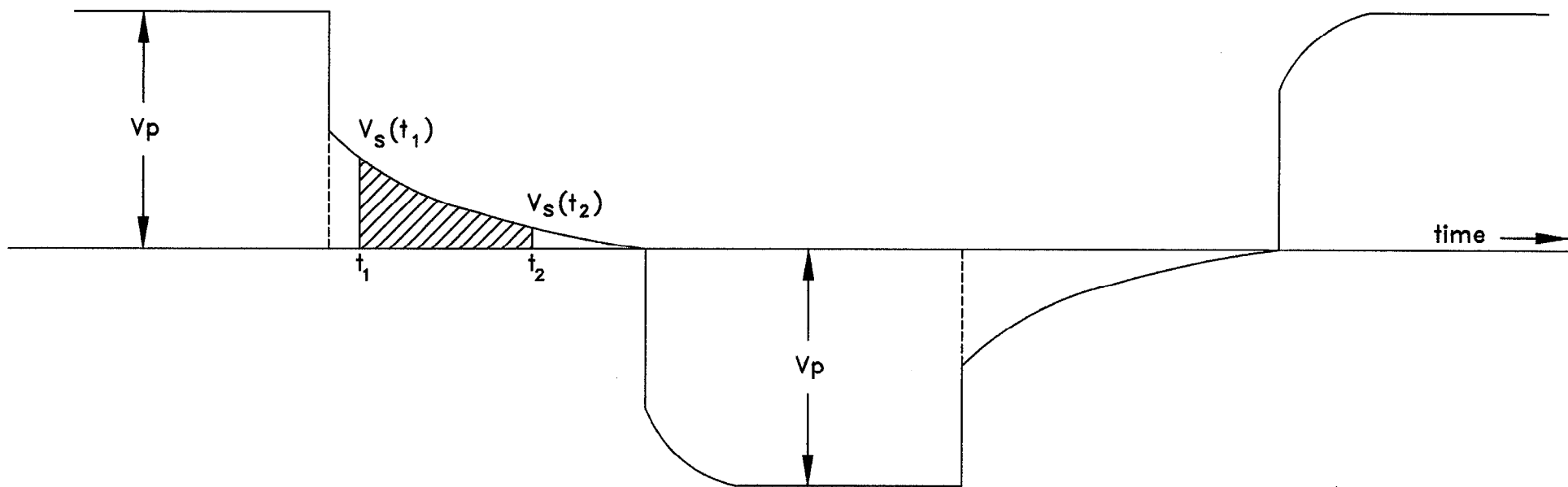
Resistivity / IP Waveform
at Receiver
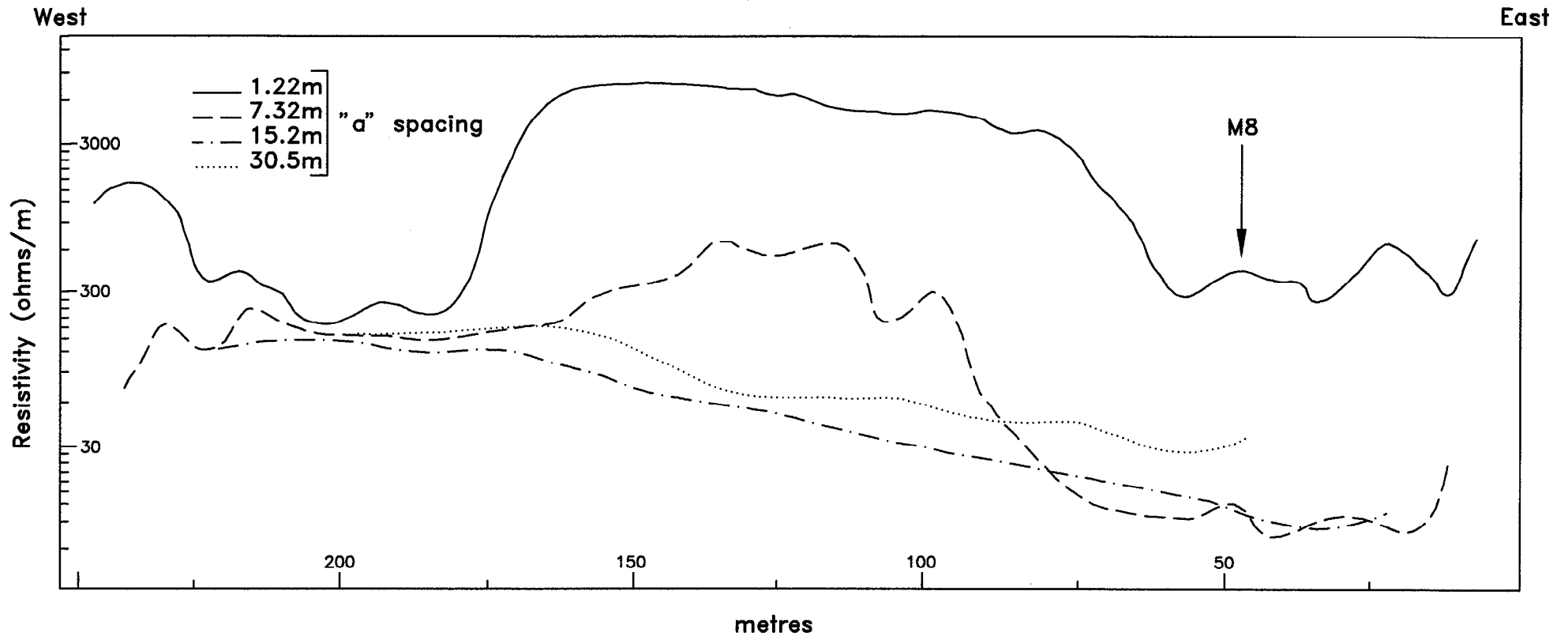
FIGURE 2.7

Resistivity Profile "B"
Wenner Array

(After Pehme, 1981)

FIGURE 2.8

M8 Sounding ———

Models
Schlumberger — — —
Wenner — · — ·

Resistivity (ohm/m.)

1000

100

10

1.0   10.0

Electrode Spacing (m.)
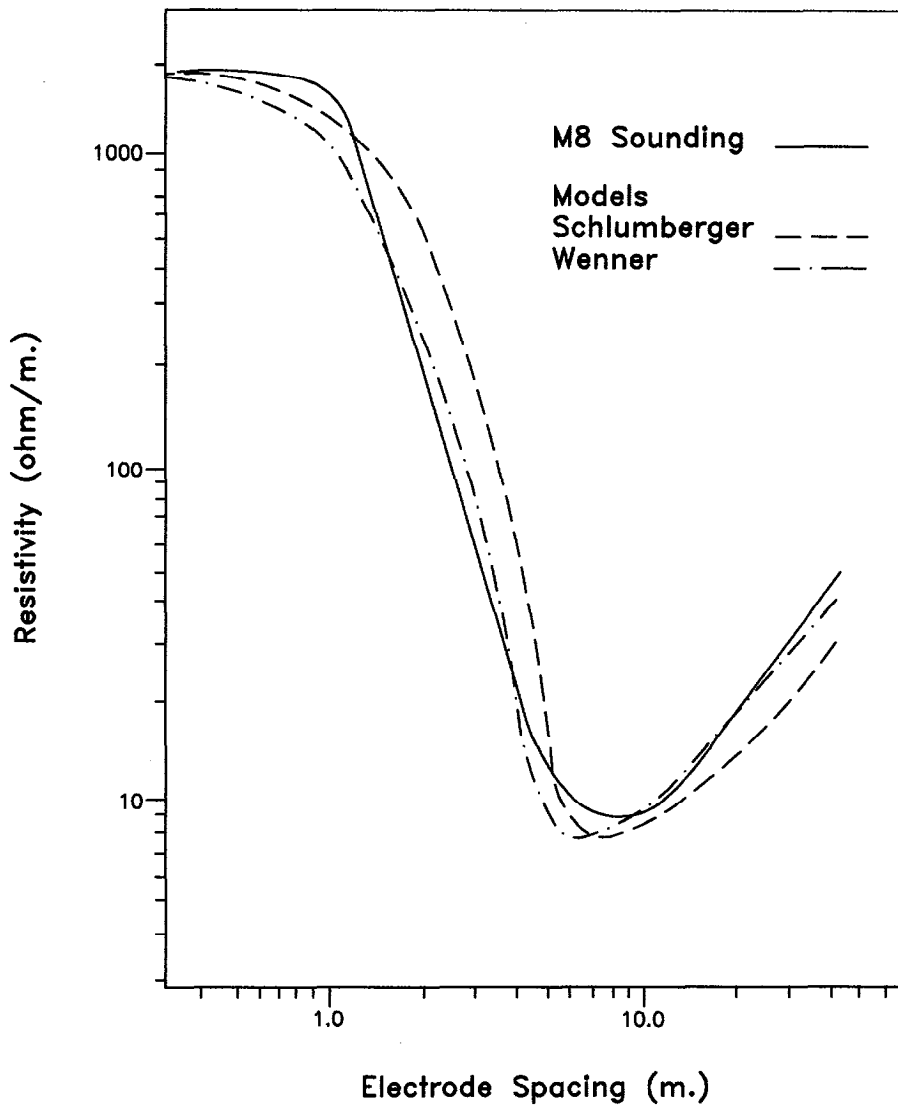
Theoretical vs. Field Sounding Curves

	0	2		4	6	8	10	12	
M8 LOG	sandy gravel		peat		sand			bedrock	
WATER RES.		1.3			1.9				
MODEL	5940	5.8	6.1	5.8	7.9			10150	
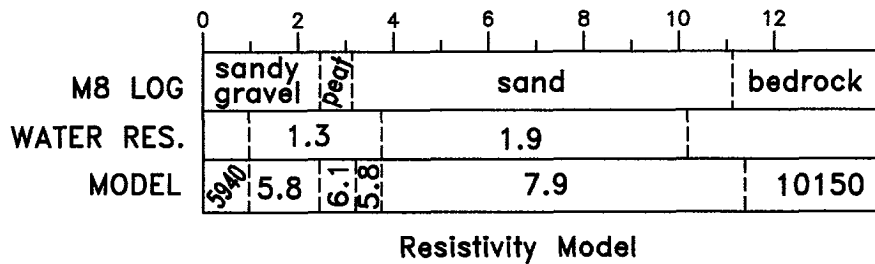
Resistivity Model

M8 Resistivity Sounding

(After Pehme, 1981)
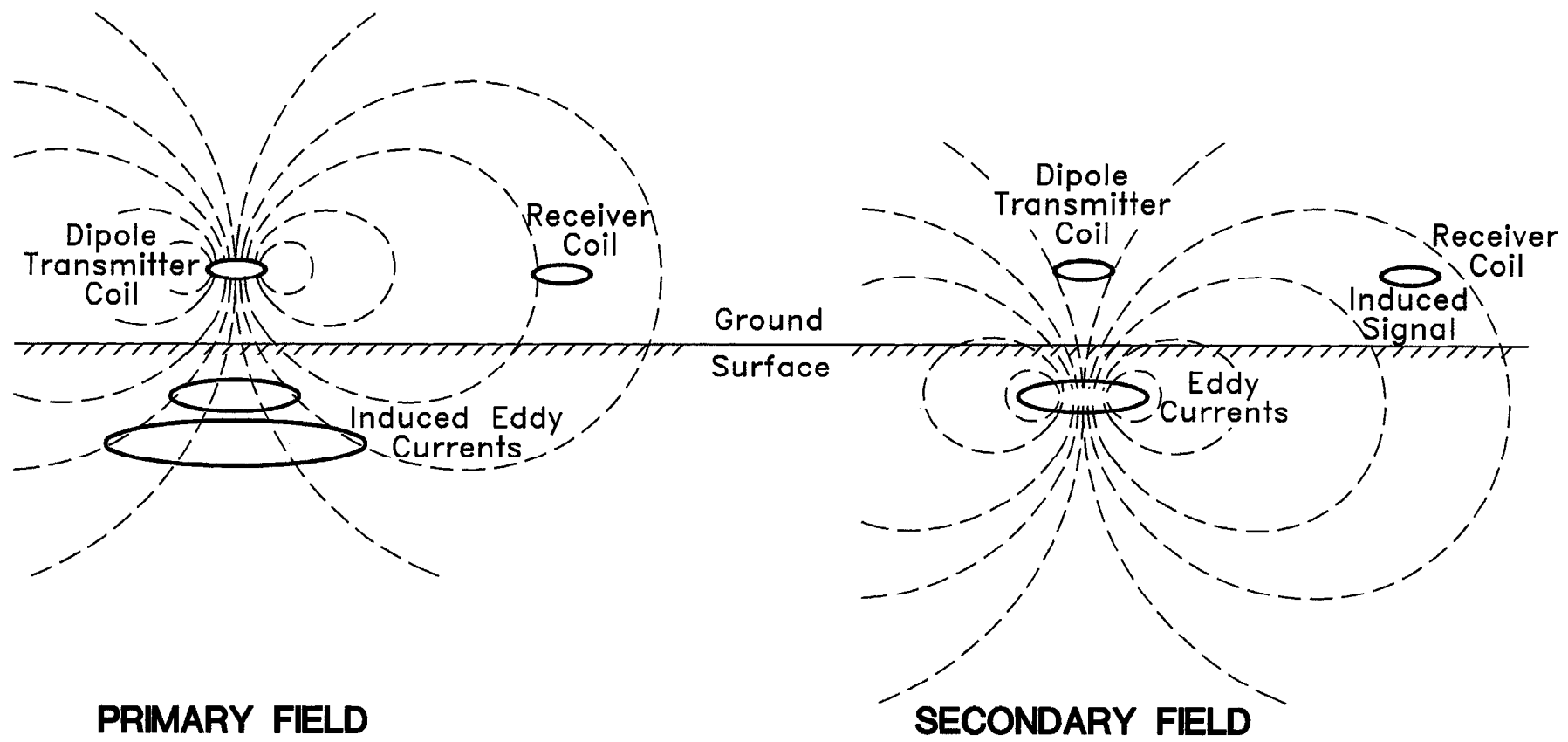
FIGURE 2.9

Principals of Electromagnetic Induction in Soil Conductivity Measurements

FIGURE 2.10

Tailings

Dam

Profile B

M8

Ditch

Buckles

Creek

100

100

25

50

100

200

400

800

25

50

100

200

400

800

−400

−800
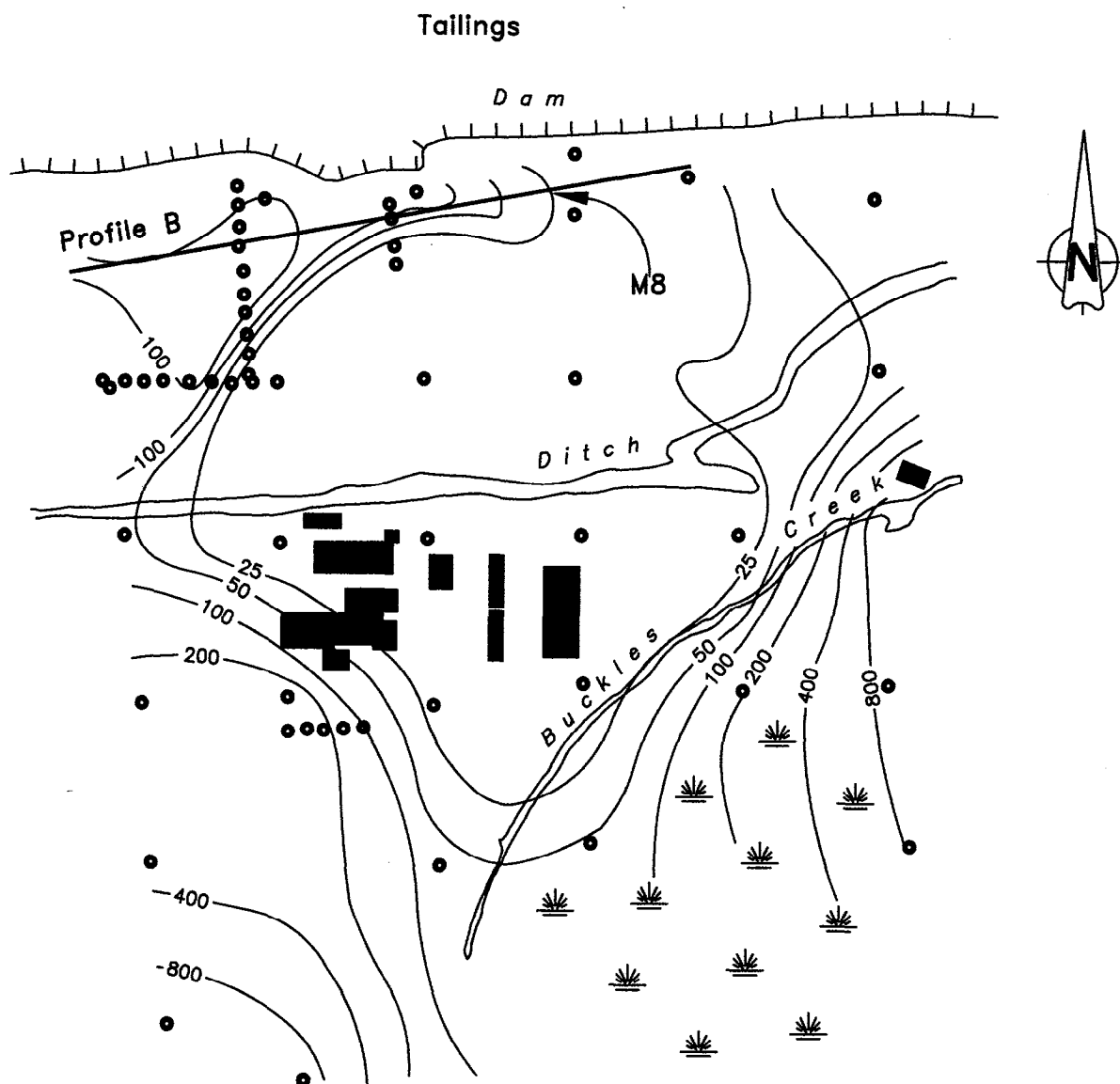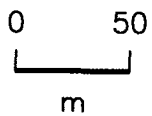
**Apparent
Resistivity**

EM 16R
(ohm/m.)
(After Pehme, 1981)

0   50

m

FIGURE 2.11
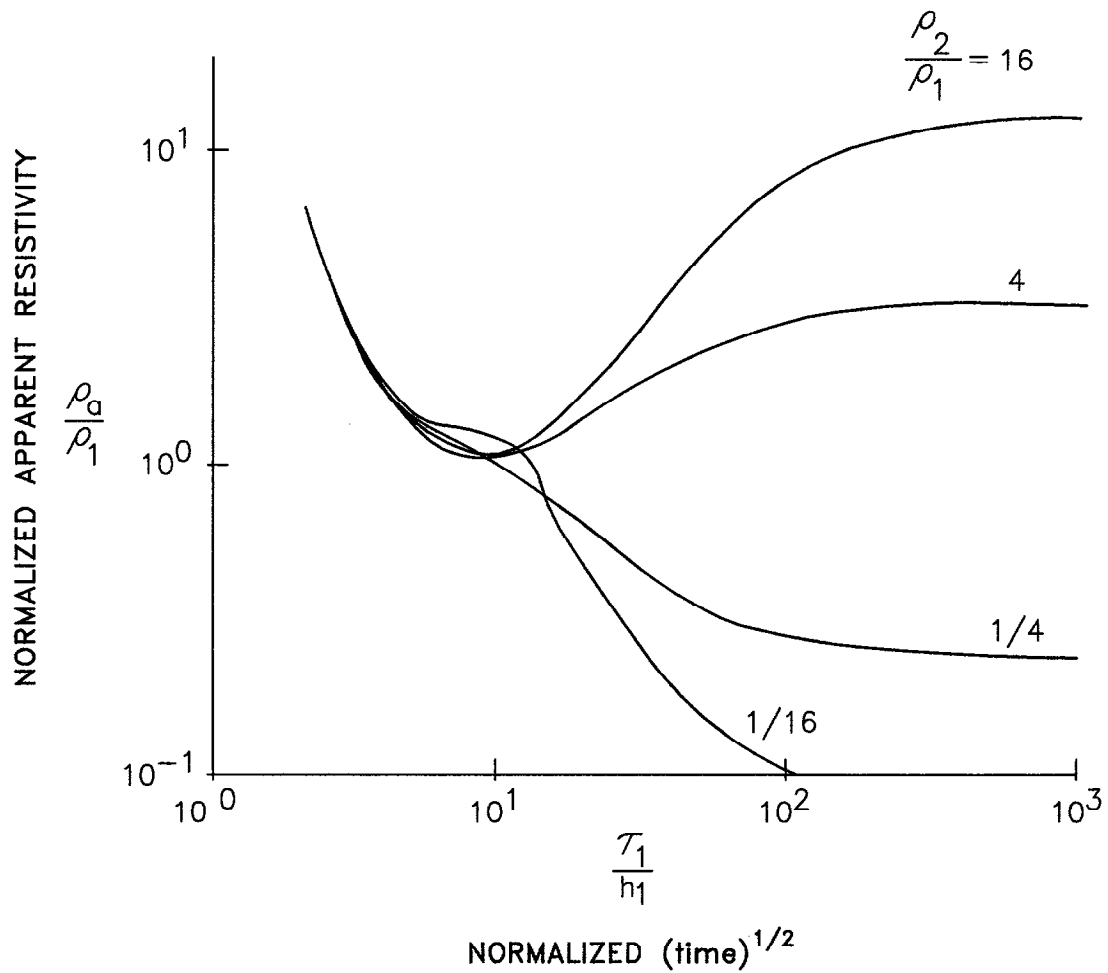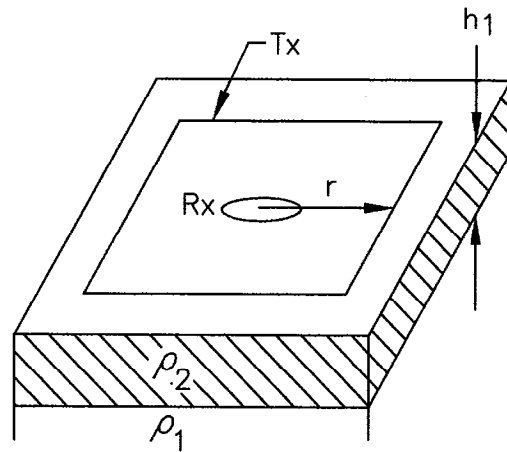
Apparent Resistivity Curves
for Two-Layer Sections

FIGURE 3.1A

Transmitter Loop

External Coil

Central Receiver Coil

Layer 1

Layer 2

Transient EM Survey Layout

Depth
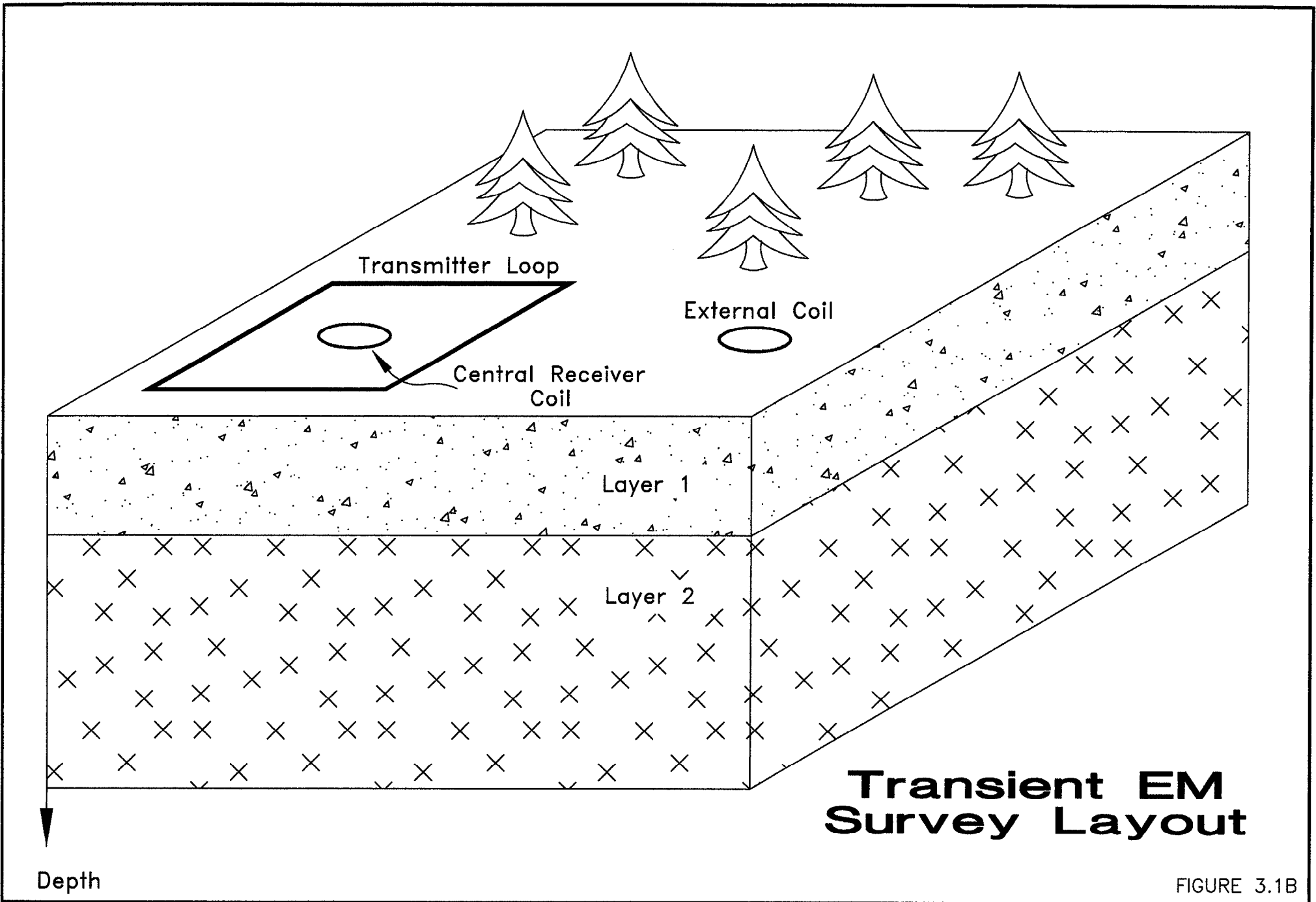
FIGURE 3.1B

On Board -
Electronic Navigation Control
Spectrometer for Geological Mapping (optional)
Video Camera

Magnetometer
and
VLF Receiver

Multi-coil EM Sensor

Tx   Rx

Airborne
EM/Magnetometer System
(from Dighem Surveys Inc. Literature)
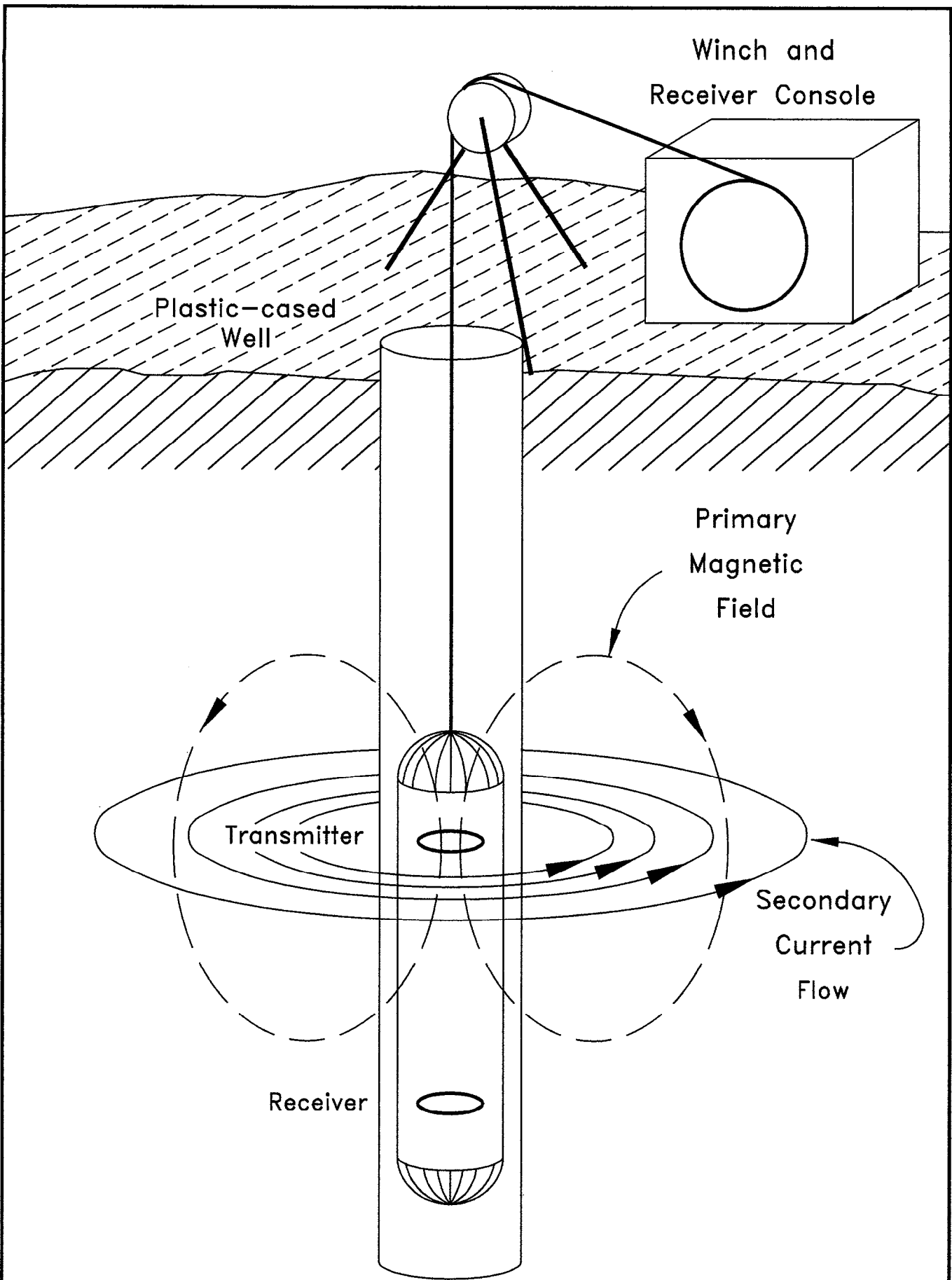
FIGURE 3.2

Borehole EM System
(from Geonics Ltd. Literature)

FIGURE 3.3

LEGEND

⊞ SUDBURY IGNEOUS COMPLEX

A.E.M. Survey Area

Levack
Tailings

Levack ◆

SUDBURY BASIN

Fault Lake
Tailings

Falconbridge ◆

0   5

Miles

Copper
Cliff
Tailings
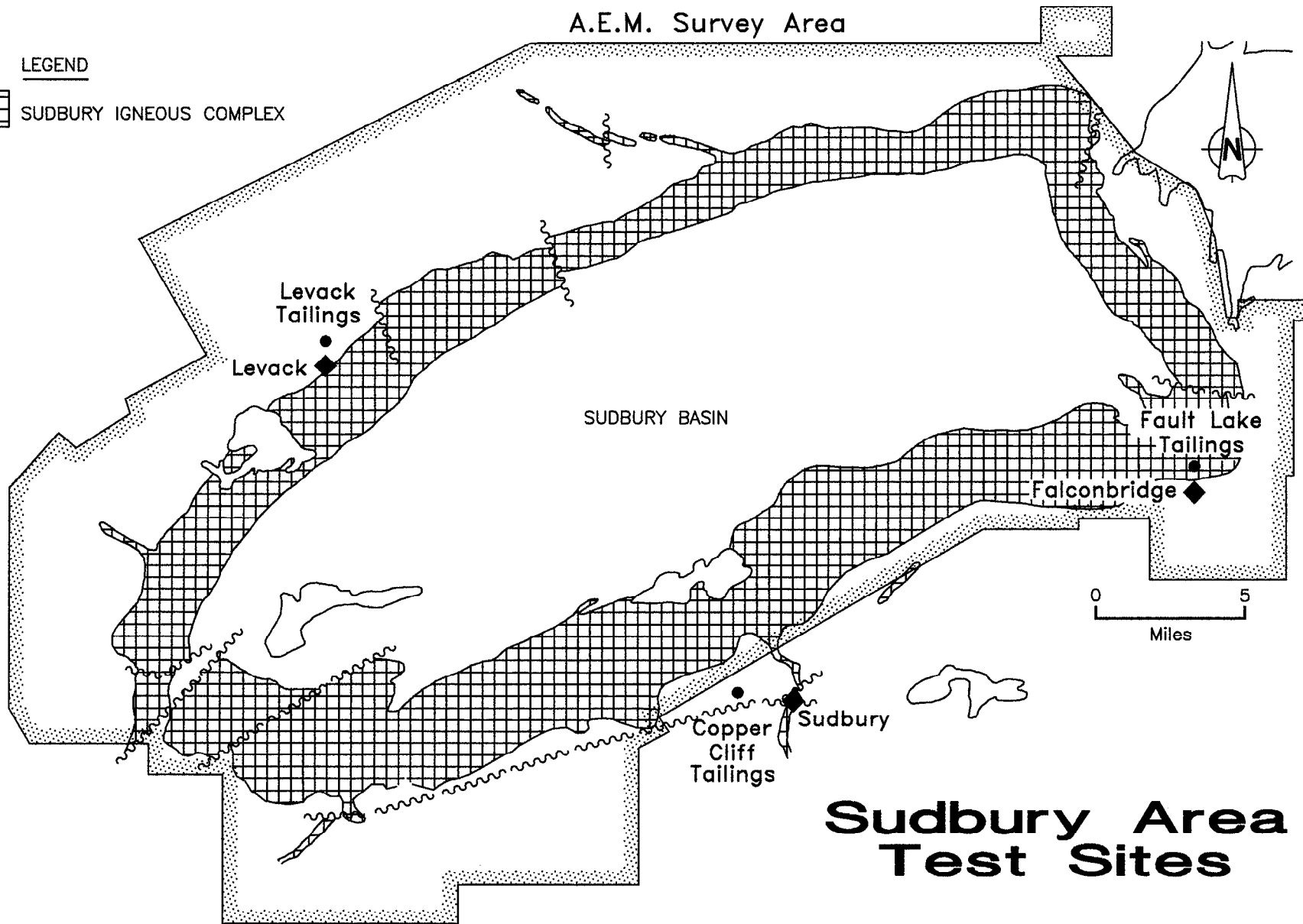
◆ Sudbury

**Sudbury Area
Test Sites**

FIGURE 4.1

Reconnaissance Conductivity Survey Line

R-2

R-3

R-1

C-D

Hill Station
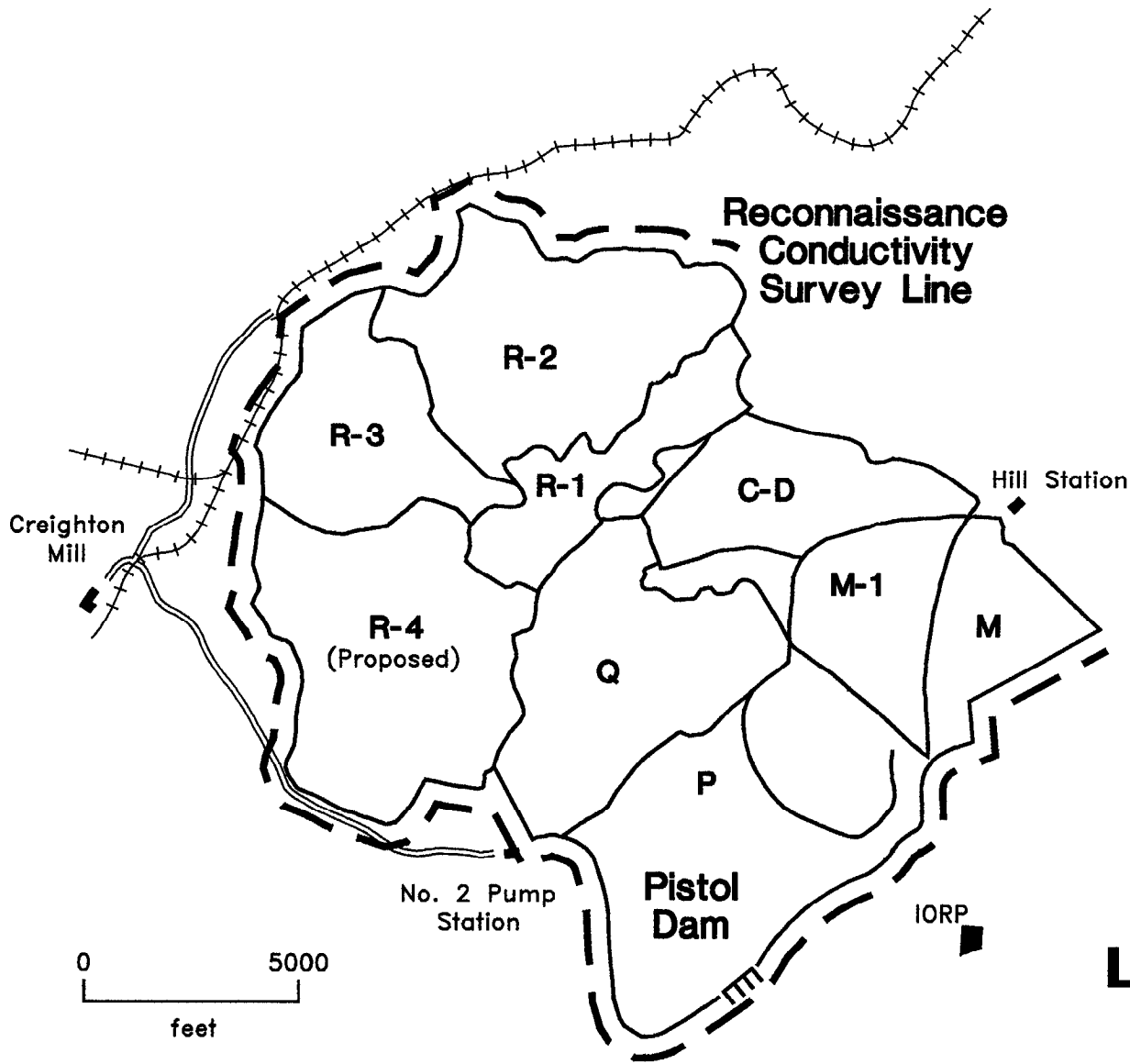
Booster Station

Copper Cliff Mill

Creighton Mill

R-4 (Proposed)

M-1

M

Q

P

No. 2 Pump Station

Pistol Dam

IORP

0   5000

feet

Location Map

Copper Cliff Tailings Area

FIGURE 5.1.1

LEGEND

• 60 Sample Wells
▬ ▬ ▬ Survey Lines

	>100 mS/m
	> 80 mS/m
	> 60 mS/m
	> 40 mS/m
	> 20 mS/m
	> 10 mS/m
	> 0 mS/m

PISTOL DAM

**Pistol Dam
EM31
Horizontal Dipole**

FIGURE 5.1.1.1

LEGEND

•⁶⁰ Sample Wells

Survey Lines

> 80 mS/m
> 60 mS/m
> 40 mS/m
> 20 mS/m
> 0 mS/m

N

PISTOL DAM

B L.60

• 14

• 15

23
82
83   21
      25   21G
           30
           30G
L3   31
L1 L2

34

28
22G
27
33
34
105
103
81
81G
L5
L6

92
92G

100

101
102

93
93G

80   93C

0   200

m
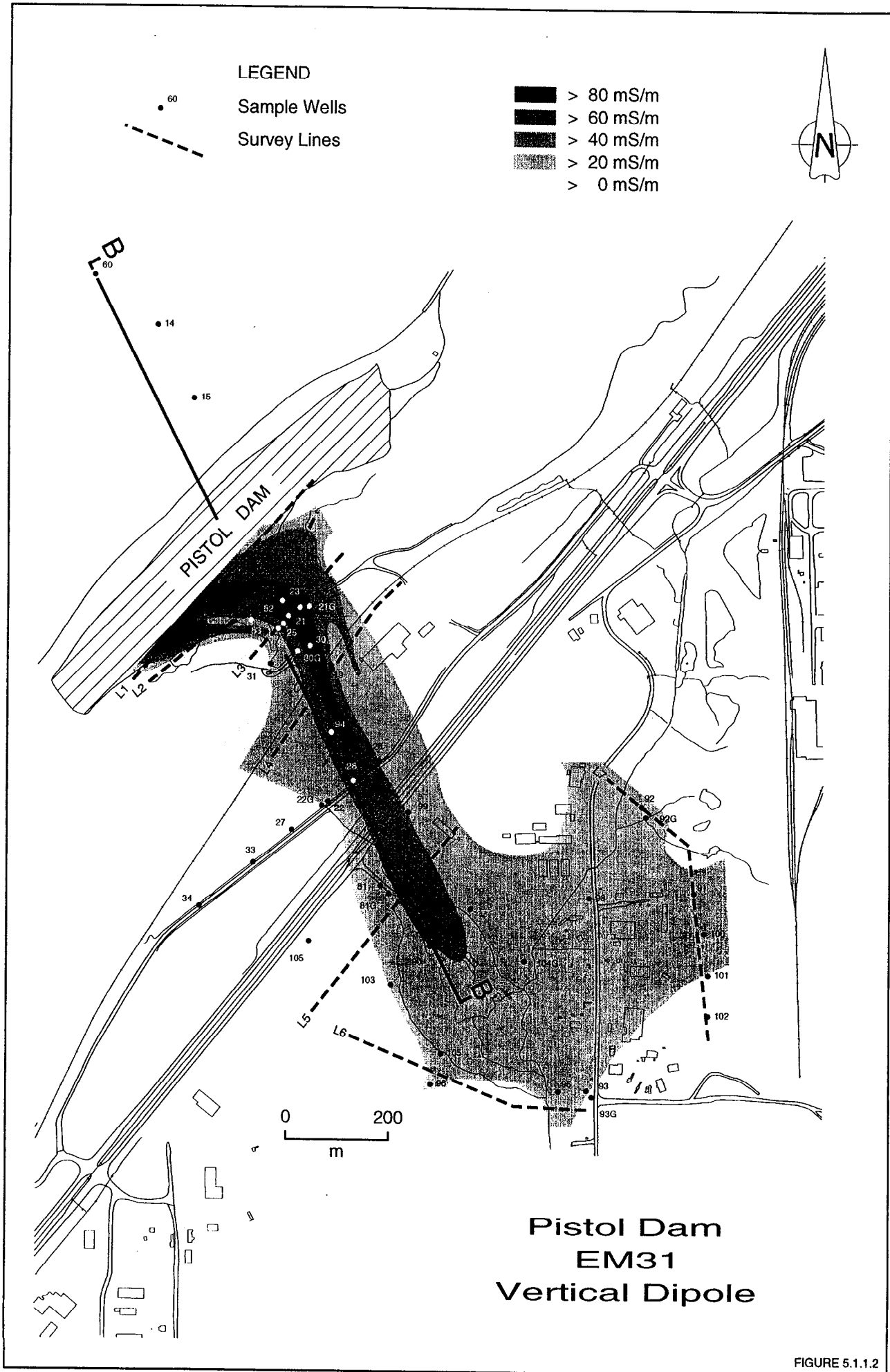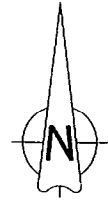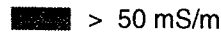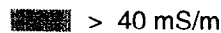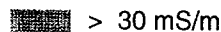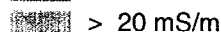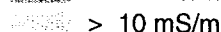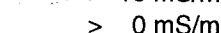
Pistol Dam
EM31
Vertical Dipole

FIGURE 5.1.1.2

LEGEND

Sample Wells

Survey Lines

> 50 mS/m
> 40 mS/m
> 30 mS/m
> 20 mS/m
> 10 mS/m
> 0 mS/m
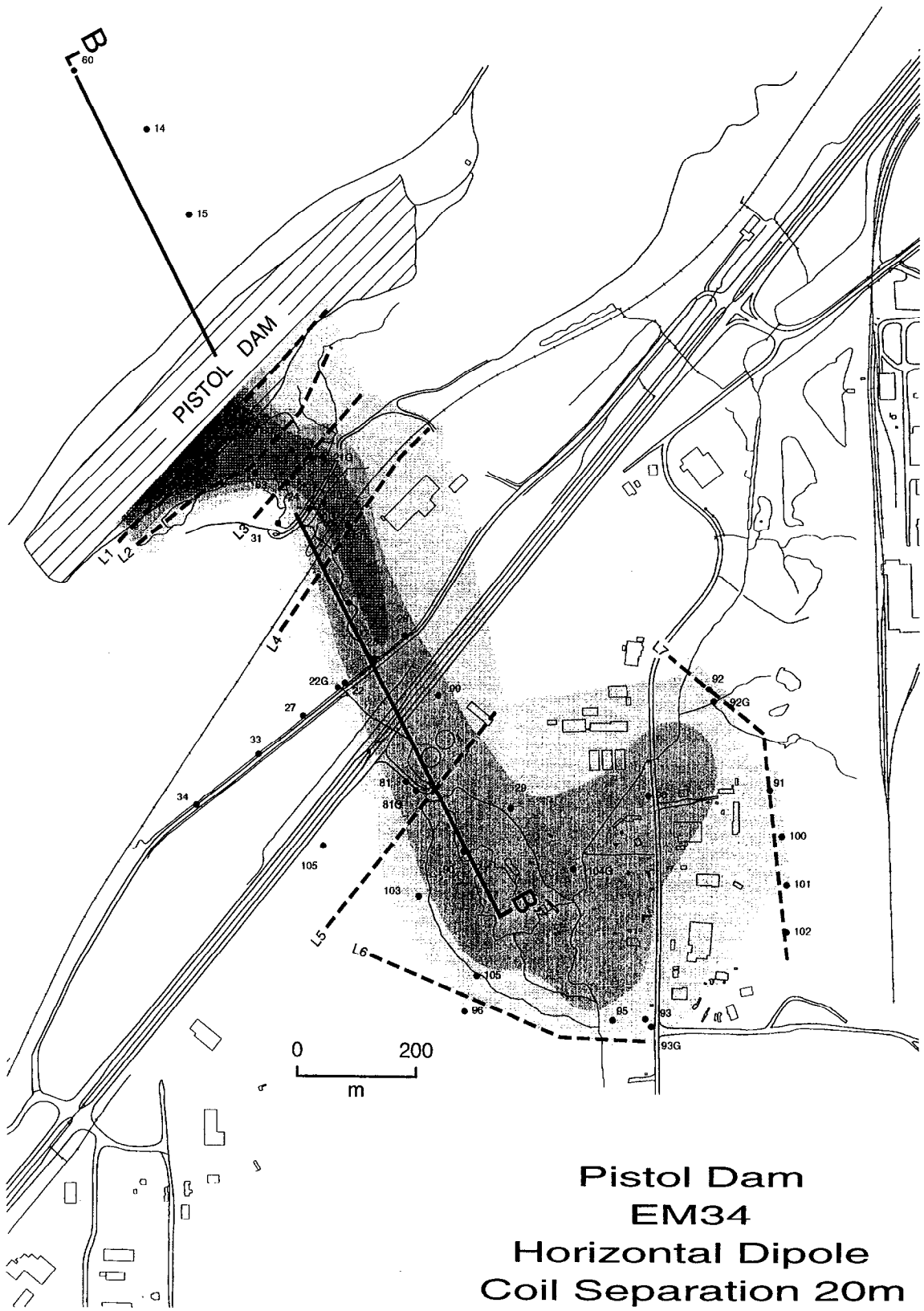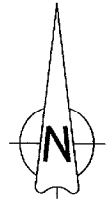
N

Pistol Dam
EM34
Horizontal Dipole
Coil Separation 20m

FIGURE 5.1.1.3

LEGEND

• 60   Sample Wells

Survey Lines

> 30 mS/m
> 20 mS/m
> 10 mS/m
> 5 mS/m
> 0 mS/m

PISTOL DAM

0   200

m

**Pistol Dam
EM34
Horizontal Dipole
Coil Separation 40m**

FIGURE 5.1.1.4

EM-31,34 Conductivity Profiles
Pistol Dam Area

Line 1

COND.(mmhos/m)

East   STATION   West

— HH + HG * VG

H=Horizontal coils
V=Vertical coils

COND.(mmhos/m)

East   STATION   West

— 20V + 40V
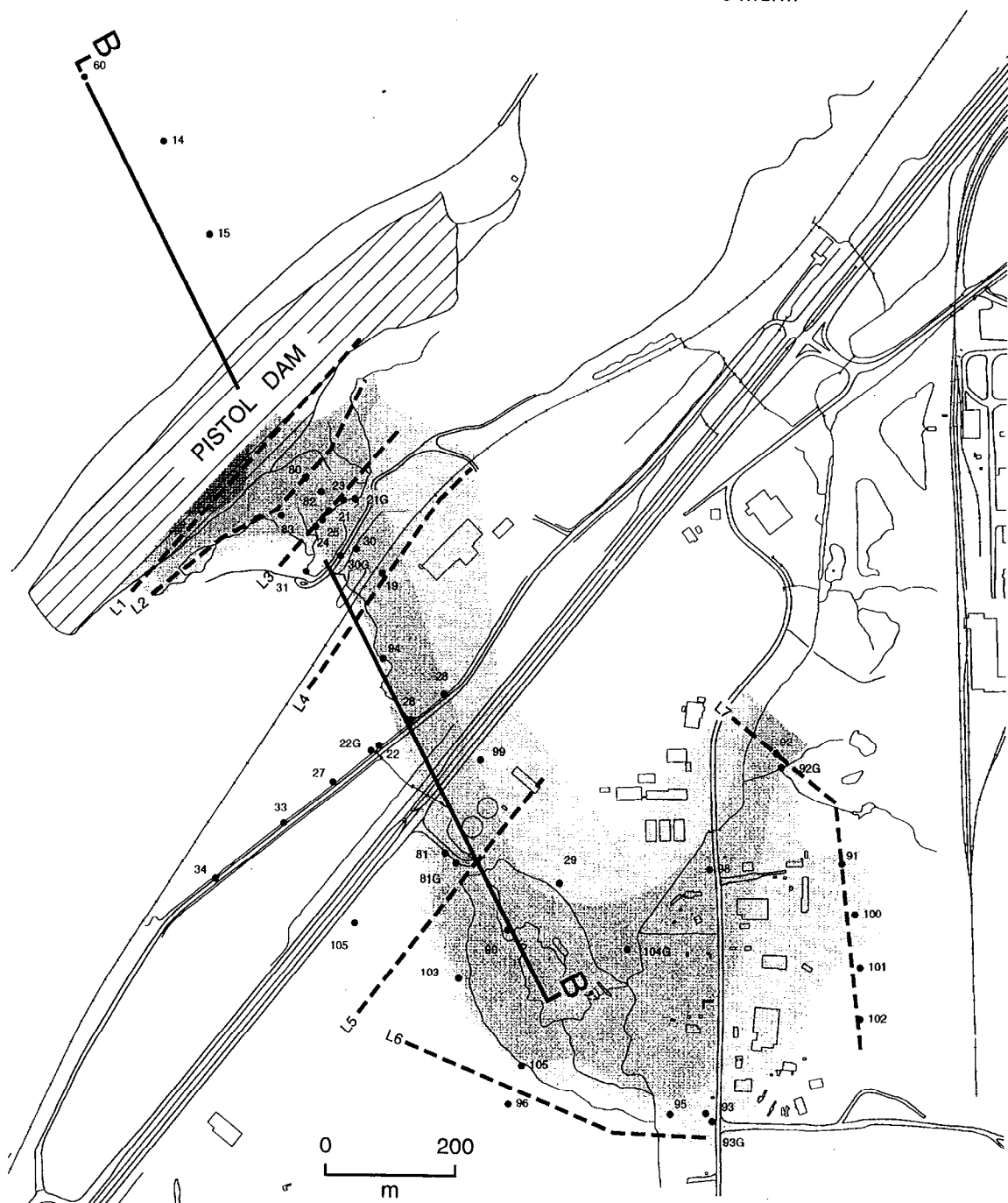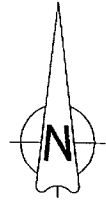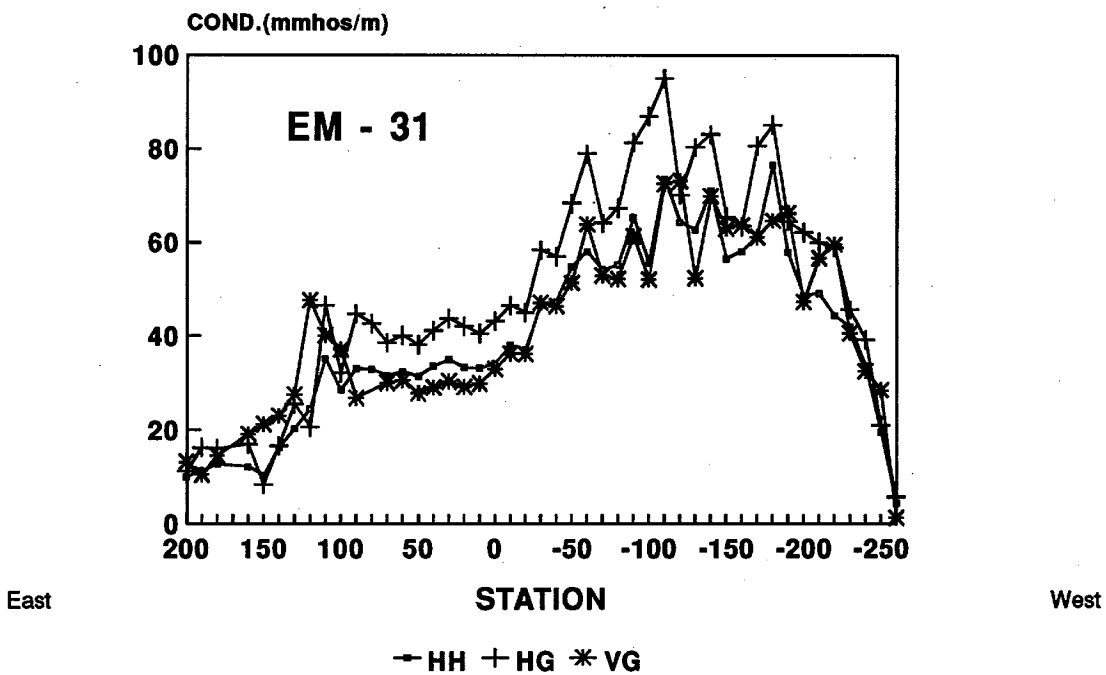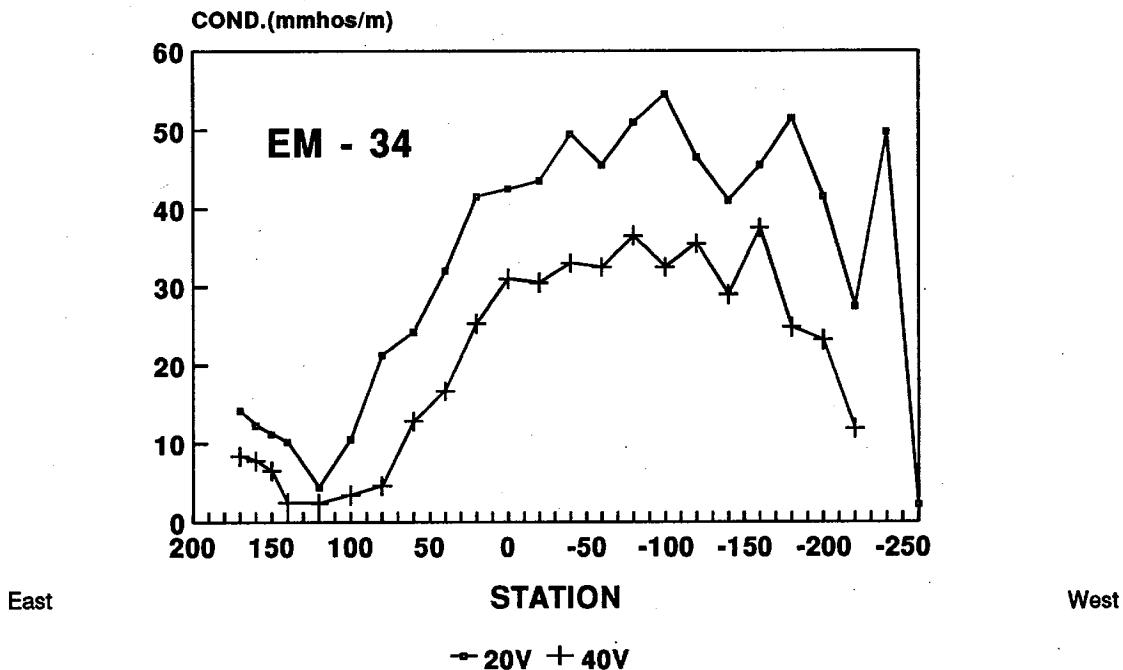
Note vertical scale

Figure 5.1.1.5

EM-31,34 Conductivity Profiles
Pistol Dam Area

Line 2

COND. (mmhos/m)

EM - 31

Heavy

Seepage

Zone

250
200
150
100
50
0

250 200 150 100 50 0 -50 -100 -150 -200

East   STATION   West

─ HH ＋ HG ＊ VG

H=Horizontal coils
V=Vertical coils

COND.(mmhos/m)

EM - 34

50
40
30
20
10
0

250 200 150 100 50 0 -50 -100 -150 -200

East   STATION   West

─ 20V ＋ 40V
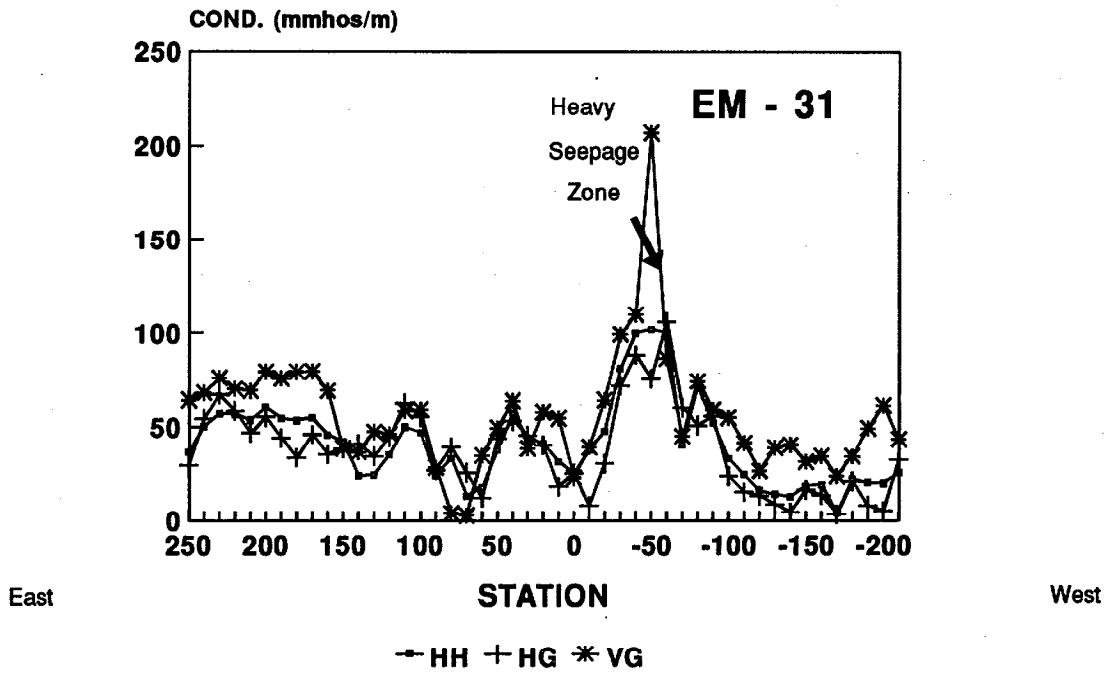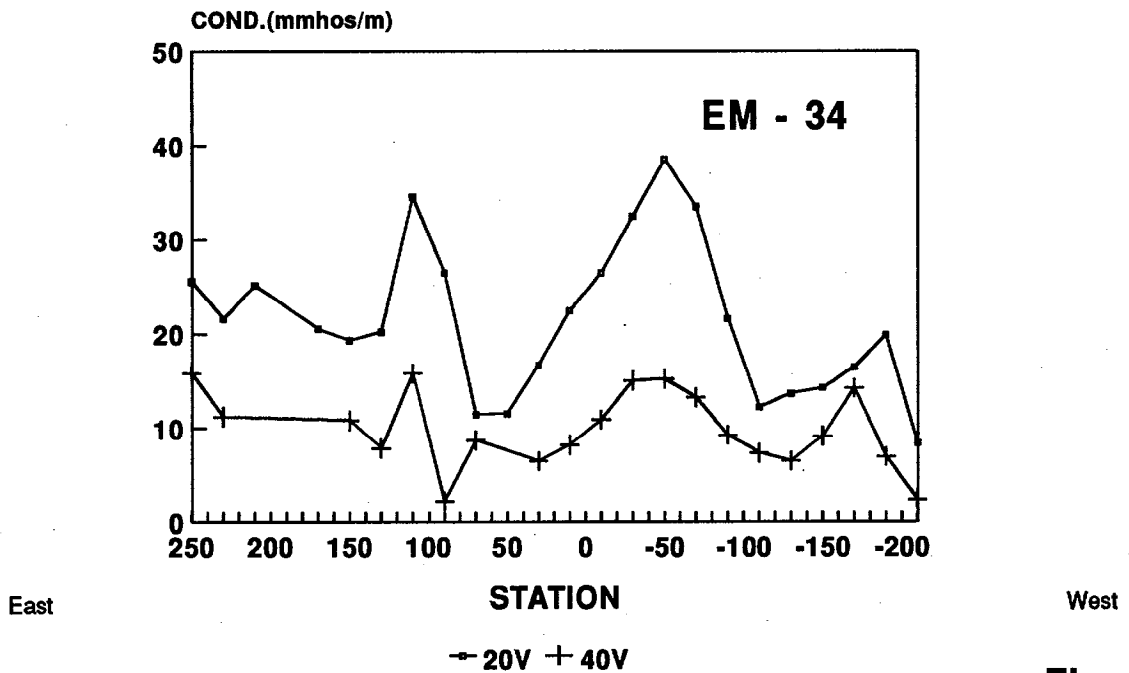
**Figure
5.1.1.6**

EM-31,34 Conductivity Profiles
Pistol Dam Area

Line 3

COND. (mmhos/m)

Swampy
Area

EM - 31

100

80

60

40

20

0

100   50   0   -50   -100

East   STATION   West

─HH +HG *VG

H=Horizontal coils
V=Vertical coils

COND.(mmhos/m)

EM - 34

50

40

30

20

10

0

100   50   0   -50   -100

East   STATION   West

─20V +40V
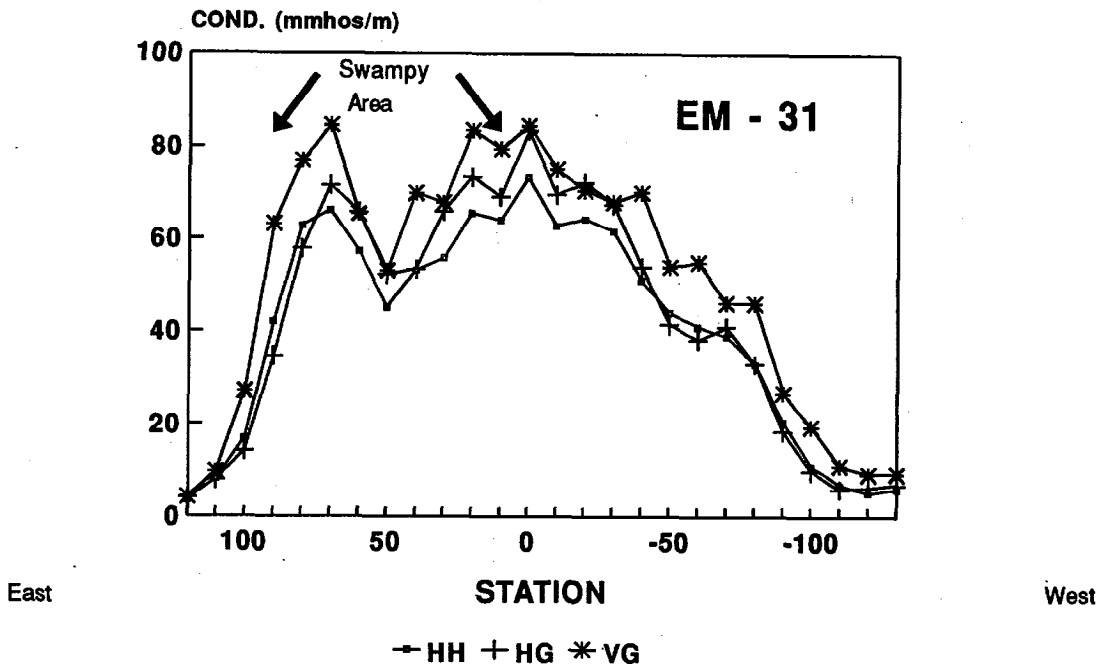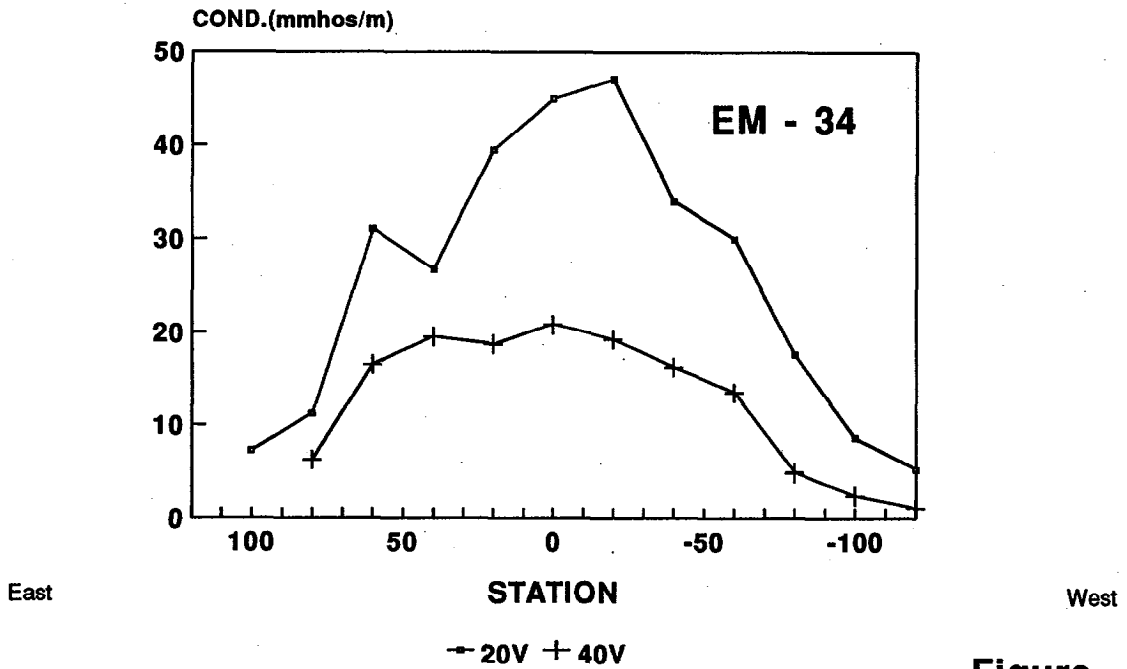
Note vertical scale

**Figure
5.1.1.7**

EM-31,34 Conductivity Profiles
Pistol Dam Area

Line 4

COND.(mmhos/m)

EM - 31

STATION

—HH +HG *VG

H=Horizontal
V=Vertical

COND.(mmhos/m)

EM - 34

STATION

— 20V
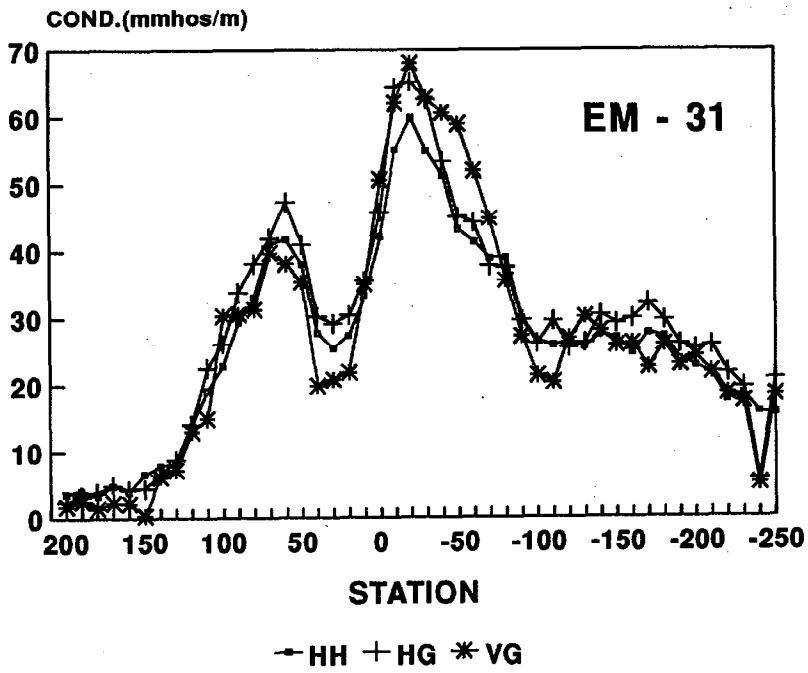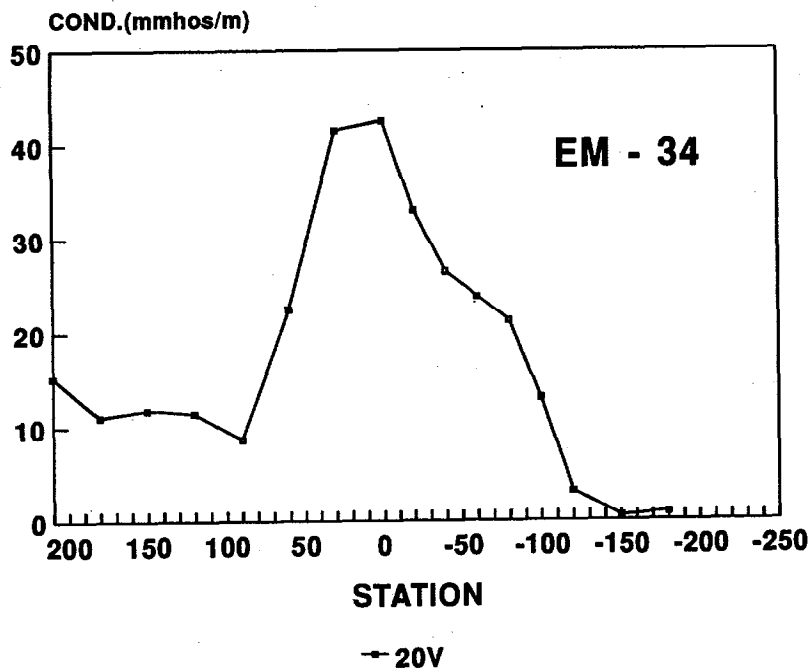
Note vertical scale

Figure
5.1.1.8

EM-31,34 Conductivity Profiles
Pistol Dam Area
Line 5

COND. (mmhos/m)

EM - 31

STATION

East   West

─ HH + HG ✳ VG

H=Horizontal coils
V=Vertical coils

COND. (mmhos/m)

Fence and
Culvert

EM - 34

STATION

East   West

─ 20V + 40V ✳ 20H ▫ 40H
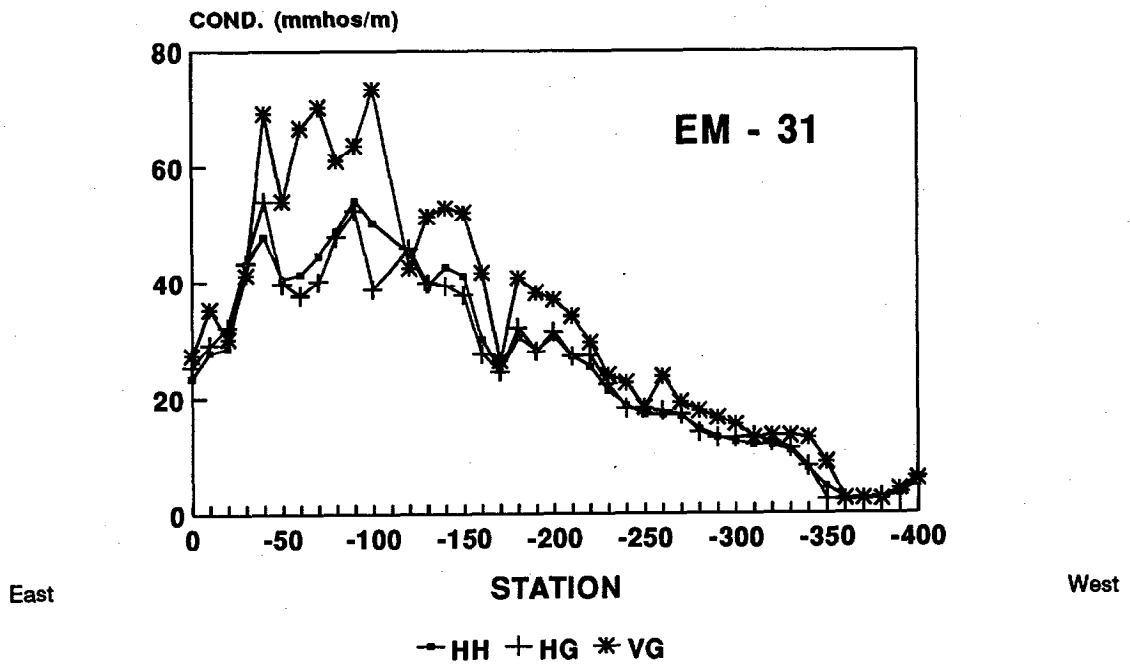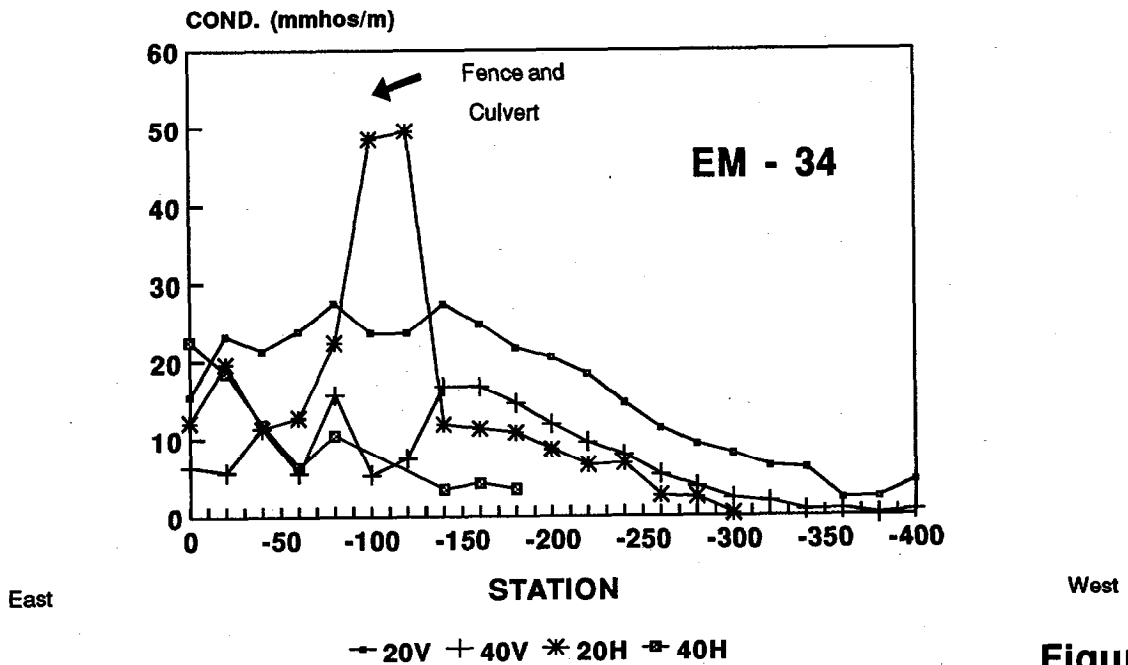
Note vertical scale

Figure
5.1.1.9

EM-31,34 Conductivity Profiles
Pistol Dam Area
Line 6

COND.(mmhos/m)

EM - 31

Fence

STATION

East

West

--- HH + HG * VG

H=Horizontal coils
V=Vertical coils

COND.(mmhos/m)

EM - 34

STATION

East

West

--- 20V + 40V
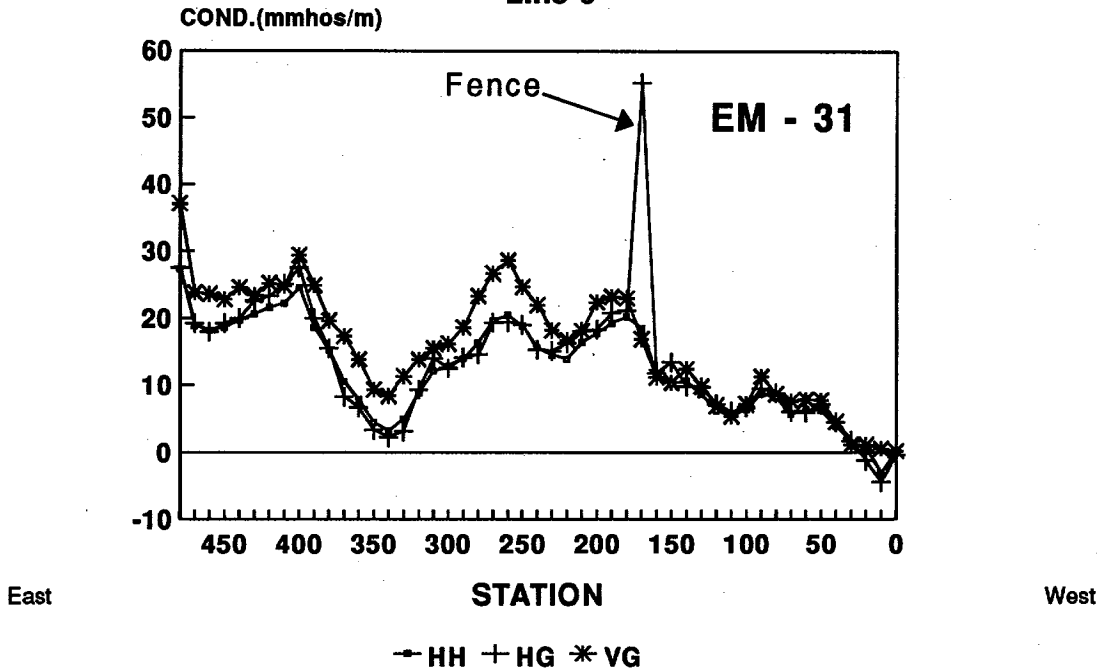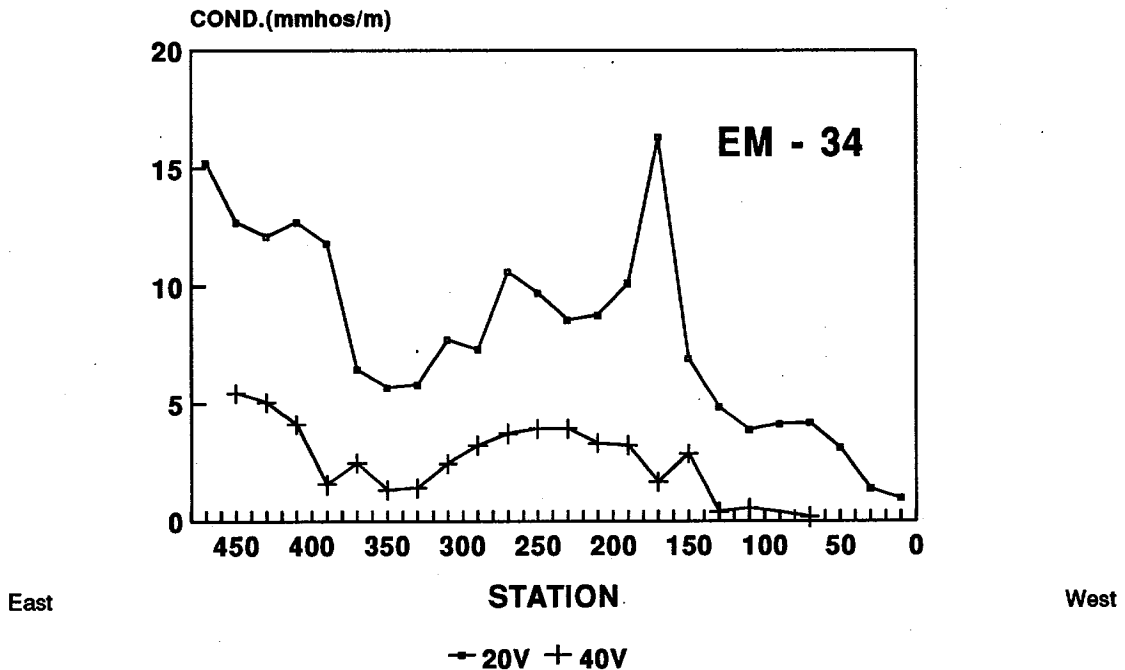
Note vertical scale

Figure
5.1.1.10

EM-31,34 Conductivity Profiles
Pistol Dam Area
Nickel Refinery Line
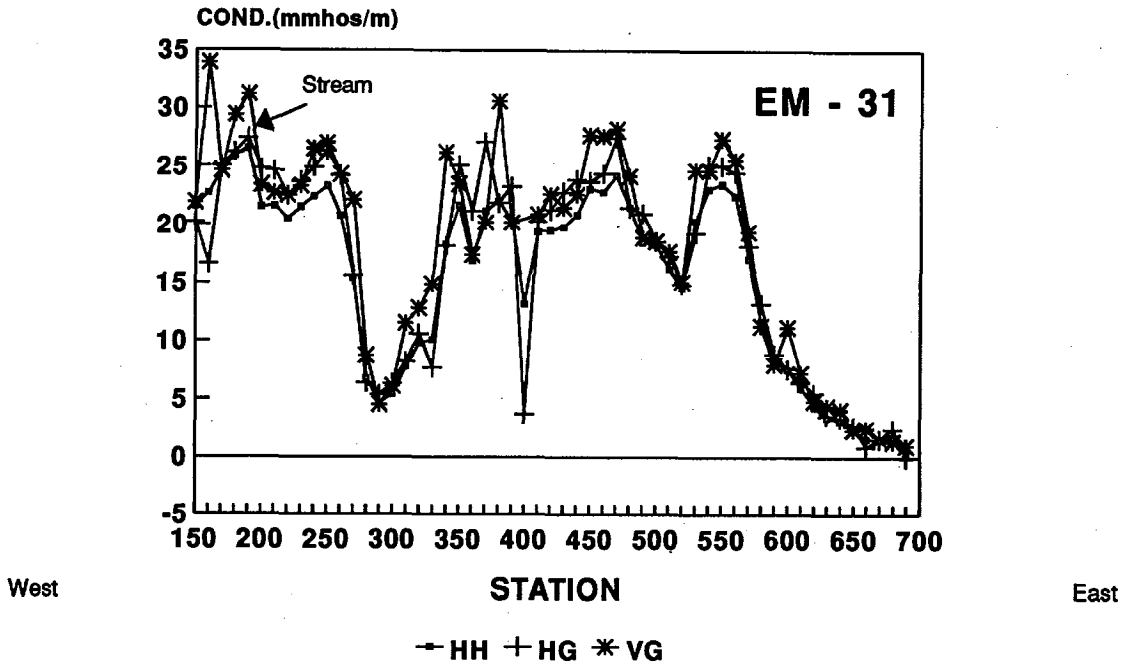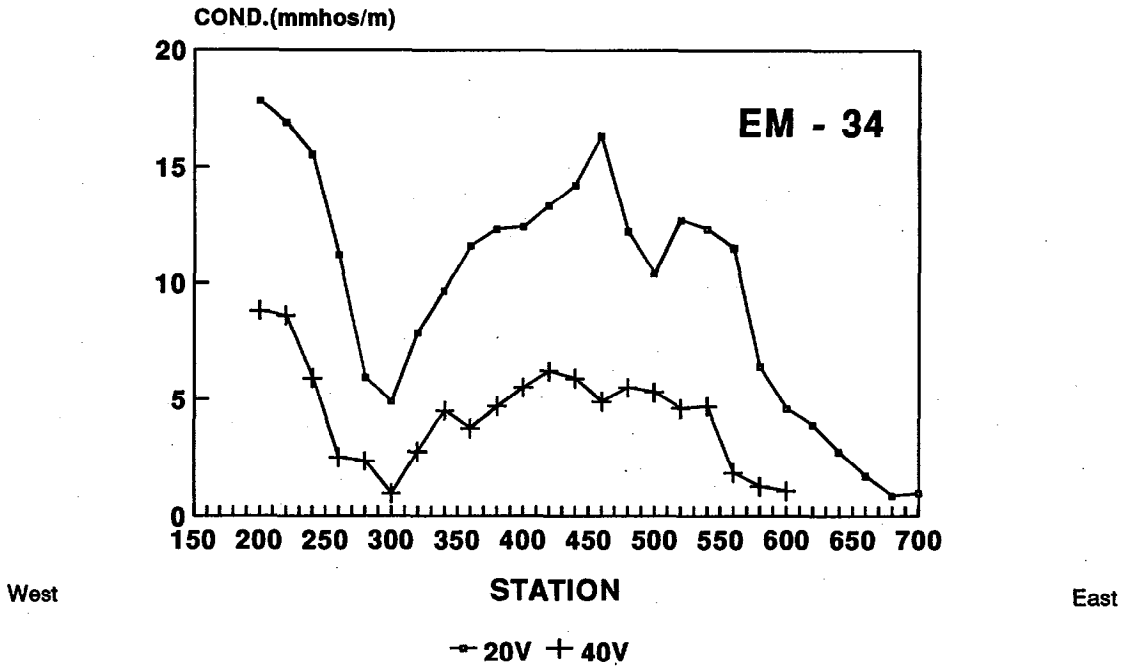
COND.(mmhos/m)

EM - 31

Stream

West   STATION   East

─ HH ＋ HG ＊ VG

H=Horizontal coils
V=Vertical coils

COND.(mmhos/m)

EM - 34

West   STATION   East

─ 20V ＋ 40V

Note vertical scale

Figure

5.1.1.11
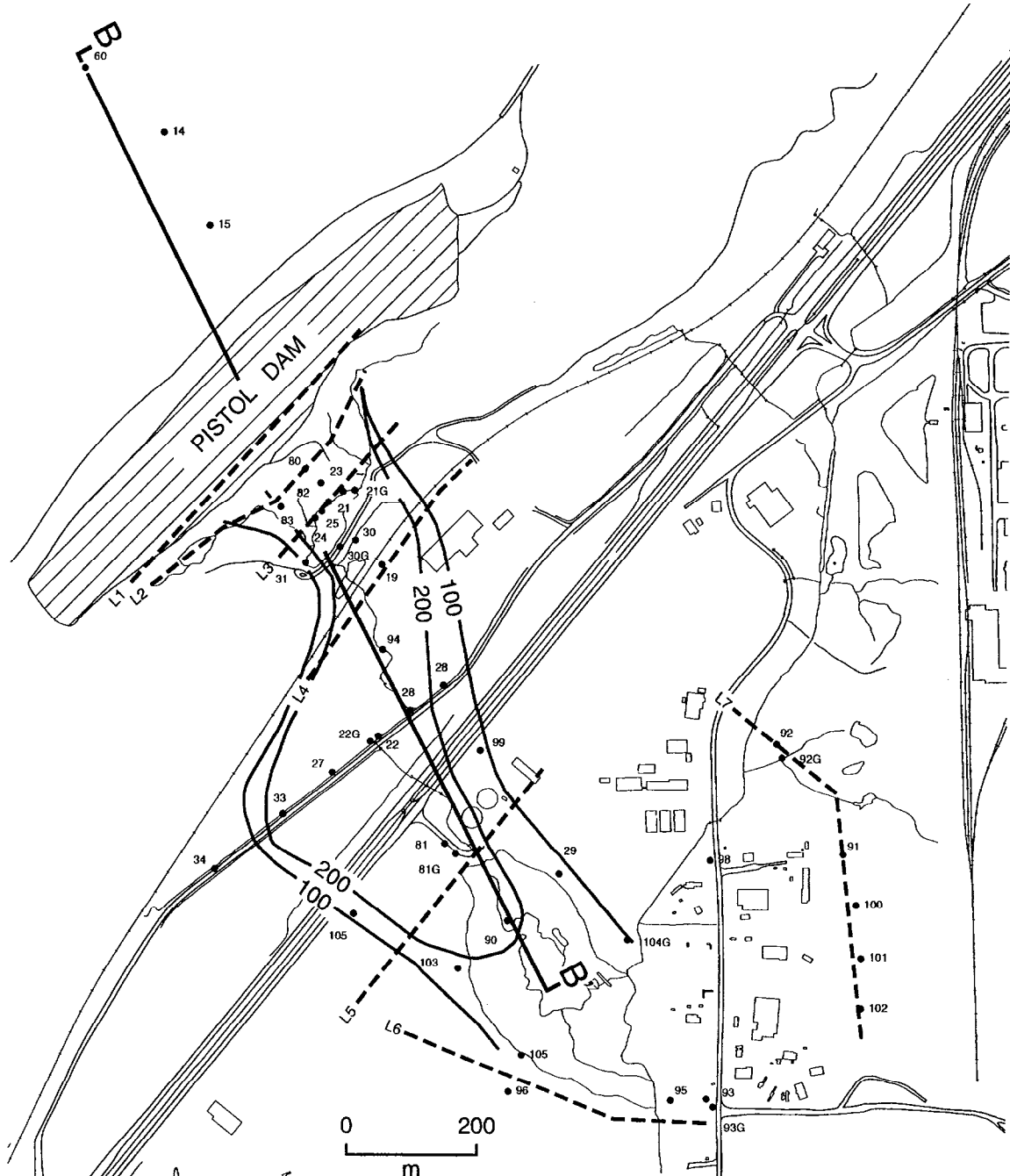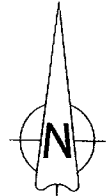
**Pistol Dam
Basal Aquifer Electrical
Conductivity Plume**
(Robertson et al., 1992)
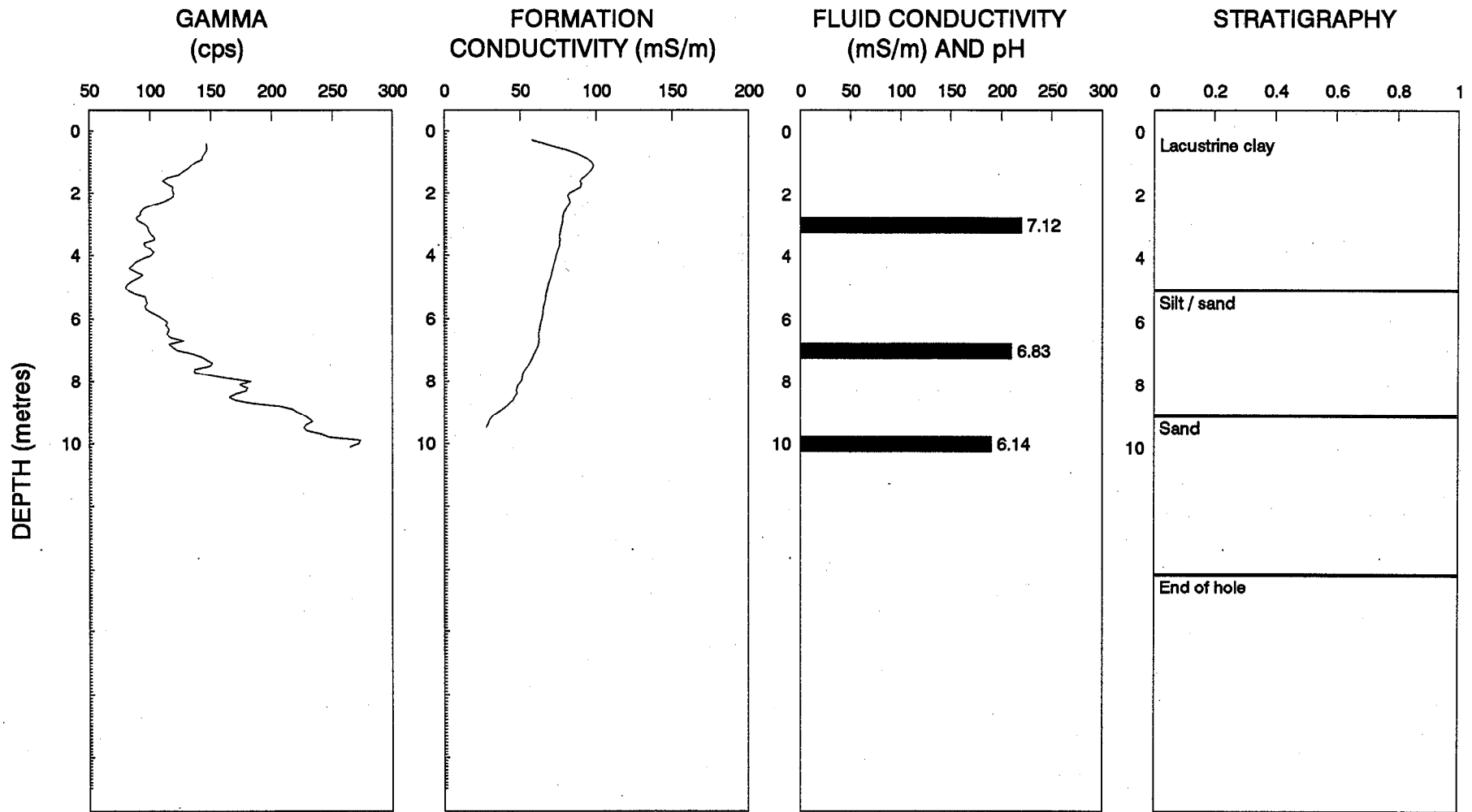
FIGURE 5.1.2

BOREHOLE LOGS – PISTOL DAM – G21

Figure 5.1.2.1
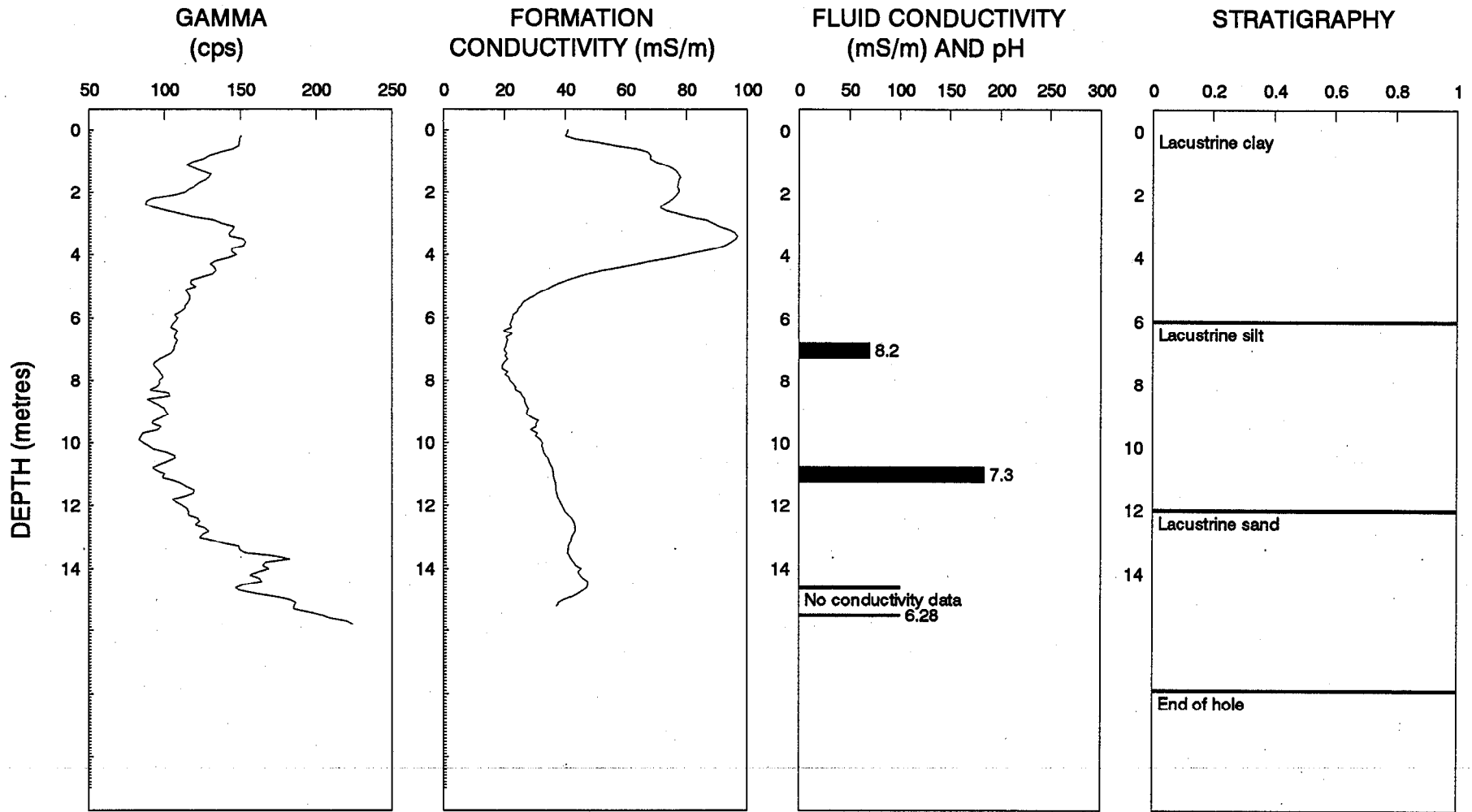
BOREHOLE DATA   G30 – PISTOL

Figure 5.1.2.2
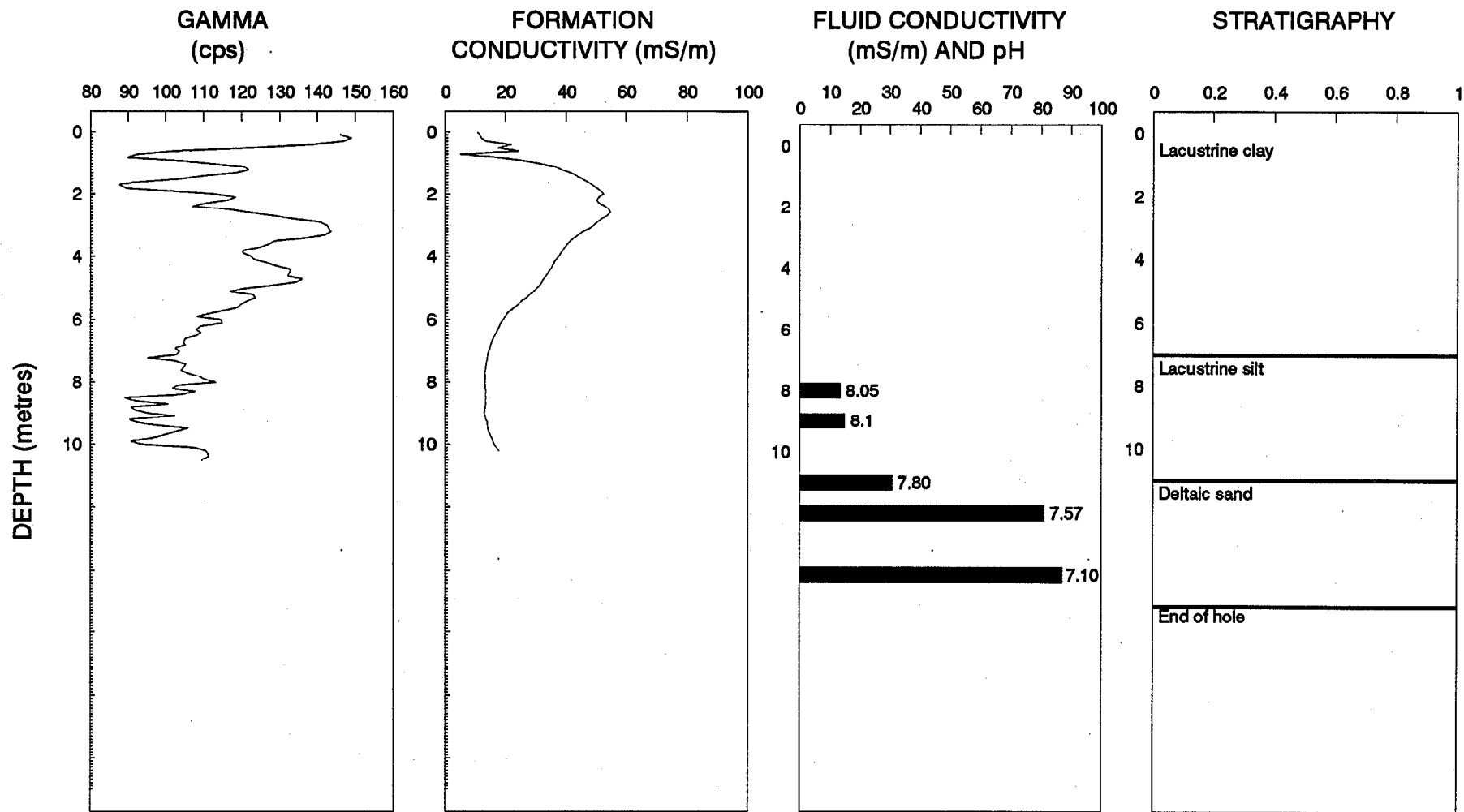
BOREHOLE DATA   G22 – PISTOL

Figure 5.1.2.3

GAMMA (CPS) — BULK CONDUCTIVITY (mS/m) — PORE FLUID CONDUCTIVITY (mS/m) — STRATIGRAPHY

DEPTH (metres)

Stratigraphy labels:
- Organics
- Sandy silt
- Soft grey clayey silt
- No data
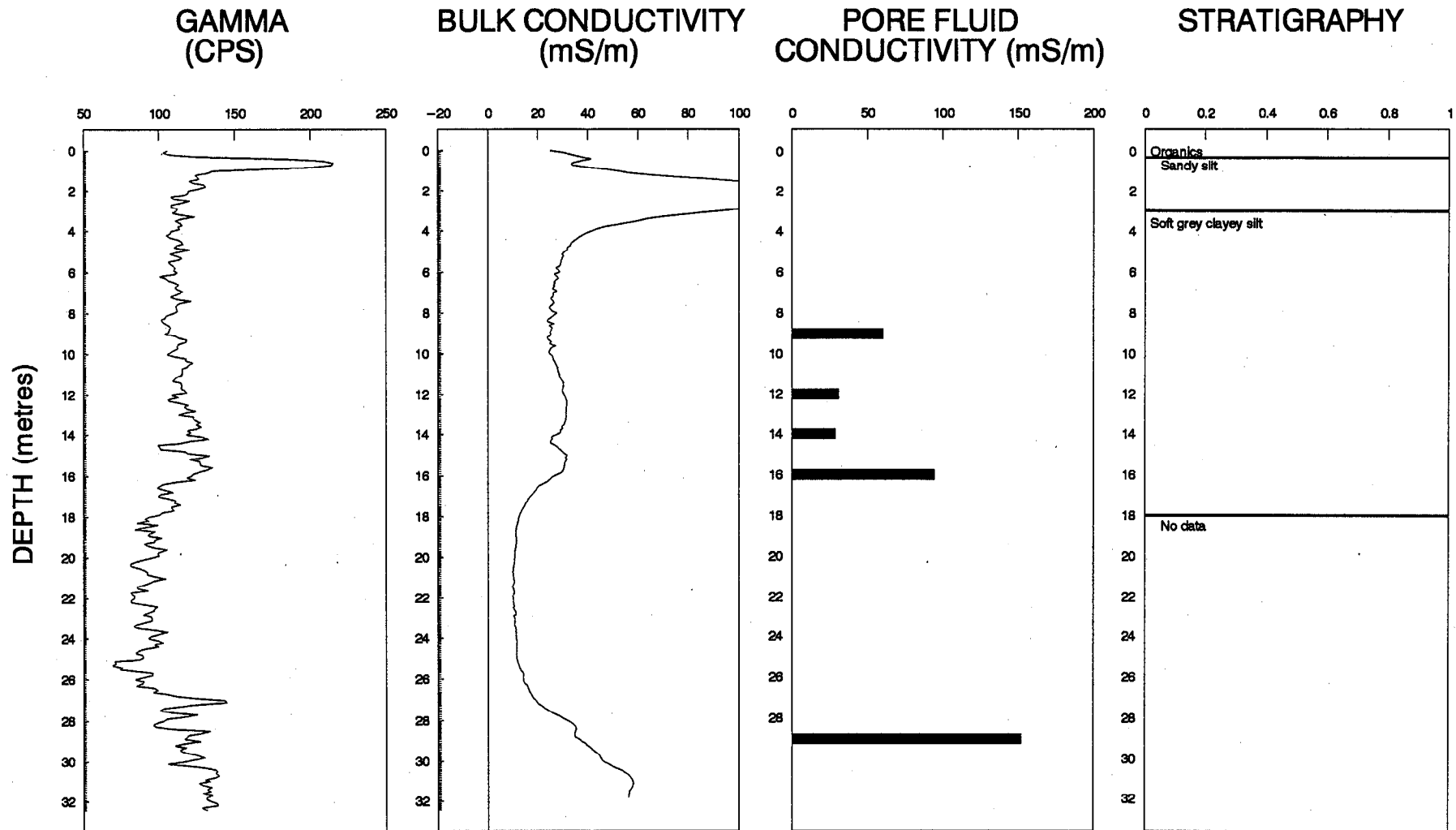
BOREHOLE LOGS – PISTOL DAM – DH 81G

Figure 5.1.2.4
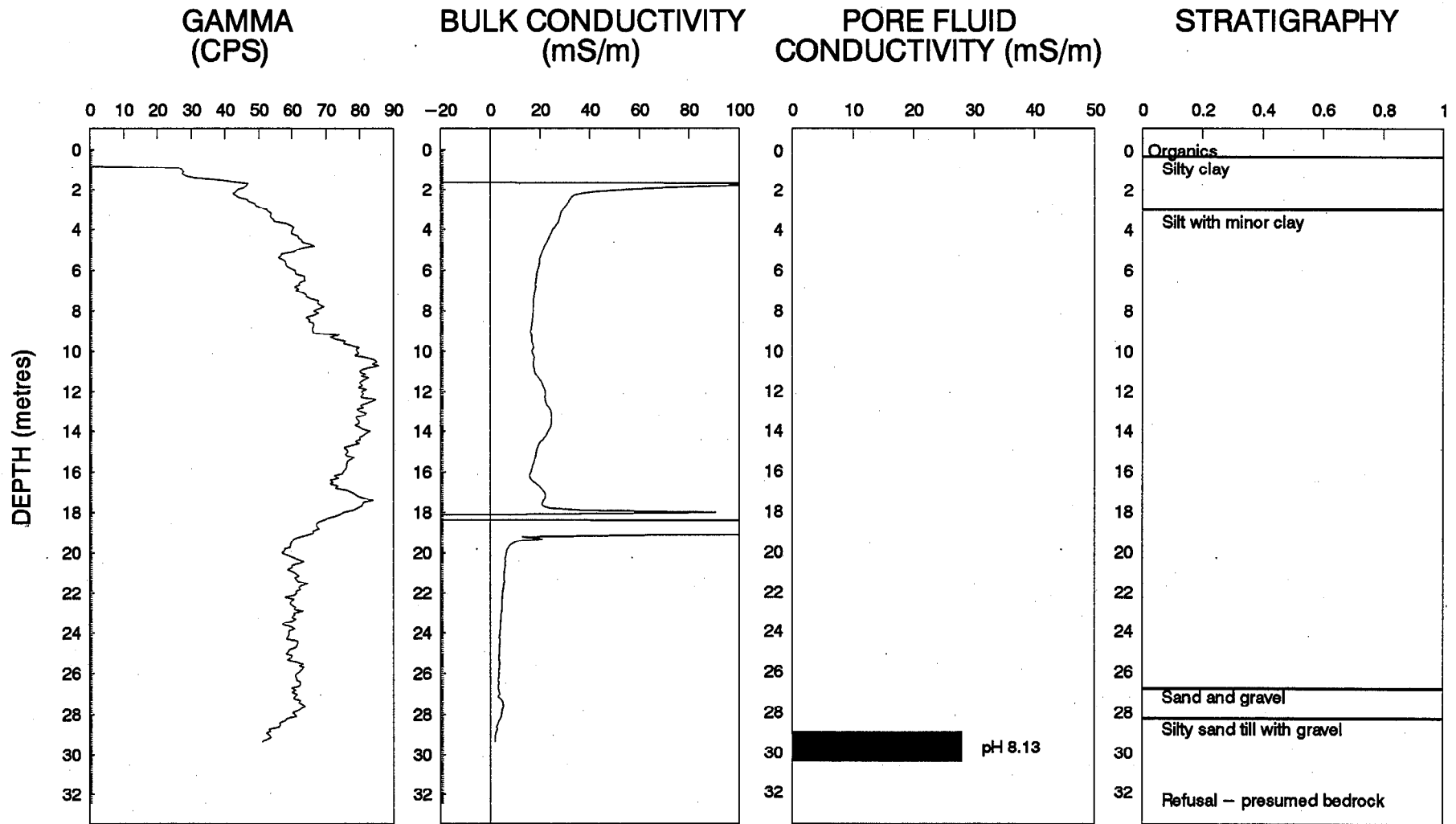
BOREHOLE LOGS – PISTOL DAM – DH 104G

Figure 5.1.2.5
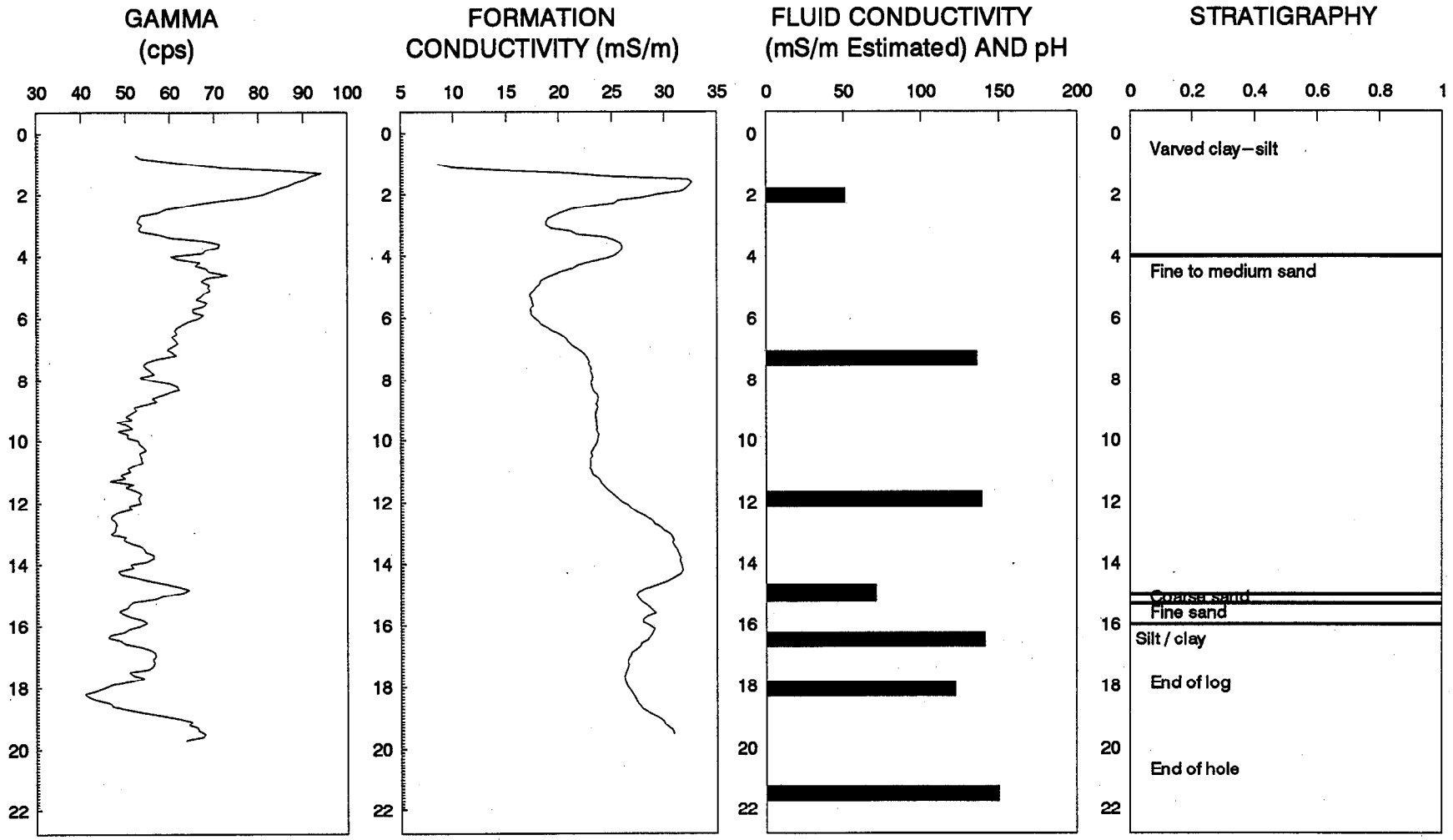
BOREHOLE DATA   G92 – PISTOL DAM

Figure 5.1.2.6
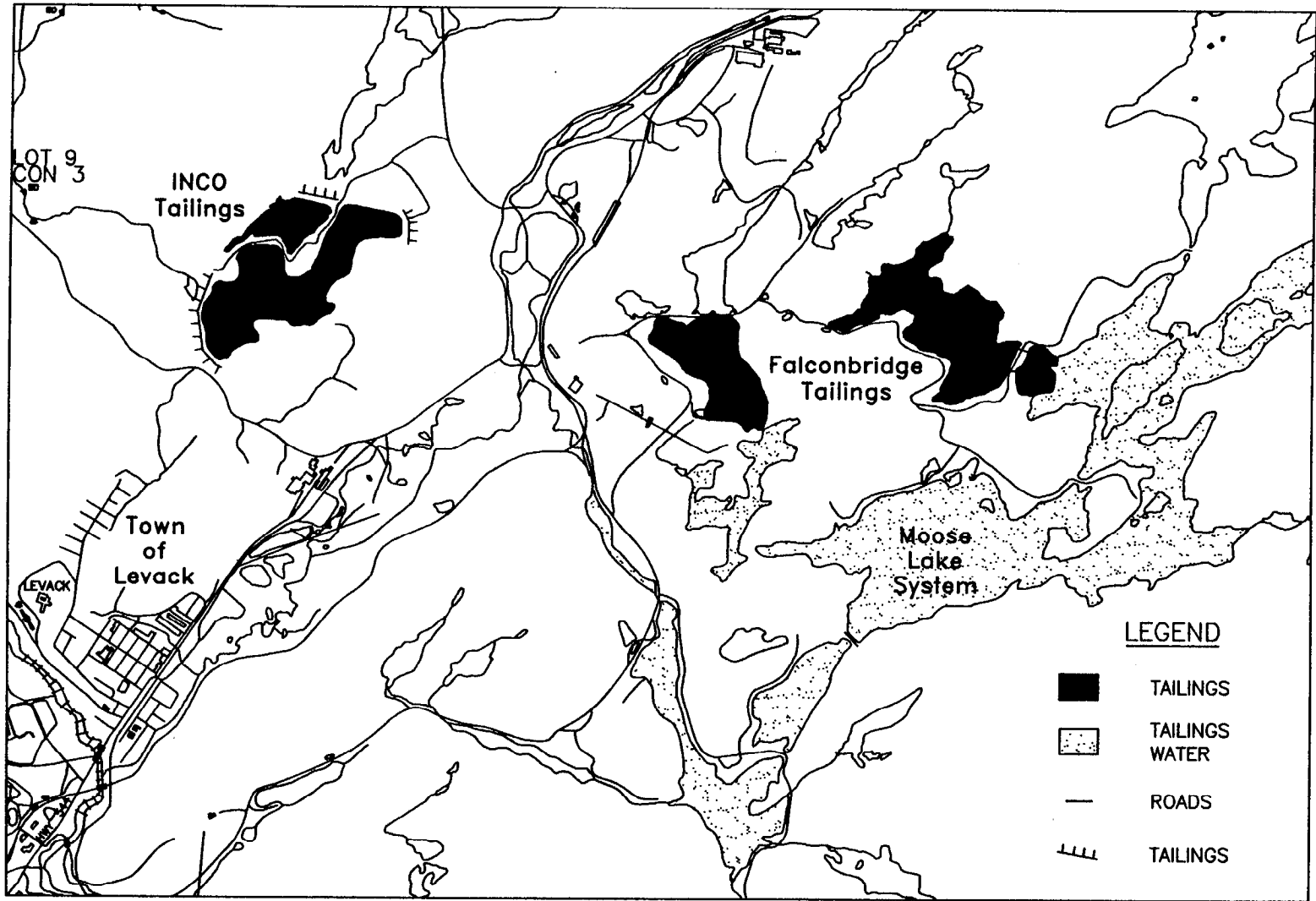
Electrical Conductivity Profile Section B (Robertson et al. 1992)

FIGURE 5.1.3

Levack Area Tailings
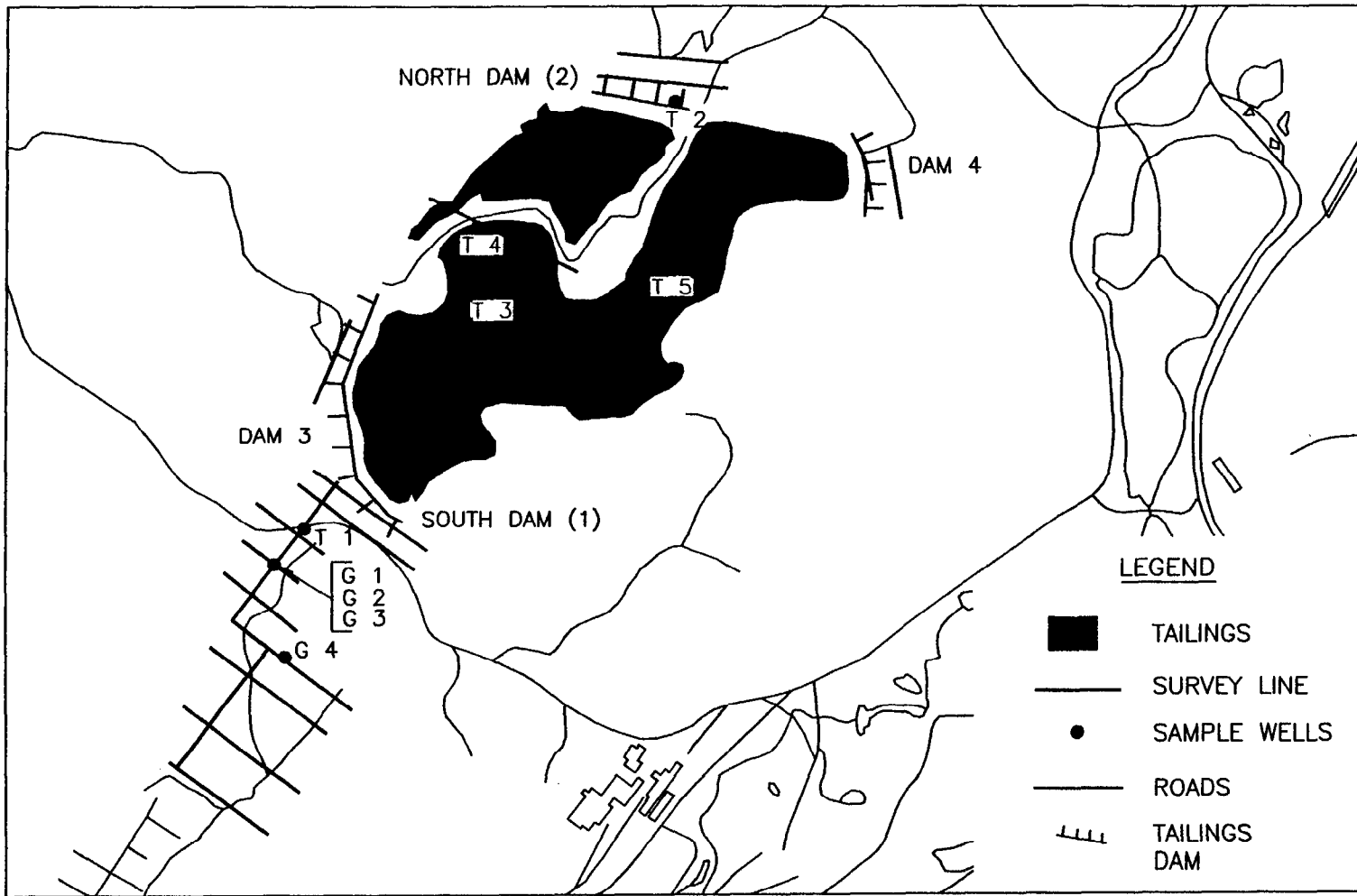
FIGURE 5.2.1

INCO Levack Tailings

LEGEND

■ TAILINGS

— SURVEY LINE

• SAMPLE WELLS

— ROADS

⊥⊥⊥ TAILINGS DAM

NORTH DAM (2)

DAM 4

T 2

T 4

T 5

T 3

DAM 3

SOUTH DAM (1)

T 1

G 1
G 2
G 3

G 4

FIGURE 5.2.2

ROCK
ROCK
DAM
1000 W
500 W
LAKE
T4●
ABANDONED
GRAVEL
PIT
●T2
ABANDONED
GRAVEL
PIT
00 10 20
mmho/m
TAILINGS
0
00
200 N
ROCK
ROCK
TAILINGS
●T5
EM 34 LEGEND
————— 20H
- - - - - 40H
ROCK

North Dam Profiles - EM34
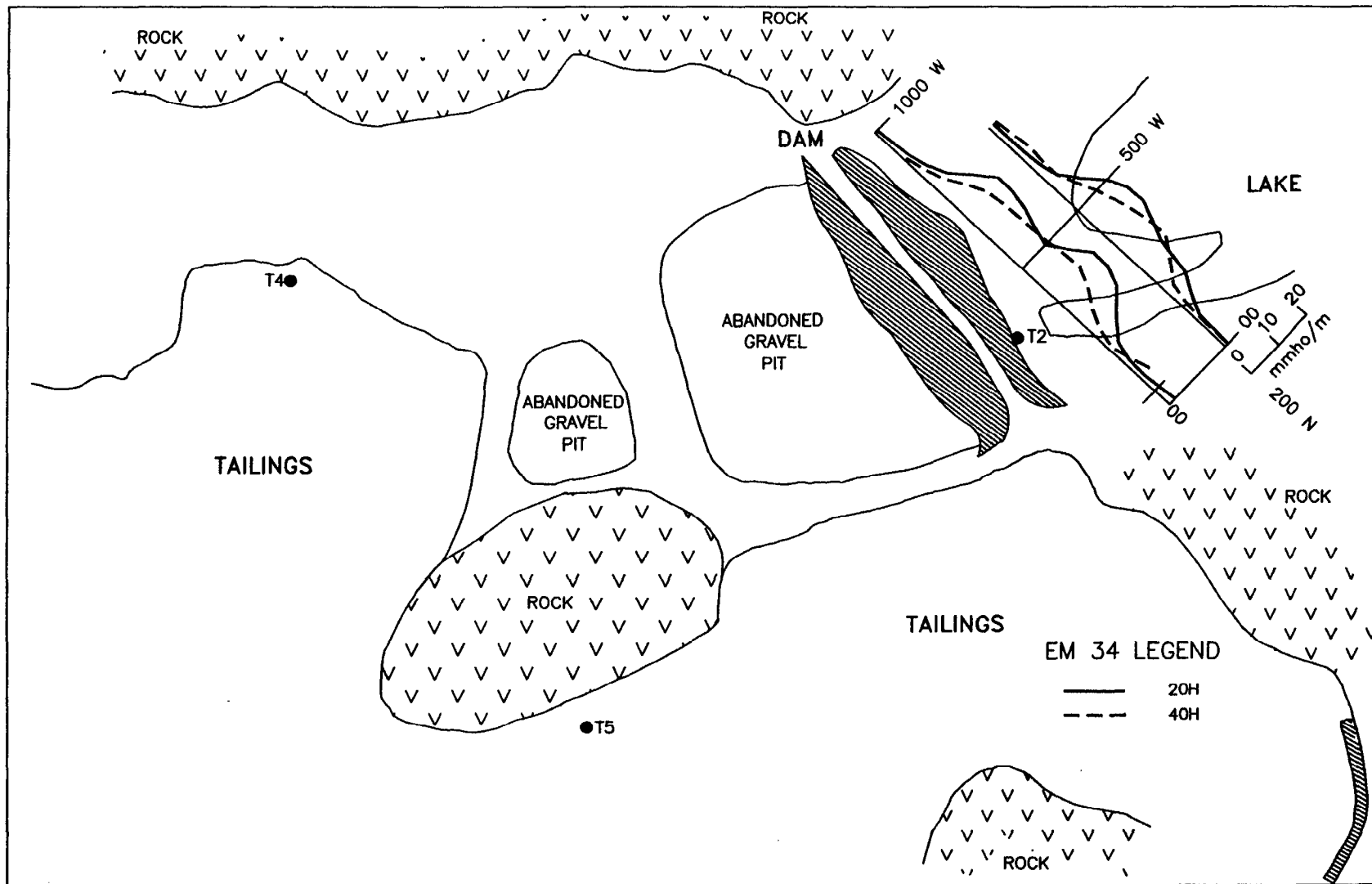
FIGURE 5.2.2.1B
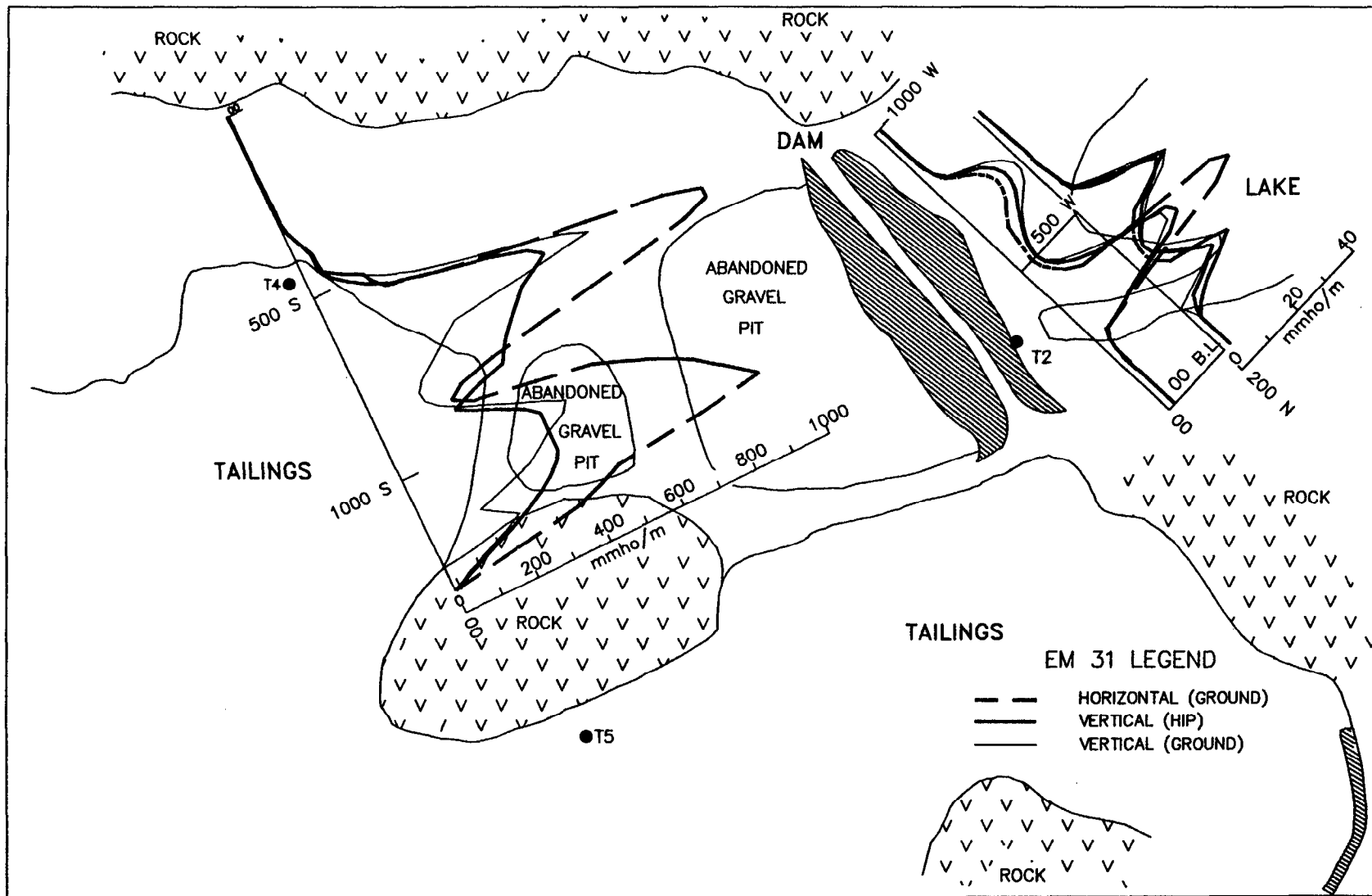
North Dam Profiles - EM31
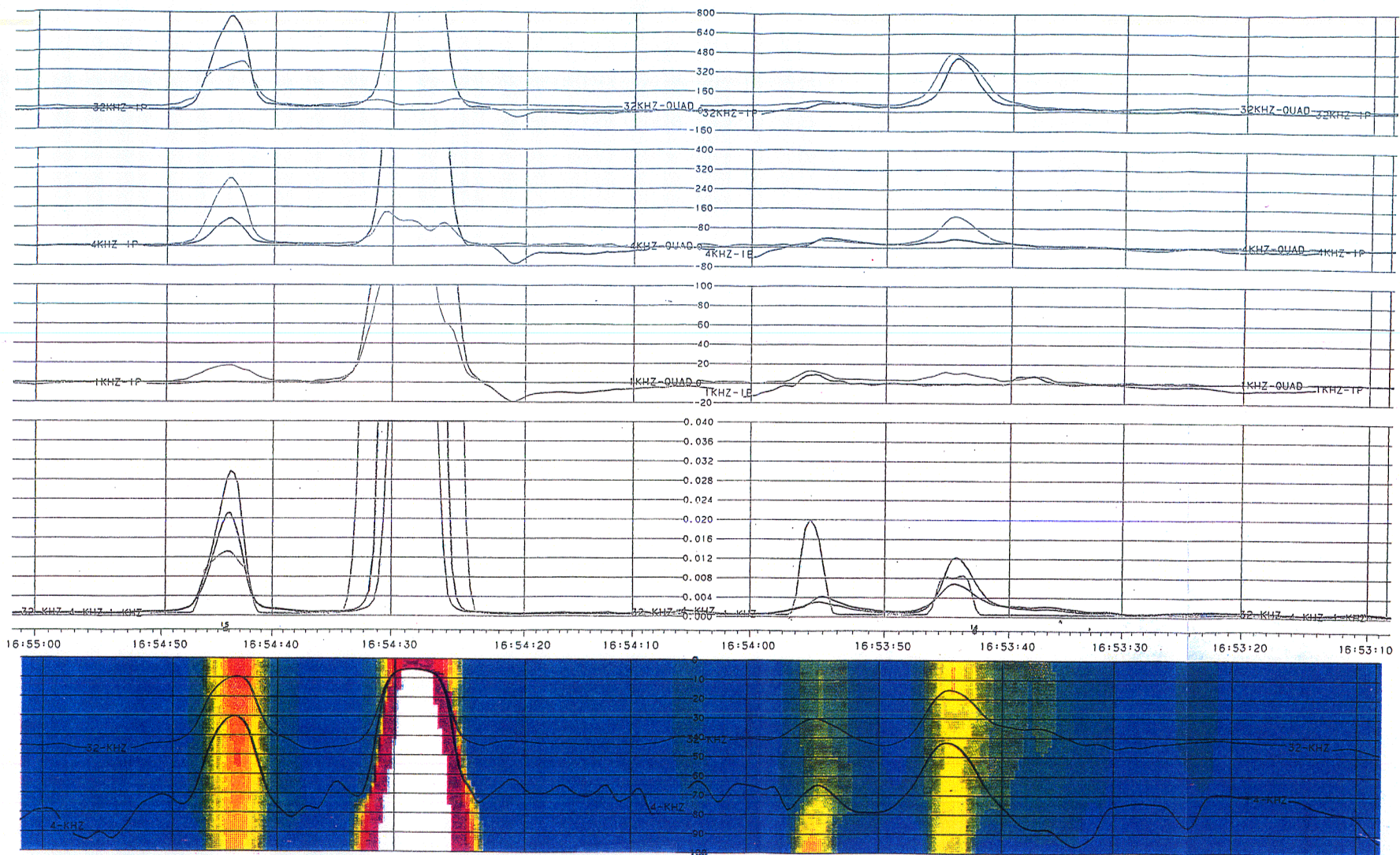
FIGURE 5.2.2.1A

STACKED PROFILES FLIGHT NO: 26

FIGURE 5.2.1.2

CONDUCTIVITY

	0.5000
	0.1000
	0.0750
	0.0500
	0.0350
	0.0270
	0.0220
	0.0180
	0.0150
	0.0120
	0.0100
	0.0080
	0.0060
	0.0040
	0.0030
	0.0020
	0.0015
	0.0010
	0.0005
	0.0000

FIGURE 5.2.1.3
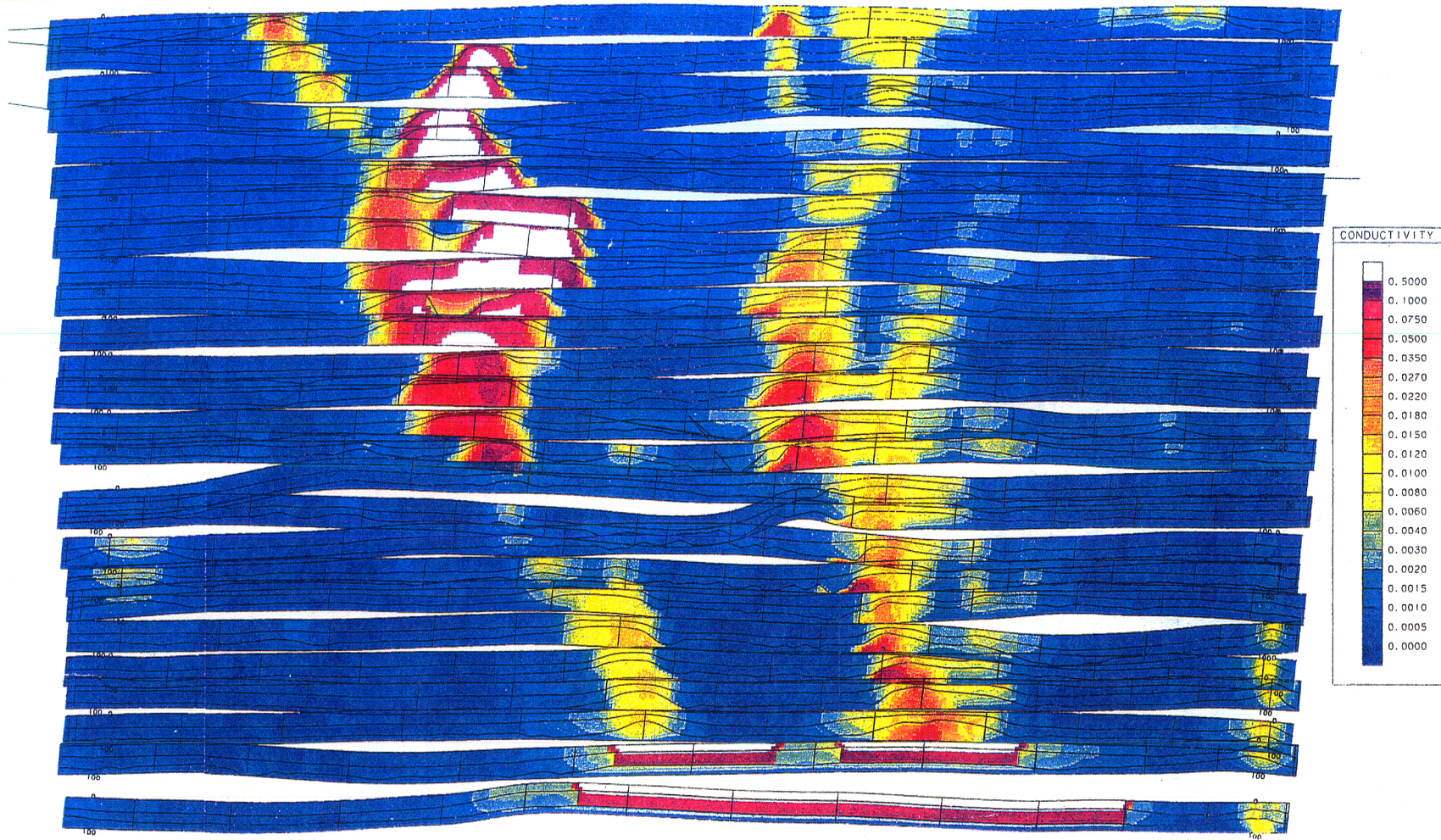
CONDUCTIVITY
(mmho/m)
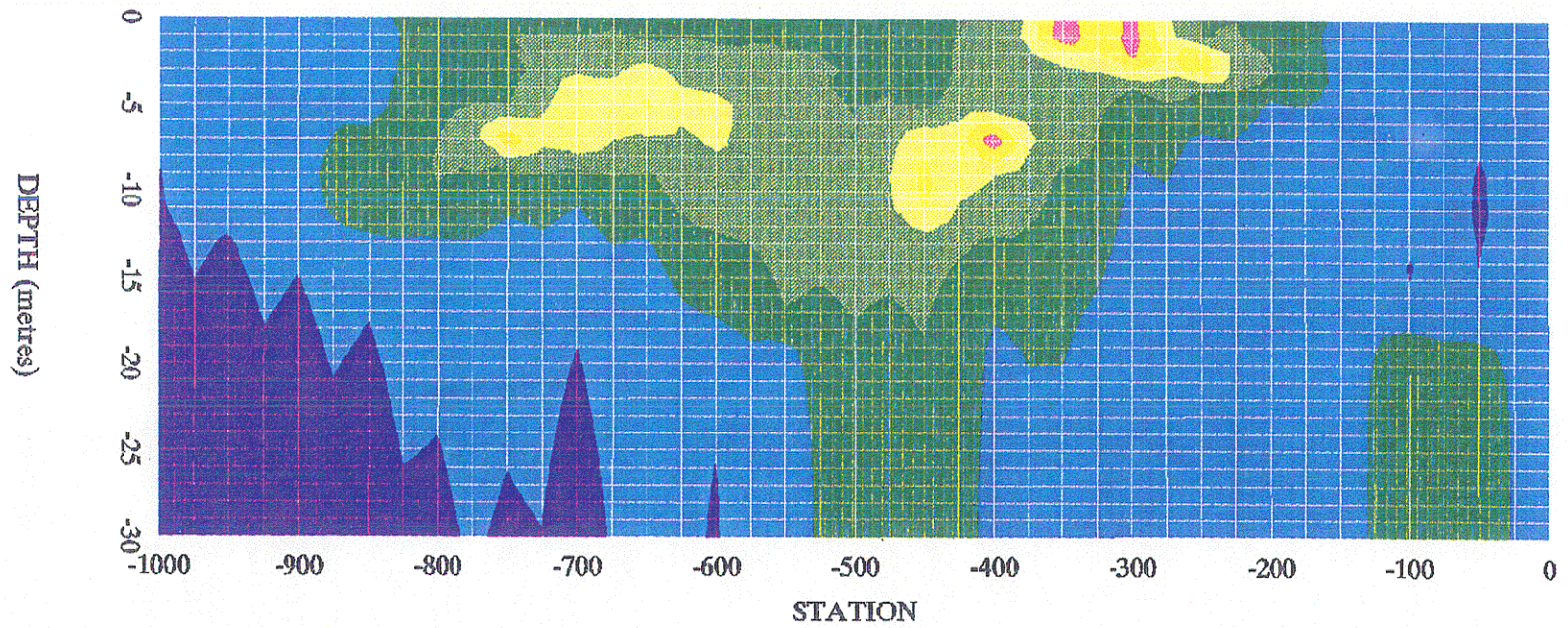
Legend:
- 0-2
- 2-5
- 5-10
- 10-20
- 20-30
- 30-40
- 40-50
- 50-

LEVACK DAM 2 00N
(DISCRETE)

FIGURE 5.2.2.2
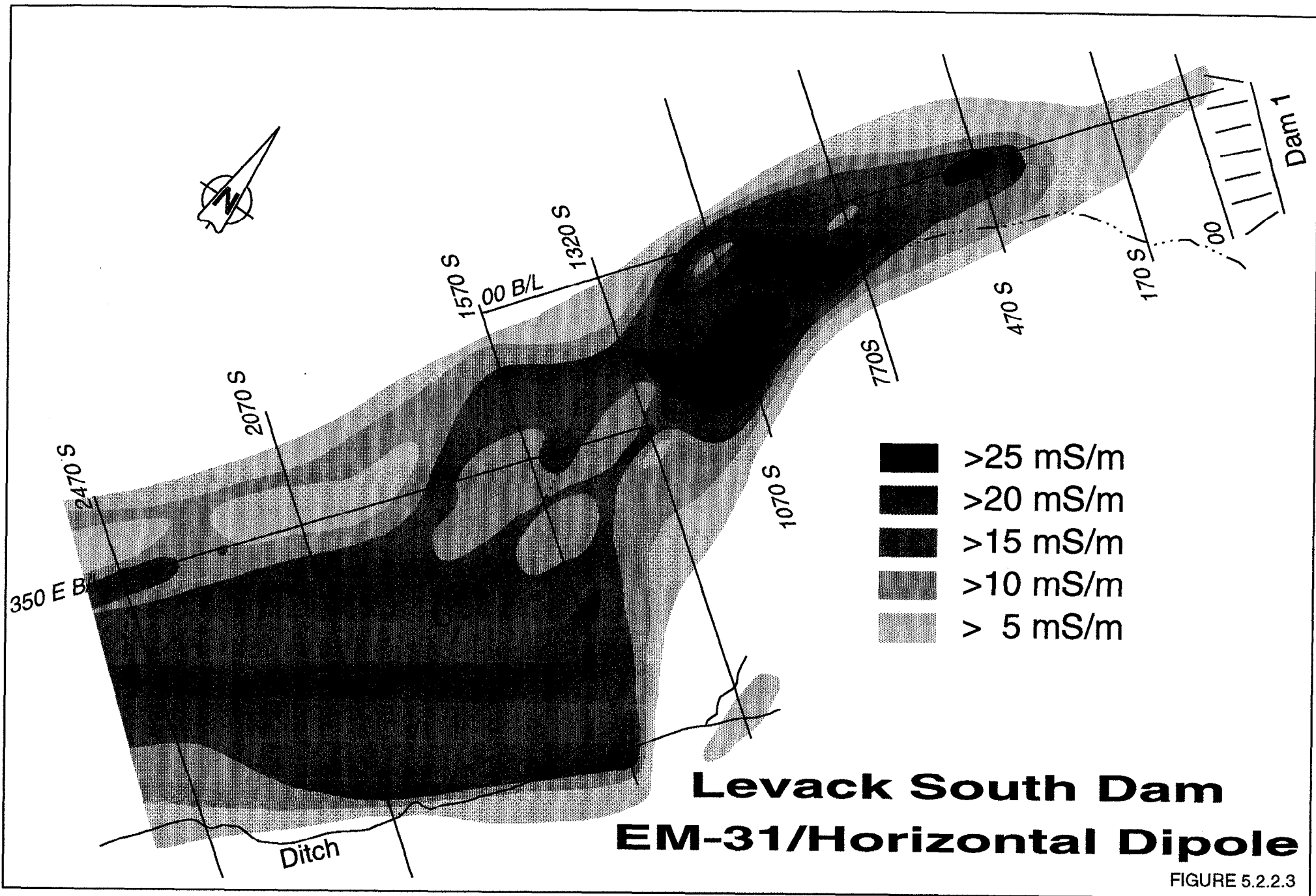
Levack South Dam
EM-31/Horizontal Dipole

■	>25 mS/m
▨	>20 mS/m
▦	>15 mS/m
▒	>10 mS/m
░	> 5 mS/m

Dam 1

00

170 S

470 S

770S

1070 S

1320 S

1570 S

00 B/L

2070 S

2470 S

350 E B/L

Ditch

FIGURE 5.2.2.3

Levack South Dam

EM-31/Vertical Dipole
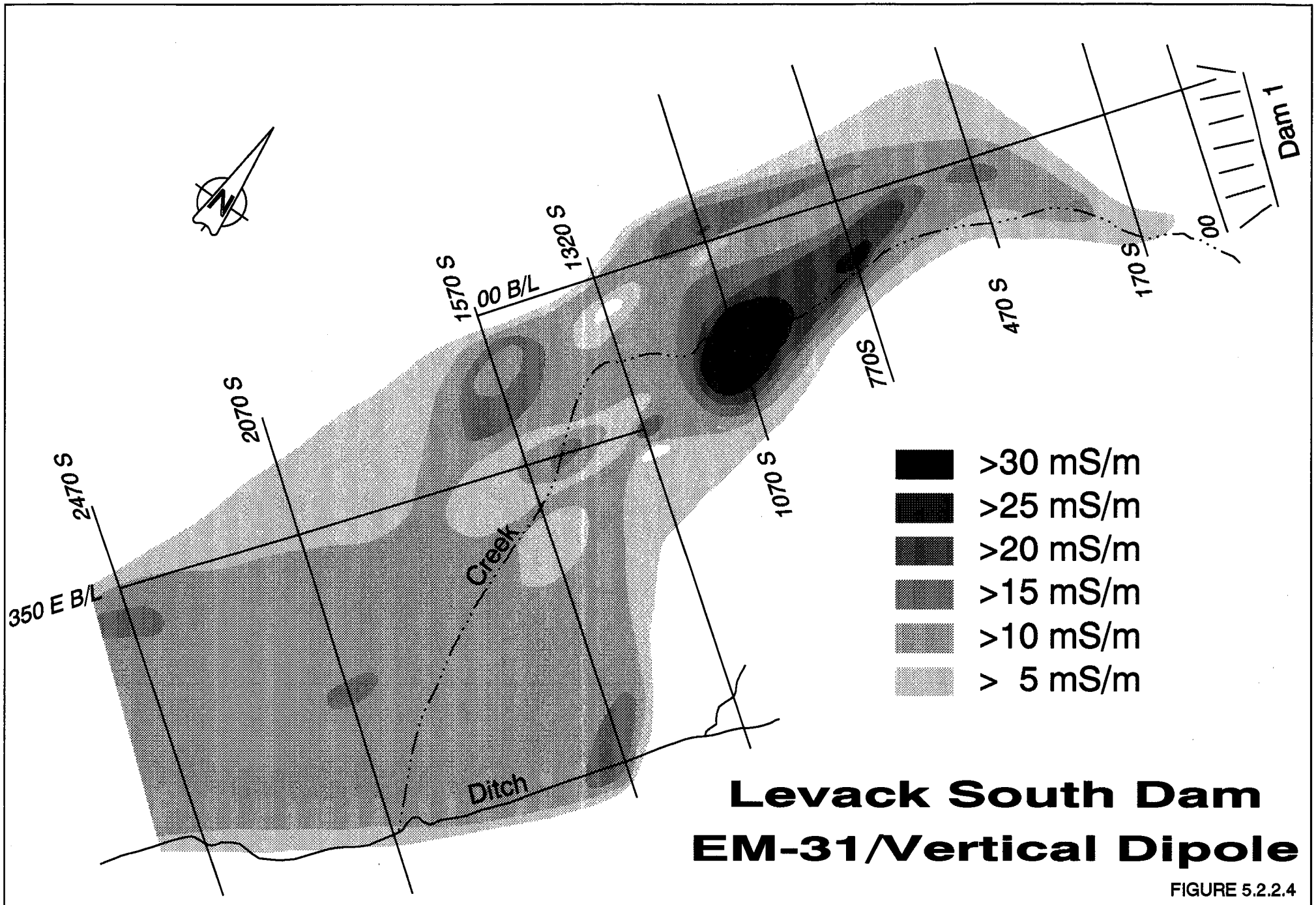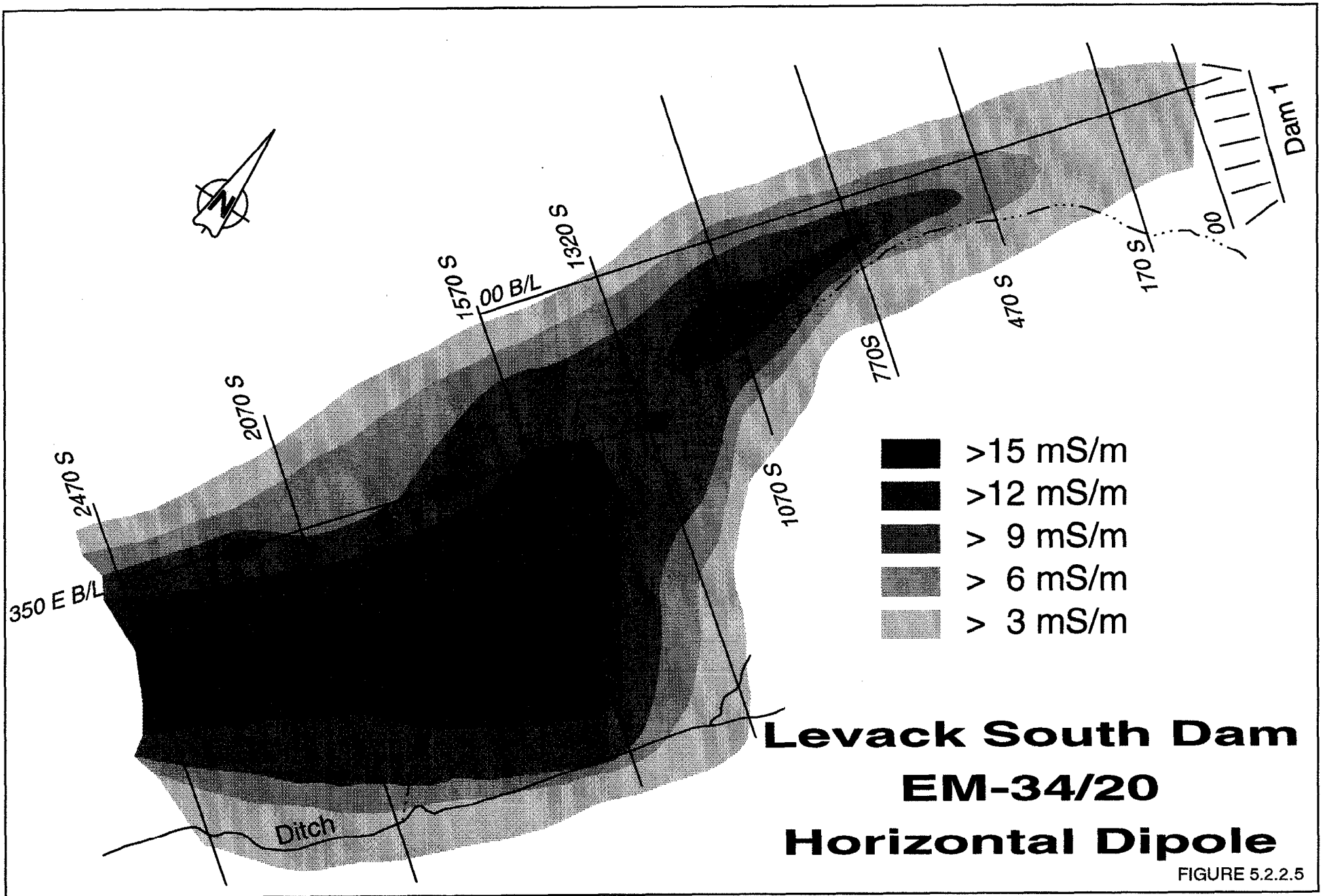
FIGURE 5.2.2.4

Levack South Dam
EM-34/20
Horizontal Dipole

■	>15 mS/m
■	>12 mS/m
▨	> 9 mS/m
▧	> 6 mS/m
░	> 3 mS/m

FIGURE 5.2.2.5

Levack South Dam

EM-34/40H

Horizontal Dipole
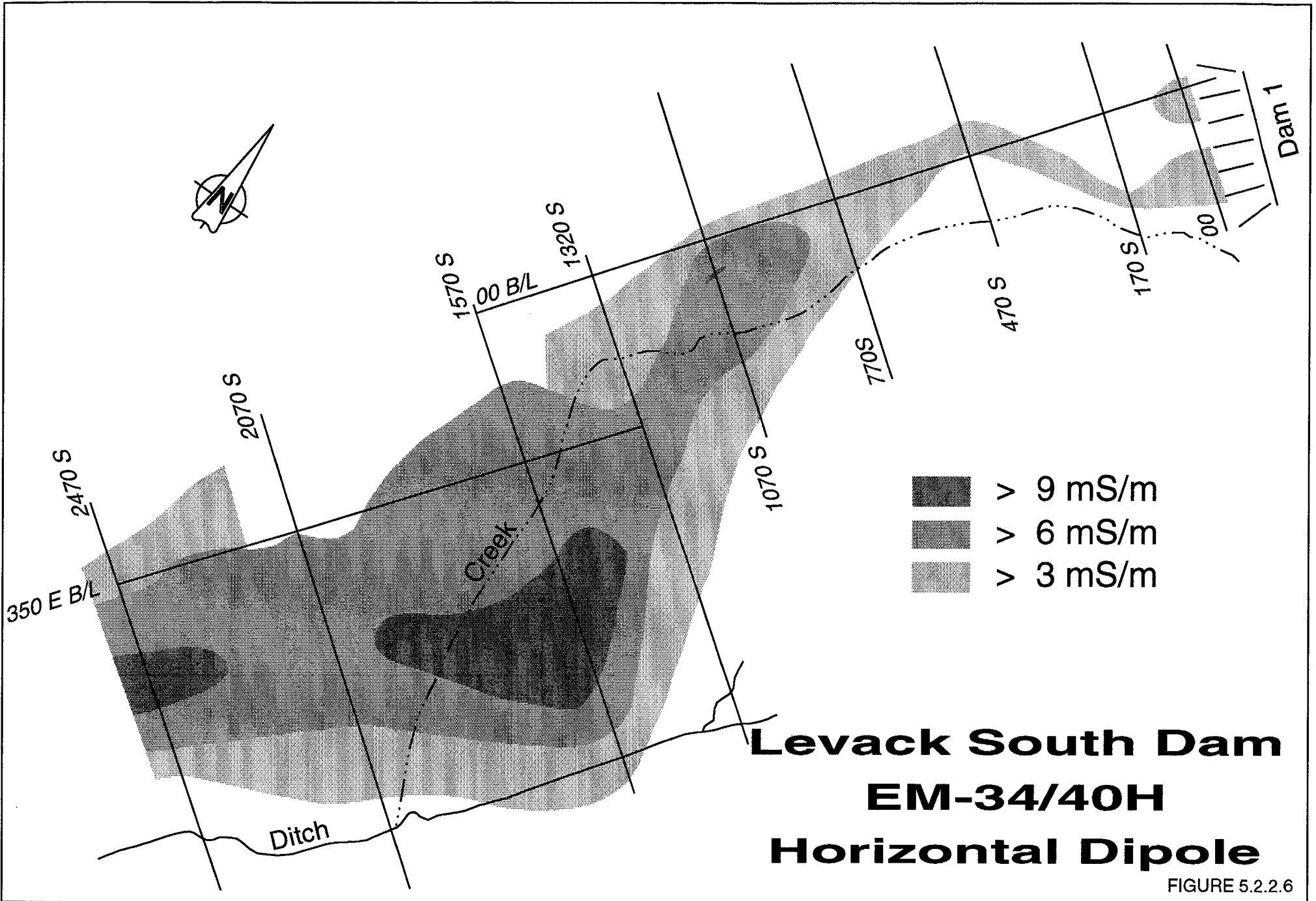
FIGURE 5.2.2.6

Contours in mS/m

LEVACK DAM 1 00S (CONTINUOUS)
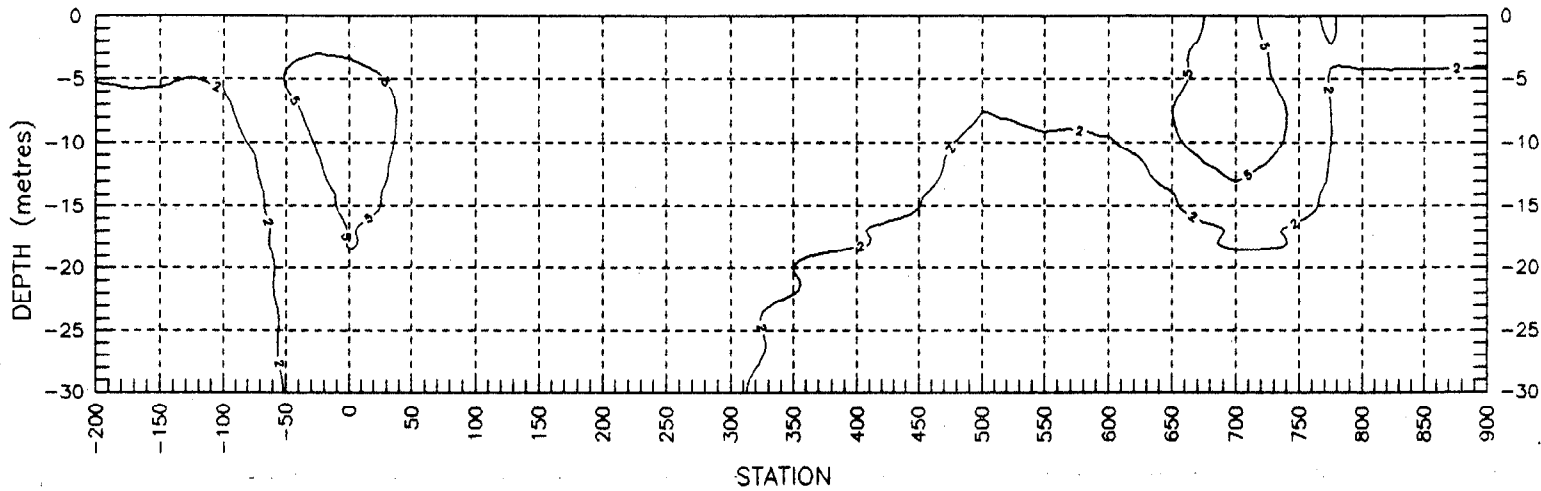
LEVACK DAM 1 170S (CONTINUOUS)

INCO EXPLORATION AND
TECHNICAL SERVICES INC.

VERTICAL CONDUCTIVITY SECTIONS
LEVACK DAM AREA
DAM I

GEO-PHYSI-CON

| SCALE | DRAWN BY | DATE March, 1992 |
| N.T.S. | PROJECT NO. C 92-10 | FIGURE |

FIGURE 5.2.2.7

LEVACK DAM 1 470S (CONTINUOUS)
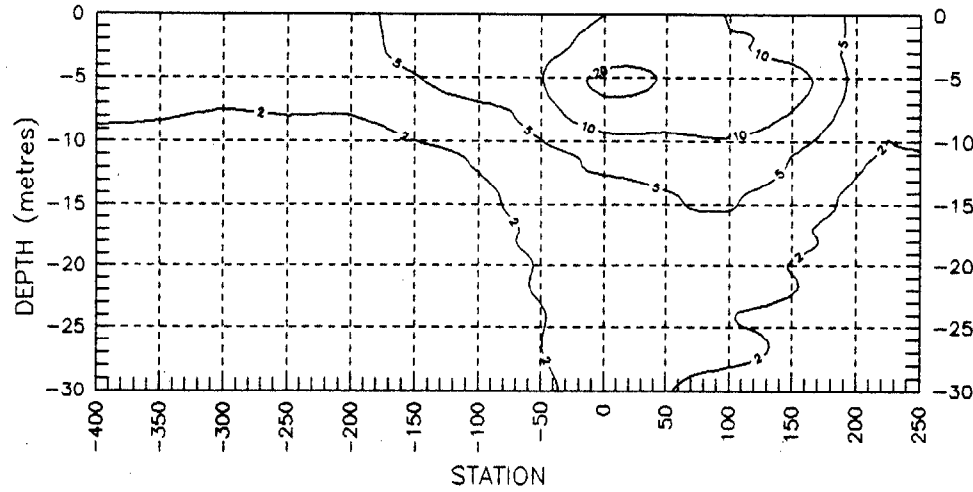
Contours in mS/m

LEVACK DAM 1 770S (CONTINUOUS)

INCO EXPLORATION AND
TECHNICAL SERVICES INC.

VERTICAL CONDUCTIVITY SECTIONS
LEVACK DAM AREA
DAM I

GEO·PHYSI·CON

SCALE	DRAWN BY	DATE March,1992
N.T.S.	PROJECT NO. C 92-10	FIGURE

FIGURE 5.2.2.8

Contours in mS/m

LEVACK DAM 1 1070S (CONTINUOUS)

FIGURE 5.2.2.9

BOREHOLE DATA   T1-1 - LEVACK

Figure 5.2.3.1

GAMMA (cps)

FORMATION CONDUCTIVITY (mS/m)

FLUID CONDUCTIVITY (mS/m) AND pH

STRATIGRAPHY

DEPTH (metres)

Sand and gravel till

End of hole

5.2
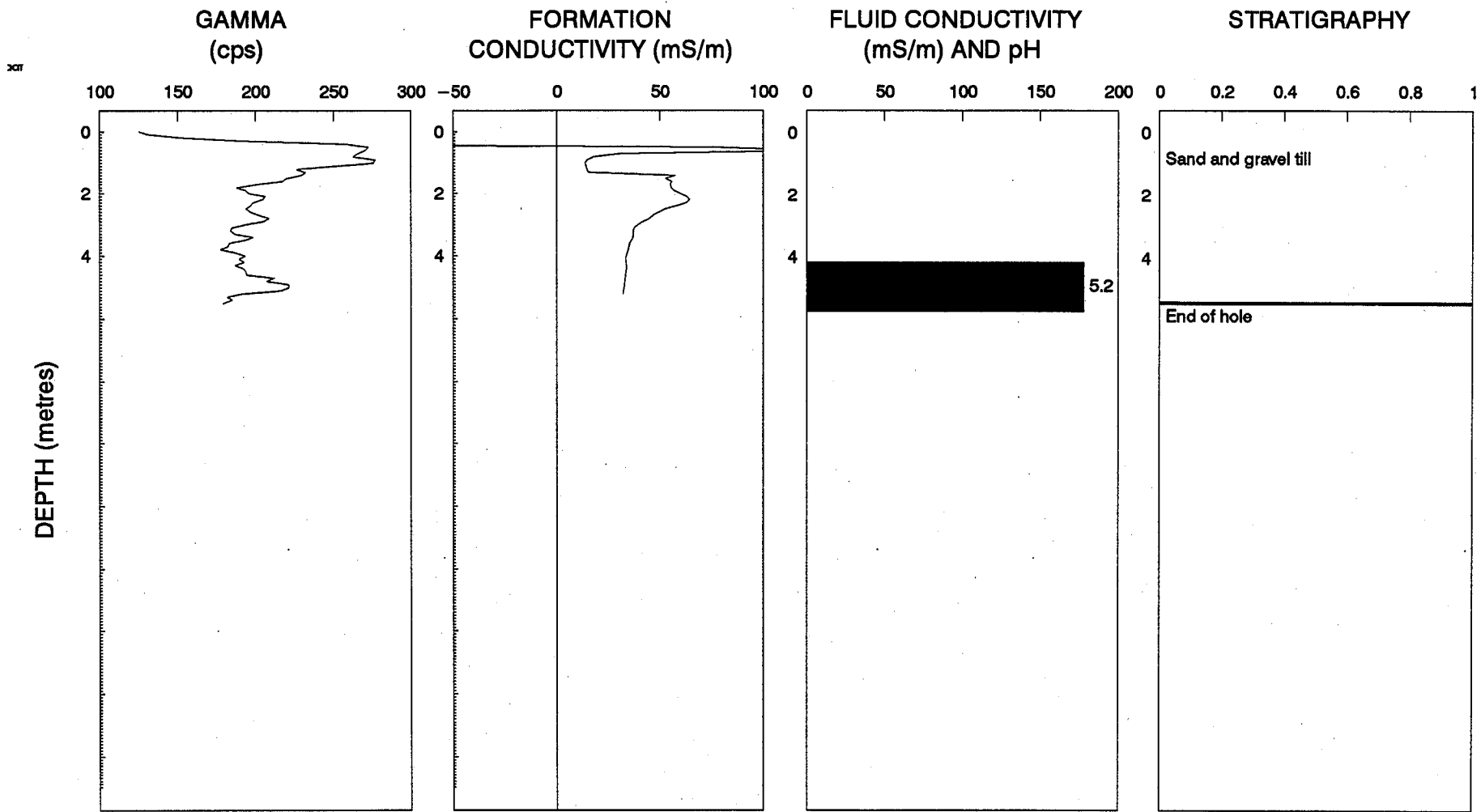
BOREHOLE DATA   G1 – LEVACK

Figure 5.2.3.2

| GAMMA (cps) | FORMATION CONDUCTIVITY (mS/m) | FLUID CONDUCTIVITY (mS/m) AND pH | STRATIGRAPHY |

DEPTH (metres)

Sand and gravel till

End of hole

5.58
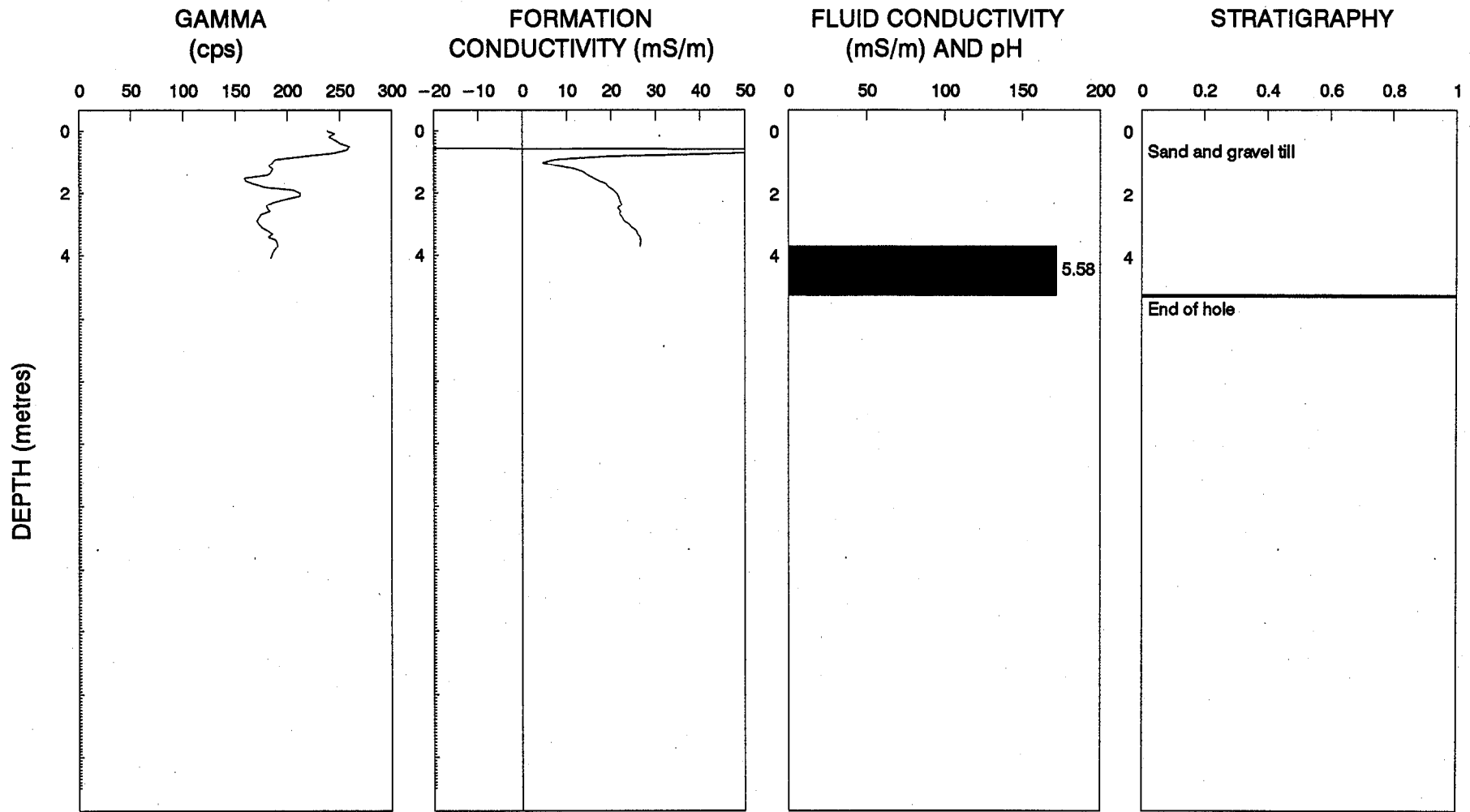
BOREHOLE DATA   G2 – LEVACK

Figure 5.2.3.3

GAMMA (cps)

50   100   150   200   250

FORMATION CONDUCTIVITY (mS/m)

−50   0   50   100

FLUID CONDUCTIVITY (mS/m) AND pH

0   50   100   150   200   250   300

STRATIGRAPHY

0   0.2   0.4   0.6   0.8   1

DEPTH (metres)

6.10

Sand and gravel till

Gravel till

Sand and gravel till

Gravel till

Sand

Cobble till

End of hole
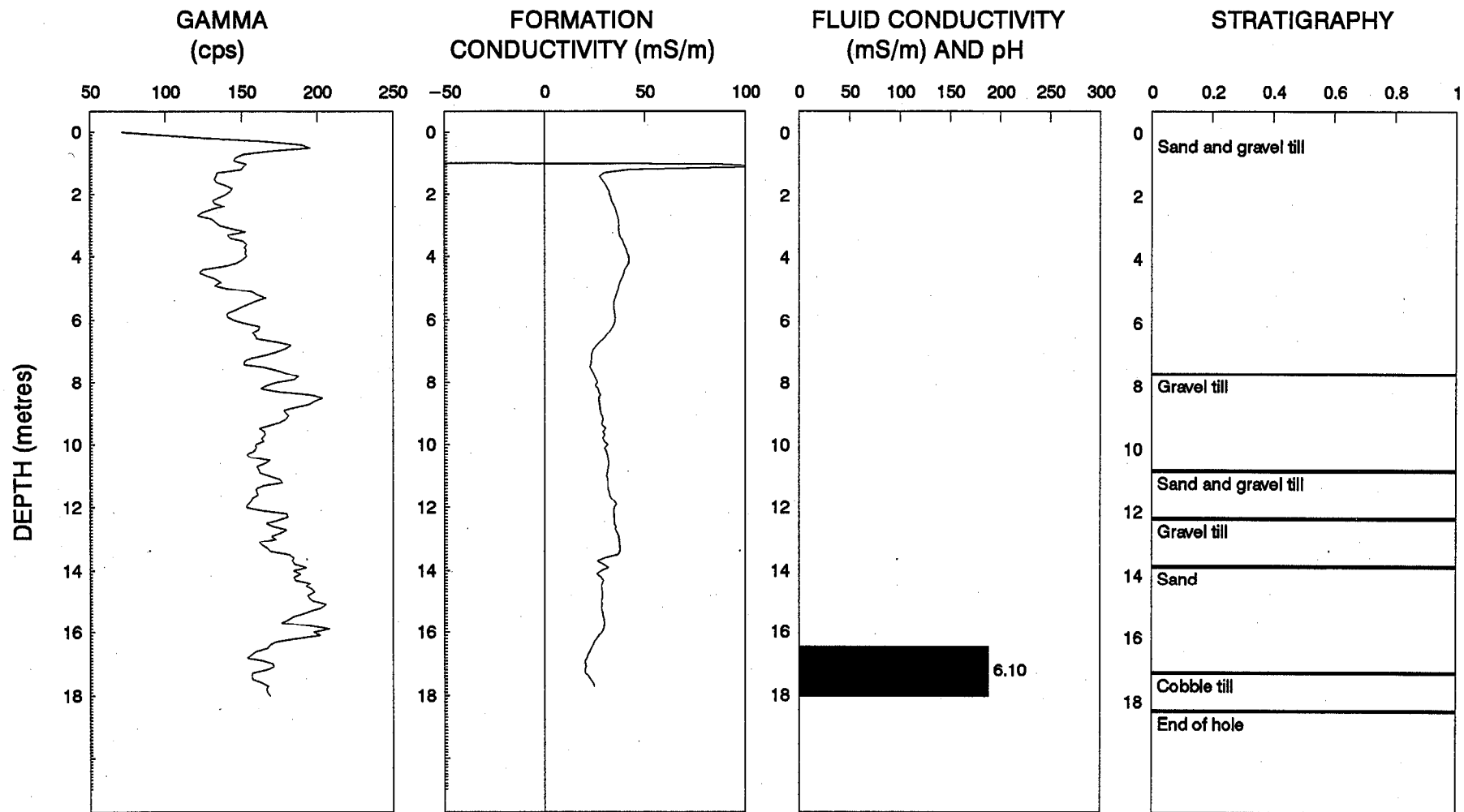
BOREHOLE DATA   G3 − LEVACK

Figure 5.2.3.4

GAMMA (cps)	FORMATION CONDUCTIVITY (mS/m)	FLUID CONDUCTIVITY (mS/m) AND pH	STRATIGRAPHY

Silty sand, some gravel

Sand, medium coarse

Sand and gravel till

6.19

End of hole

DEPTH (metres)
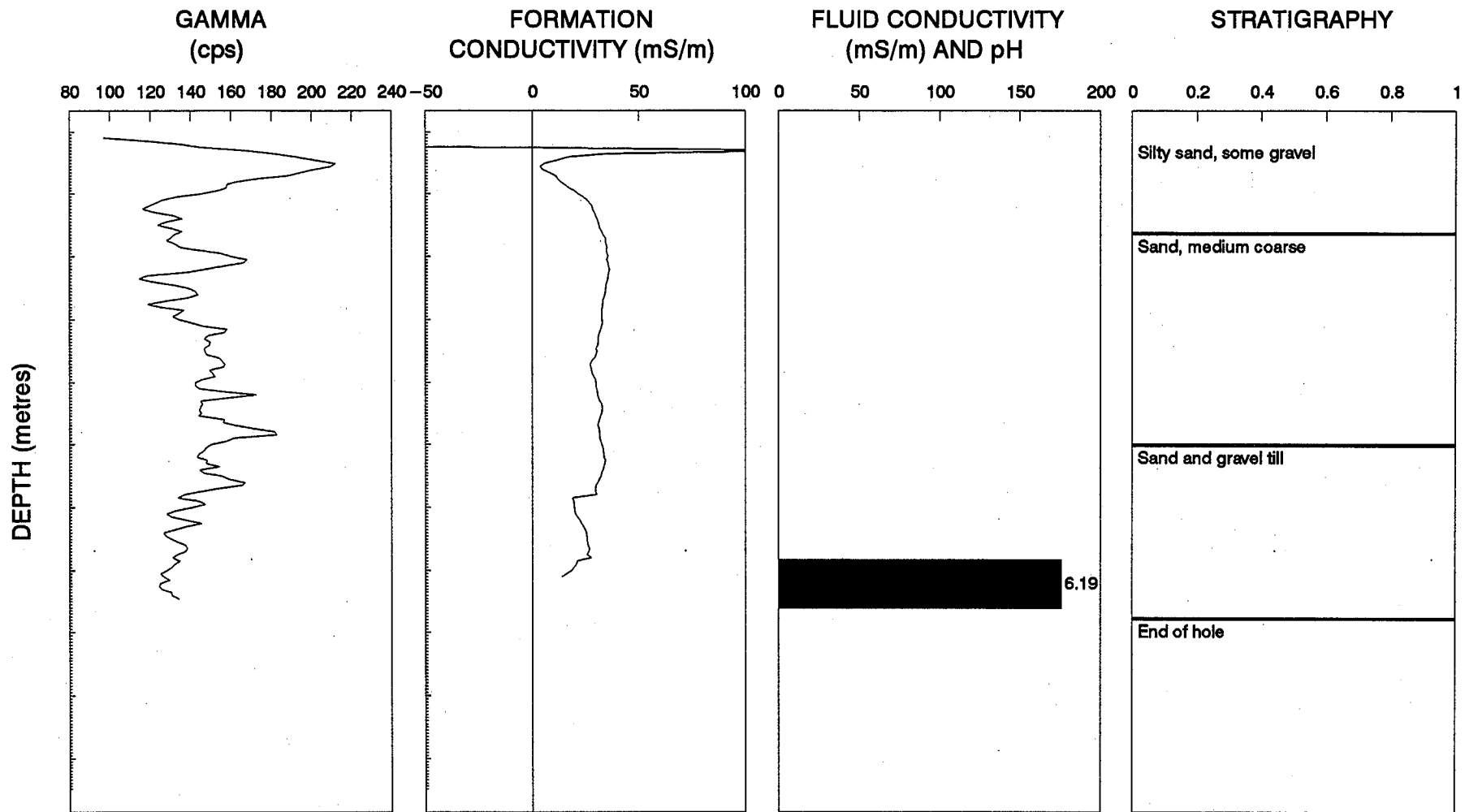
BOREHOLE DATA   G4 – LEVACK

Figure 5.2.3.5

GAMMA (cps)

FORMATION CONDUCTIVITY (mS/m) thousands

FLUID CONDUCTIVITY (mS/m) AND pH

STRATIGRAPHY

Rock Fill

Tailings

Sandy Silt

Sand and Gravel Till

pH 3.01

pH 9.72

pH 5.83
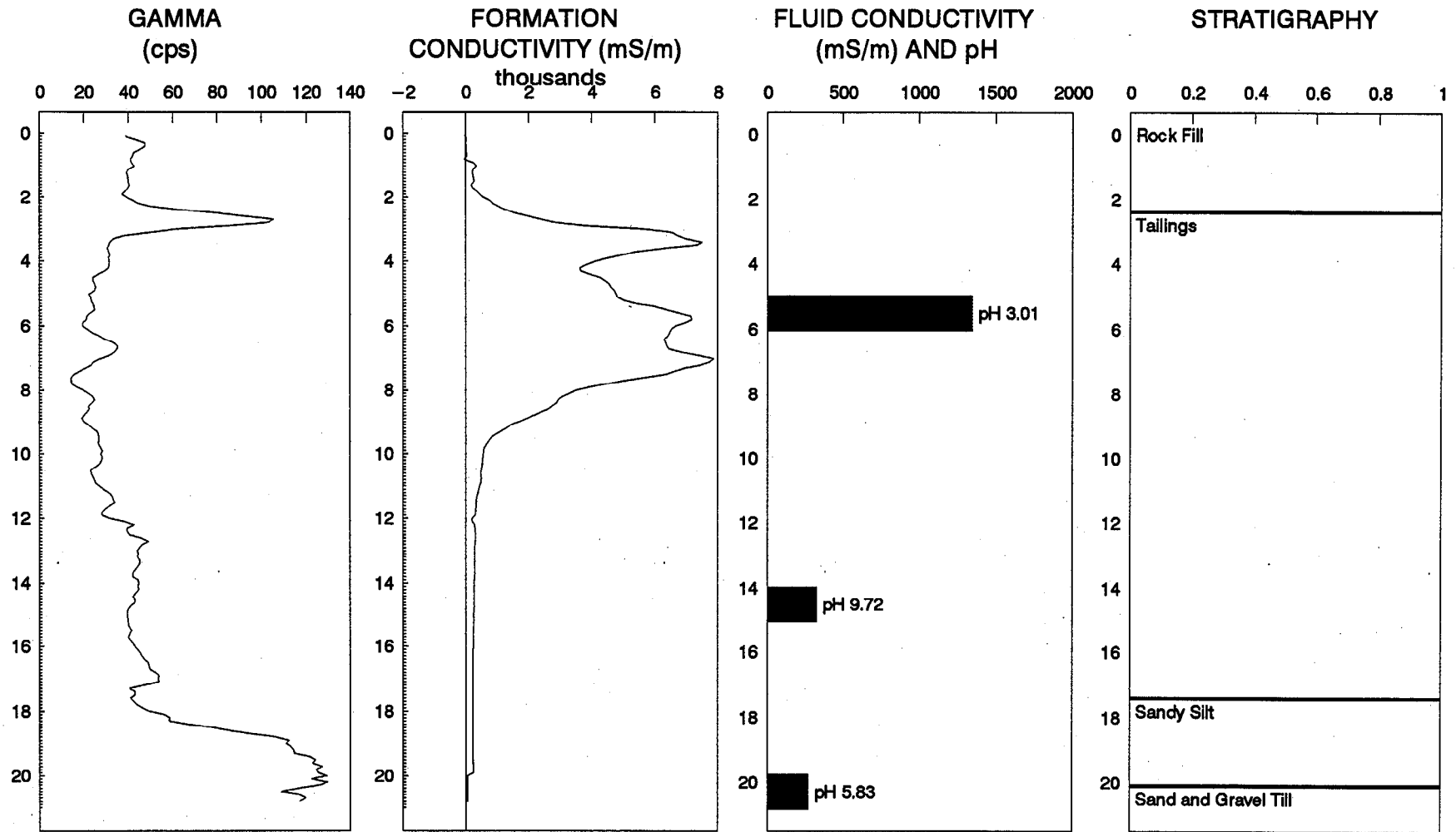
BOREHOLE DATA   T5 – LEVACK

Figure 5.2.3.6

GAMMA (cps) | **FORMATION CONDUCTIVITY (mS/m)** | **FLUID CONDUCTIVITY (mS/m) AND pH** | **STRATIGRAPHY**
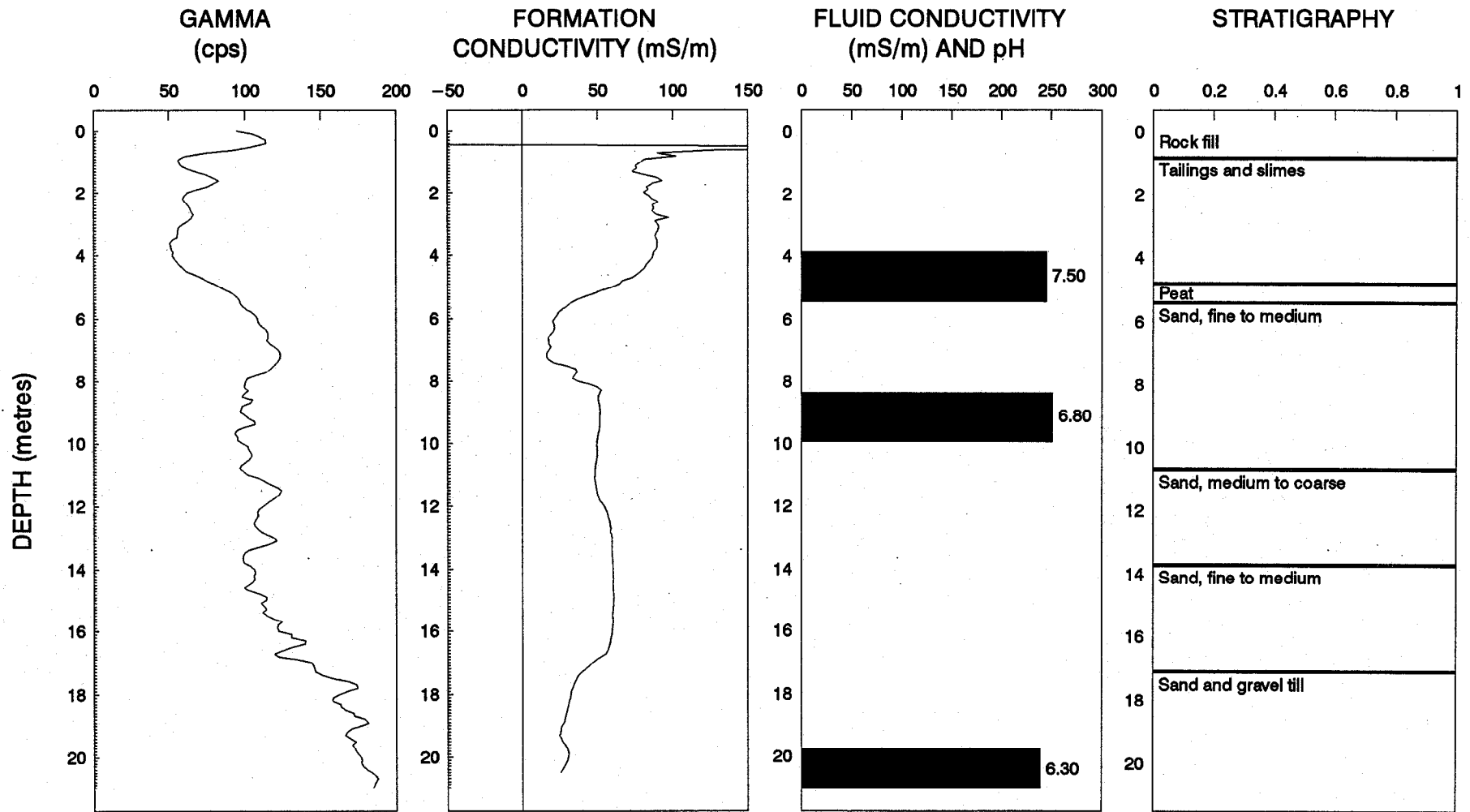
BOREHOLE DATA   T4 – LEVACK

Figure 5.2.3.7
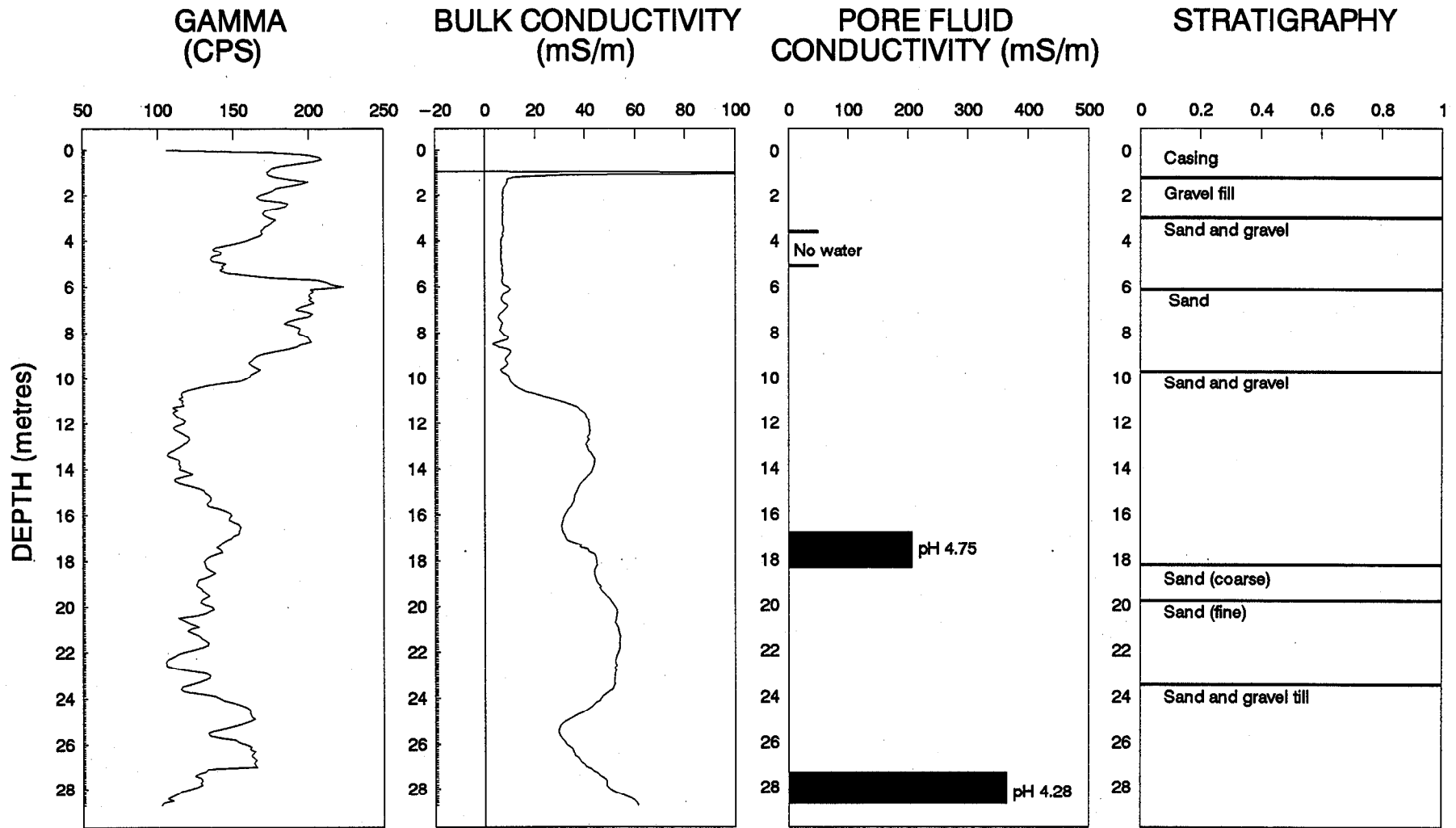
BOREHOLE LOGS – LEVACK DAM 2 – DH T2

Figure 5.2.3.8

GROUNDWATER CHEMISTRY

Well 2–1 Depth 28.9m
Total Conductivity – 4169 microS/cm
pH – 4.28

FIGURE 5.2.3.9

FIGURE 5.2.3.10

HORIZONTAL DIPOLE – GROUND LEVEL

VERTICAL DIPOLE – HIP LEVEL

VERTICAL DIPOLE – GROUND LEVEL
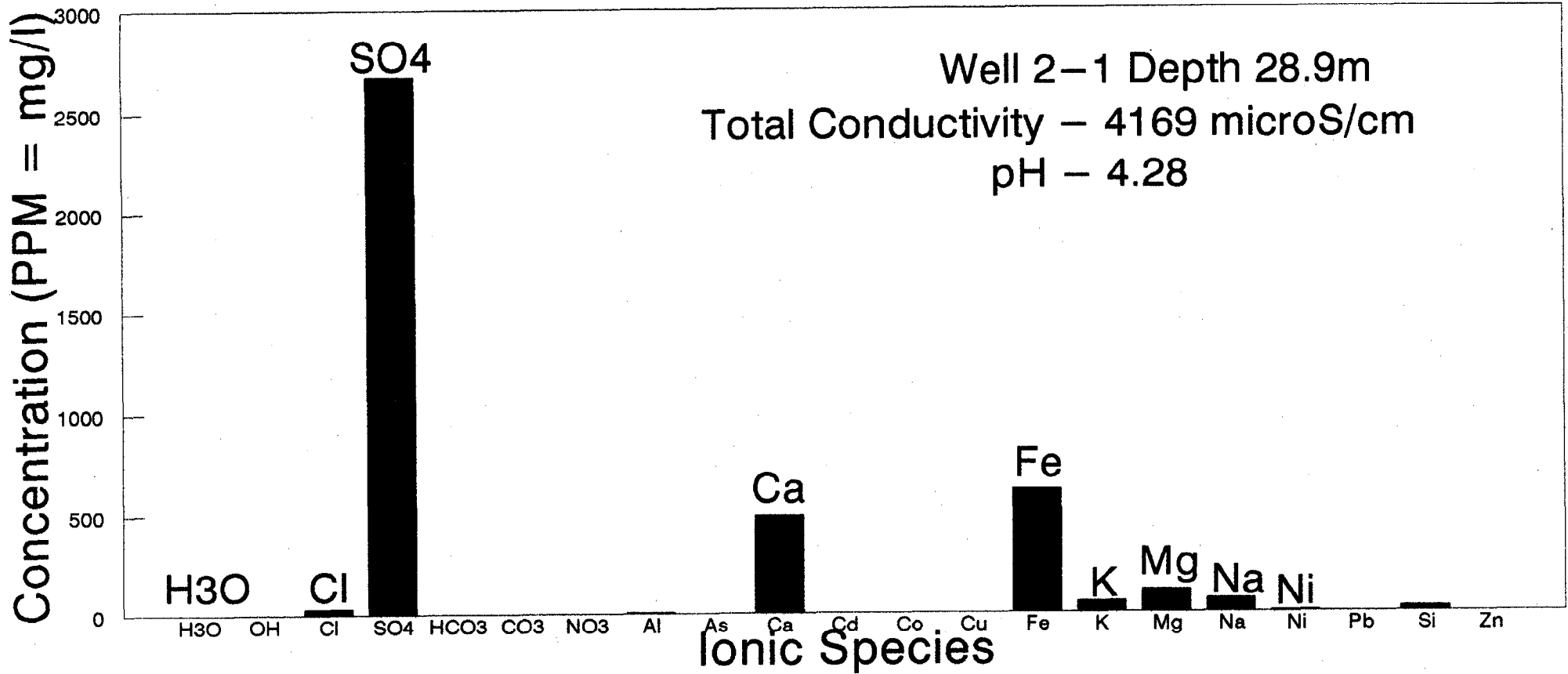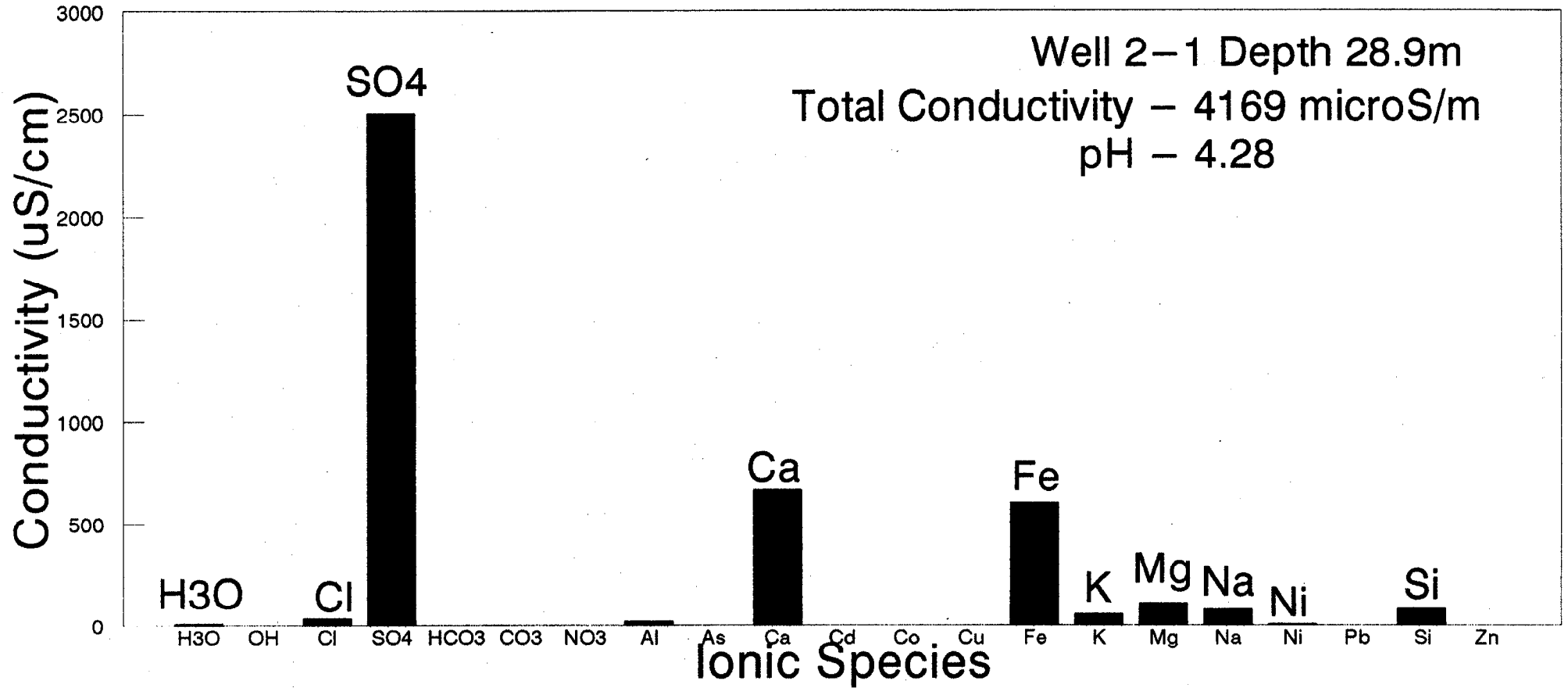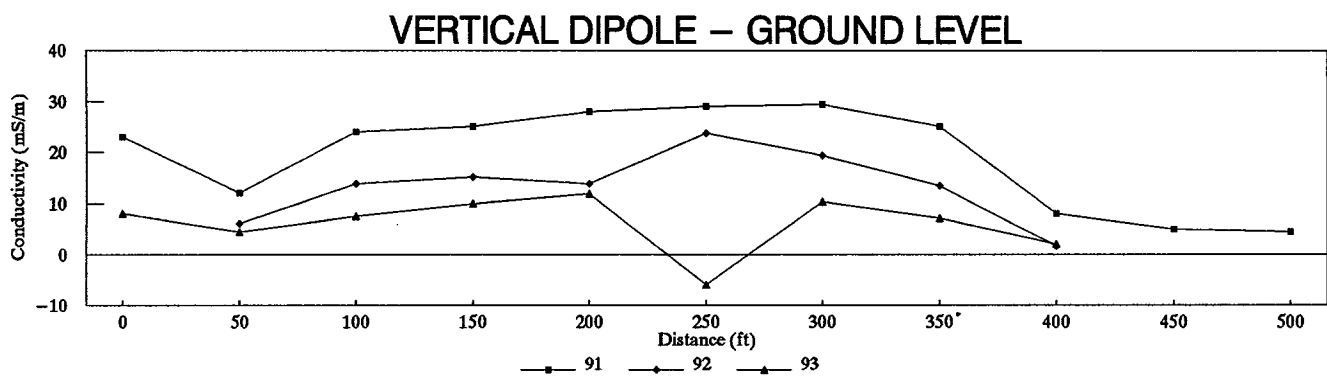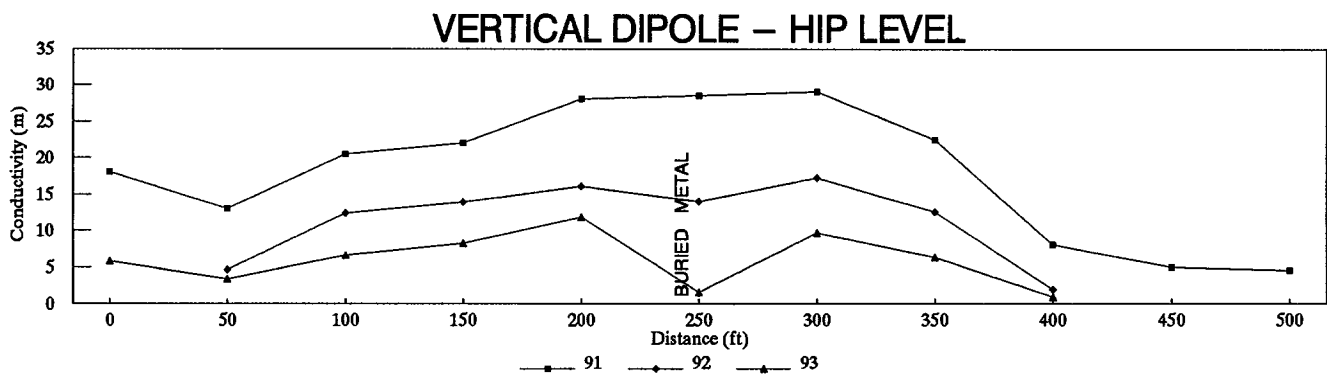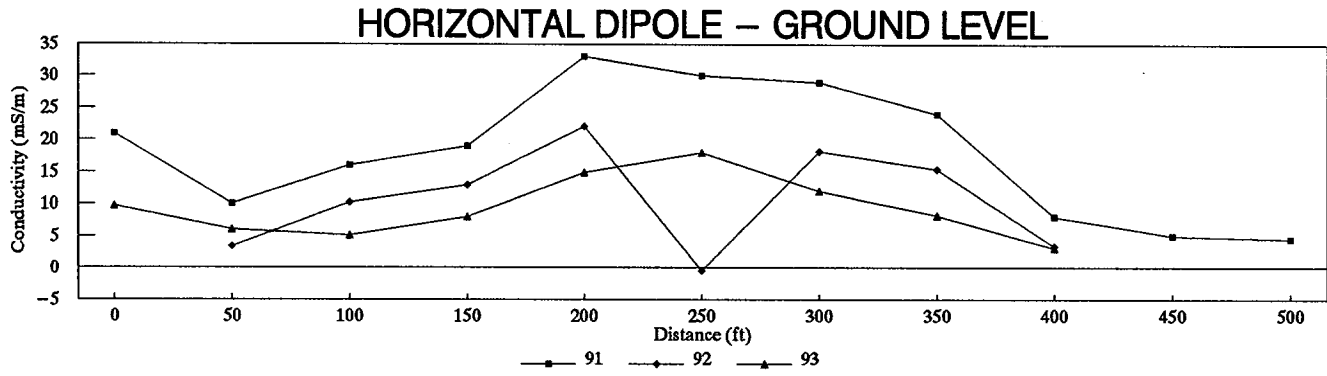
REPEAT SURVEYS – EM31 – LEVACK LINE 1070S

Figure 5.2.4
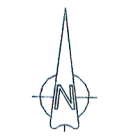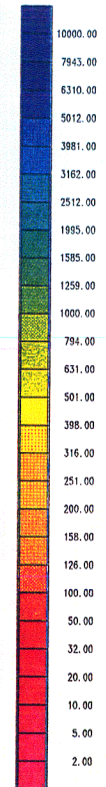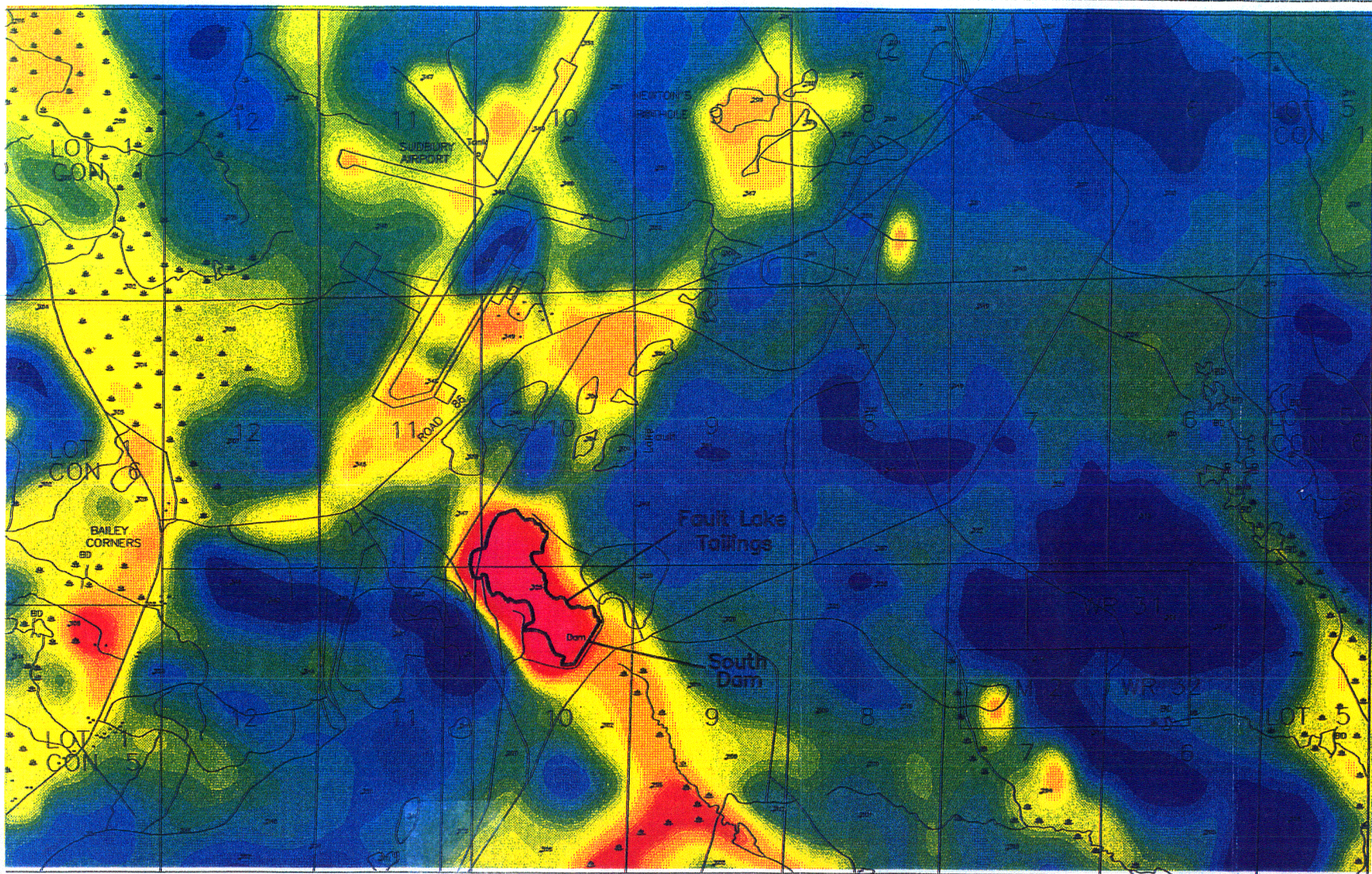
Apparent Resistivity
ohm·m
(LOGARITHMIC)

10000.00
7943.00
6310.00
5012.00
3981.00
3162.00
2512.00
1995.00
1585.00
1259.00
1000.00
794.00
631.00
501.00
398.00
316.00
251.00
200.00
158.00
126.00
100.00
50.00
32.00
20.00
10.00
5.00
2.00

Fault Lake
Tailings

South
Dam

BAILEY
CORNERS

SUDBURY
AIRPORT

LOT 1
CON 7

LOT 1
CON 6

LOT 1
CON 5

INCO Exploration & Technical Services Inc.

FAULT LAKE TAILINGS

AEM RESISTIVITY

0 100 200 300 400 500
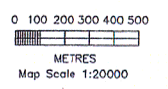
METRES
Map Scale 1:20000

Figure 5.3.1

250 W 200 W 150 W 100 W 50 W 00

100 N

SOUTH DAM

50 N

| S1 | S2 | S3 | S4 | S5 |

EXISTING
WELL O   O F1

O F2

SAMPLE WELLS
O

00

ROAD

50 S

> 8 mS/m

> 6 mS/m

> 4 mS/m

> 2 mS/m

> 0 mS/m

0   40

m

Beaver
Pond
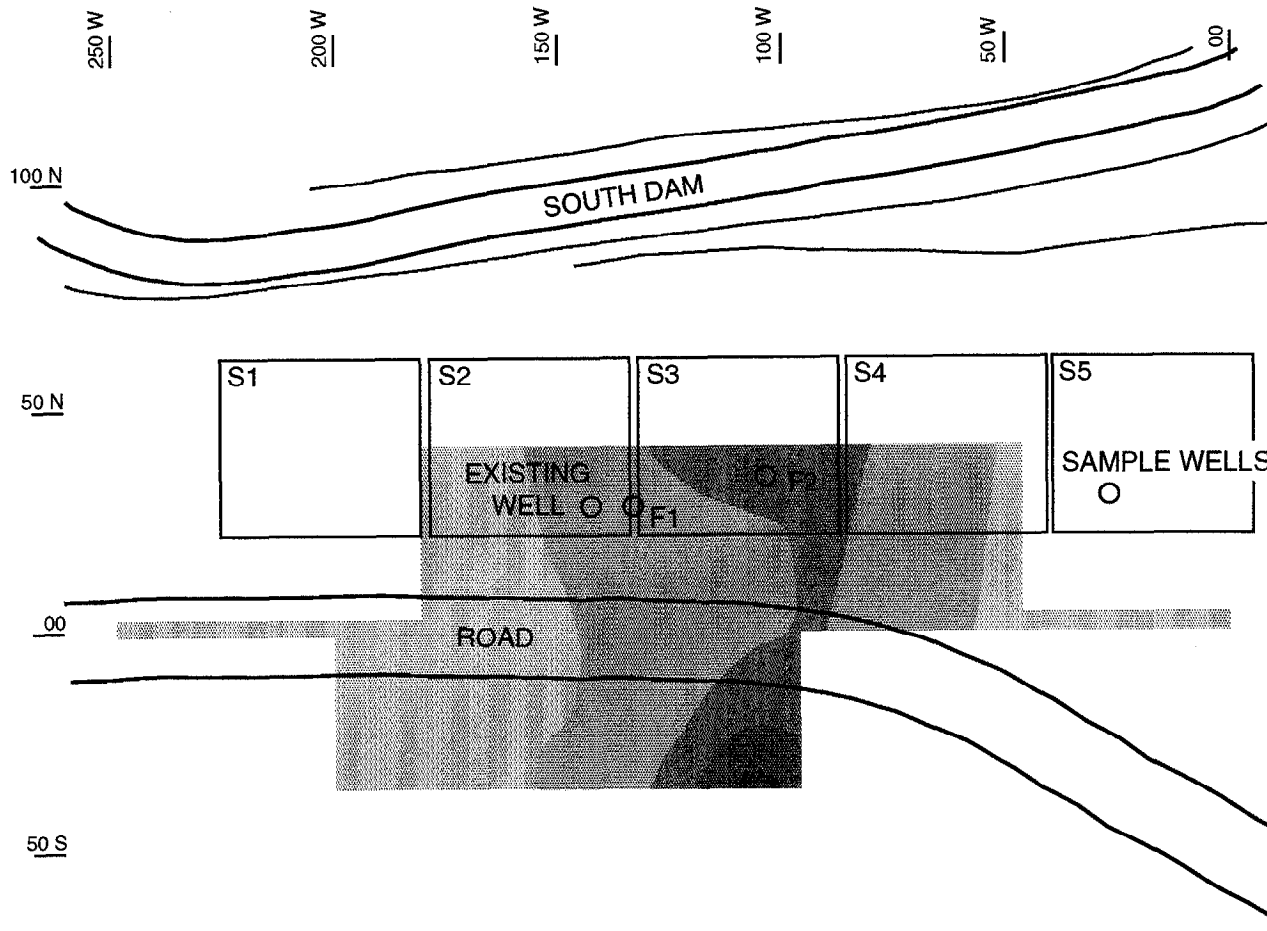
**FAULT LAKE
SOUTH DAM
EM31-DL/Vertical Dipole
Coil Separation 3.66m**
(after Geomar, 1992)

FIGURE 5.3.2.1

250 W 200 W 150 W 100 W 50 W 00

100 N

SOUTH DAM

50 N

EXISTING
WELL O O

SAMPLE WELLS
O

> 8 mS/m

> 6 mS/m

00 ROAD

> 4 mS/m

> 2 mS/m

> 0 mS/m

50 S

0   40

m

Beaver
Pond
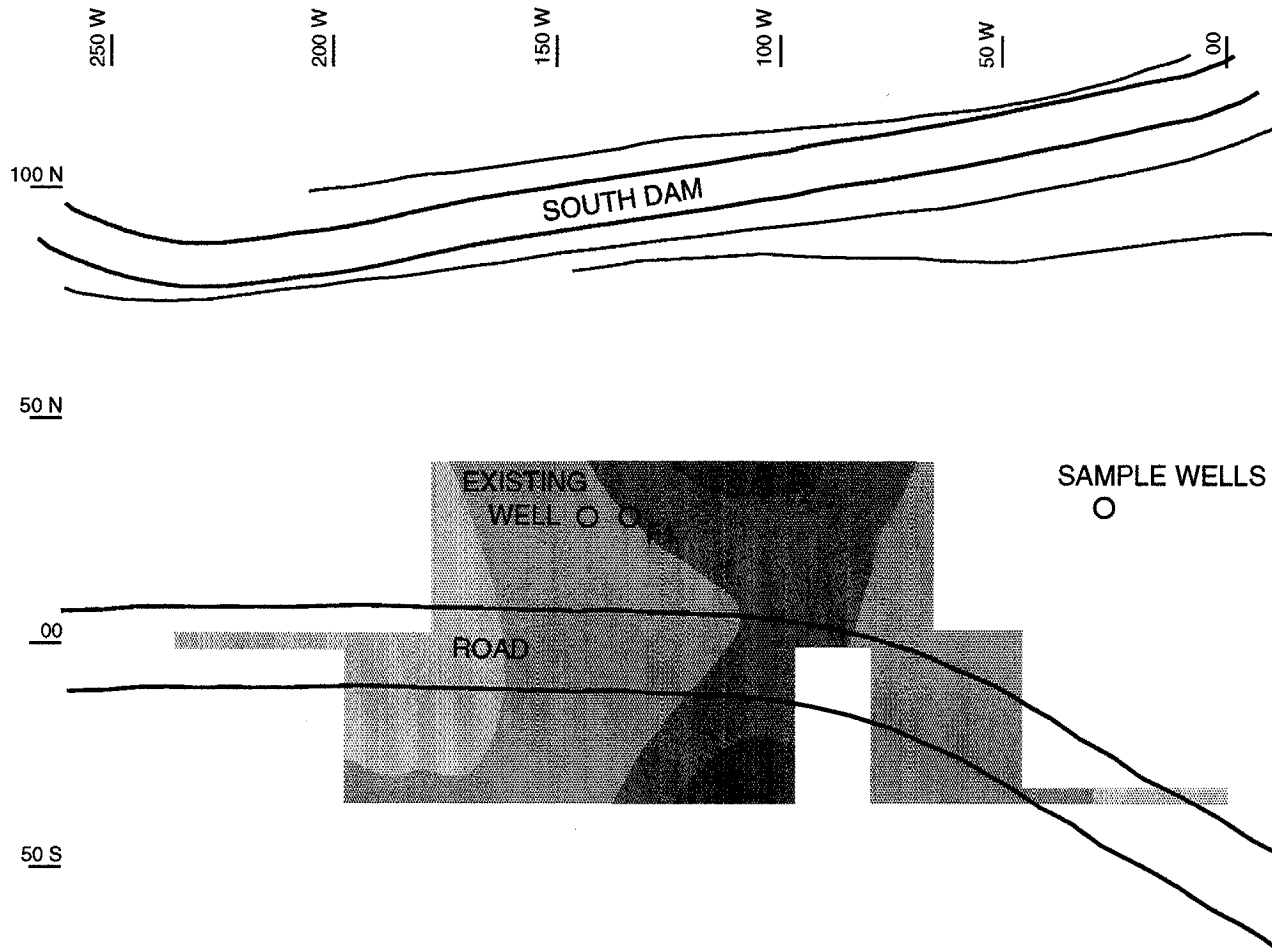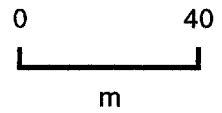
**FAULT LAKE
SOUTH DAM
EM34-3/Horizontal Dipole
Coil Separation 10m**
(after Geomar, 1992)

FIGURE 5.3.2.2
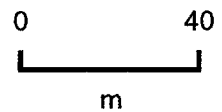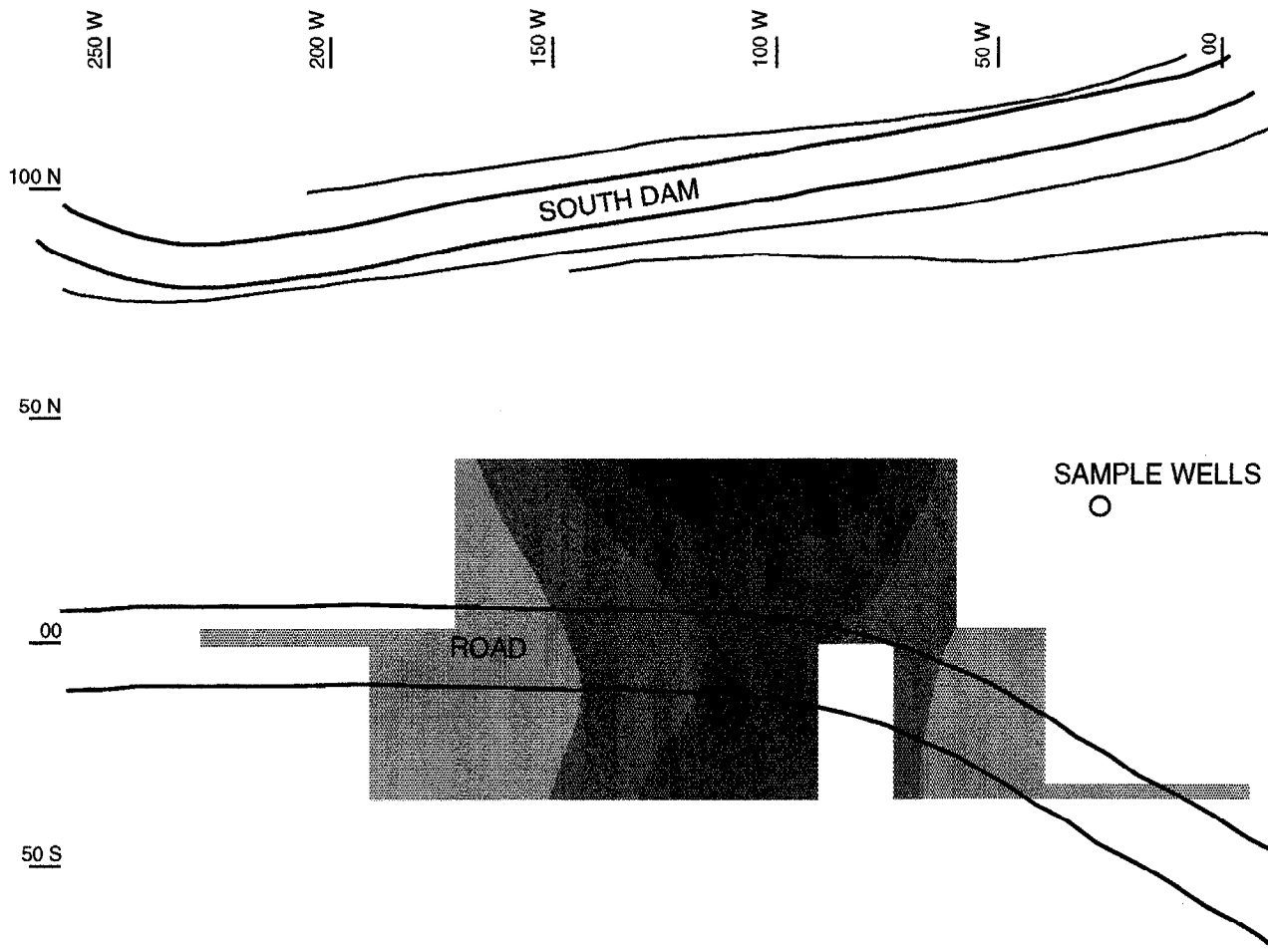
250 W 200 W 150 W 100 W 50 W 00

100 N

SOUTH DAM

50 N

>10 mS/m
> 8 mS/m
> 6 mS/m
> 4 mS/m
> 2 mS/m

SAMPLE WELLS
O

00

ROAD

50 S

0   40

m

Beaver
Pond

**FAULT LAKE
SOUTH DAM
EM34-3/Horizontal Dipole
Coil Separation 20m**
(after Geomar, 1992)
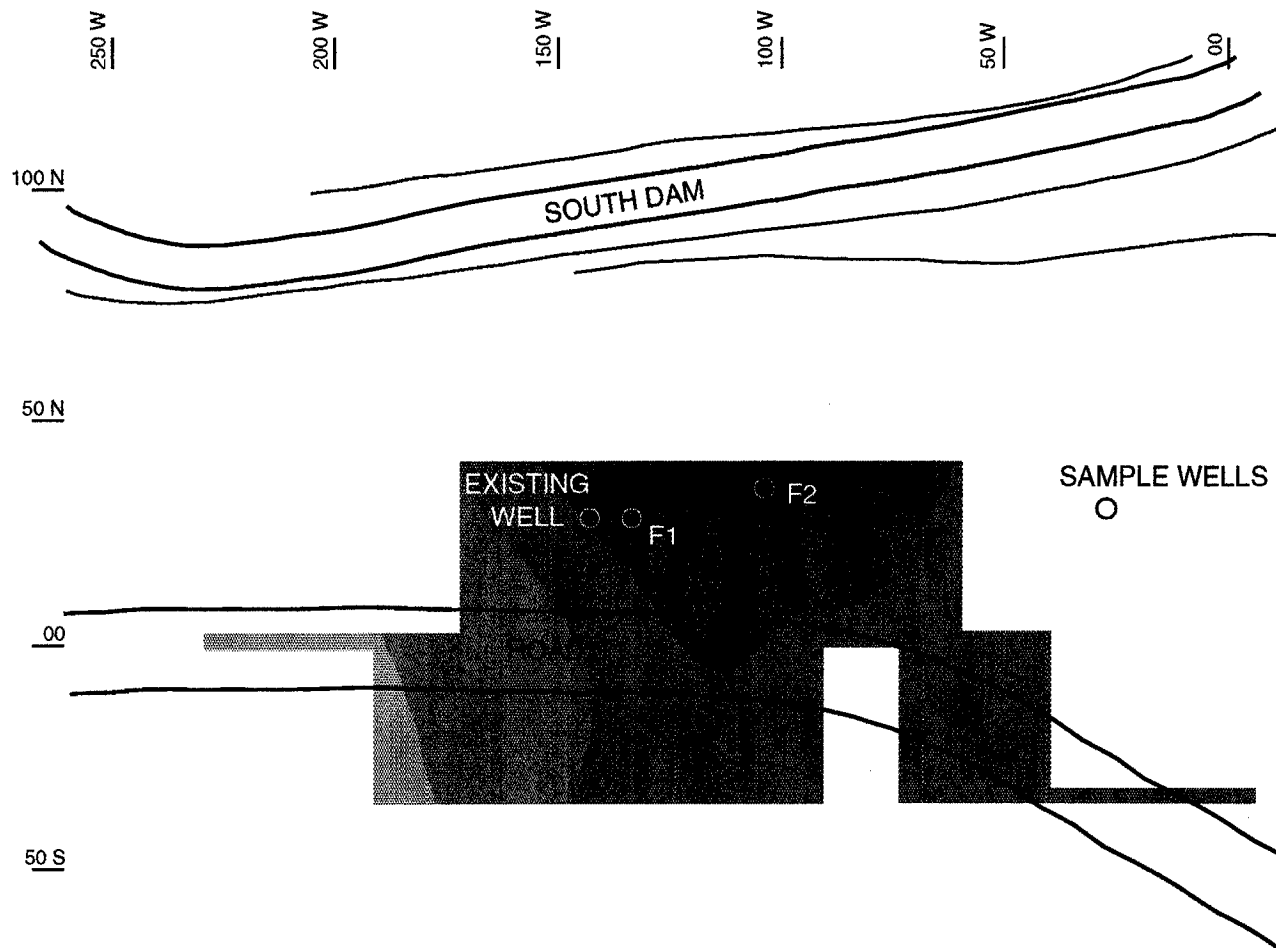
FIGURE 5.3.2.3

FAULT LAKE
SOUTH DAM
EM34-3/Vertical Dipole
Coil Separation 20m
(after Geomar, 1992)

FIGURE 5.3.2.4

S1

Apparent Resistivity (ohm-m) vs Time (msec)

S2

Apparent Resistivity (ohm-m) vs Time (msec)

S3

Apparent Resistivity (ohm-m) vs Time (msec)

S4

Apparent Resistivity (ohm-m) vs Time (msec)

S5

Apparent Resistivity (ohm-m) vs Time (msec)
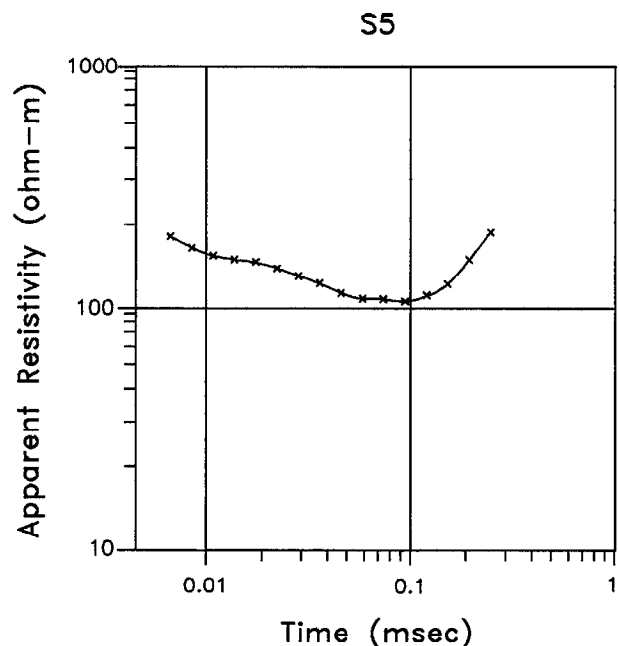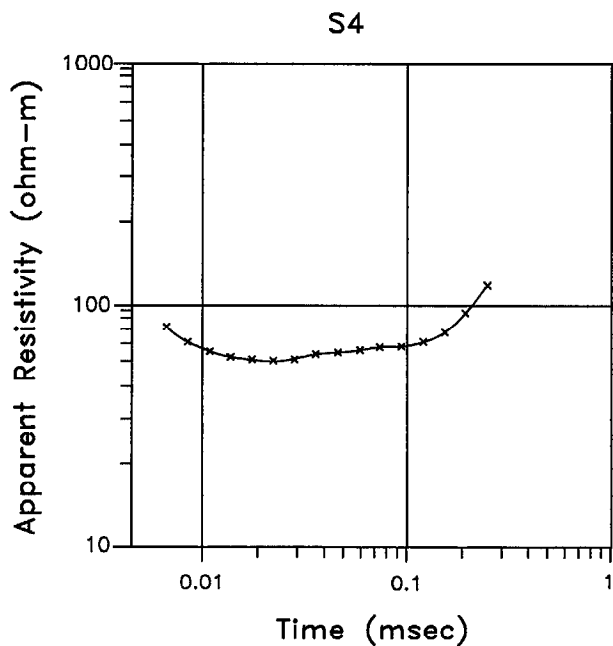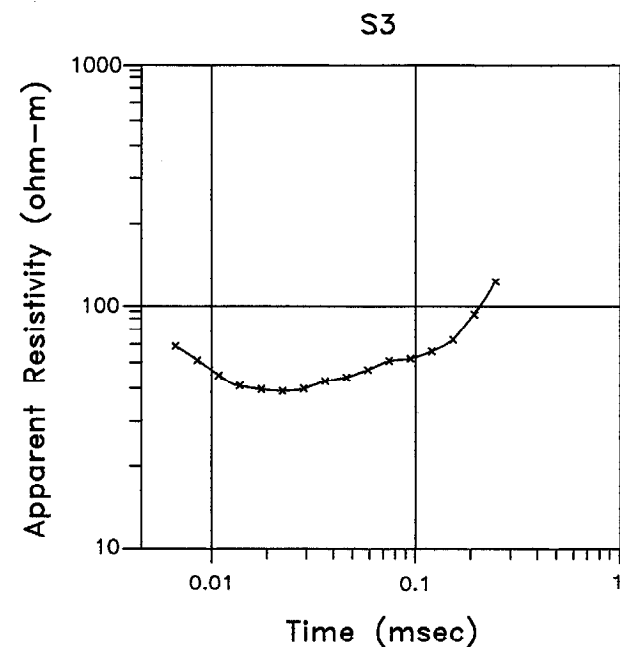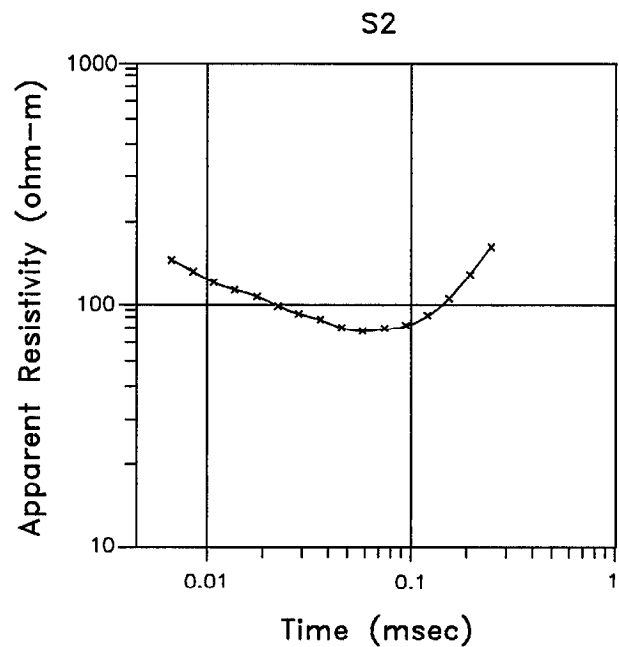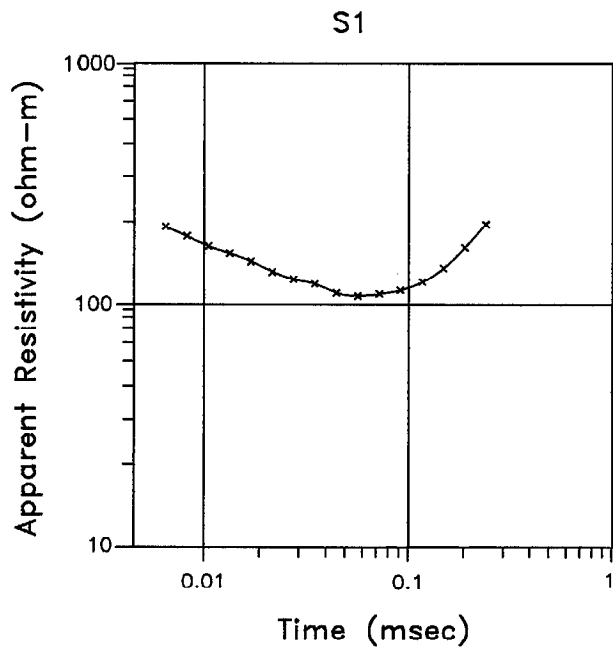
Fault Lake South Dam TEM Data

Geomar Geophysics
for Falconbridge Ltd.

FIGURE 5.3.2.5
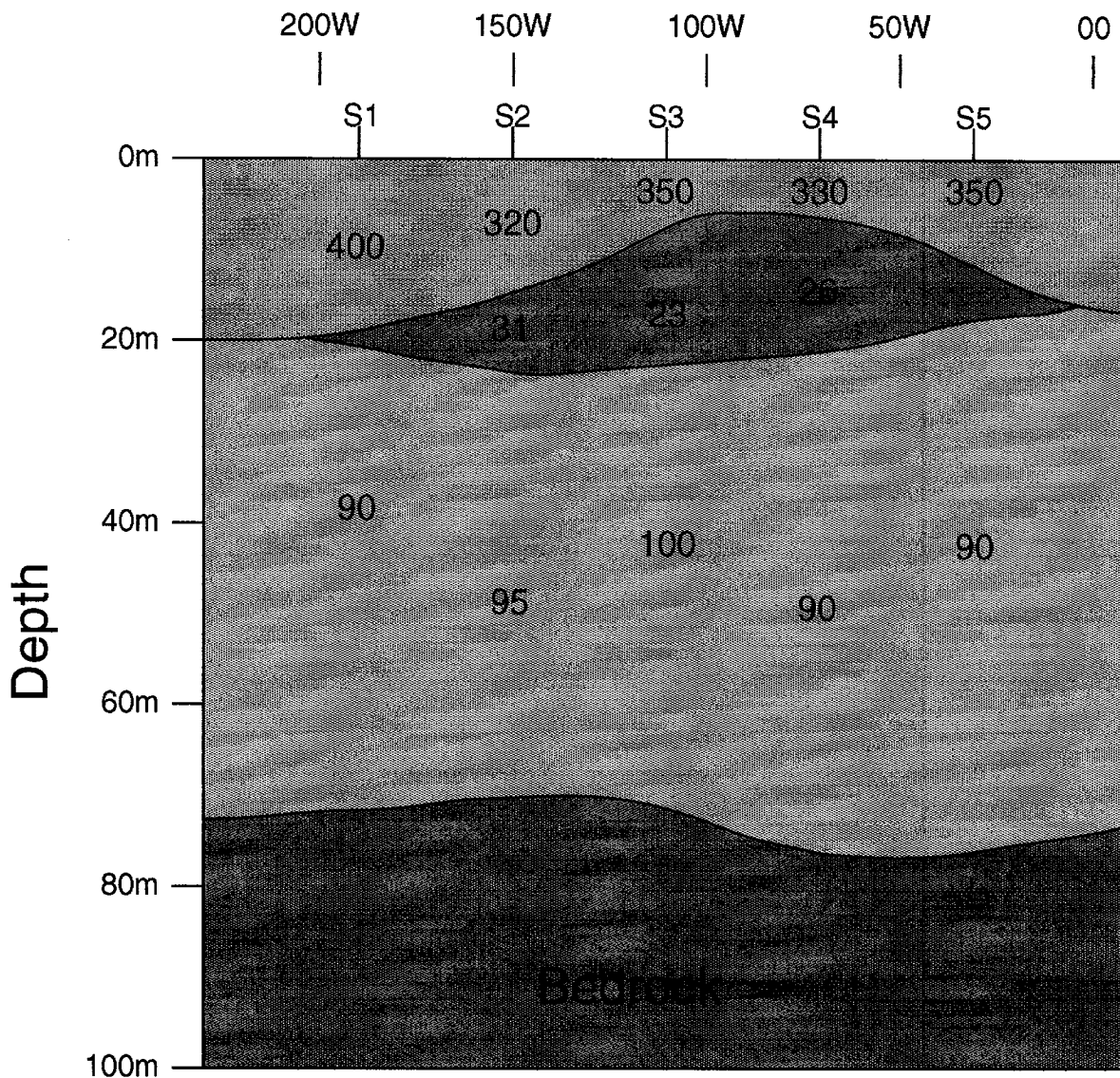
Fault Lake South Dam

Interpreted Section
Instrument EM-47
(After Geomar Geophysics Ltd.)

Resistivity Values in Ohm'm
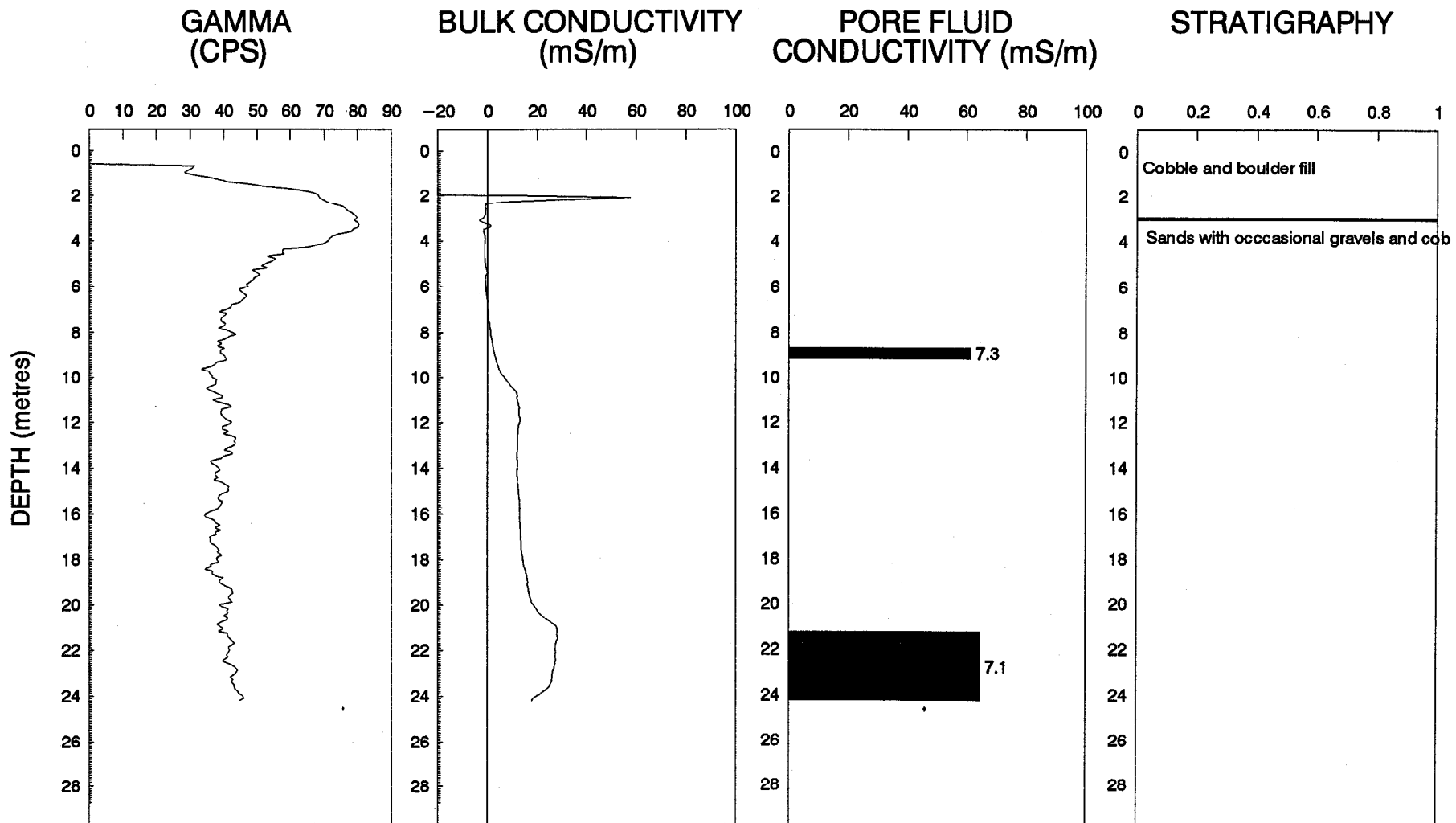
FIGURE 5.3.2.6

BOREHOLE LOGS – FAULT LAKE – DH F1

Figure 5.3.3.1

GAMMA
(CPS)

BULK CONDUCTIVITY
(mS/m)

PORE FLUID
CONDUCTIVITY (mS/m)

STRATIGRAPHY

DEPTH (metres)

Cobble and boulder fill

Sands with occasional gravels and cob

6.6

6.3

6.8
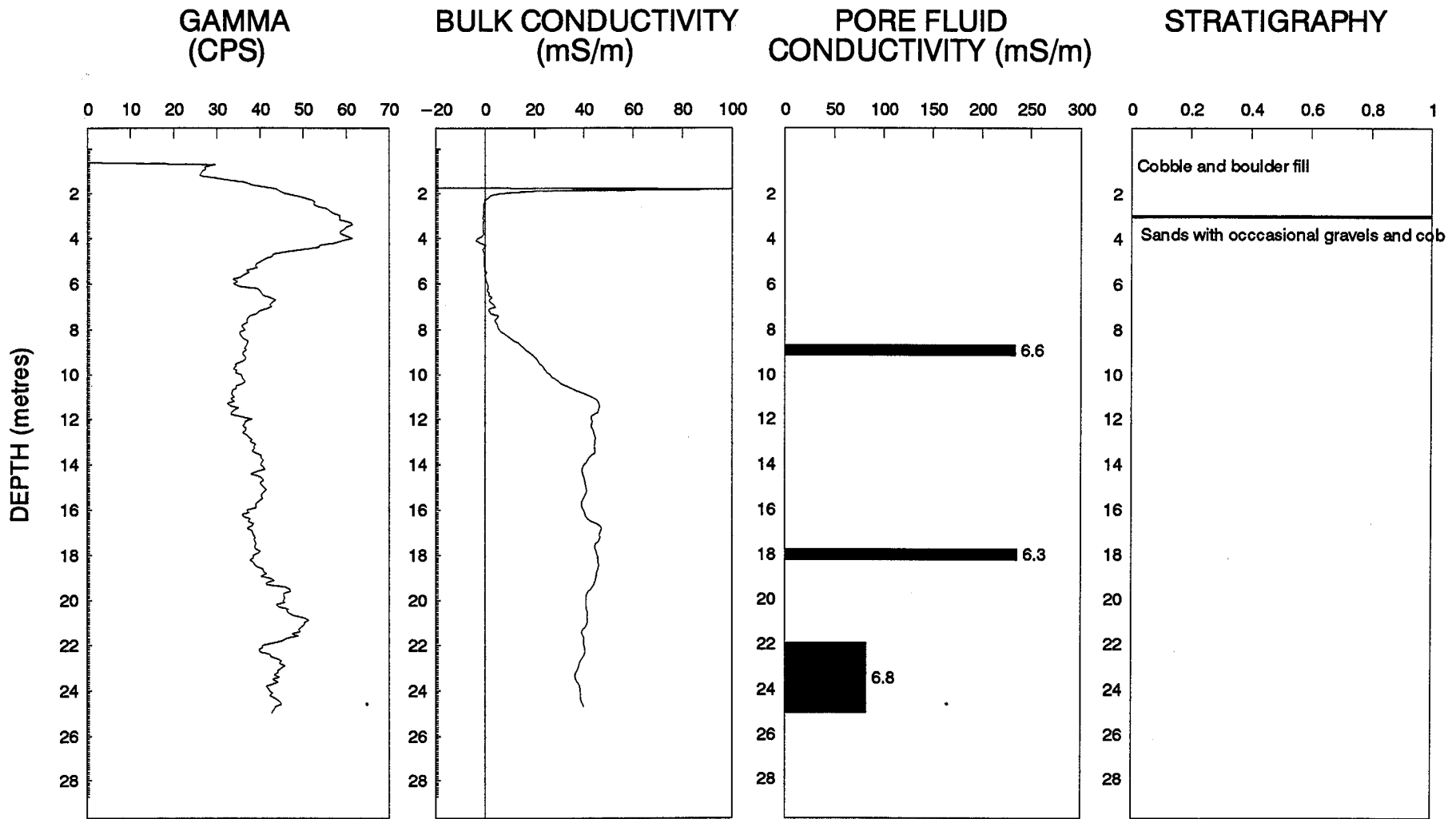
BOREHOLE LOGS – FAULT LAKE – DH F2

Figure 5.3.3.2

Copper Cliff Line Location Map

FIGURE 5.4.1

Map labels: R-2, R-3, R-1, R-4 (Proposed), C-D, M-1, M, Q, P

Pyrhotite Strorage Area Line

Creighton Mill

Hill Station

Line A, Line A East, Line A West, Line B

No. 2 Pump Station

Pistol Dam

IORP

Hwy 17

LEGEND
- 60 Piezometer Nest
- IP Lines

0 — 2500 feet

Piezometer labels: 53, 4, 1, 54, 50, 52, 51, 13, IN57, 58, 10, 62, 56, 55, 11, 61, 12, 17, 16, 18, 59, 60
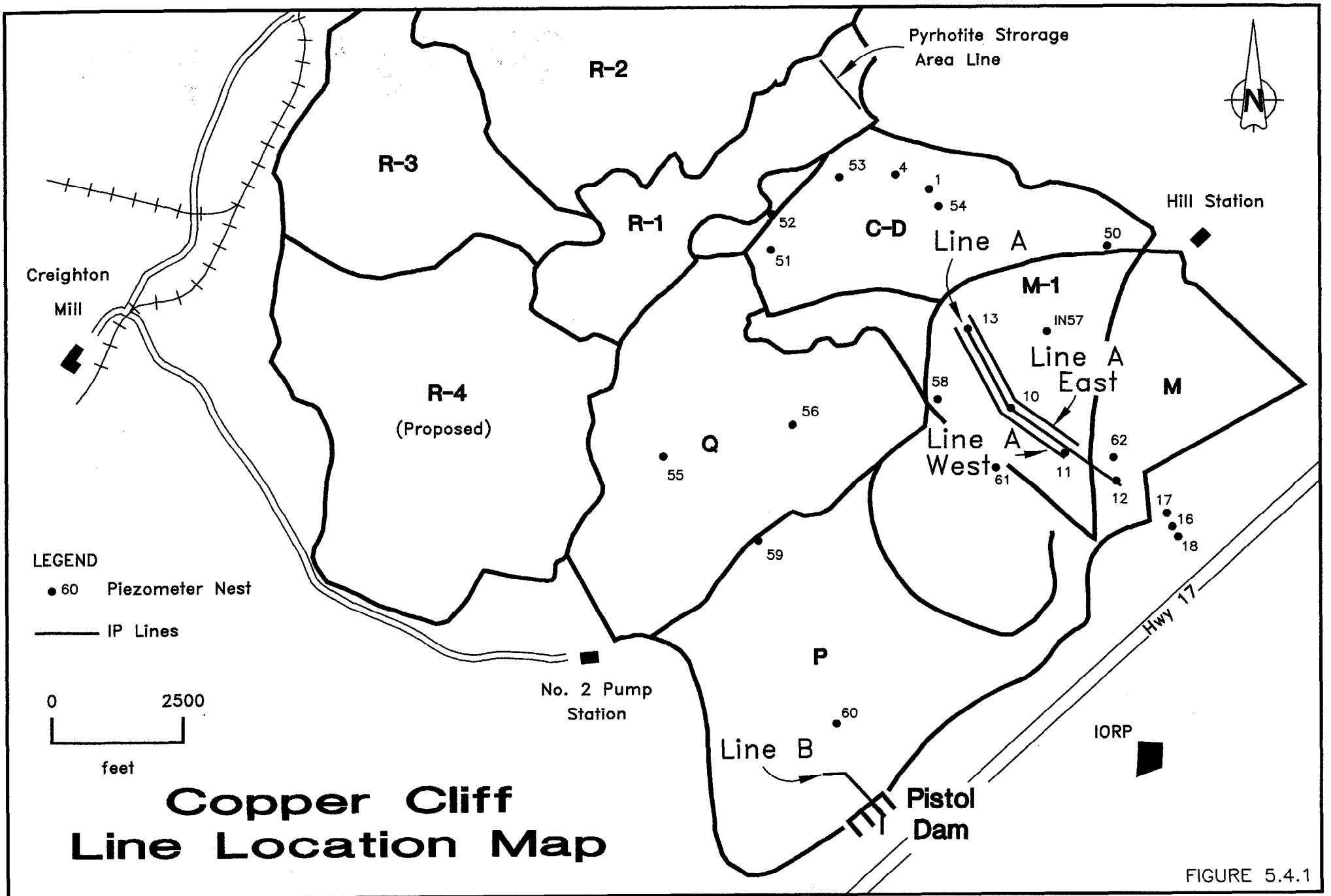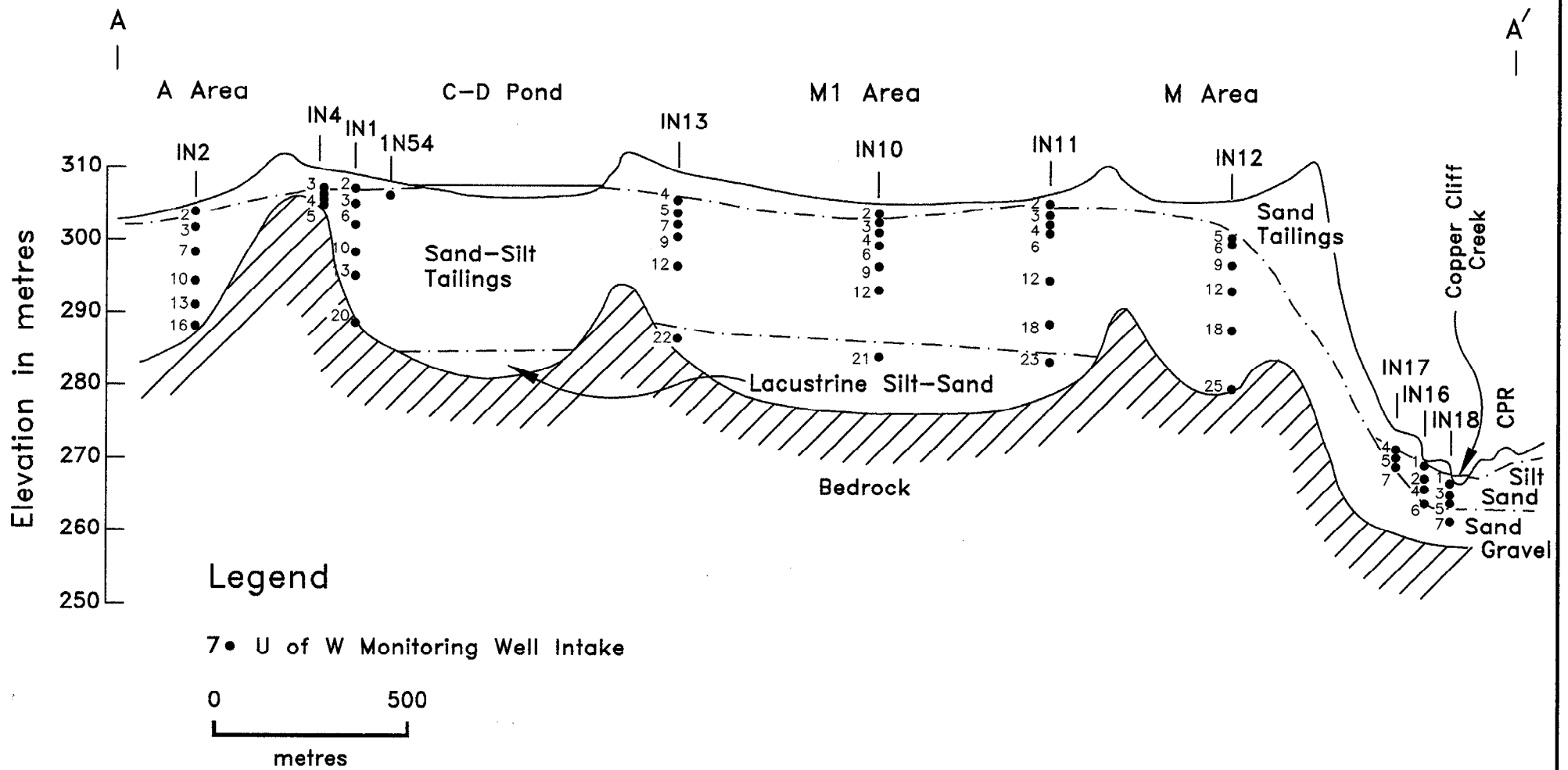
Copper Cliff Tailings
Section A (Robertson et al. 1992)

FIGURE 5.4.2
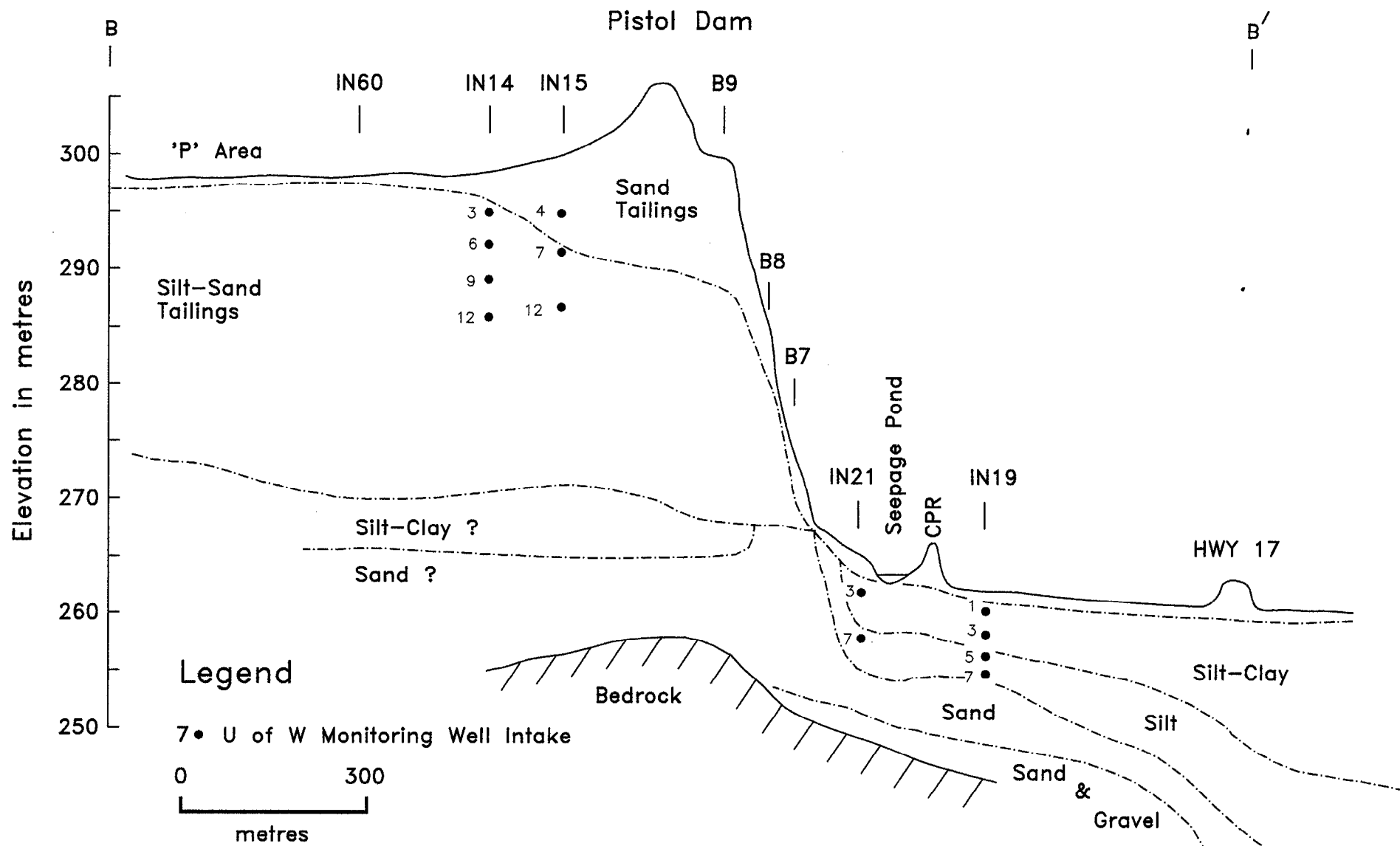
Copper Cliff Tailings
Section B (Robertson et al. 1992)

FIGURE 5.4.3
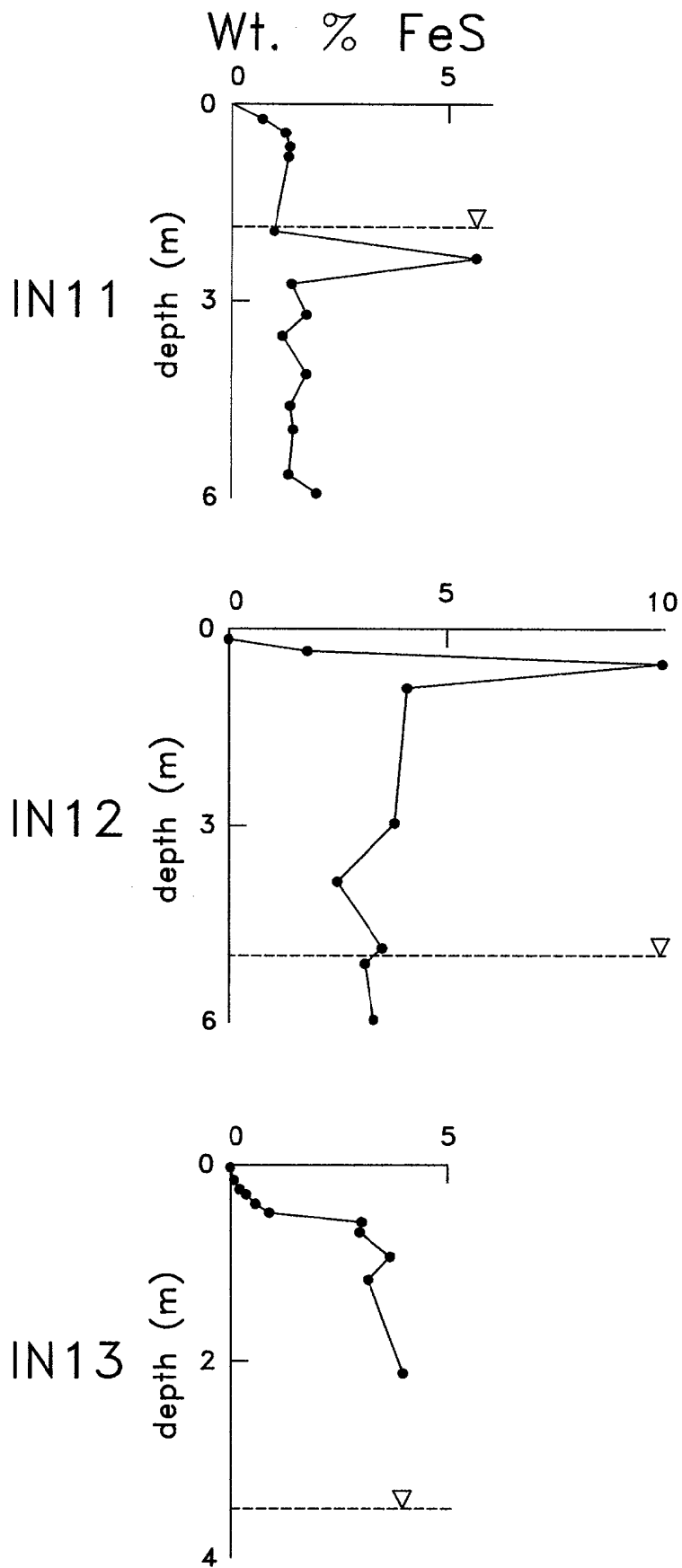
Sulphur in Boreholes

FIGURE 5.4.4
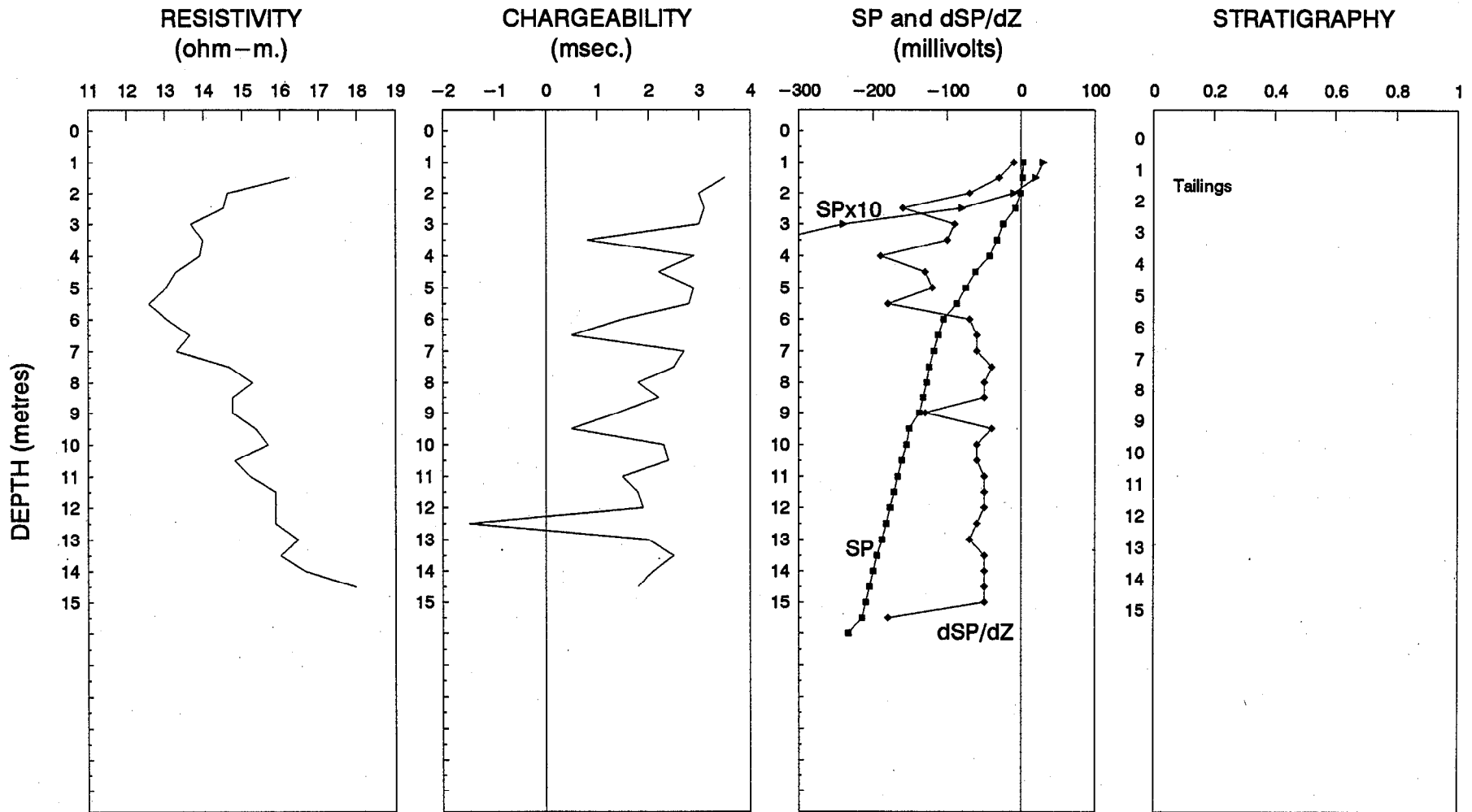
IP/SP/RESISTIVITY Hole IN10G – Copper Cliff Tailngs

Figure 5.4.5
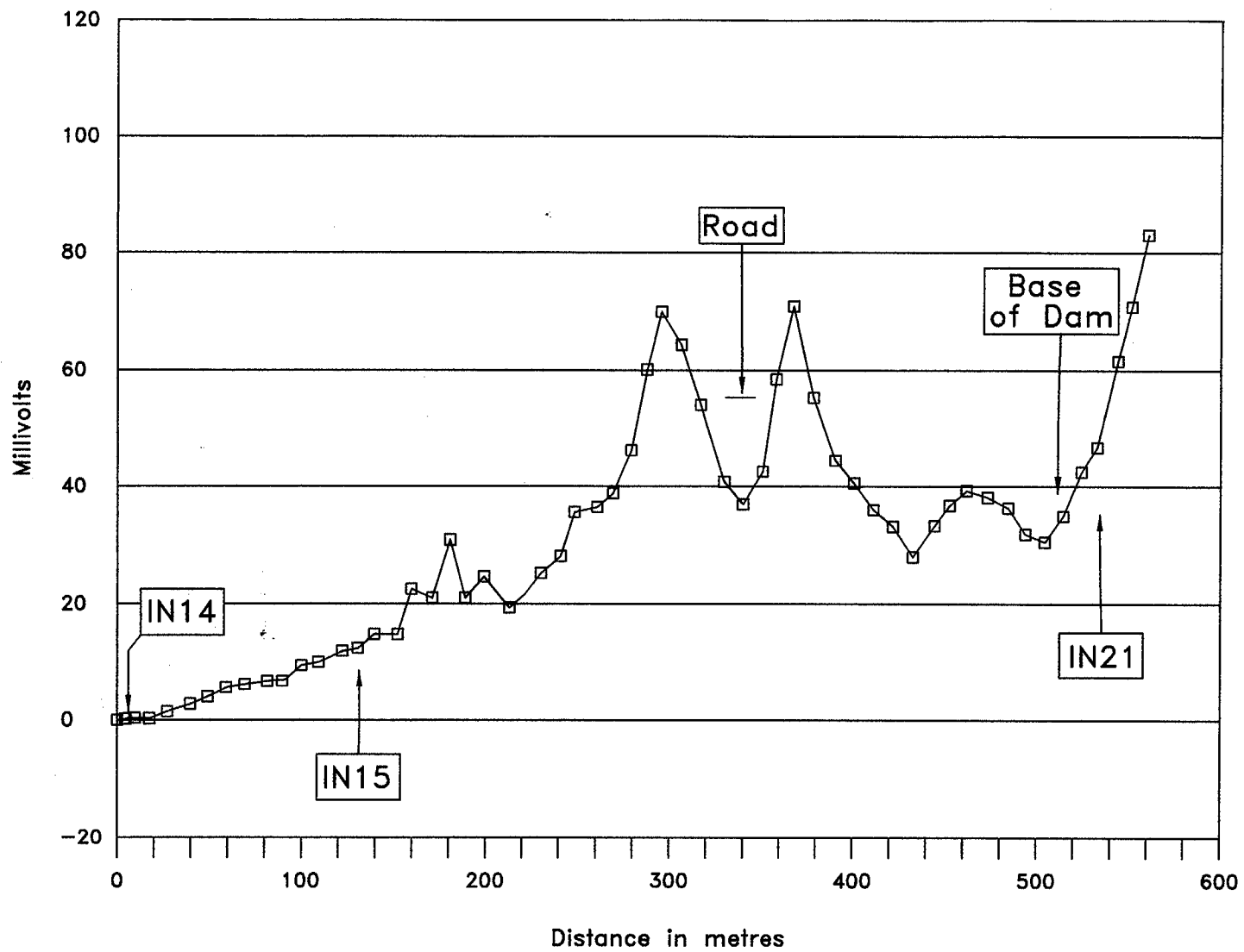
Copper Cliff Tailings – Line B
SP Survey

FIGURE 5.4.6

Base Map
Pistol Dam
EM47 Survey

81
81G

29

90

104G

103

105

96

95

93
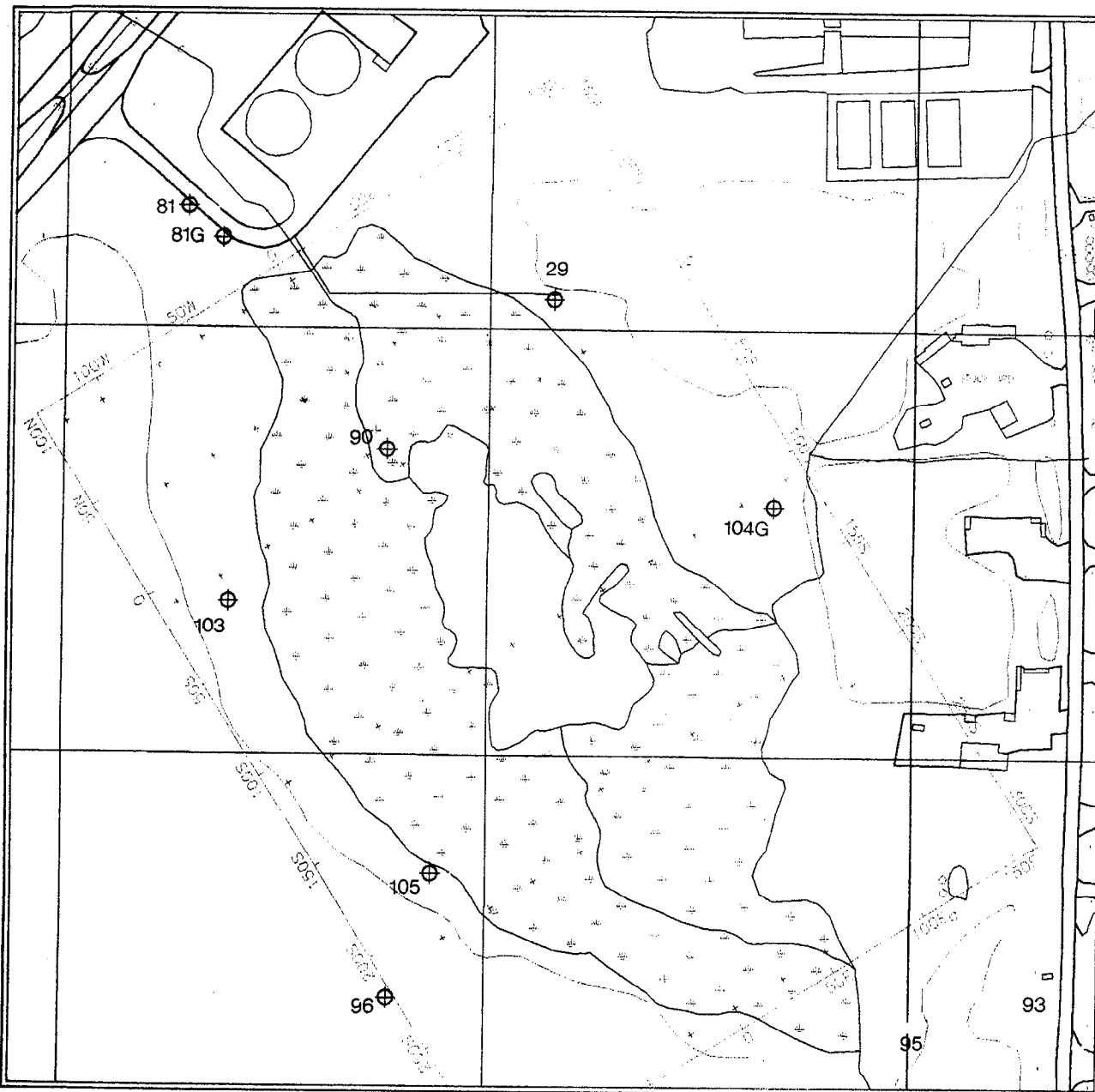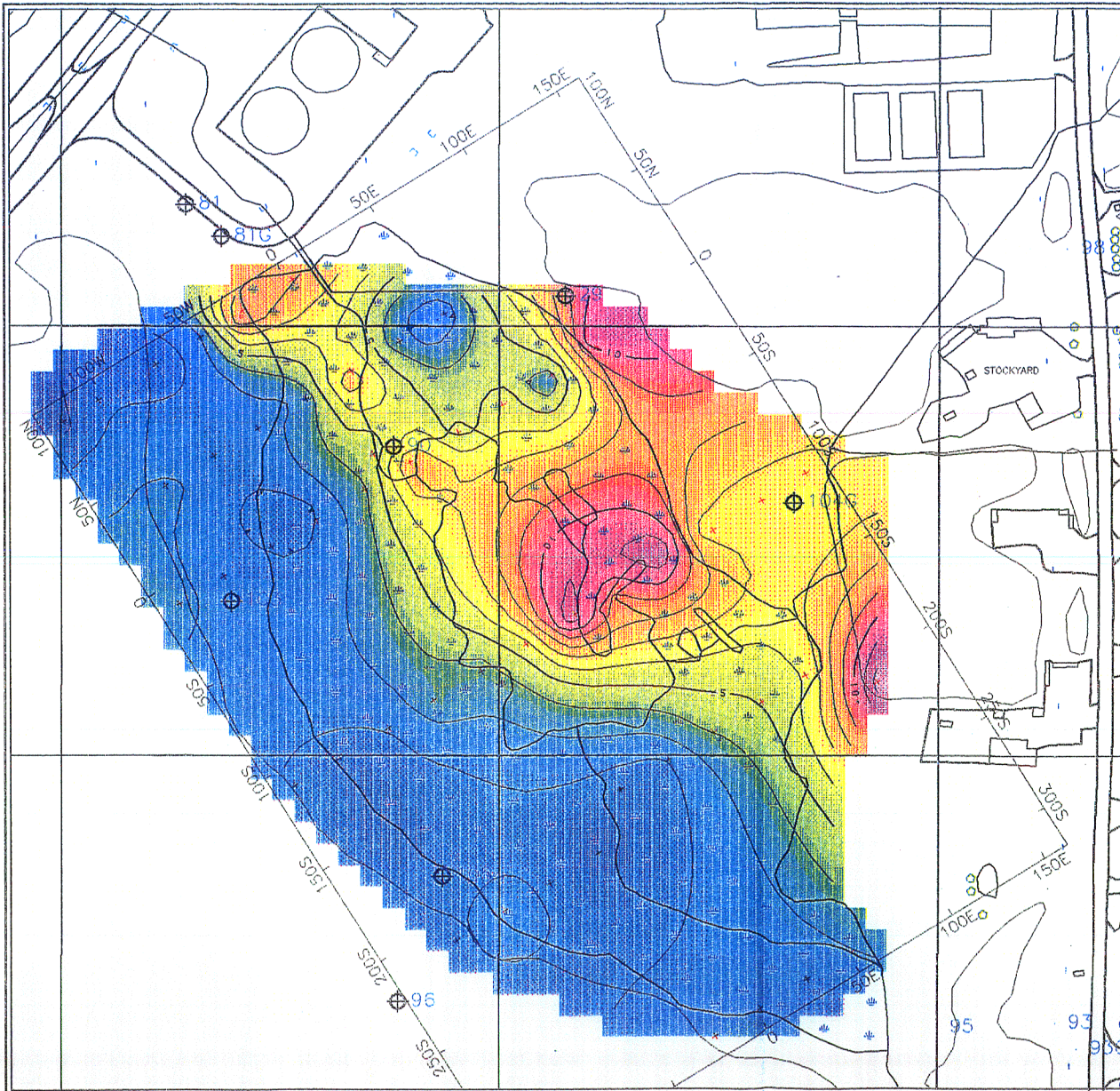
FIGURE H1

⊕ Borehole

⋅ Reading

Scale: 1:2000

Adapted from map provided by:

INCO EXPLORATION AND
TECHNICAL SERVICES INC.
Copper Cliff, Ontario
POM 1NO

Hyd-
Eng
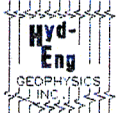
Channel 2
Voltage
Pistol Dam
EM47 Survey
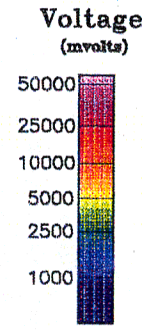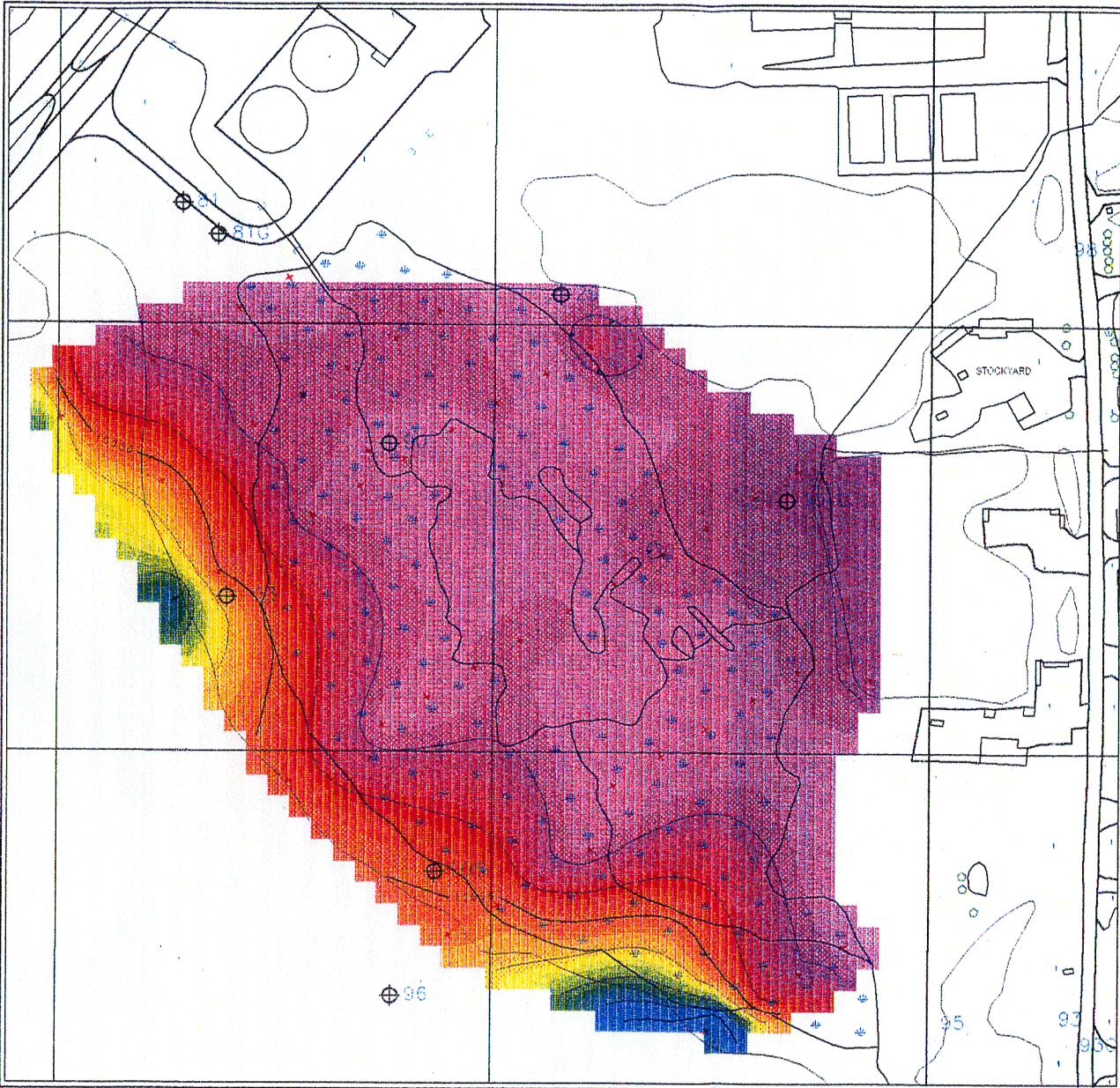
Voltage
(mvolts)

50000
25000
10000
5000
2500
1000

FIGURE H2

Note: Logarthmic contour
interval

⊕ Borehole
✗ Reading

Scale: 1:2000

Channel 6 Voltage Pistol Dam EM47 Survey
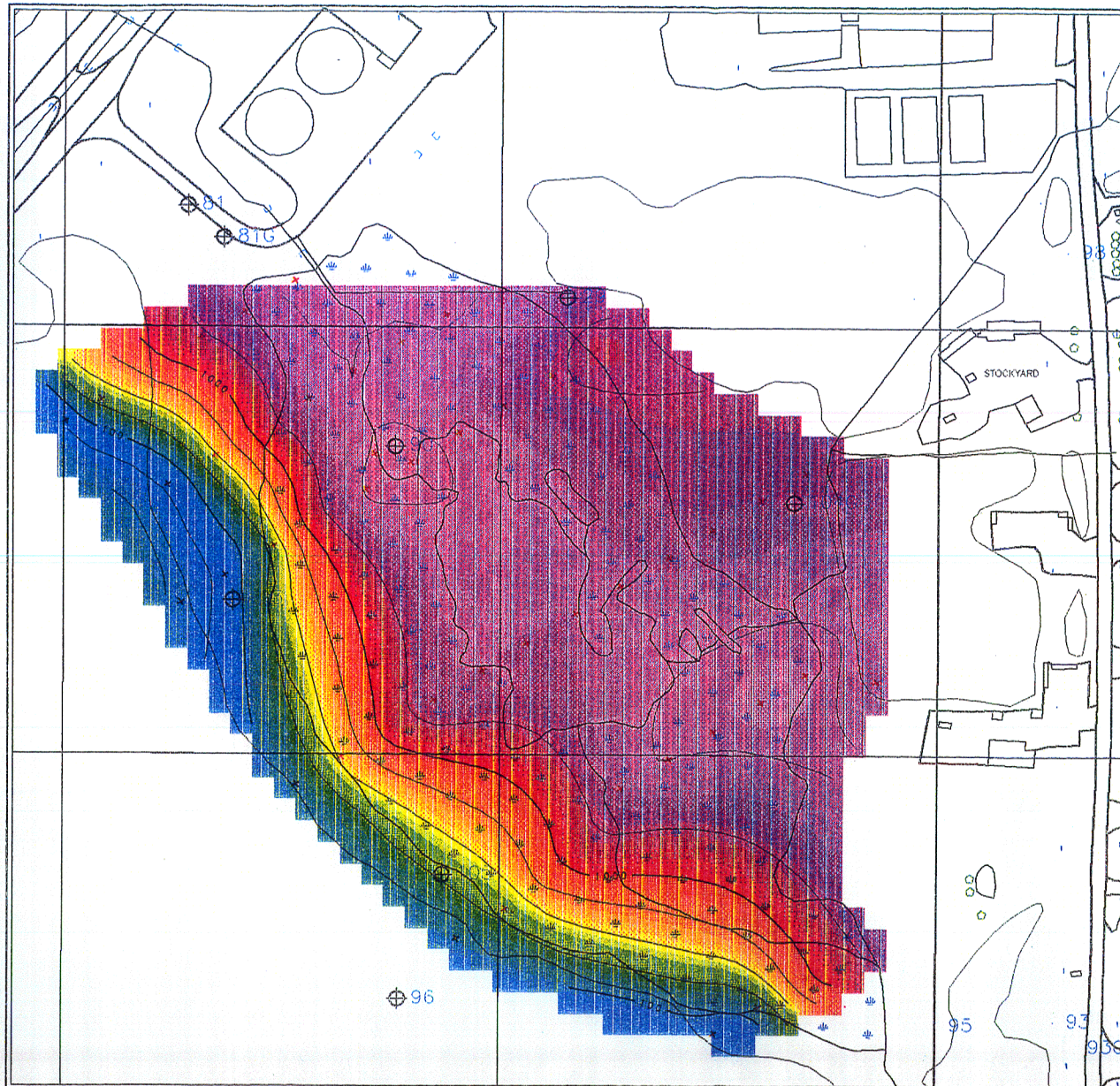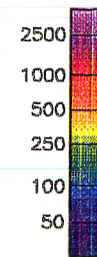
Voltage (mvolts)

2500
1000
500
250
100
50

FIGURE H3

Note: Logarthmic contour interval

⊕ Borehole
✗ Reading

Scale: 1:2000

STOCKYARD

Channel 12
Voltage
Pistol Dam
EM47 Survey

STOCKYARD

Voltage
(mvolts)

100
50
25
10
5
2.5
1
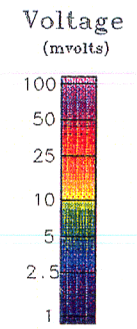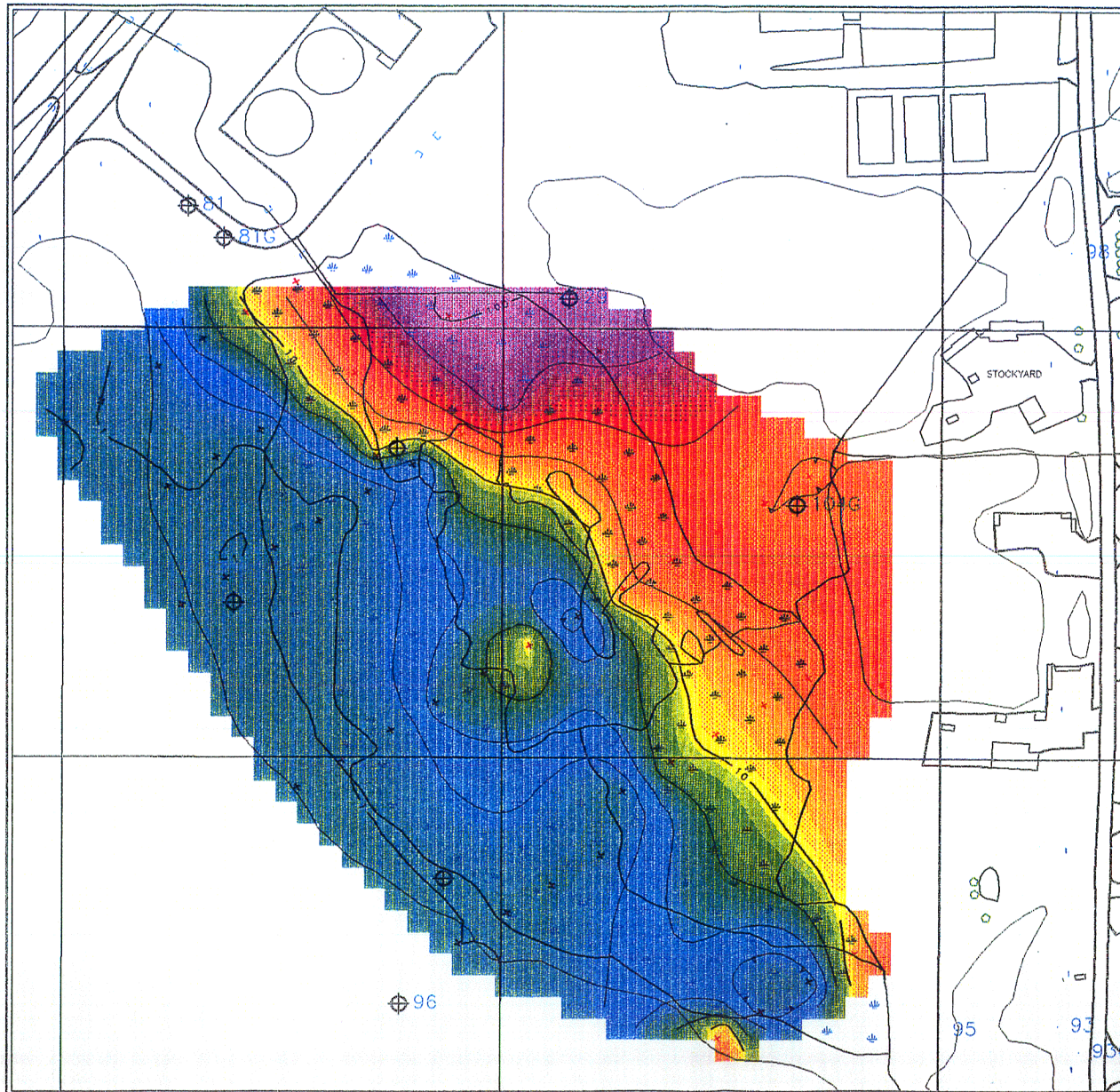
FIGURE H4

Note: Logarthmic contour
interval
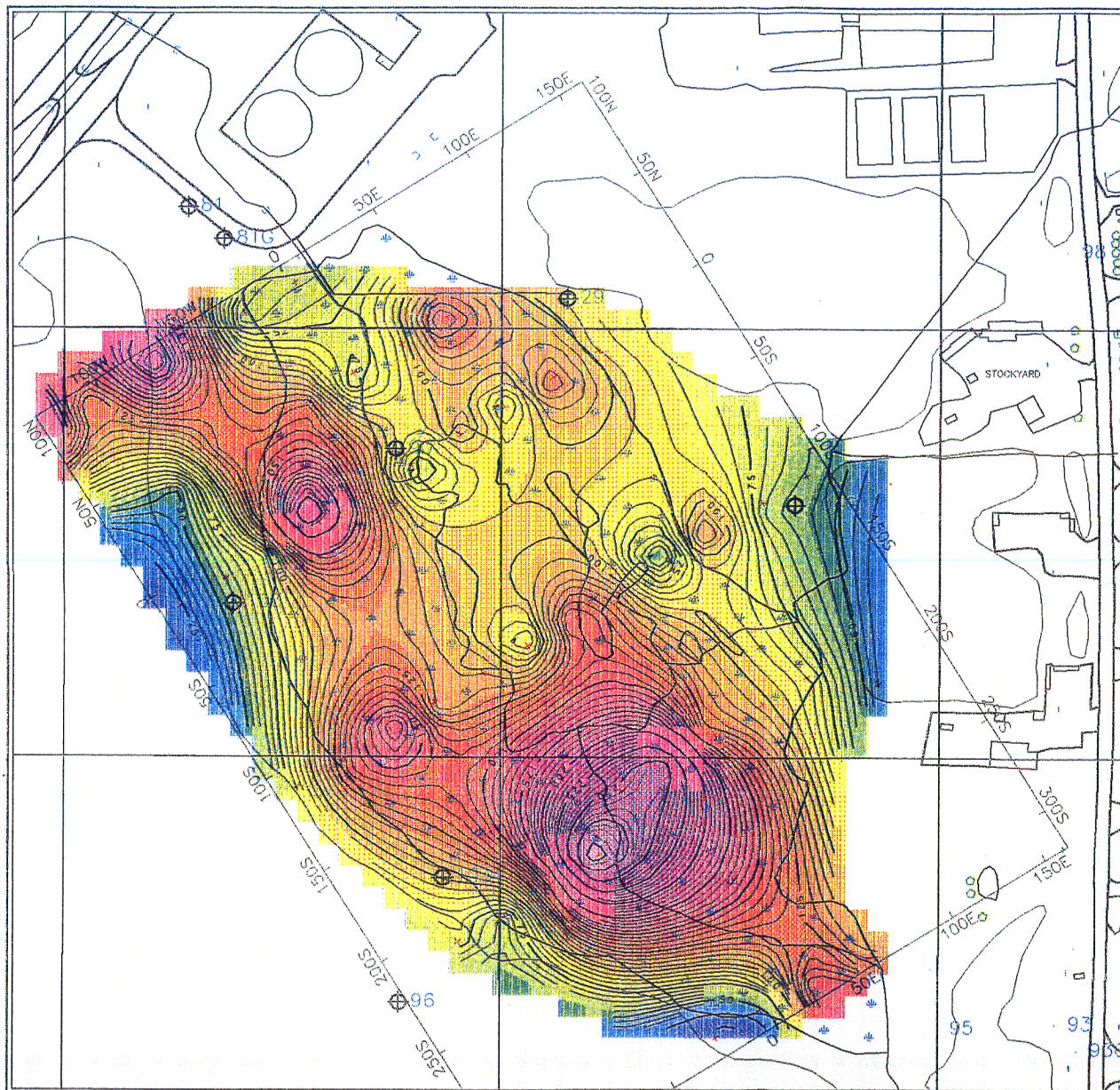
⊕ Borehole
✗ Reading

Scale: 1:2000

Adapted from map provided by:

INCO EXPLORATION AND
TECHNICAL SERVICES INC.
Copper Cliff, Ontario
POM 1N0   08/17/93

Interpreted
Overburden
Thickness

Pistol Dam
EM47 Survey

FIGURE H5

⊕ Borehole
✕ Reading

Scale: 1:2000

Adapted from map provided by:

INCO EXPLORATION AND
TECHNICAL SERVICES INC.
Copper Cliff, Ontario
P0M 1N0   08/17/93

Interpreted
Layer 1 Cond.
Pistol Dam
EM47 Survey

FIGURE H6

⊕ Borehole

× Reading

Scale: 1:2000

Adapted from map provided by:

INCO EXPLORATION AND
TECHNICAL SERVICES INC.
Copper Cliff, Ontario
PDM 1NO   08/17/93

Line A

Dipole-Dipole Array

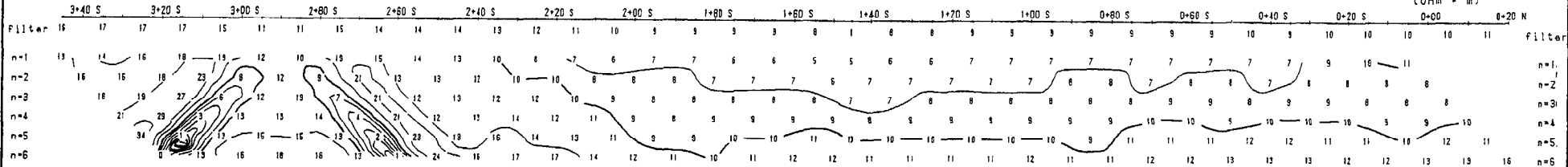a   na   a

e - 10 M
n - 1, 2, 3, 4, 5, 6
plot point

Logarithmic Contours
1, 1.5, 2, 3, 5, 7.5, 10,...

Instrument: PHOENIX IPT1.BRGM IP-6
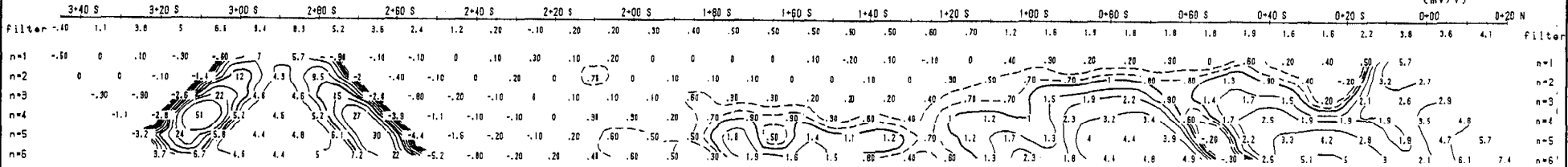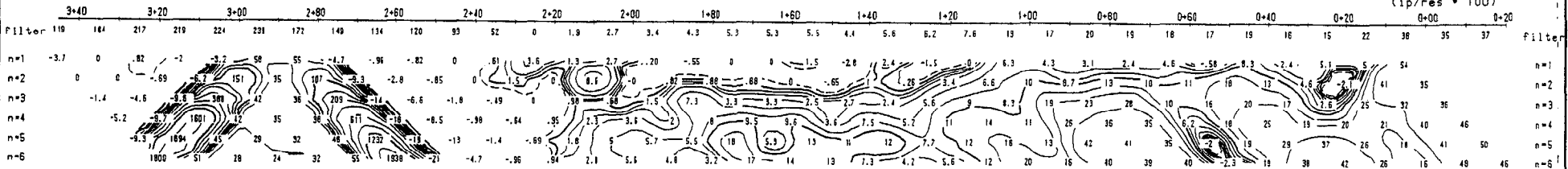Time cycle: 2 sec.
Operator: Gerry Shields

PIPE

IN13

RESISTIVITY
(Ohm * m)

CHARGEABILITY
(mV/V)

METAL FACTOR
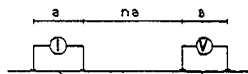(ip/res * 100)

Induced Polarization Survey

INCO EXPL. & TECHNICAL SERVICES INC.

Tailings Pond Project
Sudbury Area

Date: 94/01/11
Interpretation by:
Scale 1 : 1000

Executed by: WALCER GEOPHYSICS LTD
Compiled by: VAL D'OR GEOPHYSIQUE LTEE

Line A

Dipole-Dipole Array

a   na   b

e - 10 M
n - 1, 2, 3, 4, 5, 6
plot point

Logarithmic Contours
1, 1.5, 2, 3, 5, 7.5, 10,...

Instrument: PHOENIX IPT1, BRGM IP-6
Time cycle: 2 sec.
Operator: Gerry Shields

IN10

RESISTIVITY
(Ohm • m)

CHARGEABILITY
(mV/V)

METAL FACTOR
(ip/res • 100)

Induced Polarization Survey
INCO EXPL. & TECHNICAL SERVICES INC.
Tailings Pond Project
Sudbury Area
Date: 94/01/11
Interpretation by:
Scale 1 : 1000
Executed by: WALCER GEOPHYSICS LTD
Compiled by: VAL D'OR GEOPHYSIQUE LTEE

Line A

Dipole-Dipole Array

a   na   b

e = 10 M
n = 1, 2, 3, 4, 5, 6
plot point

Logarithmic Contours
1, 1.5, 2, 3, 5, 7.5, 10,...

Instrument: PHOENIX IPT1, BRGM IP-6
Time cycle: 2 sec.
Operator: Gerry Shields

RESISTIVITY
(Ohm * m)

CHARGEABILITY
(mV/V)

METAL FACTOR
(ip/res * 100)

Geosoft Software for the Earth Sciences

93-1035

Induced Polarization Survey

INCO EXPL. & TECHNICAL SERVICES INC.

Tailings Pond Project
Sudbury Area

Date: 94/01/11
Interpretation by:
Scale 1 : 1000

Executed by: WALCER GEOPHYSICS LTD
Compiled by: VAL D'OR GEOPHYSIQUE LTEE
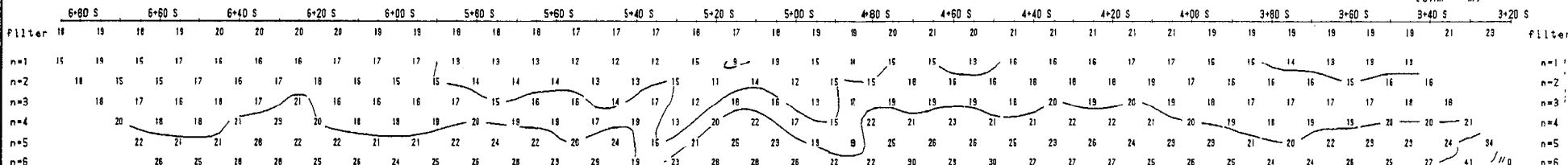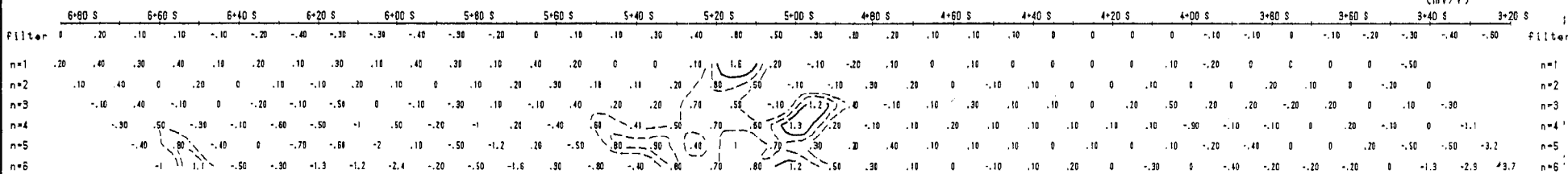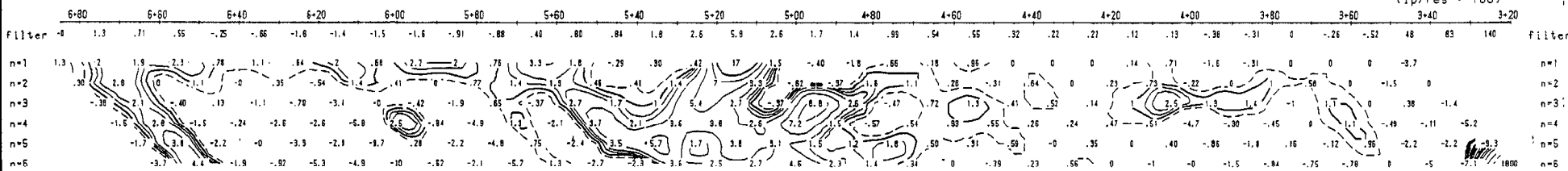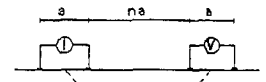
Line A

Dipole-Dipole Array

a   na   a

e - 10 M
plot point   n = 1, 2, 3, 4, 5, 6

Logarithmic Contours
1, 1.5, 2, 3, 5, 7.5, 10,...

Instrument: PHOENIX IPT1, BRGM IP-6
Time cycle: 2 sec.
Operator: Gerry Shields

IN11

RESISTIVITY
(Ohm * m)
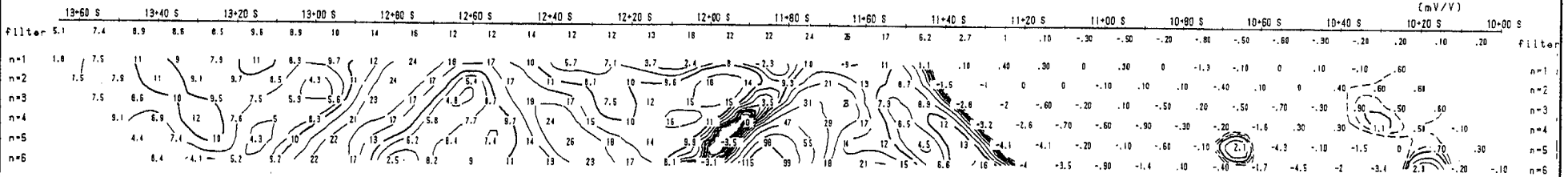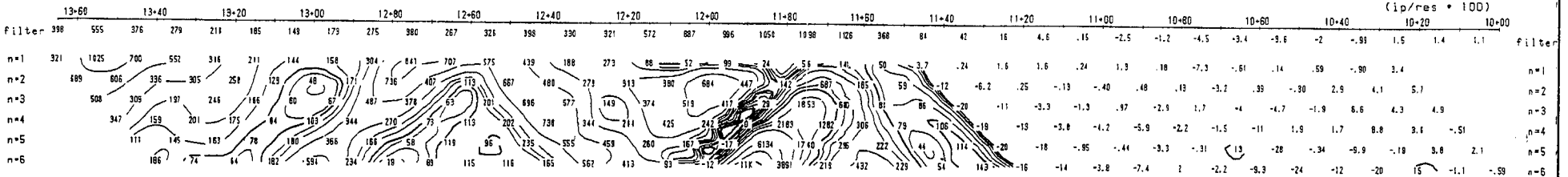
CHARGEABILITY
(mV/V)

METAL FACTOR
(ip/res * 100)

Geosoft Software for the Earth Sciences

93-1035

Induced Polarization Survey

INCO EXPL. & TECHNICAL SERVICES INC.
Tailings Pond Project
Sudbury Area

Date: 94/01/11
Interpretation by:
Scale 1 : 1000

Executed by: WALCER GEOPHYSICS LTD
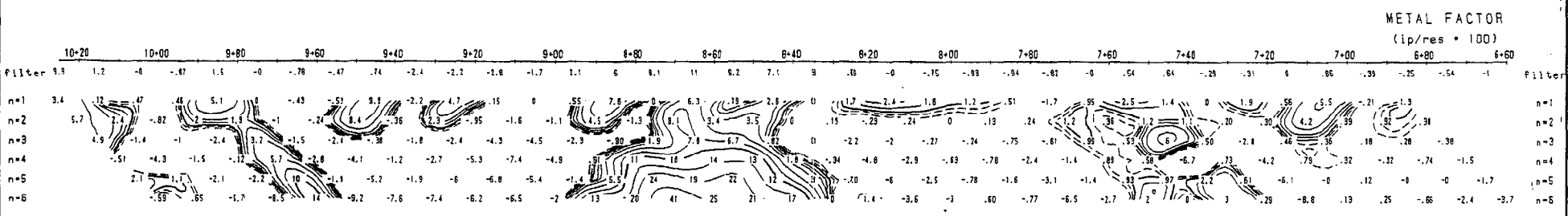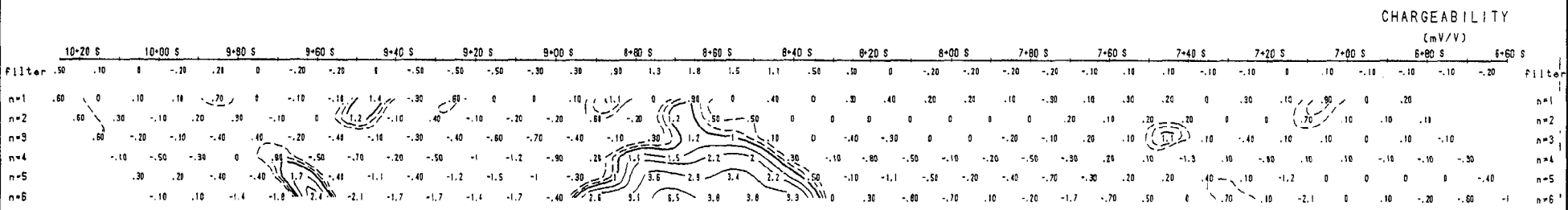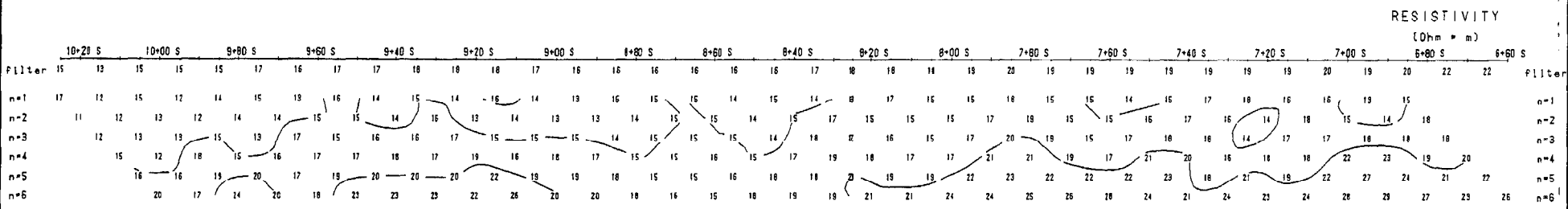Compiled by: VAL D'OR GEOPHYSIQUE LTEE

Line A

Dipole-Dipole Array

a — na — a

⓵ ⓥ

e — 10 M
n = 1, 2, 3, 4, 5, 6
plot point

Logarithmic Contours
1, 1.5, 2, 3, 5, 7.5, 10,...

Instrument: PHOENIX IPT1, BRGM IP-6
Time cycle: 2 sec.
Operator: Gerry Shields

IN12

RESISTIVITY
(Ohm • m)

CHARGEABILITY
(mV/V)

METAL FACTOR
(ip/res • 100)
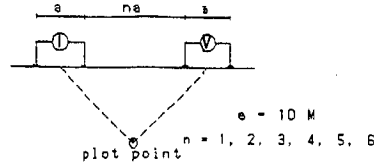
Induced Polarization Survey

INCO EXPL. & TECHNICAL SERVICES INC.
Tailings Pond Project
Sudbury Area

Date: 94/01/11
Interpretation by:
Scale 1 : 2500

Executed by: WALCER GEOPHYSICS LTD
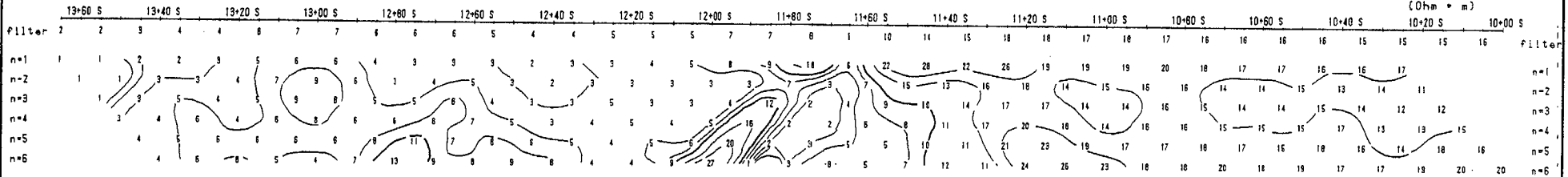Compiled by: VAL D'OR GEOPHYSIQUE LTEE

Line A

Dipole-Dipole Array

a   na   a

e = 20.0 M
n = 1, 2, 3, 4, 5, 6

plot point

Logarithmic Contours
1, 1.5, 2, 3, 5, 7.5, 10,...

Instruments: PHOENIX IPV4T, IPT1
Frequency 4 Hz
Operator: Gerry Shields

IN10   PIPE   IN13

RESISTIVITY
(Ohm • m)

CHARGEABILITY
(mV/V)

METAL FACTOR
(ip/res • 100)

Induced Polarization Survey

INCO EXPL. & TECHNICAL SERVICES INC.

Tailings Pond Project
Sudbury Area

Date: 94/01/11
Interpretation by:
Scale 1 : 2000

Executed by: WALCER GEOPHYSICS LTD
Compiled by: VAL D'OR GEOPHYSIQUE LTEE

Line B

Dipole-Dipole Array

a   na   a

e - 20 M
n = 1, 2, 3, 4, 5, 6

plot point

Logarithmic Contours
1, 1.5, 2, 3, 5, 7.5, 10,...

Instrument: PHOENIX IPT1.BRGM IPƒ6
Time cycle: 2 sec.
Operator: Gerry Shields

IN15   IN14

RESISTIVITY
(Ohm * m)

filter	4+40		4+00		3+60		3+20		2+80		2+40		2+00		1+60		1+20		0+80		0+40	filter
	29	26	26	26	22	28	24	27	26	24	24	22	20	17	16	15	14	12	11	11	10	
n=1		34	98	17	26	20	39	35	30	30	24	22	15	12	13	11	9	7	6	6		n=1
n=2	23	27	15	26	38	19	34	24	24	26	21	15	13	14	12	10	9	9	8		n=2
n=3	27	22	11	14	31	31	17	25	22	22	24	16	15	15	15	12	11	11	11		n=3
n=4	27	32	11	19	29	26	29	13	24	23	23	20	17	17	16	15	13	13	14		n=4
n=5	29	95	17	20	14	26	27	25	14	26	26	21	21	19	18	16	15	17		n=5
n=6	39	39	20	32	25	24	29	24	28	15	30	25	23	25	20	19	17	19	19		n=6

CHARGEABILITY
(mV/V)

filter	4+40		4+00		3+60		3+20		2+80		2+40		2+00		1+60		1+20		0+80		0+40	filter
	-.10	1	2.2	2.4	3.6	3.3	3.3	2.3	2.1	2	2.8	2.5	2.4	1.4	1.2	1.6	.70	.60	.50	.30	0	
n=1		3.9	2.4	2.4	2.4	5.3	3.5	4	2.8	5	2.8	3.5	.41	1.8	4.6	2.2	1.4	.70	.20		n=1
n=2	1.5	2.8	2.7	3.1	3.6	3.5	1.2	1.6	2.2	1.4	.50	1.9	1	.40	1.9	.8	-.10		n=2
n=3	-1	.10	3.4	3.3	2.4	1.1	1.1	2.3	2	1.6	1.50	-.90	1.2	.30	.50	-.40		n=3
n=4	4.9	-5.9	3.1	-5	4.3	.90	.50	2	1.3	-.10	-.60	.70	.20	.10		n=4
n=5	2.2	-5.1	2.2	6.1	5.4	4.4	1.2	2.6	1.7	4.7	3.8	.91	.20	.80	.40	.30		n=5
n=6	1.3	-14	9.4	6	6.1	6.6	1.7	-2.5	-.10	-2.7	-1.8	7.6	4.2	1.6	-.10	.10	-.20	1.5	-.40		n=6

METAL FACTOR
(ip/res * 100)

filter	4+40		4+00		3+60		3+20		2+80		2+40		2+00		1+60		1+20		0+80		0+40	filter
	3	7.6	11	13	16	12	14	9.1	8.1	8.4	11	12	12	7.7	7.7	11	5.4	6.5	5.9	3.6	.75	
n=1		9.8	6.3	14	6.4	26	8.9	12	9.3	17	12	15	3.1	14	36	11	17	15	11	3.1		n=1
n=2	6.7	10	19	9.6	18	5.8	5.7	7	11	9.5	3.5	14	14	4.4	9.5	-.71		n=2
n=3	-3.6	45	30	13	11	5.5	4.5	5.7	5.1	11	12	12	3.1	4.1	3.2	4.9	-3.4		n=3
n=4	18	-17	28	26	15	11	-4.1	5.7	9.6	8.2	18	12	7.6	-.63	4.2	5.2	.56		n=4
n=5	7.8	-14	13	30	22	17	4.7	4.1	10	6.5	23	18	1.2	-1.5	5.2	2.1	1.8		n=5
n=6	3.4	-36	48	19	24	28	5.8	-9.6	-.32	16	5.9	31	19	-5.4	-.54	.39	-1.3	7.8	-2.1		n=6

Geosoft Software for the Earth Sciences

93-1035
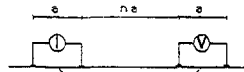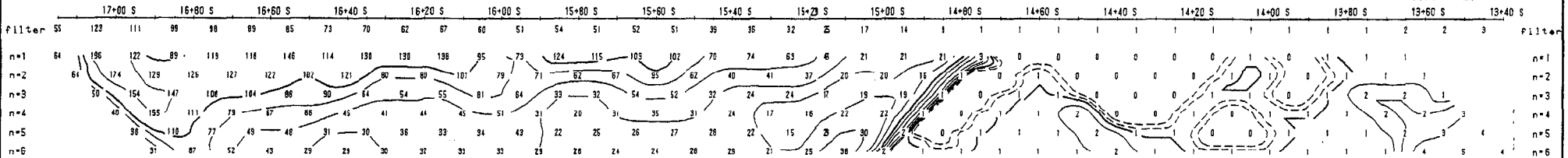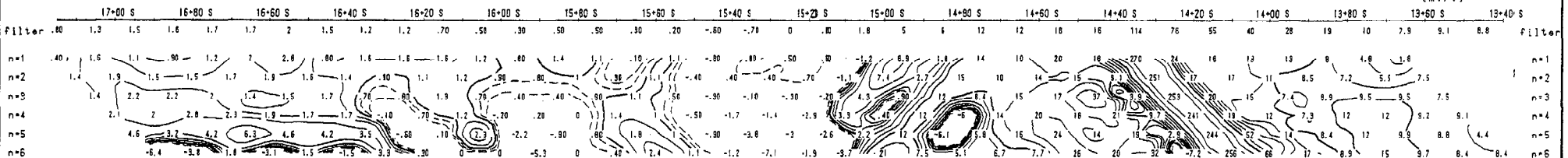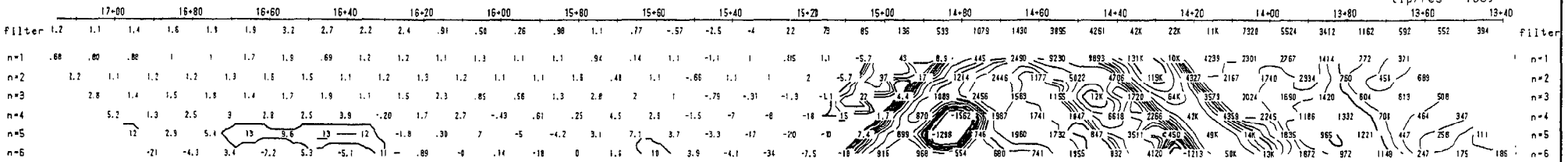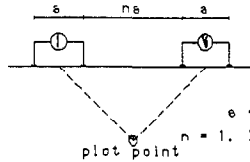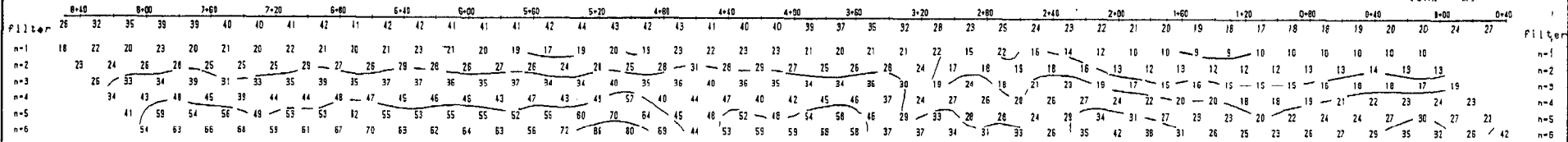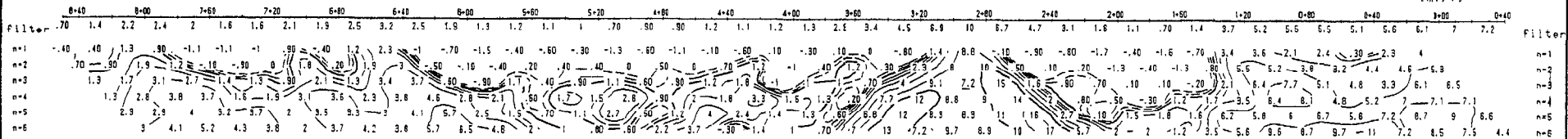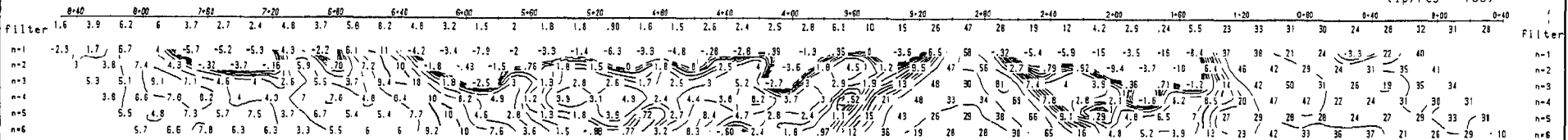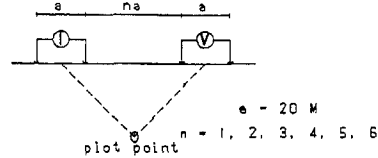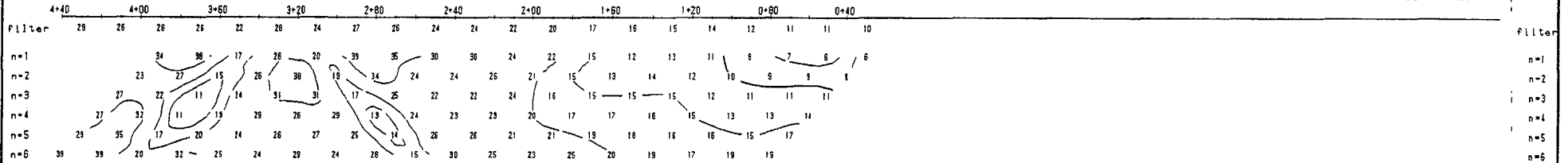
Induced Polarization Survey

INCO EXPL. & TECHNICAL SERVICES INC.

Tailings Pond Project
Sudbury Area

Date: 94/01/11
Interpretation by:
Scale 1 : 1000

Executed by: WALCER GEOPHYSICS LTD
Compiled by: VAL D'OR GEOPHYSIQUE LTEE

Po . AREA

Pole-Dipole Array

a   na   a

a - 10 M

n = 1, 2, 3, 4, 5, 6

plot point

Logarithmic Contours
1, 1.5, 2, 3, 5, 7.5, 10,...

Instrument: PHOENIX IPT1, BRGM IP-6
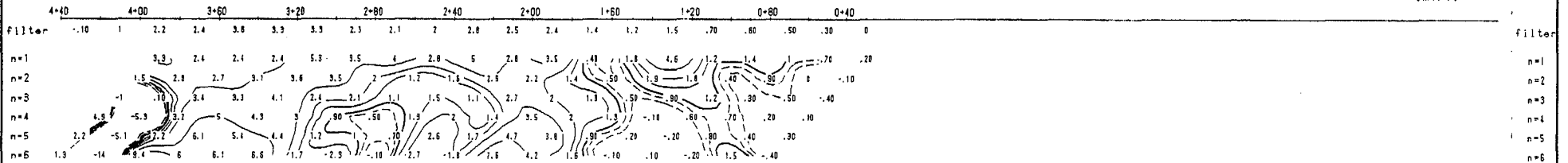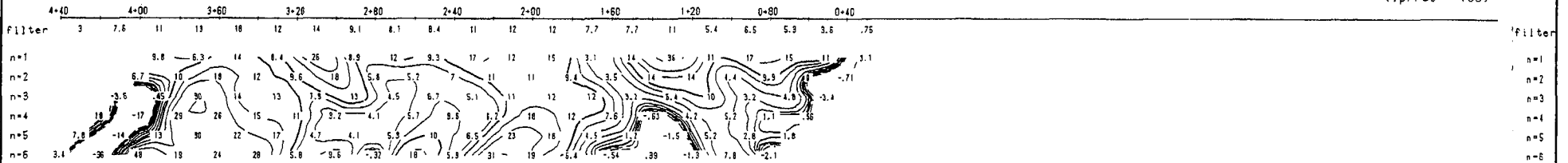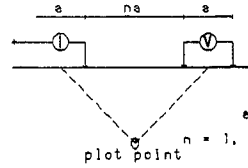Time cycle: 2 sec.
Operator: Gerry Shields

RESISTIVITY
(Ohm * m)

CHARGEABILITY
(mV/V)

METAL FACTOR
(ip/res * 100)